Consecutive Cyclization as a Simple and Efficient Synthetic Strategy for Multicyclic Polymers

A Dissertation for the Degree of Doctor of Philosophy

Yoshinobu Mato

Hokkaido University

December 2021

Acknowledgements

The study presented in this dissertation has been performed under the direction of Professor Toshifumi Satoh, Division of Applied Chemistry, Faculty of Engineering, Hokkaido University, from 2017 to 2021. I would like to express the deepest appreciation to him for his kind instruction, valuable suggestions, and encouragement throughout the course of this work as well as for his kindness in everything.

I am also grateful to Associate Professor Takuya Isono, Division of Applied Chemistry, Faculty of Engineering, Hokkaido University, for all the experimental guidance, helpful suggestions, and fruitful discussions since my first day in the laboratory.

I also would like to show my deep appreciation to Associate Professor Kenji Tajima and Associate Professor Takuya Yamamoto, Division of Applied Chemistry, Faculty of Engineering, Hokkaido University, whose kind understanding and generous supports have been indispensable throughout this work.

I also thank Professor Tesuo Deguchi, Department of Physics, Faculty of Core Research, Ochanomizu University, Lecturer Hironori Marubayashi, and Professor Hiroshi Jinnai, Institute of Multidisciplinary Research for Advanced Materials, Tohoku University, for the collaborative works, in which the broad insights for understanding polymer properties were provided.

Special thanks goes to Dr. Brian J. Ree, Kohei Honda, and Maho Sudo as well as other members of Professor Satoh's group. We have discussed the direction and interesting aspects of our works and carried out a lot of experiments together. It was a great honor to have the experiences worked together.

I am very grateful to the Research Fellowships of the Japan Society for the Promotion of Science (JSPS) for Young Scientists during 2020-2021.

The last and not the least, I wish to express my deep gratitude to my family and friends for their understanding, support, and continuous encouragement throughout his research and daily life.

December 2021

Yoshinobu Mato

Contents

Chapter 1

General Introduction

1.1 Introduction to Polymer Topology

Polymer topology describes the shapes and spatial characteristics of the polymer's backbone. While classic example includes linear and randomly branched architectures, as shown in Figure 1.1, the recent advances in precision polymerization system as well as efficient coupling reactions allowed the far broader choice, such as star, graft, dendritic, cyclic, and multicyclic topologies.[1–4] Precisely constructed non-linear type topologies give rise different polymer properties compared to those of the linear counterpart with comparable molecular weight and composition. For example, star-shaped polymer exhibits lower glass transition temperature (T_g) compared to that of the linear counterpart due to its enhanced chain mobility originating from branched main chains and chain ends. Graft and dendritic topologies have greater number of branching points and chain-ends, in which the possible chain conformation is restricted to make the rigid molecules.[5–8] These unique spatial and structural characteristics facilitate a wide range of nanomaterial applications. Controlling over not only the conventional structural parameters (*i.e.*, primary structure, tacticity, and molecular weight) but also the polymer topology is becoming important technique to realize the polymers with desired physical properties that are unachievable by the linear form. In addition, the structure-property relationship study using a series of precisely synthesized topological polymers is fundamental yet indispensable to provide a practical guideline for the design of the polymer materials with sophisticated functions.

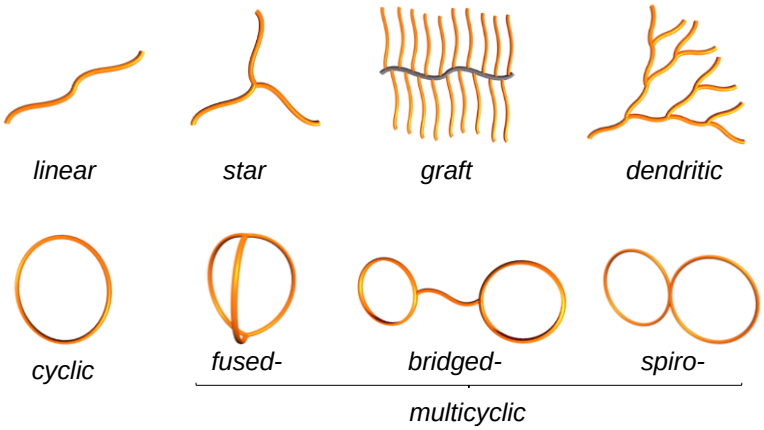

Figure 1.1. General examples of polymer topologies, including linear, star, graft, dendritic, cyclic, and diverse multicyclic topologies.

Among the polymer topologies, cyclic-type topologies (cyclic and multicyclic topologies) are classified to a distinctive category due to the lack of chain ends and are believed to be key variables for designing the synthetic polymers with tailor-made properties. In fact, structure-relationship studies of cyclic polymers that adopt a ring-like shape have revealed unique physical properties and functions. Examples includes higher density,[9] smaller hydrodynamic volume,[10] and superior optical properties[11] compared to its linear counterparts, which stems from the lack of chain-ends. In this context, the synthesis of "multicyclic" topological polymers that consist of more than two macromolecular rings have been attempted, as shown in Figure 1.1.[12] Multicyclic topologies are typically classified into three categories: *fused*- (such as θ-shaped), *bridged*- (such as manacle-shaped), and *spiro*-type (such as 8-shaped) topologies by identifying the main ring, branching points, and bridges. Their unique multicyclic architectures could be used for not only controlling polymer properties but also developing diverse novel materials. For example, cage-shaped polymers should have a large and isolated three-dimensional cavity like the cryptands with macromolecular frame, which are expected as supramolecular materials enabling the inclusion of the giant guests, such as metal clusters[13,14] (Figure 1.2(a)). Also, the development of additive for modifying material's

properties utilizing the entanglement where a linear chain penetrates a cyclic chain is envisaged (Figure 1.2(b)). Such applications are unachievable by conventional low-molecular-weight cyclic compounds. Another interest aspect of synthesizing cyclic-type topological polymers is that this could provide a basis for mimicking and replicating the unique properties of naturally-occurring folded peptides with superior bioactivities using synthetic polymers.[15,16] Despite such potentials, study on systematic investigation of structure-property relationships remains elusive due to the synthetic difficulty of multicyclic polymers with controllable ring number (*i.e.*, arm number) and its size. Thus, the development of facile yet universal synthetic pathway to multicyclic polymers remains major task in the field of polymer science.

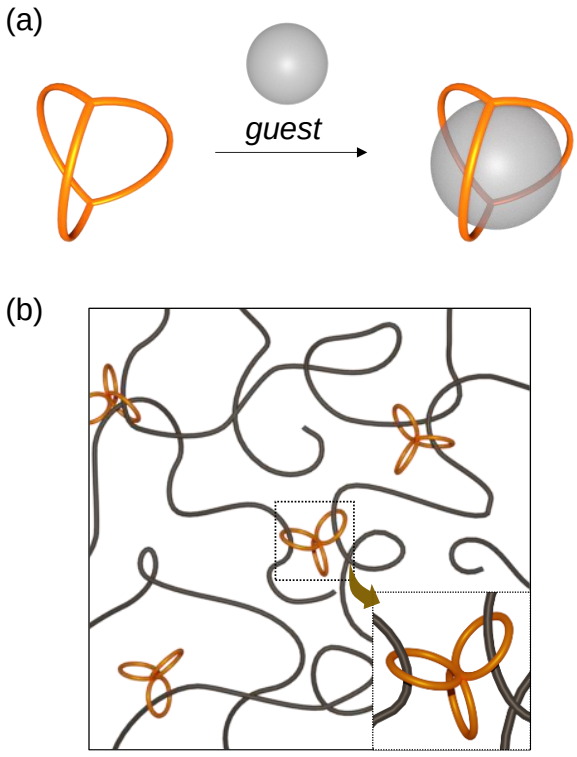

Figure 1.2. Potential applications of multicyclic polymers. (a) Guest molecule uptake into the three-dimensional compartment of a cage-shaped polymer which can be used for supramolecular applications. (b) Multicyclic polymer as additive for modifying material's properties through the penetration of linear chains into cyclic chains, as shown in the inset.

1.2 Synthesis of Monocyclic Polymers

The well-defined monocyclic polymer is generally synthesized via (a) ring-closure reactions, (b) ring-expansion polymerization, and (c) topology transformation (Figure 1.3).

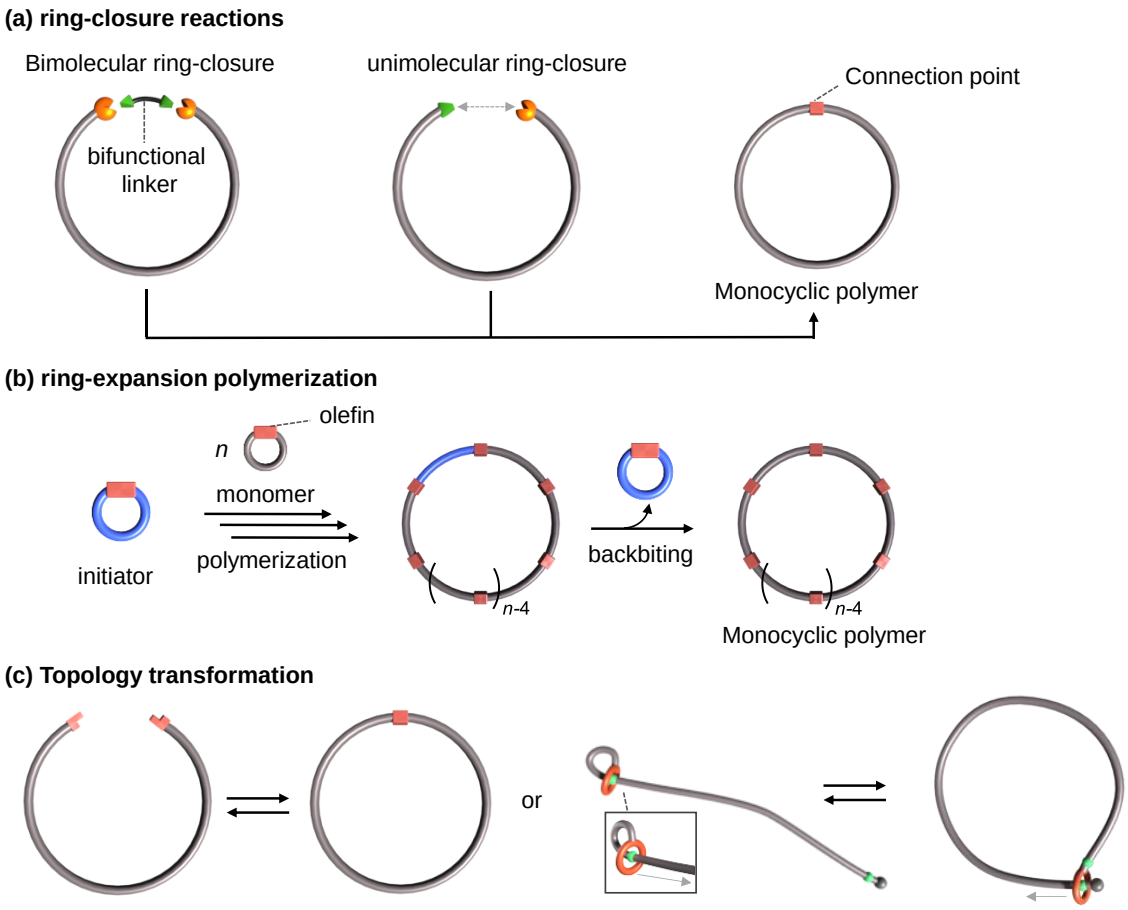

Figure 1.3. Synthetic pathways to monocyclic polymers via (a) ring-closure reactions, (b) ring-expansion polymerization, and (c) topology transformations.

The ring-closure reactions (*i.e.*, cyclization reaction) are the simplest synthetic strategy to monocyclic polymers, and they are divided into two subcategories: bimolecular ring-closure and unimolecular ring-closure. For any ring-closure reactions, the high dilution is required to selectively promote the intramolecular reaction rather than the intermolecular reaction. In the bimolecular ring-closure, the selective intermolecular coupling reaction between polymer chain

ends and a bifunctional linker. For example, the pioneering work by Hocker et al. demonstrated the synthesis of monocyclic polystyrene (PS) via the combination of anionic polymerization and bimolecular coupling with dichloro-*p*-xylene as a coupling agent (Scheme 1.1(a)).[17] It is notable that such typical bimolecular reactions are performed with strictly equimolar amounts of the functionalized polymers and the coupling reagent. Tezuka et al. reported the efficient coupling reaction, so-called Electrostatic Self-Assembly and Covalent Fixation (ESA-CF) method (Scheme 1.1(b)), where monocyclic ammonium ion and carboxylate ion are electrostatically assembled and heated to form covalent bonds. Specifically, the telechelic poly(tetrahydrofuran) (PTHF) having *N*-phenylpyrrolidinium group at each chain end was reacted with a dicaroboxylate linker to produce the monocyclic form in high yield.[18] The robustness of ESA-CF method has enabled the construction of not only monocyclic but also diverse multicyclic and cyclic-linear hybrid polymer topologies (see Section 1.3 below).

Scheme 1.1. Synthesis of cyclic polymers via intermolecular cyclization, based on (a) bimolecular coupling of dichloro-*p*-xylene and polystyreyl anion (b) ESA-CF method.

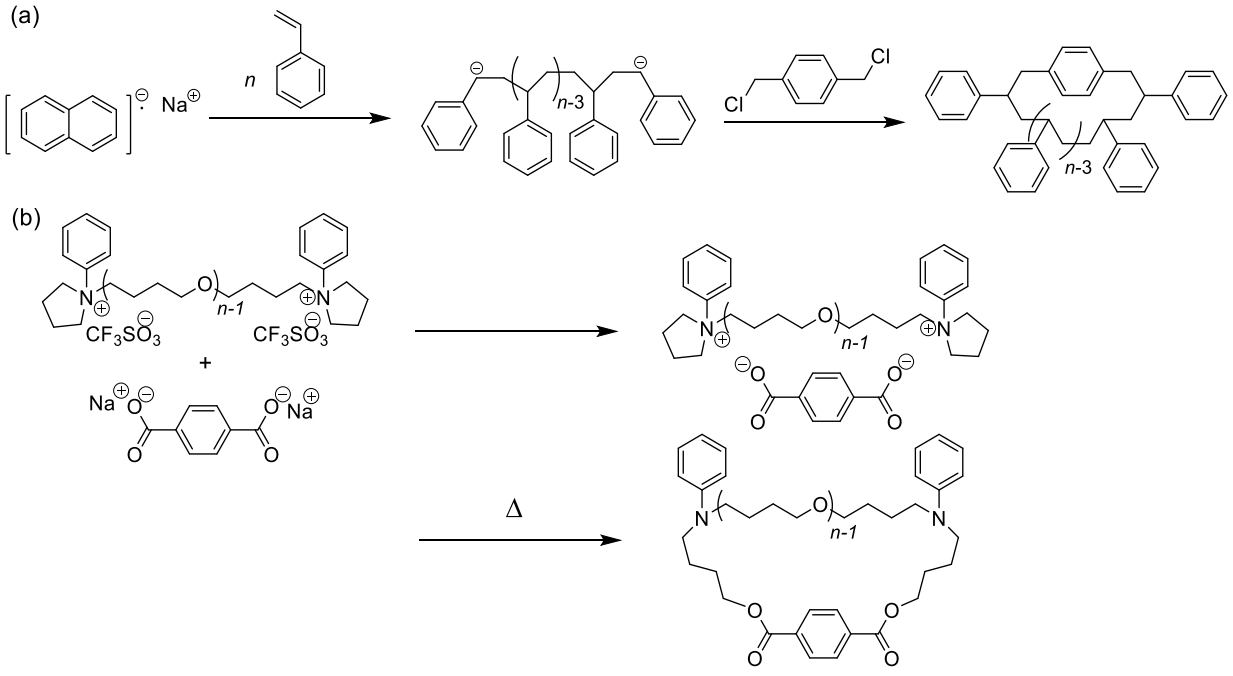

On the other hand, unimolecular ring-closure (*i.e.*, intramolecular cyclization) has also been exploited for the synthesis of monocyclic polymers. Many examples achieved the construction of monocyclic polymers by taking the advantage of highly efficient ‘‘click’’ reactions, specifically cupper(I)-catalyzed azido-alkyne cycloaddition (CuAAC) reaction; It is featured by the tolerance to a wide range of functional groups and the ability to form a covalent bond in qualitative yield. Grayson et al. synthesized the monocyclic polystyrene (PS) by intramolecular cyclization of the α-ethynyl-ω-azido end-functionalized linear PS based on the CuAAC (Scheme 1.2).[19] This method has been recognized as one of the most reliable cyclization techniques as of date. Due to the potential toxicity of the cupper catalyst, alternative click reactions have been employed for the cyclization, such as strain-promoted azido-alkyne cycloadditions (SPAAC),[20] the Diels-Alder reaction of maleimide and furan end groups,[21] and various photoactivated cycloaddition reactions.[22,23]

Scheme 1.2. Synthesis of monocyclic polymers via intramolecular cyclization based on CuAAC reaction.

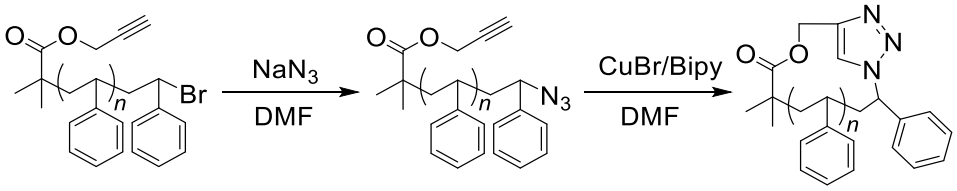

Ring-expansion polymerization also efficiently produce the monocyclic polymers. Early efforts by Lee et al. revealed that ring-opening polymerization of lactones with cyclic tin alkoxide initiator affords monocyclic polyesters, as shown in Scheme 1.3(a).[24] Grubbs et al. reported the synthesis of high molecular weight monocyclic polybutadiene from 1,5-cyclooctadiene using ruthenium-based metathesis catalyst via ring-expansion metathesis polymerization (REMP), in which the repeating monomer insertion into the cyclic initiators take place, followed by the elimination of catalyst via backbiting (Scheme 1.3(b)).[25] Veige et

al. have also demonstrated the cyclic tungsten catalyst allowed the REMP of alkyne derivatives to produce the monocyclic polyacetylenes (Scheme 1.3(c)).[26,27] Since the ring-expansion strategies do not involve ring-closure process, scalable synthesis of monocyclic polymer with high molecular weight (>100 kDa) is possible in high purity. On the other hand, some drawbacks remain, such as broad dispersity (*Đ*), poor controllability of the molecular weight and availability of limited polymer species (*i.e.*, limited monomers). The recent study on the optimization of the catalyst structure for the REMP enabled accessing monocyclic polymers with controlled molecular weight.[28] In addition, many research groups have also developed the ring-expansion polymerization systems based on radical,[29,30] cationic,[31–33] and anionic polymerization.[34,35] Thus, a wide range of polymer backbone could be used for the ring-expansion polymerization to get diverse monocyclic polymers.

Scheme 1.3. Synthesis of monocyclic polymers by (a) tin-catalyzed ring-expansion polymerization of the lactone and (b) ruthenium-catalyzed REMP of cycloalkene. (c) tungsten-catalyzed REMP of alkyne.

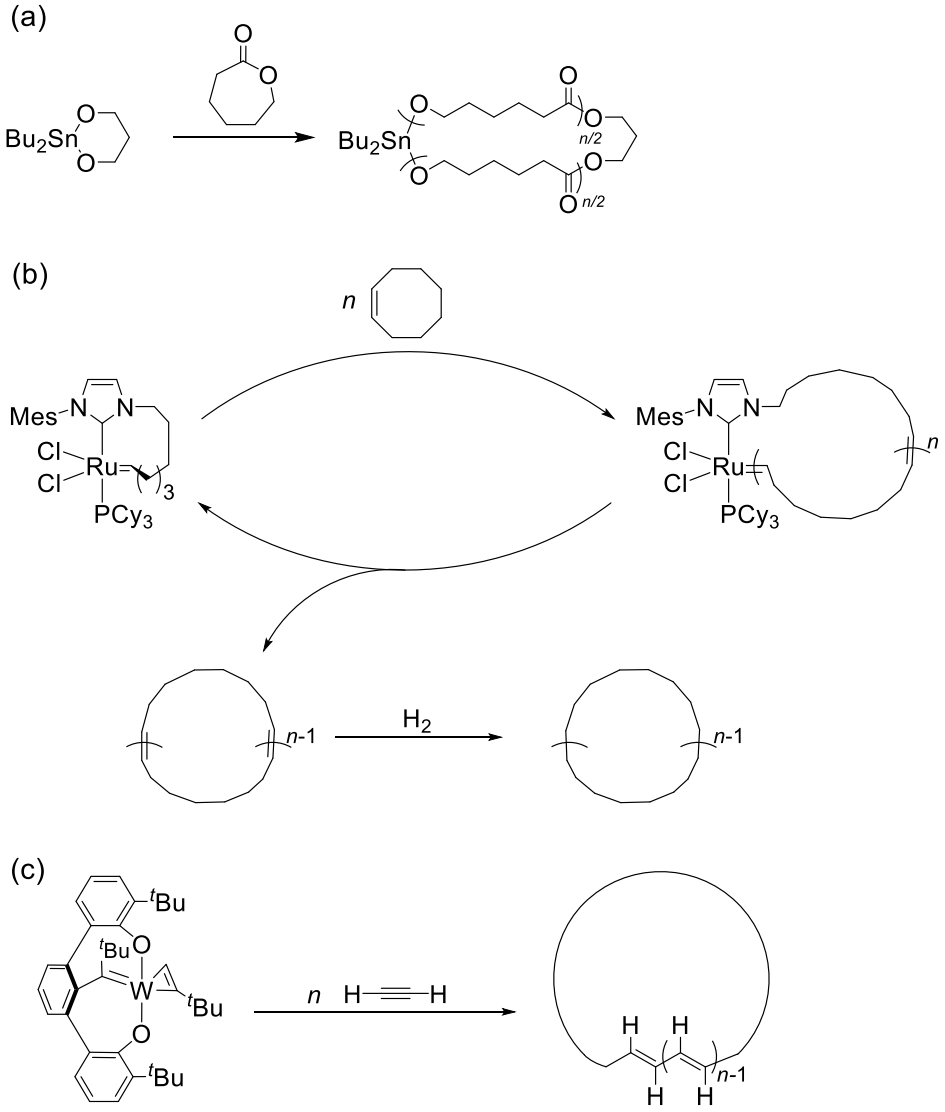

Besides the aforementioned synthetic approaches, the topology transformation systems from linear to monocyclic topology are of particular interest from the viewpoints of expanding the scope of stimuli-responsive polymers and understanding structure-property relationships.[36] A general concept of the topology transformation systems is based on the highly efficient disassembly and assembly processes of the reversible linkages connected to a constitutional polymer segment. The various stimuli can be used for the topology

transformation by introducing the thermo-responsive, photo-responsive, mechano-responsive, and redox-responsive moieties into the polymers.[22,37–39] For example, Monteiro et al. reported that redox-responsible linear PS with *α*,*ω*-thiol ends, which can form intermolecular disulfide bond under the dilute condition to give the monocyclic PS (Scheme 1.4(a)).[40] The obtained monocyclic PS can be transformed to its linear form by reduction reaction. Besides, Yamamoto and coworkers developed the reversible linear-cyclic topology transformation based on dimerization and cleavage of anthracenyl group of the telelchelics which are triggered by the light and heat, respectively (Scheme 1.4(b)).[38] In the past two decades, the topology transformation system was expanded with the rotaxane chemistry.[41] Takata et al. demonstrated the topology transformation of linear PTHF having a crown ether wheel threading onto the polymer axle, through the shuttling by protection/deprotection reactions (Scheme 1.4(c)).[42–44]

As described above, the development of precise synthesis and cyclization methods will accelerate the investigation of material applications. However, the reported cyclization strategies are mostly specialized for monocyclic polymer synthesis, and the precise synthesis of cyclic polymer with narrow *Đ* and controlled molecular weight are still limited. Therefore, robust synthetic strategies are required for preparing not only the well-defined monocyclic polymers and but also much architecturally multicyclic polymers.

Scheme 1.4. Construction of monocyclic polymers via topology transformation based on (a) disulfide, (b) anthracene, and (c) rotaxane chemistries.

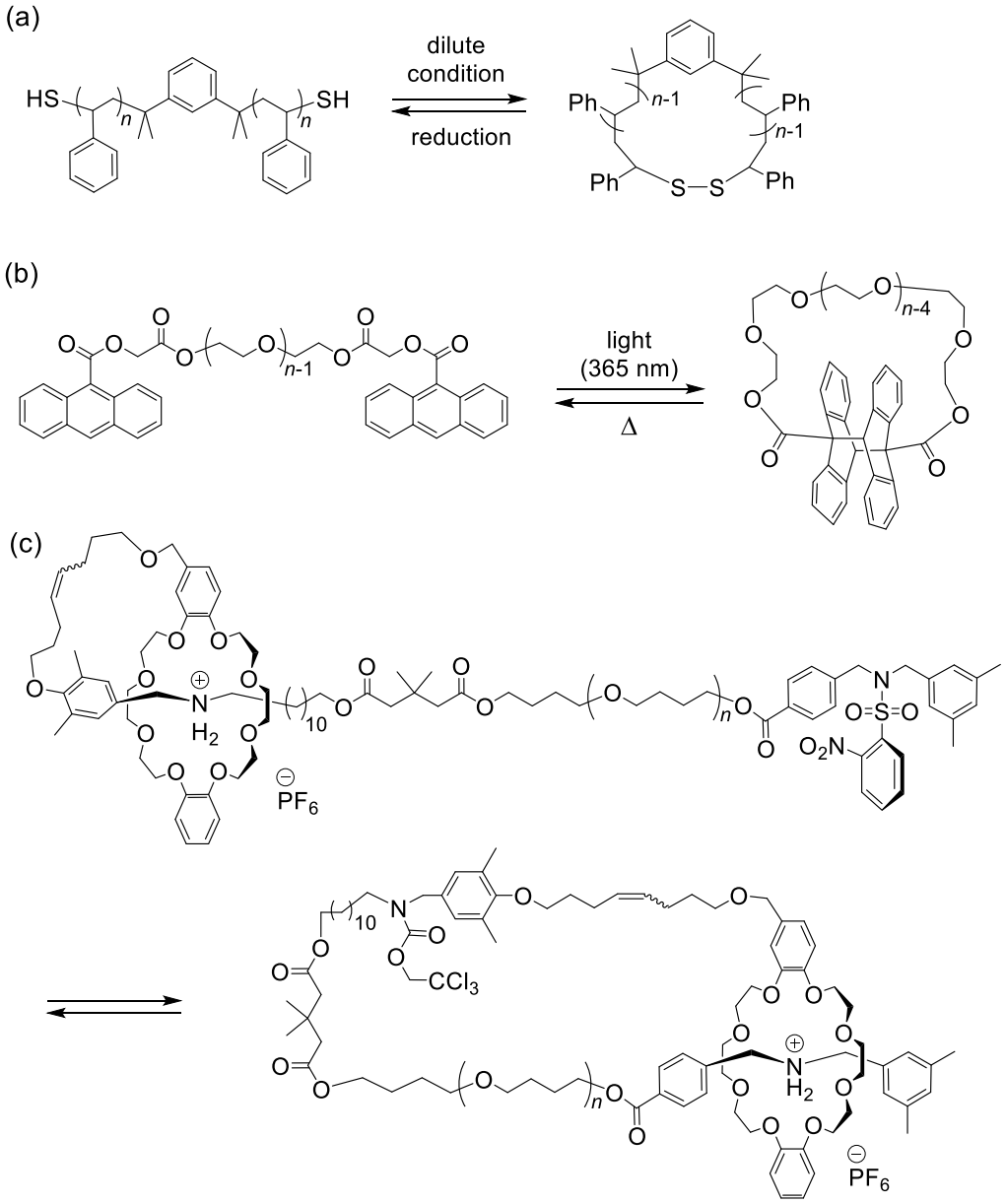

1.3 Synthesis of Multicyclic Polymers

As the fascinating physical properties of monocyclic polymers have been revealed, those of multicyclic polymer have also attracted more attentions. Since 1988, when Antonietti et al. firstly reported the synthesis of 8-shaped PS as a multicyclic polymer,[45] the synthesis of multicyclic polymers having diverse backbones and topologies (*fused*- (such as θ-shaped), *bridged*- (such as manacle-shaped), and *spiro*-types (such as 8-shaped)) have attempted up to date. As described in Section 1.1, the synthetic studies of multicyclic polymers could enable the structure-property relationships as well as provide a basis to replicate the folded peptides with superior bioactivities by synthetic polymers. Among the aforementioned synthetic pathways for monocyclic polymers, only the efficient ring-closure methods, which are capable forming the covalent bond in high selectivity and high efficiency (*i.e.*, CuAAC,[46–48] SPAAC,[49,50] and ESA-CF method[12,18,51,52]), can be applied to the multicyclic polymer synthesis. This is because all the predetermined reactive sites in a polymer chain must be connected each other to precisely construct the complicated multicyclic architectures. Other synthetic methods (ring-expansion polymerization, topology-transformation, and etc.) are hardly utilized for the universal synthesis of multicyclic polymers due to their daunting preparation of specially-designed initiators or catalysts and poor monomer choice.[53–55] To date, several synthetic pathways for the multicyclic polymers have been developed: (i) intermolecular coupling of monocyclic constituents, (ii) intermolecular cyclization of linear/star polymers with the multifunctionalized linker, and (iii) intramolecular cyclization of linear/star polymer precursors bearing functional groups at predetermined positions, as shown in Schemes 1.5–1.7.

Monteiro and Tezuka groups independently reported the coupling reaction of monocyclic units (*i.e.*, strategy (i)) to produce 8-shaped, trefoil-shaped, quatrefoil-shaped, and more architecturally complicated multicyclic polymers.[46,51,56] For example, Monteiro and colleagues synthesized 8-shaped PS via CuAAC of the azido-functionalized monocyclic PS and

ethynyl-functionalized monocyclic PS (Scheme 1.5(a)). They also succeeded to obtain trefoil-shaped PS by attaching two azido-functionalized monocyclic PS onto a di-ethynyl-functionalized monocyclic PS.[57] The same group also reported the iterative CuAAC reaction of constitutional PS ring in a step-by-step manner to produce well-defined pentacyclic PS (Scheme 1.5(b)). However, it requires laborious efforts and time-consuming processes. They additionally proposed an elegant one-shot preparation method of multicyclic polymers (Scheme 1.5(c)): the CuAAC polymerization of bifunctional monocyclic PS carrying an azido group and an ethynyl group afforded the multicyclic PS with greater number of ring units up to 20. However, aforementioned strategies require the elaborated synthesis of monocyclic polymers having a reactive functional group as well as a tedious purification process to remove the excessive monocyclic reactant. Another drawback of this strategy is poor control over the number of cyclic units because its step-growth polymerization nature provides the broad distribution of ring number to give ill-defined products.

Scheme 1.5. Synthesis of multicyclic polymers via intermolecular coupling of monocyclic constituents.

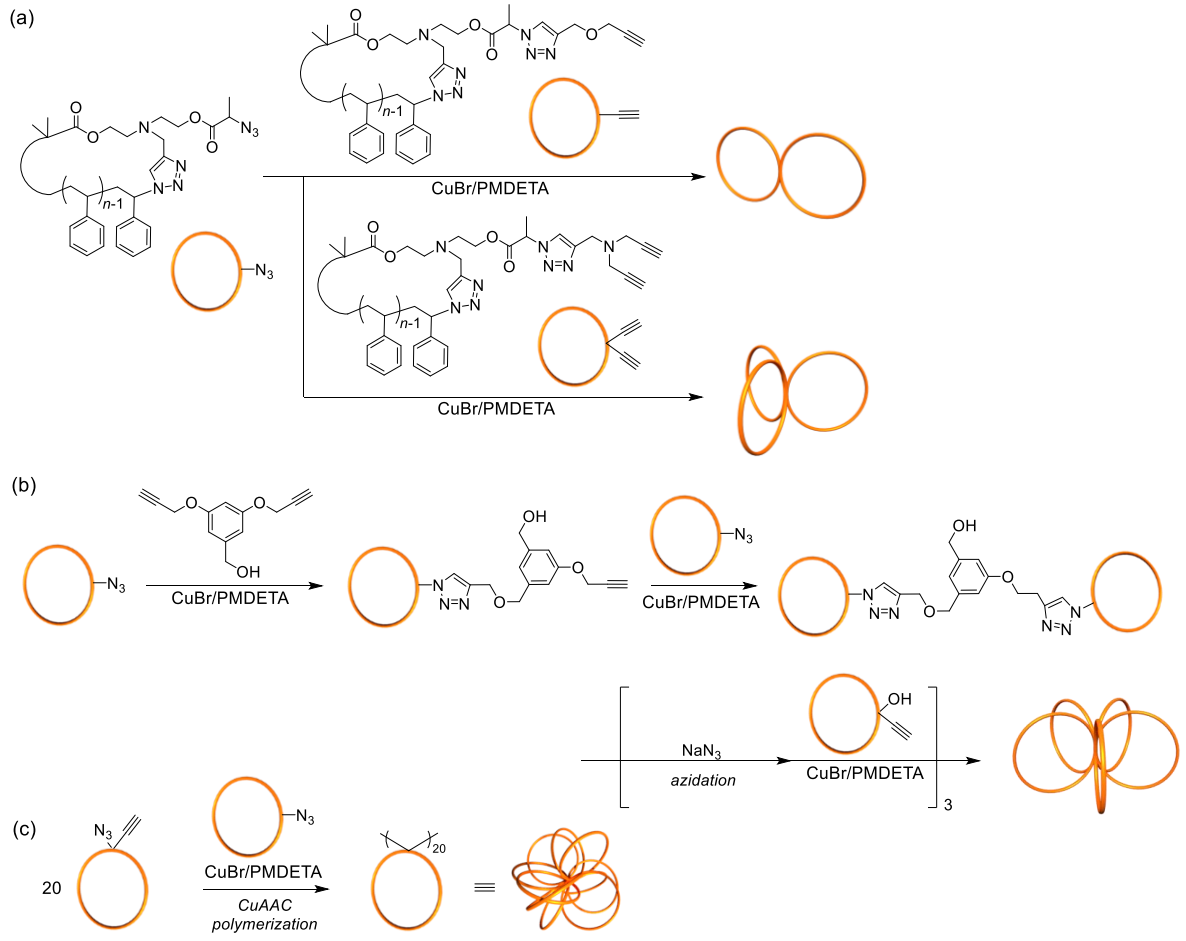

Scheme 1.6 shows the examples of intermolecular cyclization of linear/star polymers with the multifunctionalized linker (strategy (ii)). Paik et al. achieved the synthesis of 8-shaped and four-armed cage-shaped PS via the click coupling of ω-azido-functionalized star-shaped PS and ethynyl-functionalized linkers (Scheme 1.6(a)).[58,59] Tezuka et al. synthesized the four-armed cage-shaped polymer by applying the ESA-CF protocol to two telechelic PTHF with olefin at the chain center and a tetrafunctional linker, followed by the intramolecular olefin metathesis reaction (Scheme 1.6(b)).[60] Recently, six-armed cage-shaped polymer was successfully constructed by Zhang via SPAAC reaction using a multifunctional linker (Scheme 1.6(c)).[50] Note that no one achieved the synthesis of cage-shaped polymers having more than

seven arms due to the synthetic difficulty of the precursor and/or linkers with different functional groups at specific positions. While some reports regarding the construction of complicated multicyclic polymer topologies have recently been published, the formidable preparation of not only multifunctional linear/star precursors but also multifunctional linkers pose a major hurdle to systematically investigate structure-property relationships.

Scheme 1.6. Synthesis of multicyclic polymers via intermolecular cyclization of linear/star precursor with multifunctional linker.

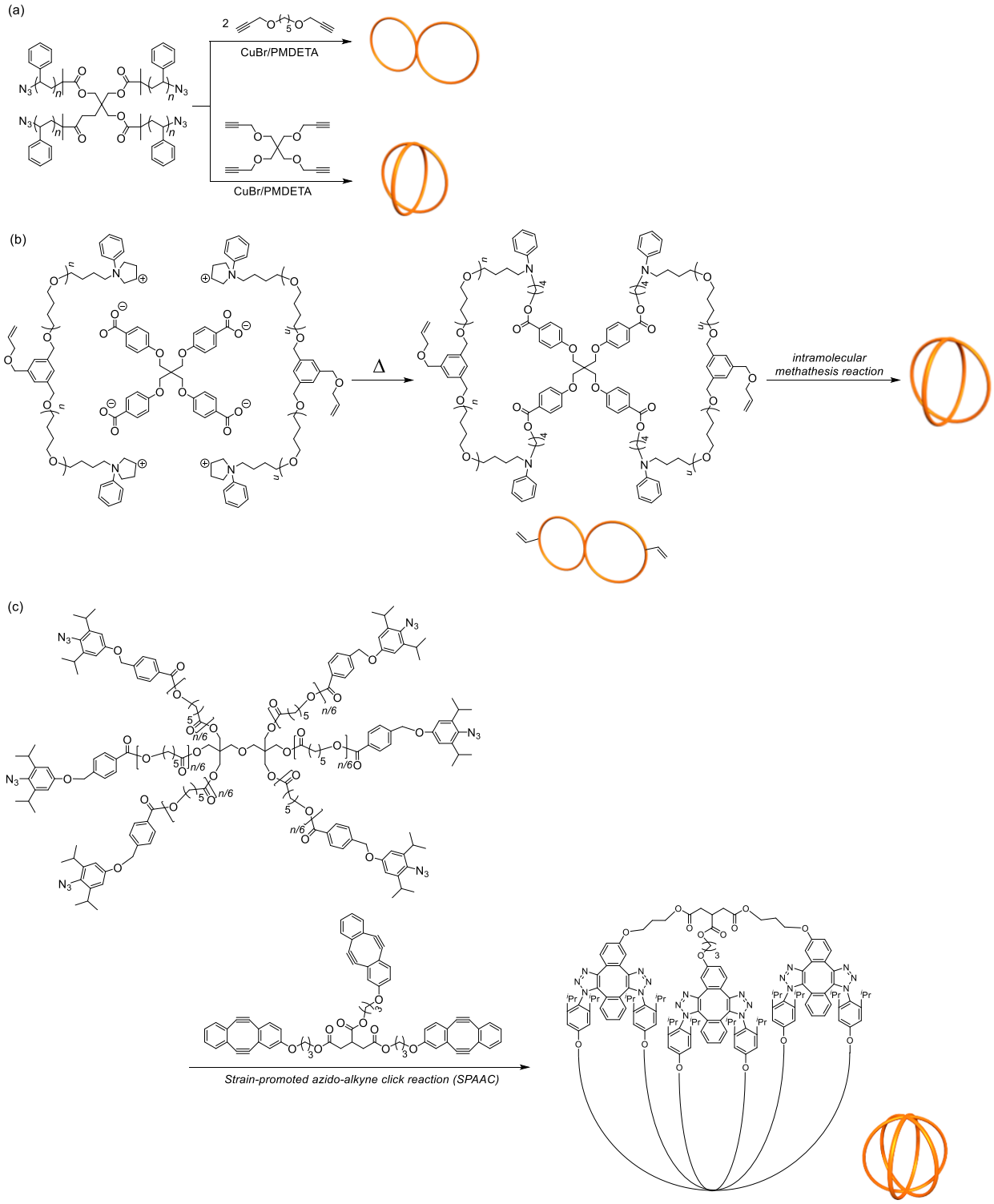

The intramolecular cyclization of linear/star polymer precursors (strategy (iii)) using coupling reactions is one of most reliable methods for multicyclic polymer synthesis. Because if the only intramolecular unimolecular ring-closure occurs, the desired multicyclic topologies should be precisely constructed. For example, Pan et al. reported the synthesis of the 8-shaped PS via the CuAAC of a linear PS possessing two ethynyl groups at the chain center and an azido group at each ω-end (Scheme 1.7(a)).[61] Satoh et al. have extended this approach to synthesize 8-, trefoil-, and quatrefoil-, and cage-shaped polyether and polyester system, in which their film morphology and self-assembly properties were systematically investigated.[47,62–66] Pan and Theato et al. independently developed the intramolecular cyclization strategies to afford the cage-shaped polymers using three- and four-armed star-shaped polymers with azido and alkyne groups at proper positions (Scheme 1.7(b) and (c), respectively).[67,68] To eliminate the intermolecular reaction kinetic issues, more complex precursor structures were also investigated: the topological conversions of trefoil- and quatrefoil-shaped polyethers into three- and four-arm cages, respectively, via selective hydrogenolysis of the benzyl ether linkages at the focal point were reported by Satoh and colleagues (Figure 1.7 (c)).[48] A major drawback is that these approaches require elaborated synthesis of linear or star polymer precursors with different functional groups at predetermined positions.

Scheme 1.7. Synthesis of multicyclic polymers via intramolecular cyclization of linear/star polymer precursors bearing functional groups at predetermined positions.

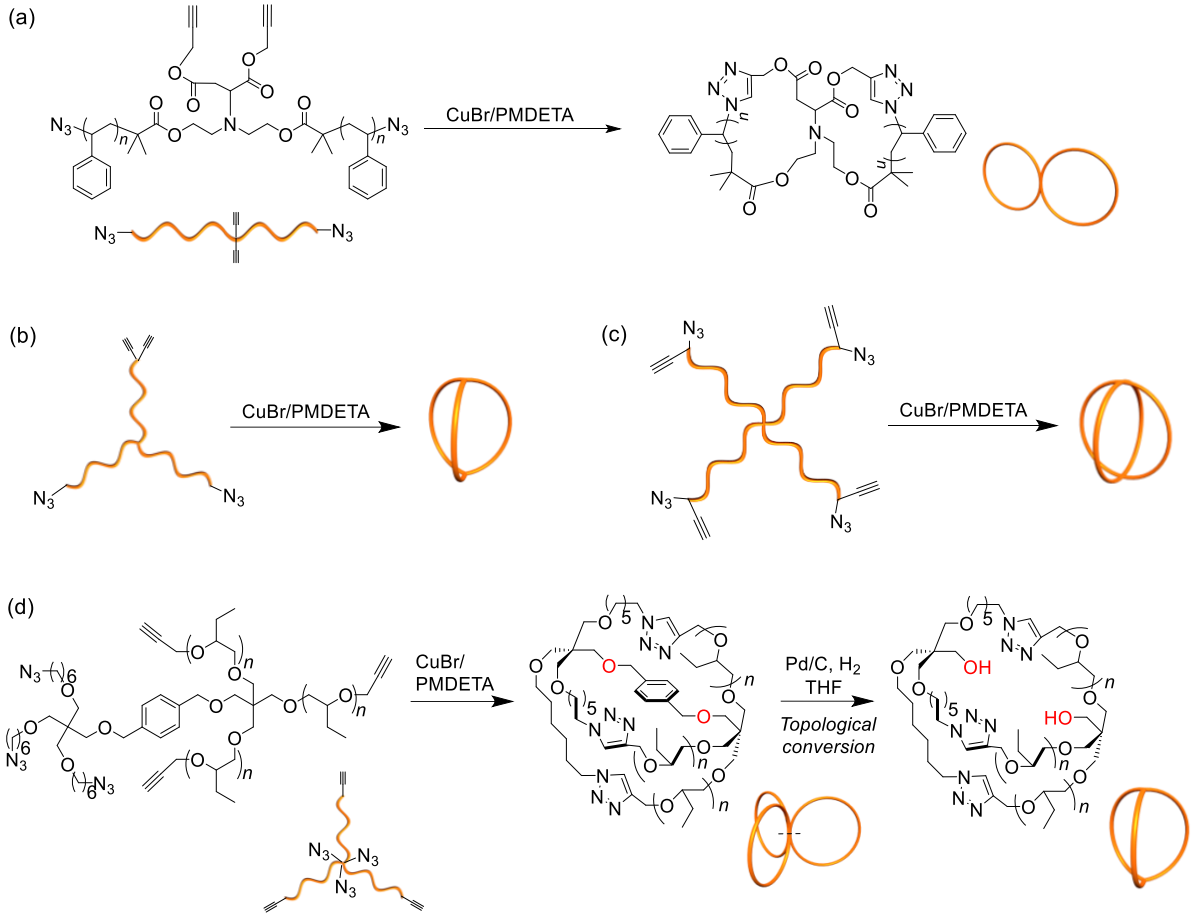

As described above, however, the sophisticated molecular design and daunting synthesis of polymer precursors are required for the current synthetic pathways for multicyclic polymers. Accordingly, even today, only few examples reached the stage for exploring the fundamental physical properties stemming from the multicyclic topologies.[69,70] Thus, the development of simple, efficient, and universal cyclization approach based on novel reaction manner for the synthesis of multicyclic polymers have been desired.

1.4 Ring-opening Metathesis Polymerization

The term olefin metathesis refers to a family of reactions involving the rearrangement of carbon-carbon double bonds. The metathesis reaction was expanded to the polymerization of cyclic olefins, so-called ring-opening metathesis polymerization (ROMP), which produces linear polyolefins (Scheme 1.8).[71] While various organometallic catalyst and organocatalysts have been found to mediate the ROMP, ruthenium-centered catalysts (Hoveyda and Grubbs catalysts) are widely used due to their excellent tolerance to water, air, and solvents as well as many functional groups. Specifically, Grubbs catalysts have the variation from first- to third-generations by optimizing and varying the ligands, as shown in Chart 1.1. While all of them catalyze the ROMP, only the third-generation Grubbs catalysts (G3) having the pyridinium-type ligands enable the well-controlled and fast-initiating ROMP of strained cyclic olefins such as cyclopentenes and norbornenes. Indeed, the G3 having the 3-bromopyridinium ligands catalyzes the ROMP of norbornenes in 106 times higher initiation rate compared to that of second-generation catalyst, in which the well-defined linear polynorbornenes with narrow $Đ$ (<1.1) and controlled molecular weight can be obtained at high conversion (>99%) even in the case that norbornene-functionalized macromonomers are used.[72,73] Diverse functional groups (such as carboxyl, hydroxyl, and azide group as well as polymer chains) can be introduced at the α- and ω-chain-ends in the polymer using functional initiator and chain transfer agents, respectively (Scheme 1.9), which facilitates materials applications.[74]

Scheme 1.8. Proposed mechanism for the ROMP of cyclic olefin.

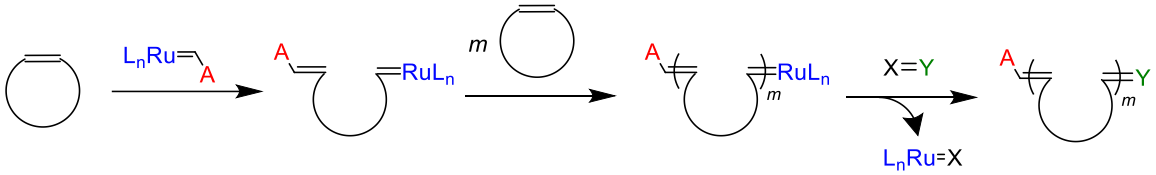

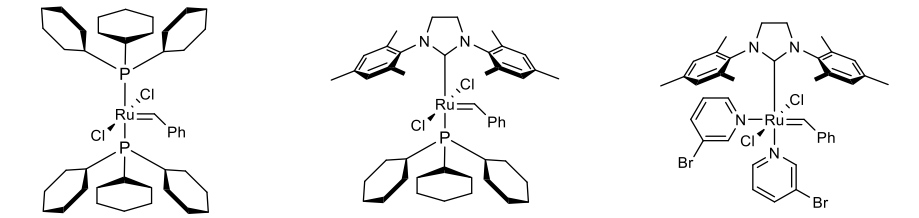

Chart 1.1. A list of ruthenium-based olefin metathesis catalysts from 1st to 3rd generations.

Scheme 1.9. The *α*,*ω*-end functionalization of polyolefin in ROMP using chain transfer agents. FG and FG': functional groups.

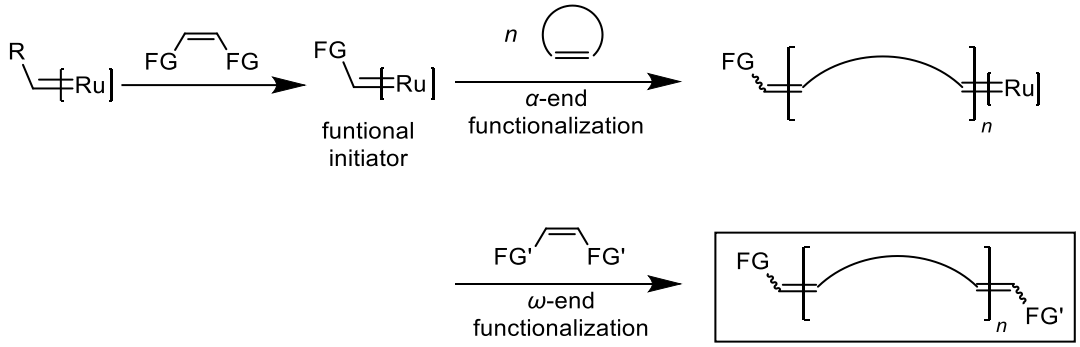

Given the aforementioned features, ROMP mediated by G3 could be a favorable candidate for developing the new macrocyclization method with universality, simplicity, and robustness. In fact, Satoh et al. established a robust synthetic pathway to multicyclic polymers: the cyclopolymerization of *α*,*ω*-norbornenyl-functionalized bifunctional linear macromonomers produces well-defined multicyclic polymers through ROMP (Scheme 1.10).[75] The cyclopolymerization is facilitated by the significantly quicker intramolecular cyclization compared to the intermolecular propagation under diluted conditions. This method enabled the facile yet universal synthesis of multicyclic polymers with desired numbers of macrocyclic units from a single *α*,*ω*-end-functionalized macromonomer by varying $[\text{macromonomer}]_0/[\text{G3}]_0$ ratio. In addition, the ring size can also be controlled by changing the molecular weight of the macromonomer, which is useful for elucidating the structure-property relationships. It is

noteworthy that the requisite reactive group is only the norbornene, indicating the facile precursor preparation. This report is the only example of universal ROMP-based macrocyclization strategy without specially designed monomers,[55] and its features render the usefulness on developing the efficient synthetic routes to a variety of multicyclic polymers. Furthermore, gaining the mechanistic insights into cyclopolymerization may provide elementary yet crucial knowledge to expand the ROMP-based syntheses of a variety of architecturally complex macromolecules. For instance, none reported the precise construction of graft polymers with multicyclic side chains (*i.e.*, graft polymer in which the multicyclic polymer is a repeating unit). Thus, expanding the cyclization strategies based on ROMP should make significant progress in the research field of topological polymer, involving the multicyclic polymer synthesis, structure-property investigations, and functional materials applications.

Scheme 1.10. Multicyclic polymer synthesis through the cyclopolymerization of *α*,*ω*-norbornenyl-functionalized bifunctional linear macromonomers.

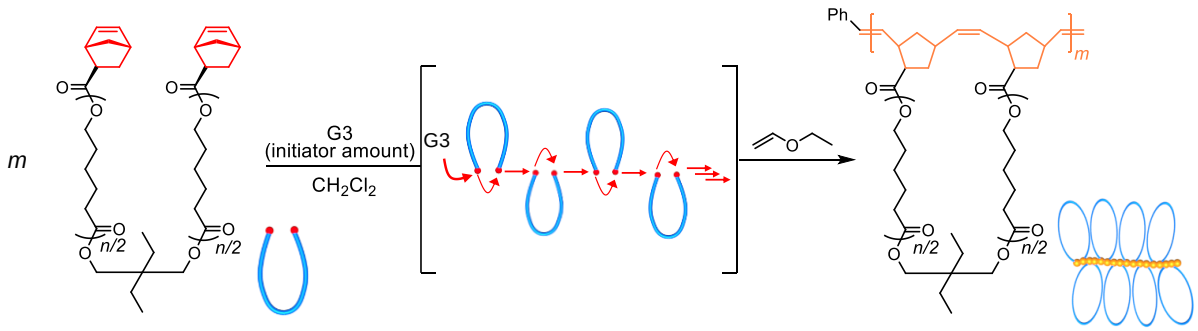

1.5 Objective and Outline of the Dissertation

The polymer topology, which describes the spatial features of the polymer's backbone, plays crucial role for controlling of polymer properties as mentioned in Section 1.1. Particularly, the effect of multicyclic polymer topologies is of significant importance to create advanced materials that are unachievable by conventional low-molecular-weight cyclic compounds. Despite the numerous efforts over the last two decades on the synthesis of multicyclic polymers, simple yet universal synthetic methods for multicyclic polymers remain elusive. This is because precise construction of the complex multicyclic structures is quite challenging, which is unachievable by simple extension from the monocyclic polymer synthesis. In addition to the fact that the current synthetic pathways for multicyclic polymers requires the sophisticated molecular design and daunting synthesis of polymer precursors (and linkers), the stepwise cyclization nature makes the poor ring-formation efficiency. The aforementioned drawbacks give rise to difficulty in controlling the number of cyclic units and ring sizes of multicyclic polymers. Accordingly, the very limited structure-relationship studies are reported so far, and one suffers from designing and fabricating the functional materials using multicyclic polymers.

To overcome this situation, the development of simple yet universal cyclization method for multicyclic polymers is desired. Here, the model multicyclic polymers that used in the structure-relationship study regarding multicyclic topology have to satisfy following three requirements from the viewpoint of polymer characteristics. First, the multicyclic polymer must possess well-defined primary structure (*i.e.*, main chain structure), which unambiguously defines its physical (molecular weight, density, and crystallinity), thermal (T_g, melting temperature, and crystallization temperature), and mechanical (Young's modulus, toughness, and etc.) properties. Second, the preparation of the multicyclic polymers with the controlled molecular weight and narrow $Đ$ is necessary, which guarantee the well-controlled size of ring units in the multicyclic polymers. Third, polymer precursor with the defined chain-end structure

is also required, which allow us to quantitatively introduce the desired functional group into the predetermined positions in a polymer chain. Unless all the requirements are ensured, the cyclization reactions should give ill-defined products and by-products, making it difficult to elucidate the correlation between the multicyclic structures and physical properties. The precision polymerization techniques (*i.e.*, controlled/living polymerization systems) may satisfy aforementioned requirements and provide a synthetic platform for the studies regarding multicyclic polymers.

The author hypothesized that if the chain-reaction-type multiple macrocyclization is possible, a simple yet efficient synthesis of multicyclic polymer can be realized. In fact, some multicyclic small molecules composed of 5-7 membered rings (such as, ladder polyethers) are constructed via cascade cyclization of the multifunctionalized precursors with low degree of freedom. As shown in Figure 1.4(a), Jamison et al. demonstrated the efficient construction of inherently complex ladder oligoether having four tetrahydropyran rings via cascade cyclization of triepoxide precursor, in which the consecutive ring-opening oligomerization of epoxides takes place.[76] However, a significant challenge here is how to perform such consecutive cyclization on multifunctionalized macromolecular precursor to afford muticyclic polymers (Figure 1.4(b)). Since the aforementioned ROMP-based macrocyclization method reported by Satoh produces the ~300-membered macrocycle in maximum, the author thought that the system could enable the envisioned consecutive cyclization method with the aid of extraordinarily fast kinetics and functional group tolerance of ROMP, as described in Section 1.4. In addition, the end-functionalization of ROMP facilitates the facile preparation functional multicyclic polymers for diverse materials applications.

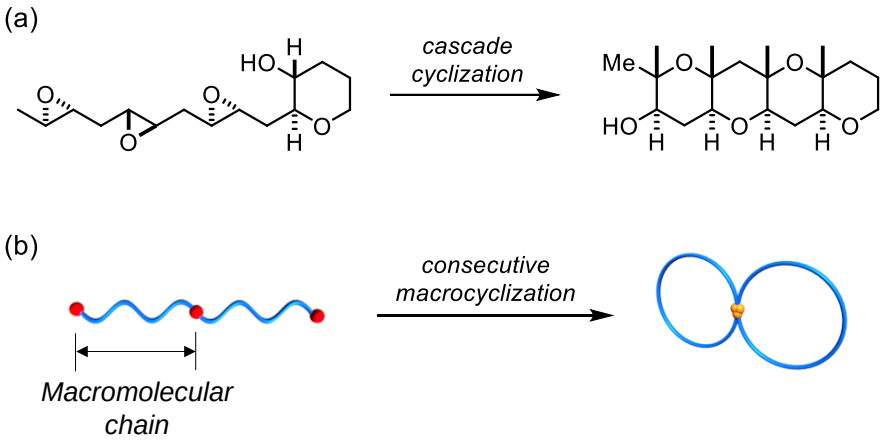

Figure 1.4. (a) Cascade cyclization of trifunctional precursor to produce a multicyclic small molecule. (b) Consecutive macrocyclization of trifunctional polymer precursor to afford the 8-shaped polymer.

Therefore, the primary objective of this dissertation is the establishment of "consecutive cyclization" strategy based on ROMP, involving the formation of multiple cyclic units via chain-reaction manner. Such novel multicyclization which taken place in chain-reaction manner should be highly useful for the systematic synthesis and characterization of various multicyclic polymers. Note that polycaprolactone (PCL) was selected as model polymer due to the ease of preparation with sufficient chain-end-fidelity and narrow $Đ$ (<1.1). The author firstly addressed the synthesis and characterization of *spiro*-type (8-, trefoil-, and quatrefoil-shaped) and cage-shaped multicyclic PCLs via the intramolecular ring-opening metathesis oligomerization (ROMO) of norbornenes attached on linear and star-shaped precursor polymers. Then, the established method was applied to cyclopolymerization of star-shaped macromonomers for the precise synthesis of novel graft polymers with macromolecular cage side chains by optimizing the reaction condition. With a series of multicyclic polymers with comparable molecular weight and narrow $Đ$, systematic characterization was carried out to reveal the effect of the multicyclic topology on the physical properties.

An outline of this dissertation is as follows:

Chapter 2 describes a novel cyclization strategy (namely, intramolecular consecutive cyclization) based on intramolecular ROMO for synthesizing *spiro*-type multicyclic polymers. A series of linear, three-armed star-, four-armed star-shaped PCLs with norbornenyl group at the chain center and each end were easily synthesized by the following three reaction steps: (1) ring-opening polymerization of ε-caprolactone using polyol initiator having a protected hydroxyl group, (2) the deprotection reaction, and (3) end-norbornenyl-functionalization. Then, the obtained linear, three-armed star-, four-armed star-shaped polymer precursors were subjected to the intramolecular ROMO using G3 catalyst under a highly diluted condition to produce the 8-, trefoil-, and quatrefoil-shaped PCLs, respectively (Figure 1.5). The desired *spiro*-multicyclic topologies were successfully obtained in efficient manner with a narrow $Đ$. The cyclization using different solvents under varied temperatures revealed the robustness of intramolecular ROMO. In addition, the universality of proposed cyclization strategy was confirmed by applying to diverse polymer species, such as poly(glycidyl ether) and polylactide. One-pot functionalization of the oligonorbornene chain ends was also demonstrated to make the functional multicyclic polymers for the materials applications. Comprehensive study on the structure-property relationships of the *spiro*-type multicyclic PCLs revealed enhanced crystallization ability in the 8-shaped topology.

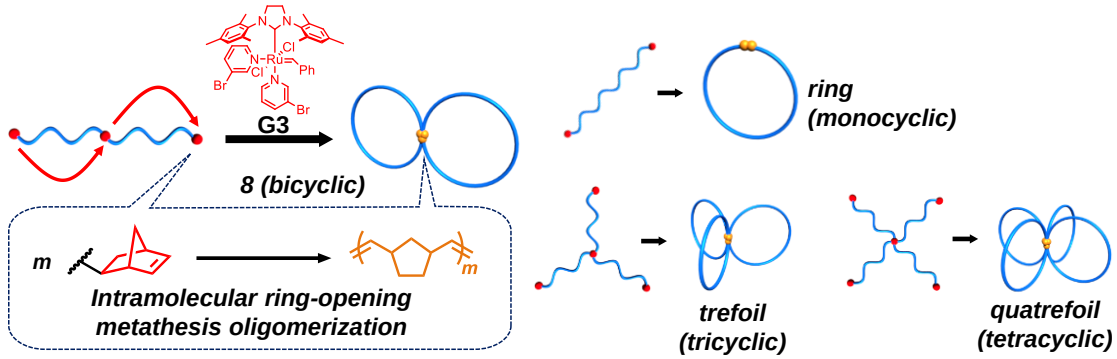

Figure 1.5. Schematic illustration of the synthetic strategy for *spiro*-multicyclic polymers through intramolecular ROMO mediated by G3 catalyst.

Chapter 3 describes the systematic synthesis of cage-shaped polymers (namely, macromolecular cages) with varied arm numbers and ring size via intramolecular ROMO of the end-norbornenyl-functionalized star-shaped PCL precursors (Figure 1.6). Firstly, the three-, four-, six-, and eight-armed star-shaped PCL precursors were prepared in two steps: the ring-opening polymerization of ε-caprolactone using polyol initiators and subsequent end-norbornenyl-functionalization. The established intramolecular ROMO of the star-shaped precursors successfully afforded the desired cage-shaped PCL in sufficient yields with high purity. It is notable that the intramolecular consecutive cyclization enabled the facile yet precise synthesis of six and eight-armed cage-shaped polymers, while conventional syntheses present a practical limitation to the systematic synthesis of macromolecular cages with arm numbers greater than seven. With a series of cage-PCLs, the polymer properties associated with a cage-shaped architecture have systematically evaluated for the first time, which revealed that the hydrodynamic diameter, viscosity, and crystallization behavior of macromolecular cages are strongly affected by the arm number and arm length.

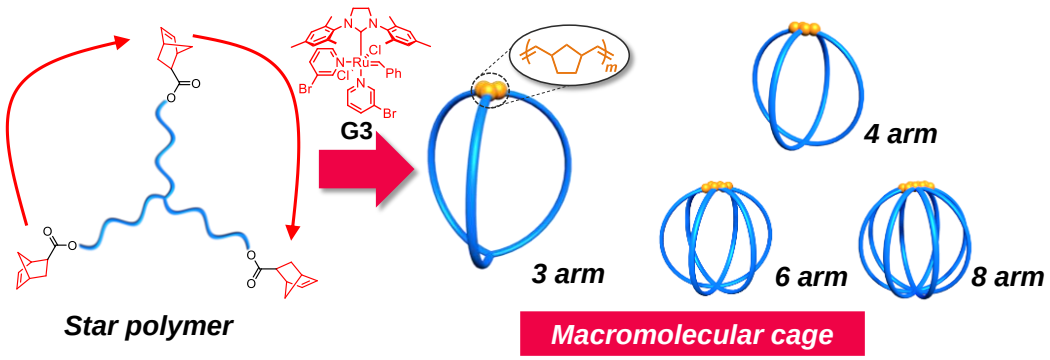

Figure 1.6. Schematic illustration of the synthetic strategy for cage-shaped multicyclic polymers (namely, macromolecular cages) through intramolecular ROMO mediated by G3 catalyst.

Chapter 4 describes the precise synthesis of novel graft polymers with macromolecular cage side chains (*cage*-GPs) through the cyclopolymerization of end-norbornenyl-functionalized star-shaped macromonomers (Figure 1.7). The three- and four-armed star-shaped macromonomers, that can be easily prepared in the same manner as Chapter 3, were subjected to the ROMP in the highly diluted condition to produce the *cage*$_x$-GPs (where x denotes the arm number of the caged-side-chain unit, x = 3 and 4). The comprehensive structural analysis revealed that the present cyclopolymerization affords the desired *cage*$_x$-GPs with well-defined microstructure. In addition, kinetic study suggested that the cyclopolymerization of star polymer proceeds in an accurately controlled manner, which is composed of the repetition of rapid intramolecular consecutive cyclization and subsequent rate-determining intermolecular addition reaction. Systematic characterization on a series of GPCLs with varying molecular weights and side-chain topologies have elucidated the fact that the cage-shaped side-chain topologies significantly affected the crystallization behavior, hydrodynamic diameter, and viscosity.

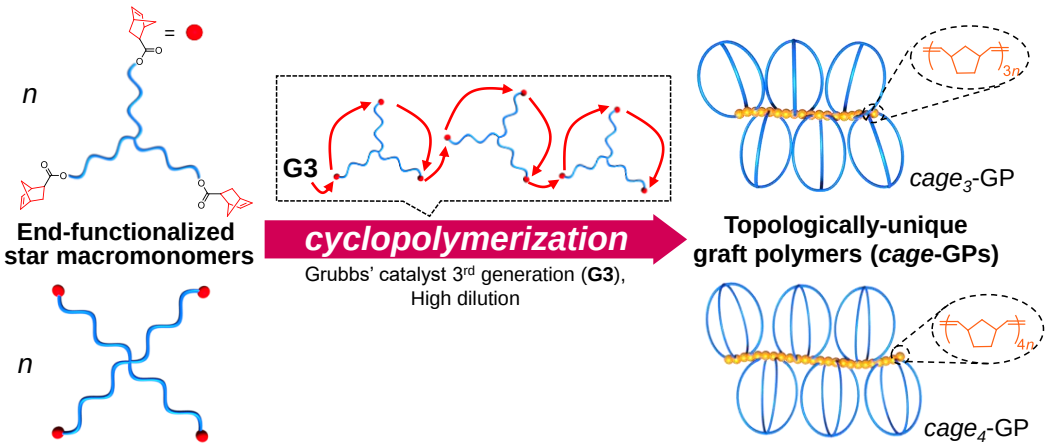

Figure 1.7. Schematic representation of synthetic strategy for graft polymers with cage-shaped side chains via cyclopolymerization of end-norbornenyl-functionalized star-shaped macromonomers using G3.

Chapter 5 summarizes the established consecutive cyclization strategies as simple, efficient, and universal synthetic methods for multicyclic polymers, enabling the investigation of structure-property relationships.

1.6 References

(1) Polymeropoulos, G.; Zapsas, G.; Ntetsikas, K.; Bilalis, P.; Gnanou, Y.; Hadjichristidis, N. 50th Anniversary Perspective: Polymers with Complex Architectures. *Macromolecules* **2017**, *50*, 1253–1290.

(2) Ren, J. M.; McKenzie, T. G.; Fu, Q.; Wong, E. H. H.; Xu, J.; An, Z.; Shanmugam, S.; Davis, T. P.; Boyer, C.; Qiao, G. G. Star Polymers. *Chem. Rev.* **2016**, *116*, 6743–6836.

(3) Haque, F. M.; Grayson, S. M. The Synthesis, Properties and Potential Applications of Cyclic Polymers. *Nat. Chem.* **2020**, *12*, 433–444.

(4) Yamamoto, T.; Tezuka, Y. Topological Polymer Chemistry: A Cyclic Approach toward Novel Polymer Properties and Functions. *Polym. Chem.* **2011**, *2*, 1930–1941.

(5) Sheiko, S. S.; Sumerlin, B. S.; Matyjaszewski, K. Cylindrical Molecular Brushes: Synthesis, Characterization, and Properties. *Prog. Polym. Sci.* **2008**, *33*, 759–785.

(6) Feng, C.; Li, Y.; Yang, D.; Hu, J.; Zhang, X.; Huang, X. Well-Defined Graft Copolymers: From Controlled Synthesis to Multipurpose Applications. *Chem. Soc. Rev.* **2011**, *40*, 1282–1295.

(7) Carlmark, A.; Hawker, C.; Hult, A.; Malkoch, M. New Methodologies in the Construction of Dendritic Materials. *Chem. Soc. Rev.* **2009**, *38*, 352–362.

(8) Peterson, G. I.; Bang, K. T.; Choi, T. L. Mechanochemical Degradation of Denpols: Synthesis and Ultrasound-Induced Chain Scission of Polyphenylene-Based Dendronized Polymers. *J. Am. Chem. Soc.* **2018**, *140,* 8599–8608.

(9) Clarson, S. J.; Semlyen, J. A. Cyclic Polysiloxanes: 1. Preparation and Characterization of Poly(Phenylmethylsiloxane). *Polymer.* **1986**, *27*, 1633–1636.

(10) Zimm, B. H.; Stockmayer, W. H. The Dimensions of Chain Molecules Containing Branches and Rings. *J. Chem. Phys.* **1949**, *17*, 1301–1314.

(11) Zhu, X.; Zhou, N.; Zhang, Z.; Sun, B.; Yang, Y.; Zhu, J.; Zhu, X. Cyclic Polymers with Pendent Carbazole Units: Enhanced Fluorescence and Redox Behavior. *Angew. Chemie* **2011**, *123* , 6745–6748.

(12) Tezuka, Y. Topological Polymer Chemistry Designing Complex Macromolecular Graph Constructions. *Acc. Chem. Res.* **2017**, *50*, 2661–2672.

(13) Lu, Y.; Chen, W. Sub-Nanometre Sized Metal Clusters: From Synthetic Challenges to the Unique Property Discoveries. *Chem. Soc. Rev.* **2012**, *41*, 3594–3623.

(14) Chakraborty, I.; Pradeep, T. Atomically Precise Clusters of Noble Metals: Emerging Link between Atoms and Nanoparticles. *Chem. Rev.* **2017**, *117*, 8208–8271.

(15) Schmidt, B. V. K. J.; Fechler, N.; Falkenhagen, J.; Lutz, J. F. Controlled Folding of Synthetic Polymer Chains through the Formation of Positionable Covalent Bridges. *Nat. Chem.* **2011**, *3*, 234–238.

(16) Kyoda, K.; Yamamoto, T.; Tezuka, Y. Programmed Polymer Folding with Periodically

Positioned Tetrafunctional Telechelic Precursors by Cyclic Ammonium Salt Units as Nodal Points. *J. Am. Chem. Soc.* **2019**, *141*, 7526–7536.

(17) Geiser, D.; Höcker, H. Synthesis and Investigation of Macrocyclic Polystyrene. *Macromolecules* **1980**, *13*, 653–656.

(18) Oike, H.; Imaizumi, H.; Mouri, T.; Yoshioka, Y.; Uchibori, A.; Tezuka, Y. Designing Unusual Polymer Topologies by Electrostatic Self-Assembly and Covalent Fixation. *J. Am. Chem. Soc.* **2000**, *122*, 9592–9599.

(19) Laurent, B. A.; Grayson, S. M. An Efficient Route to Well-Defined Macrocyclic Polymers via "Click" Cyclization. *J. Am. Chem. Soc.* **2006**, *128*, 4238–4239.

(20) Sun, P.; Tang, Q.; Wang, Z.; Zhao, Y.; Zhang, K. Cyclic Polymers Based on UV-Induced Strain Promoted Azide-Alkyne Cycloaddition Reaction. *Polym. Chem.* **2015**, *6*, 4096–4101.

(21) Glassner, M.; Blinco, J. P.; Barner-Kowollik, C. Diels-Alder Reactions as an Efficient Route to High Purity Cyclic Polymers. *Macromol. Rapid Commun.* **2011**, *32*, 724–728.

(22) Josse, T.; Altintas, O.; Oehlenschlaeger, K. K.; Dubois, P.; Gerbaux, P.; Coulembier, O.; Kowollik, C. B. Ambient Temperature Catalyst-Free Light-Induced Preparation of Macrocyclic Aliphatic Polyesters. *Chem. Commun.* **2014**, *50*, 2024–2026.

(23) Tang, Q.; Wu, Y.; Sun, P.; Chen, Y.; Zhang, K. Powerful Ring-Closure Method for Preparing Varied Cyclic Polymers. *Macromolecules* **2014**, *47*, 3775–3781.

(24) Kricheldorf, H. R.; Lee, S. Polylactones. 35. Macrocyclic and Stereoselective Polymerization of *β*-D,L-Butyrolactone with Cyclic Dibutyltin Initiators. *Macromolecules* **1995**, 28, 6718–6725.

(25) Bielawski, C. W.; Benitez, D.; Grubbs, R. H. An "Endless" Route to Cyclic Polymers. *Science* **2002**, *297*, 2041–2044.

(26) Roland, C. D.; Li, H.; Abboud, K. A.; Wagener, K. B.; Veige, A. S. Cyclic Polymers from Alkynes. *Nat. Chem.* **2016**, *8*, 791–796.

(27) Miao, Z.; Gonsales, S. A.; Ehm, C.; Mentink-Vigier, F.; Bowers, C. R.; Sumerlin, B. S.; Veige, A. S. Cyclic Polyacetylene. *Nat. Chem.* **2021**.

(28) Wang, T.-W.; Huang, P.-R.; Chow, J. L.; Kaminsky, W.; Golder, M. R. A Cyclic Ruthenium Benzylidene Initiator Platform Enhances Reactivity for Ring-Expansion Metathesis Polymerization. *J. Am. Chem. Soc.* **2021**, *143*, 7314–7319.

(29) Narumi, A.; Hasegawa, S.; Yanagisawa, R.; Tomiyama, M.; Yamada, M.; Binder, W. H.; Kikuchi, M.; Kawaguchi, S. Ring Expansion-Controlled Radical Polymerization: Synthesis of Cyclic Polymers and Ring Component Quantification Based on SEC-MALS Analysis. *React. Funct. Polym.* **2016**, *104*, 1–8.

(30) Narumi, A.; Yamada, M.; Unno, Y.; Kumaki, J.; Binder, W. H.; Enomoto, K.; Kikuchi, M.; Kawaguchi, S. Evaluation of Ring Expansion-Controlled Radical Polymerization

System by AFM Observation. *ACS Macro Lett.* **2019**, *8*, 634–638.

(31) Kammiyada, H.; Konishi, A.; Ouchi, M.; Sawamoto, M. Ring-Expansion Living Cationic Polymerization via Reversible Activation of a Hemiacetal Ester Bond. *ACS Macro Lett.* **2013**, *2*, 531–534.

(32) Daito, Y.; Kojima, R.; Kusuyama, N.; Kohsaka, Y.; Ouchi, M. Magnesium Bromide ($MgBr_2$) as a Catalyst for Living Cationic Polymerization and Ring-Expansion Cationic Polymerization. *Polym. Chem.* **2021**, *12*, 702–710.

(33) Kusuyama, N.; Daito, Y.; Kubota, H.; Kametani, Y.; Ouchi, M. Construction of Ring-Based Architectures: Via Ring-Expansion Cationic Polymerization and Post-Polymerization Modification: Design of Cyclic Initiators from Divinyl Ether and Dicarboxylic Acid. *Polym. Chem.* **2021**, *12*, 2532–2541.

(34) Takahashi, A.; Yuzaki, R.; Ishida, Y.; Kameyama, A. Controlled Ring-Expansion Polymerization of Thiiranes Based on Cyclic Aromatic Thiourethane Initiator. *J. Polym. Sci. Part A Polym. Chem.* **2019**, *57*, 2442–2449.

(35) Kudo, H.; Naritomi, K.; Onishi, S.; Maekawa, H.; Mondarte, E. A. Q.; Suthiwanich, K.; Hayashi, T.; Hayashi, T. Living Ring-Expansion Polymerization of Thiirane with Cyclic Monocarbamothioates. *Macromolecules* **2020**, *53*, 4733–4740.

(36) Sun, H.; Kabb, C. P.; Sims, M. B.; Sumerlin, B. S. Architecture-Transformable Polymers: Reshaping the Future of Stimuli-Responsive Polymers. *Prog. Polym. Sci.* **2019**, *89*, 61–75.

(37) Sun, H.; Kabb, C. P.; Dai, Y.; Hill, M. R.; Ghiviriga, I.; Bapat, A. P.; Sumerlin, B. S. Macromolecular Metamorphosis via Stimulusinduced Transformations of Polymer Architecture. *Nat. Chem.* **2017**, *9*, 817–823.

(38) Yamamoto, T.; Yagyu, S.; Tezuka, Y. Light- and Heat-Triggered Reversible Linear-Cyclic Topological Conversion of Telechelic Polymers with Anthryl End Groups. *J. Am. Chem. Soc.* **2016**, *138*, 3904–3911.

(39) Sugai, N.; Asai, S.; Tezuka, Y.; Yamamoto, T. Photoinduced Topological Transformation of Cyclized Polylactides for Switching the Properties of Homocrystals and Stereocomplexes. *Polym. Chem.* **2015**, *6*, 3591–3600.

(40) Whittaker, M. R.; Goh, Y. K.; Gemici, H.; Legge, T. M.; Perrier, S.; Monteiro, M. J. Synthesis of Monocyclic and Linear Polystyrene Using the Reversible Coupling/Cleavage of Thiol/Disulfide Groups. *Macromolecules* **2006**, *39*, 9028–9034.

(41) Aoki, D.; Takata, T. Mechanically Linked Supramolecular Polymer Architectures Derived from Macromolecular [2]Rotaxanes: Synthesis and Topology Transformation. *Polymer* **2017**, *128*, 276–296.

(42) Ogawa, T.; Usuki, N.; Nakazono, K.; Koyama, Y.; Takata, T. Linear-Cyclic Polymer Structural Transformation and Its Reversible Control Using a Rational Rotaxane Strategy.

Chem. Commun. **2015**, *51*, 5606–5609.

(43) Ogawa, T.; Nakazono, K.; Aoki, D.; Uchida, S.; Takata, T. Effective Approach to Cyclic Polymer from Linear Polymer: Synthesis and Transformation of Macromolecular [1]Rotaxane. *ACS Macro Lett.* **2015**, *4*, 343–347.

(44) Aoki, D.; Aibara, G.; Uchida, S.; Takata, T. A Rational Entry to Cyclic Polymers via Selective Cyclization by Self-Assembly and Topology Transformation of Linear Polymers. *J. Am. Chem. Soc.* **2017**, *139*, 6791–6794.

(45) Antonietti, M.; Folsch, K. J. Synthesis and Characterization of "Eight-Shaped" Polystyrene. *Makromol. Chem., Rapid Commun.* **1988**, *9*, 423–430.

(46) Lonsdale, D. E.; Monteiro, M. J. Various Polystyrene Topologies Built from Tailored Cyclic Polystyrene via CuAAC Reactions. *Chem. Commun.* **2010**, *46*, 7945–7947.

(47) Isono, T.; Kamoshida, K.; Satoh, Y.; Takaoka, T.; Sato, S. I.; Satoh, T.; Kakuchi, T. Synthesis of Star- and Figure-Eight-Shaped Polyethers by *t*-Bu-P_4-Catalyzed Ring-Opening Polymerization of Butylene Oxide. *Macromolecules* **2013**, *46*, 3841–3849.

(48) Satoh, Y.; Matsuno, H.; Yamamoto, T.; Tajima, K.; Isono, T.; Satoh, T. Synthesis of Well-Defined Three- and Four-Armed Cage-Shaped Polymers via "Topological Conversion" from Trefoil- and Quatrefoil-Shaped Polymers. *Macromolecules* **2017**, *50*, 97–106.

(49) Zhang, L.; Wu, Y.; Li, S.; Zhang, Y.; Zhang, K. Scalable Bimolecular Ring-Closure Method for Cyclic Polymers. *Macromolecules* **2020**, *53*, 8621–8630.

(50) Zhang, Y.; Wu, Y.; Zhao, Y.; Zhang, L.; Zhang, K. Versatile Bimolecular Ring-Closure Method for Cage-Shaped Polymers. *Macromolecules* **2021**, *54*, 6901–6910. h

(51) Ko, Y. S.; Yamamoto, T.; Tezuka, Y. Click Construction of Spiro- and Bridged-Quatrefoil Polymer Topologies with Kyklo-Telechelics Having an Azide Group. *Macromol. Rapid Commun.* **2014**, *35*, 412–416.

(52) Tezuka, Y.; Tsuchitani, A.; Yoshioka, Y.; Oike, H. Synthesis of θ-Shaped Poly(THF) by Electrostatic Self-Assembly and Covalent Fixation with Three-Armed Star Telechelics Having Cyclic Ammonium Salt Groups. *Macromolecules* **2003**, *36*, 65–70.

(53) Kricheldorf, H. R.; Lee, S. R. Polylactones. 40. Nanopretzels by Macrocyclic Polymerization of Lactones via a Spirocyclic Tin Initiator Derived from Pentaerythritol. *Macromolecules* **1996**, *29*, 8689–8695.

(54) Zhang, Z.; Nie, X.; Wang, F.; Chen, G.; Huang, W. Q.; Xia, L.; Zhang, W. J.; Hao, Z. Y.; Hong, C. Y.; Wang, L. H.; You, Y. Z. Rhodanine-Based Knoevenagel Reaction and Ring-Opening Polymerization for Efficiently Constructing Multicyclic Polymers. *Nat. Commun.* **2020**, *11*, 1–10.

(55) Chen, J.; Li, H.; Zhang, H.; Liao, X.; Han, H.; Zhang, L.; Sun, R.; Xie, M. Blocking-Cyclization Technique for Precise Synthesis of Cyclic Polymers with Regulated Topology. *Nat. Commun.* **2018**, *9*, 1–9.

(56) Sugai, N.; Heguri, H.; Ohta, K.; Meng, Q.; Yamamoto, T.; Tezuka, Y. Effective Click Construction of Bridged-and Spiro-Multicyclic Polymer Topologies with Tailored Cyclic Prepolymers (Kyklo-Telechelics). *J. Am. Chem. Soc.* **2010**, *132*, 14790–14802.

(57) Gavrilov, M.; Amir, F.; Kulis, J.; Hossain, M. D.; Jia, Z.; Monteiro, M. J. Densely Packed Multicyclic Polymers. *ACS Macro Lett.* **2017**, *6*, 1036–1041.

(58) Jeong, J.; Kim, K.; Lee, R.; Lee, S.; Kim, H.; Jung, H.; Kadir, M. A.; Jang, Y.; Jeon, H. B.; Matyjaszewski, K.; Chang, T.; Paik, H. J. Preparation and Analysis of Bicyclic Polystyrene. *Macromolecules* **2014**, *47*, 3791–3796.

(59) Lee, T.; Oh, J.; Jeong, J.; Jung, H.; Huh, J.; Chang, T.; Paik, H. J. Figure-Eight-Shaped and Cage-Shaped Cyclic Polystyrenes. *Macromolecules* **2016**, *49*, 3672–3680.

(60) Tezuka, Y.; Fujiyama, K. Construction of Polymeric δ-Graph: A Doubly Fused Tricyclic Topology. *J. Am. Chem. Soc.* **2005**, *127*, 6266–6270.

(61) Shi, G. Y.; Pan, C. Y. Synthesis of Well-Defined Figure-of-Eight-Shaped Polymers by a Combination of ATRP and Click Chemistry. *Macromol. Rapid Commun.* **2008**, *29*, 1672–1678.

(62) Isono, T.; Satoh, Y.; Miyachi, K.; Chen, Y.; Sato, S. I.; Tajima, K.; Satoh, T.; Kakuchi, T. Synthesis of Linear, Cyclic, Figure-Eight-Shaped, and Tadpole-Shaped Amphiphilic Block Copolyethers via *t*-Bu-P_4-Catalyzed Ring-Opening Polymerization of Hydrophilic and Hydrophobic Glycidyl Ethers. *Macromolecules* **2014**, *47*, 2853–2863.

(63) Ree, B. J.; Satoh, Y.; Isono, T.; Satoh, T. Bicyclic Topology Transforms Self-Assembled Nanostructures in Block Copolymer Thin Films. *Nano Lett.* **2020**, *20*, 6520–6525.

(64) Ree, B. J.; Mato, Y.; Xiang, L.; Kim, J.; Isono, T.; Satoh, T. Topologically Controlled Phase Transitions and Nanoscale Film Self-Assemblies of Cage Poly(ε-Caprolactone) and Its Counterparts . *Polym. Chem.* **2021**, *12*, 744–758.

(65) Ree, B. J.; Satoh, Y.; Isono, T.; Satoh, T. Influence of Topological Confinement on Nanoscale Film Morphologies of Tricyclic Block Copolymers. *Macromolecules* **2021**, *54*, 4120–4127.

(66) Ree, B. J.; Satoh, Y.; Isono, T.; Satoh, T. Correlations of Nanoscale Film Morphologies and Topological Confinement of Three-Armed Cage Block Copolymers. *Polym. Chem.* **2021**, *12*, 3451–3460.

(67) Shi, G. Y.; Pan, C. Y. An Efficient Synthetic Route to Well-Defined Theta-Shaped Copolymers. *J. Polym. Sci. Part A Polym. Chem.* **2009**, *47*, 2620–2630.

(68) Gauthier-Jaques, M.; Theato, P. Synergy of Macrocycles and Macromolecular Topologies: An Efficient [3_4]Triazolophane-Based Synthesis of Cage-Shaped Polymers. *ACS Macro Lett.* **2020**, *9*, 700–705.

(69) Pipertzis, A.; Hossain, M. D.; Monteiro, M. J.; Floudas, G. Segmental Dynamics in Multicyclic Polystyrenes. *Macromolecules* **2018**, *51*, 1488–1497.

(70) Hossain, M. D.; Reid, J. C.; Lu, D.; Jia, Z.; Searles, D. J.; Monteiro, M. J. Influence of Constraints within a Cyclic Polymer on Solution Properties. *Biomacromolecules* **2018**, *19*, 616–625.

(71) Bielawski, C. W.; Grubbs, R. H. Living Ring-Opening Metathesis Polymerization. *Prog. Polym. Sci.* **2007**, *32*, 1–29.

(72) Love, J. A.; Morgan, J. P.; Trnka, T. M.; Grubbs, R. H. A Practical and Highly Active Ruthenium-Based Catalyst That Effects the Cross Metathesis of Acrylonitrile. *Angew. Chem. Int. Ed.* **2002**, *41*, 4035–4037.

(73) Choi, T. L.; Grubbs, R. H. Controlled Living Ring-Opening-Metathesis Polymerization by a Fast-Initiating Ruthenium Catalyst. *Angew. Chem. Int. Ed.* **2003**, *42*, 1743–1746.

(74) Hilf, S.; Kilbinger, A. F. M. Functional End Groups for Polymers Prepared Using Ring-Opening Metathesis Polymerization. *Nat. Chem.* **2009**, *1*, 537–546.

(75) Isono, T.; Sasamori, T.; Honda, K.; Mato, Y.; Yamamoto, T.; Tajima, K.; Satoh, T. Multicyclic Polymer Synthesis through Controlled/Living Cyclopolymerization of α,ω-Dinorbornenyl-Functionalized Macromonomers. *Macromolecules* **2018**, *51*, 3855–3864.

(76) Vilotijevic, I.; Jamison, T. F. Epoxide-Opening Cascades Promoted by Water. *Science* **2007**, *317*, 1189–1192.

Chapter 2

Systematic Synthesis of Spiro-multicyclic Polymers via Intramolecular Consecutive Cyclization

2.1 Introduction

Precise folding of a biopolymer chain is an essential process to attain sophisticated higher-ordered structures, such as DNA packing and three-dimensional (3D) protein structures, which is responsible for their outstanding functions in living systems.[1–3] Inspired by the folding process of biopolymers, significant efforts have been dedicated to the folding of synthetic polymers. The synthesis of topologically unique polymers from linear polymers can be regarded as mimicking biopolymer folding processes.[4–6] One successful example of this approach is the intramolecular crosslinking of linear polymers to afford single-chain nanoparticles (SCNPs) that feature a densely packed single-chain globule with a 3D nanostructure.[7,8] However, the resulting SCNP is a statistical mixture of undefined-shape chains since the intramolecularly crosslinked formations randomly occur along the main chain.

Another remarkable approach that has been demonstrated is the programmed folding of polymer chains into predetermined cyclic-type topologies.[6,9,10] The simplest case involves intramolecular coupling between the chain ends of a linear polymer to form a monocyclic polymer with unique properties attributed to the lack of chain ends.[9–12] In addition, multicyclic topological polymers that consist of multiple macromolecular rings, have also been intriguing synthetic targets due to their interesting 3D structures.[13,14] Among these multicyclic topological polymers, effective construction of *spiro*-multicyclic topologies remains the most challenging due to inherently complicated architectures consisting of multiple cyclic units tethered at a single junction point.

Although several synthetic strategies to prepare *spiro*-multicyclic polymers have been developed over the past decade, as mentioned in Section 1.3, only few comprehensive studies have been attempted to control the size and number of cyclic units due to lack of an effective synthetic platform. Thus, the structure–property relationships associated with this folded topology are not well-defined.[15,16]

In this chapter, to overcome the aforementioned challenges, the author reports the ruthenium-catalyzed intramolecular ring-opening metathesis oligomerization (ROMO) of *exo*-norbornenyl group attached to linear and star-shaped polymers as the intramolecular consecutive cyclization, leading to not only a monocyclic polymer but also *spiro*-type (8-, trefoil-, and quatrefoil-shaped) multicyclic polymers with controllable ring size and ring numbers. First, the simplest monocyclic polymer was synthesized via intramolecular ROMO of the telechelic linear PCL with norbornenyl group using G3 under a highly diluted condition. Then, a series of linear, three-armed star-, four-armed star-shaped PCLs with norbornenyl group at the chain center and each end was subjected to the intramolecular ROMO to produce the 8-, trefoil-, and quatrefoil-shaped PCLs, respectively (Figure 2.1). All the desired *spiro*-multicyclic topologies were formed in efficient manner while retaining a narrow *Đ*. The cyclization using different solvents under varied temperatures revealed the robustness of intramolecular ROMO. In addition, the universality of proposed cyclization strategy was confirmed by applying to diverse polymer species, such as poly(glycidyl ether) and polylactide. One-pot functionalization of the oligonorbornene backbone was also demonstrated to make the functional multicyclic polymers for the materials applications. Comprehensive study on the structure-property relationships of the folded PCLs revealed enhanced crystallization ability in the 8-shaped topology.

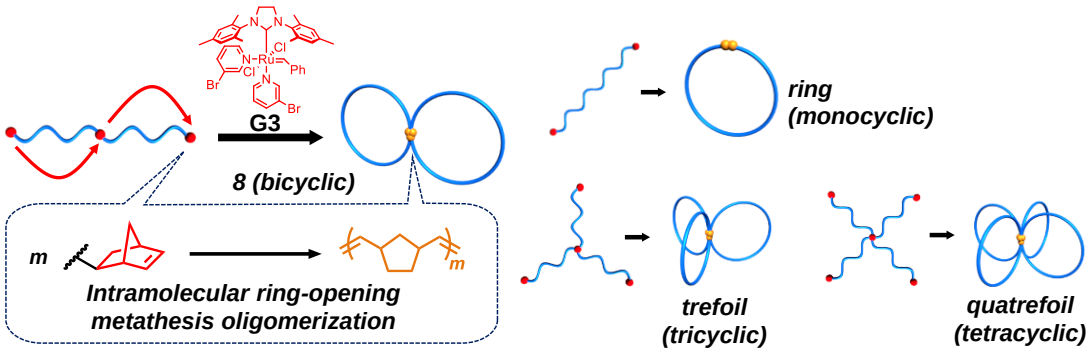

Figure 2.1. Schematic illustration of the synthetic strategy for *spiro*-multicyclic polymers through intramolecular consecutive ROMO mediated by G3.

2.2 Experimental Section

2.2.1 Materials

Grubbs' catalyst 3rd generation (G3),[17] 1,3-bis((1-methyl-1,1-bis(hydroxymethyl))-2-ethoxy)-2-((*p*-methoxybenzoxy)methyl)propane (**I3**),[18] and 4-(hydroxymethyl)styrene[19] were prepared according to previously reported method. Amberlyst® A21 (Organo Co., Ltd), *N*,*N*-dimethyl-4-aminopyridine (DMAP; Tokyo Chemical Industry Co., Ltd. (TCI), >99.0%), 1-ethyl-3-(3-(dimethylamino)-propyl)carbodiimide hydrochloride (EDC; TCI, >98.0%), ethyl vinyl ether (TCI, >98.0%), 2,3-dichloro-5,6-dicyano-1,4-benzoquinone (DDQ; TCI, >97.0%), *p*-methoxybenzyl chloride (PMBCl; TCI, >98.0%), (±)-*exo*-5-norbornenecarboxylic acid (*exo*-NB-COOH; Aldrich, 97%), *cis*-2-butene-1,4-diol (TCI, >94.0%), *t*-Bu-P_4 (in hexane as ~0.8 mol L^{-1} solution; Sigma-Aldrich Chemicals), sodium iodide (NaI; Wako Pure Chemical Industry Co. Ltd., >99.5%), and 2, 5-dihydroxybenzoic acid (DHB; Sigma-Aldrich, >98.0%) were used as received. ε-Caprolactone (ε-CL; TCI, >99%), 2-ethylhexyl glycidyl ether (TCI, >98.0%), 1,8-diazabicyclo[5.4.0]-7-undecene (DBU; TCI, >98.0%) were purified by distillation over CaH_2 under reduced pressure and stored in the glovebox. L-Lactide (TCI, >98.0%) was purified twice by recrystallization using dry toluene and stored in the glovebox. Diphenyl phosphate (DPP; TCI, >99.0%) and synthesized initiators were purified by azeotropic distillation with dry toluene and stored in the glovebox.

2.2.2 Instruments

The polymerization experiments were carried out in an MBRAUN stainless steel glovebox equipped with a gas purification system (molecular sieves and copper catalyst) in a dry argon atmosphere (H_2O, O_2<0.1 ppm). The moisture and oxygen contents in the glovebox were monitored by an MB-MO-SE 1 moisture sensor and an MB-OX-SE 1 oxygen sensor, respectively. Dry toluene (>99.5%; water content, <0.001%, Kanto Chemical Co., Inc.) used

for the polymerization was purified by passing through an MBRAUN solvent purification system (MB SPS COMPACT) consisting of a column of activated alumina and a column with activated copper catalyst. The ^{1}H (400 MHz) and ^{13}C nuclear magnetic resonance (NMR) (100 MHz) spectra were recorded using a JEOL JNM-ECS400 instrument at room temperature in $CDCl_3$ or methanol-d_4. The size exclusion chromatography (SEC) was performed at 40 °C in THF (flow rate, 1.0 mL min^{-1}) using a Shodex GPC-101 gel permeation chromatography system (Shodex DU-2130 dual pump, Shodex RI-71-S reflective index detector, and Shodex ERC-3125SN degasser) equipped with a Shodex KF-G guard column (4.6 mm × 10 mm; particle size, 8 μm) and two Shodex KF-804L columns (linear, 8 mm × 300 mm) or a Jasco high-performance liquid chromatography system (PU-980 Intelligent HPLC Pump, CO-2065 Plus Intelligent Column Oven, RI-2031 Plus Intelligent RI Detector, and DG-2080-53 Degasser) equipped with a Shodex KF-G guard column (4.6 mm × 10 mm; particle size, 8 μm) and two Shodex KF-804L columns (linear; particle size 7 μm; 8.0 mm × 300 mm; exclusion limit, 4×10^4). The number-average molecular weight ($M_{n,SEC}$) and the dispersity ($Đ$) of the polymers were calculated on the basis of polystyrene calibrations. The absolute weight-averaged molecular weights ($M_{w,MALS}$) of the samples were determined by SEC with multiangle light scattering detection (SEC-MALS-Visco) in THF (flow rate, 1.0 mL min^{-1}) at 40 °C using an Agilent 1100 series instrument equipped with a DG 1100 degasser, a Shodex KF-G guard column (4.6 mm × 10 mm; particle size, 8 μm), a Shodex KF-800D solvent-peak separation column (linear, 8.0 mm × 100 mm; particle size, 10μm), two Shodex KF-805L columns (linear, 8.0 mm × 300 mm; exclusion limit, 4.0×10^6; particle size, 10 μm), a DAWN 8+ multiangle laser light scattering detector (Wyatt Technology), an Optilab rEX refractive index detector (Wyatt Technology), and a Viscostar viscosity detector (Wyatt Technology). The preparative SEC for Grubbs' catalyst removal was performed at r.t. in $CHCl_3$ (flow rate, 3.5 mL min^{-1}) using LC-9201 liquid chromatography system (Japan Analytical Industry Co. Ltd.) equipped

with a BG-12 degasser, a PI-50 pump, a RI-50S RI detector, a JAIGEL-H-P guard column (8 mm × 40 mm; Japan Analytical Industry Co. Ltd.), and a Shodex K-2004 column (linear, 20.0 mm × 300 mm; exclusion limit, 1.4×10^4; particle size, 7 μm). The matrix-assisted laser desorption ionization time-of-flight mass spectrometry (MALDI-TOF MS) of the obtained polymers was performed using an Applied Biosystems Voyager-DE STR-H equipped with a 337 nm nitrogen laser (3 ns pulse width). Two hundred shots were accumulated for the spectra at a 20 kV acceleration voltage in the reflector mode and calibrated using PSt as the internal standard. Samples for the MALDI-TOF MS were prepared as follows: (i) the THF solution of polymer sample (4.0 mg mL^{-1}) and the THF solution of matrix (DHB; 60 mg mL^{-1}) were mixed at a volume ratio of 1:1. (ii) Then, the sample plate was spotted by the THF solution of cationic agent (NaI; 1.0 mg mL^{-1}, 1.0 μL), followed by the mixed solution (1.0 μL). The thermal properties of the polymer samples were measured from −50 to 100 °C during the second heating by a Bruker AXS DSC 3100 differential scanning calorimeter under a nitrogen atmosphere with the heating rate of 10 °C min^{-1} and cooling rate 20 °C min^{-1}. The melting temperature (T_m) was determined as peak maxima of transition during 2nd heating run. Thermogravimetric analysis (TGA) was performed from 20 to 500 °C with a heating rate of 10 C min^{-1} by a Bruker AXS DSC 3100 under a nitrogen atmosphere. Synchrotron small-angle X-ray scattering (SAXS) and wide-angle X-ray diffraction (WAXD) measurements of the obtained polymers were performed with an X-ray beam of 1.5Å at the BL-6A in the Photon Factory (Tsukuba, Japan). The 2D SAXS and WAXD profiles were obtained with a Pilatus 1M and 100K detectors, respectively, which were circularly averaged to produce the 1D plots of log I (intensity) and q (scattering vector). The q value was calibrated using a silver behenate. The powder sample of the polymer was put into a Hilgenberg lindemann glass capillary (1.5 mm × 80 mm), which was annealed at 100 °C for 1 h in a pre-heated oven to erase a thermal history and then cooled to room

temperature. The crystallinity (X_{WAXD}) was determined by the peak deconvolution of WAXD profile.

2.2.3 Synthetic details

General synthetic procedure for the polymer precursors

A linear PCL with a reactive *exo*-norbornenyl grup at each chain end (**Pre$_{ring}$-a**) was prepared in two steps consisting of polymerization of ε-CL and subsequent end-functionalization with *exo*-norbornene carboxylic acid (*exo*-NB-COOH). The diphenyl phosphate (DPP)-catalyzed ring-opening polymerization of ε-CL was carried out using 2,2-diethyl-1,3-propanediol as an initiator with the [ε-CL]$_0$/[I]$_0$/[DPP] ratio of 50/1/0.05 to afford linear PCL (**HO-PCL-OH-a**; $M_{n,NMR}$ = 4,890, $Đ$ = 1.05). Subsequently, **HO-PCL-OH-a** was treated with *exo*-NB-COOH in the presence of EDC and DMAP ([**HO-PCL-OH-a**]$_0$/[*exo*-NB-COOH]$_0$/[DMAP]/[EDC] = 1/4/6/6) to generate **Pre$_{ring}$-a**. In the ^{1}H NMR spectrum of **Pre$_{ring}$-a**, a proton signal attributed to the methylene adjacent to each chain end (*i*: 3.65 ppm) were observed. After the subsequent condensation reaction with *exo*-NB-COOH, the ^{1}H NMR signals due to the norbornenyl groups (*x, y*: 6.13 ppm; *z*: 3.04 ppm; *w*: 2.93 ppm; *v*: 2.22 ppm; *u*: 1.91 ppm) appeared and suggested quantitative introduction of the norbornenyl group to the chain ends. In addition, the SEC traces of **Pre$_{ring}$-a** retained the monomodal peak with $Đ$ = 1.05. These results supported the successful synthesis of **Pre$_{ring}$-a** ($M_{n,NMR}$ = 5,110, $M_{n,SEC}$ = 9,790, $Đ$ = 1.05).

Synthesis of liner PCL (HO-PCL-OH)

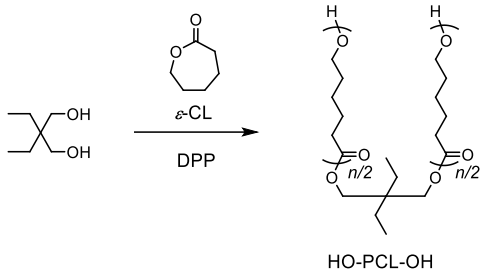

A typical procedure for the polymerization is as follows (method A): Under Ar atmosphere, ε-CL (1.50 g, 13.1 mmol), 2,2-diethyl-1,3-propanediol (21.7 mg, 164 μmol), and DPP (33.7 mg, 164 μmol) were placed in a reaction vessel. The reaction mixture was stirred at 80 °C for 2.5 h. The polymerization was quenched by the addition of Amberlyst® A21. The polymer crude was purified by the reprecipitation from CH_2Cl_2 into cold methanol/*n*-hexane (v/v = 10/1) to give **HO-PCL-OH-a** as a white solid. Yield: 65.3%.

$M_{n,NMR}$ = 4,890 g mol^{-1} ($CDCl_3$), $M_{n,SEC}$ = 9,600 g mol^{-1} (THF), $Đ$ = 1.05.

^{1}H NMR (400 MHz, $CDCl_3$): δ (ppm) 4.27-3.96 (m, $(CH_3CH_2)_2CCH_2$, -OCO$(CH_2)_4CH_2$–), 3.91 (s, $(CH_3CH_2)_2C$–), 3.65 (q, J = 6.1, –CH_2OH), 2.52-2.16 (m, –OCO$CH_2(CH_2)_4$–), 1.83-1.53 (m, –OCO$CH_2CH_2(CH_2)_3$–, –OCO$(CH_2)_3CH_2CH_2$–), 1.48-1.21 (m, CH_3CH_2–, –OCO$(CH_2)_2CH_2(CH_2)_2$–), 0.82 (t, J = 7.5, CH_3CH_2–).

Synthesis of *ω*-norbornenyl end-functionalized linear PCL (Pre$_{ring}$)

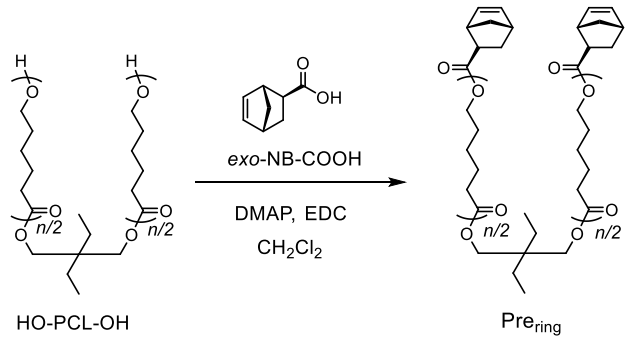

A typical procedure for the condensation reaction is as follows (method B): In a Schlenk flask, **HO-PCL-OH** ($M_{n,NMR}$ = 4,890 g mol^{-1}, 1.10 g, 224 μmol), *exo*-NB-COOH (78.7

mg, 570 µmol), DMAP (104 mg, 855 µmol), and EDC (221 mg, 855 µmol) were dissolved in CH_2Cl_2 (10 mL) and the mixture was stirred at r.t. for 24 h. The polymer crude was purified by reprecipitation from CH_2Cl_2 into cold methanol to give **Pre$_{ring}$-a** as a white solid. Yield: 62.2%. $M_{n,NMR}$ = 5,110 g mol^{-1} ($CDCl_3$), $M_{n,SEC}$ = 9,790 g mol^{-1} (THF), $Đ$ = 1.05.

^{1}H NMR (400 MHz, $CDCl_3$): δ (ppm) 6.13 (m, –C*H*=C*H*– in norbornene ring), 4.28-3.98 (m, $CH_3CH_2CCH_2$-, –OCO$(CH_2)_4CH_2$–), 3.92 (s, $(CH_3CH_2)_2C$–), 3.04 (s, –C*H*-CH-CH_2O– in norbornene ring), 2.93 (s, –C*H*–CH_2–CH–CH_2O– in norbornene ring), 2.51-2.16 (m, –OCO$CH_2(CH_2)_4$–), 1.91 (m, *exo*-C*H*– of –CH–CH_2–CH–CH_2O– in norbornene ring), 1.77-1.54 (m, –OCO$CH_2CH_2(CH_2)_3$–, –OCO$(CH_2)_3CH_2CH_2$–), 1.49-1.24 (m, CH_3CH_2–, –OCO$(CH_2)_2CH_2(CH_2)_2$–, bridge head –CH_2– in norbornene ring, *endo*-C*H*- of –CH–CH_2–CH–CH_2O–), 0.92-0.79 (t, J =7.5, CH_3CH_2–).

Synthesis of cyclic PCL (ring)

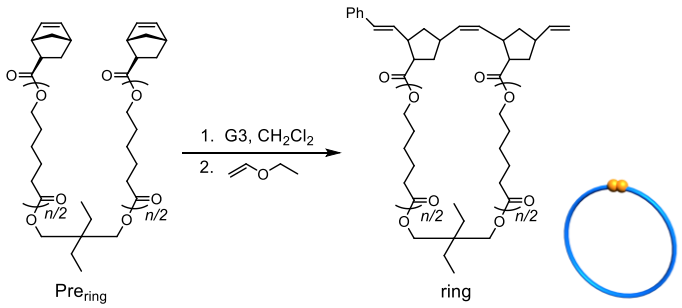

A typical procedure for the intramolecular ring-opening metathesis oligomerization is as follows (method C): G3 (31.2 mg, 35.2 µmol) was added to a three-necked flask and dissolved in deggased-CH_2Cl_2 (230 mL). Then, a solution of **Pre$_{ring}$-a** ($M_{n,NMR}$ = 5,110 g mol^{-1}, 30.0 mg, 5.87 µmol, 170 µM in CH_2Cl_2) was added dropwise to the G3 solution through the additional funnel over 30 min. After 10 min, the reaction was quenched by the addition of ethyl vinyl ether (300 µL). The metal residue in the crude product was removed by preparative SEC (solvent, CH_3Cl) to give **ring-a** as a pale brown solid. Yield: 92.3%.

$M_{n,SEC}$ = 7,520 g mol^{-1} (THF), $Đ$ = 1.09.

^{1}H NMR (400 MHz, $CDCl_3$): δ (ppm) 7.70, 7.53 (Aromatic), 6.59-4.82 (br, alkenyl of poly(norbornene) backbone), 3.91 (s, $(CH_3CH_2)_2C$–), 2.39-2.22 (m, –$OCOCH_2(CH_2)_4$–), 3.49-1.12 (br, cyclopentane ring of poly(norbornene) backbone), 1.77-1.58 (m, -$OCOCH_2CH_2(CH_2)_3$-, -$OCO(CH_2)_3CH_2CH_2$-), 1.47-1.29 (m, CH_3CH_2–, –$OCO(CH_2)_2CH_2(CH_2)_2$–), 0.83 (t, J = 7.5, CH_3CH_2–).

Synthesis of 2-ethyl-2-(((4-methoxybenzyl)oxy)methyl)propane-1,3-diol (I1)

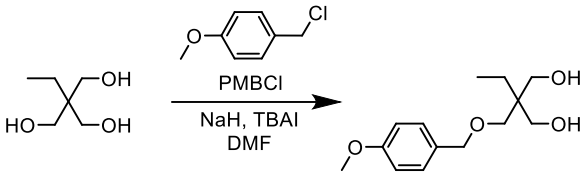

I1

A typical procedure for the protection with *p*-methoxybenzyl chloride is as follows (method D): Under an argon atmosphere, trimethylolpropane (34.8 g, 259 mmol) was added to a solution of NaH (3.84 g, 96.0 mmol; 60% in mineral oil) and tetrabutylammonium iodide (TBAI; 2.59 g, 7.01 mmol) in DMF (400 mL), then the solution was stirred at 70 °C for 30 min. A solution of *p*-methoxybenzyl chloride (PMBCl; 10.0 g, 63.9 mmol) in DMF (100 mL) was added dropwise to the reacting mixture, and the resulting mixture was stirred at 70 °C for 24 h under an argon atmosphere. After removing the solvent by evaporation, the obtained residue was dissolved in AcOEt and washed with brine. The organic layer was dried over anhydrous Na_2SO_4, filtrated, and then concentrated. The residue was purified by silica gel column chromatography (AcOEt/*n*-hexane = 8/2, R_f = 0.30) to give **I1** as a white solid. (11.1 g). Yield: 68.3%

^{1}H NMR (400 MHz, $CDCl_3$): δ (ppm) 7.23 (d, 2H, J = 8.70, aromatic), 6.87 (d, 2H, J = 8.70, aromatic), 4.42 (s, 2H, -PhCH_2O-), 3.80 (s, 3H, -CCH_2CH_3), 3.68 (d, 2H, J = 11.0, -OCH_2C-),

3.57 (d, 2H, J = 11.0, -CCH_2OH), 3.43 (s, 2H, -CCH_2CH$_3$), 2.90 (s, 2H, -OH), 0.80 (t, 3H, J = 7.50, -OCH$_3$). HRMS (ESI, in methanol solution): *m/z* calcd for $C_{14}H_{22}O_4Na$: 277.1410 $[M+Na]^+$; found: 277.1410.

Synthesis of PMBO-(PCL-OH)$_2$

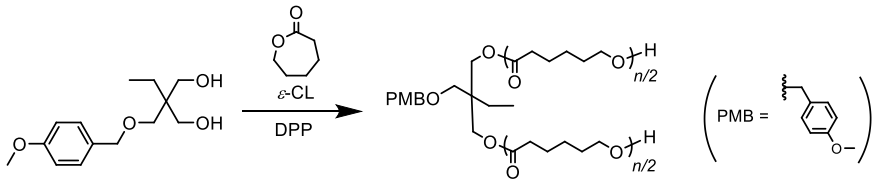

I1 PMBO-(PCL-OH)$_2$

Method A was used for the polymerization of ε-CL (3.0 g, 26.3 mmol) with **I1** (134 mg, 525 μmol), and DPP (132 mg, 525 μmol) in toluene (20.2 mL) at r.t. for 3 h to give **PMBO-(PCL-OH)$_2$** as white solid (2.49 g) Yield: 89.3%

$M_{n,NMR}$ = 5,670 g mol^{-1}, $M_{n,SEC}$ = 9,640 g mol^{-1} (THF), $Đ$ = 1.06

^{1}H NMR (400 MHz, $CDCl_3$): δ (ppm) 7.21 (d, J = 8.70, aromatic), 6.86 (d, J = 8.70, aromatic), 4.39 (s, -PhCH_2O-), 4.15-3.93 (m, -OCO(CH$_2$)$_4$CH_2-), 3.80 (s, -CCH$_2$CH_3), 3.69-3.61 (m, -CH_2OH), 3.30 (d, J = 8.20, -OCH_2C-), 2.43-2.22 (m, -OCOCH_2(CH$_2$)$_4$-), 1.86-1.52 (m, -OCOCH$_2$CH_2(CH$_2$)$_3$-, -OCO(CH$_2$)$_3$CH_2CH$_2$-), 1.50-1.24 (m, -OCO(CH$_2$)$_2$CH_2(CH$_2$)$_2$-, -CH_2CH$_3$), 0.84 (t, J = 7.50 Hz, -CH$_2$CH_3).

Synthesis of HO-(PCL-OH)$_2$

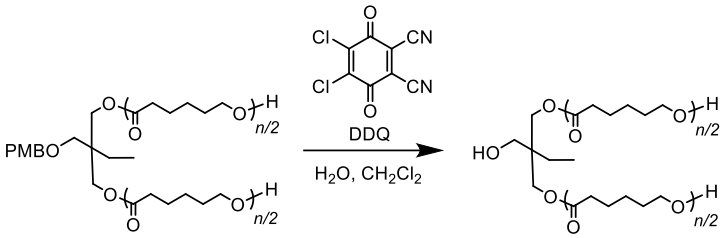

PMBO-(PCL-OH)$_2$ HO-(PCL-OH)$_2$

A typical procedure for the deprotection reaction is as follows (Method E): 1,2-Dichloro-4,5-dicyano-*p*-benzoquinone (DDQ; 161 mg, 708 mmol) was added to the solution of **PMBO-(PCL-OH)$_2$** ($M_{n,NMR}$ = 5,670 g mol^{-1}, 2.0 g, 351 μmol) in CH_2Cl_2/water (30.0 mL, v/v = 2/1), and the reaction mixture was stirred at r.t. for 24 h. The polymer crude was purified by reprecipitation twice from CH_2Cl_2 into cold methanol to give **HO-(PCL-OH)$_2$** as a white solid (1.04 mg). Yield: 52.0%

$M_{n,NMR}$ = 5,650 g mol^{-1}, $M_{n,SEC}$ = 9,690 g mol^{-1} (THF), $Đ$ = 1.06

^{1}H NMR (400 MHz, $CDCl_3$): δ (ppm) 4.31-3.83 (m, -OCO$(CH_2)_4$CH_2-), 3.66 (t, J = 6.40, -$(CH_2)_4$CH_2OH), 3.42 (d, J = 6.40, -CCH_2OH), 2.54-2.11 (m, -OCOC$H_2(CH_2)_4$-), 1.90-1.53 (m, -OCOCH$_2$C$H_2(CH_2)_3$-, -OCO$(CH_2)_3$CH_2CH$_2$-), 1.52-1.32 (m, -OCO$(CH_2)_2$C$H_2(CH_2)_2$-, -CCH_2CH$_3$), 0.90 (t, J = 7.50, -CCH$_2$CH_3).

2.6 Synthesis of Pre$_{fig8}$-a

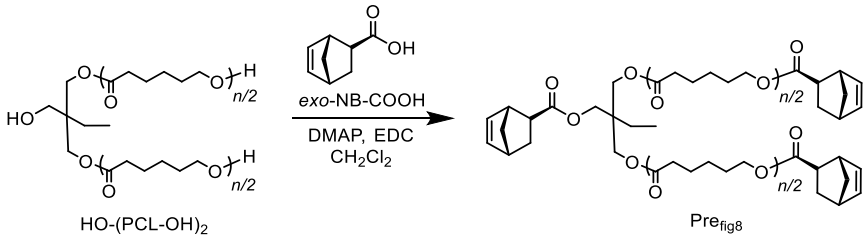

Method D was used for the condensation reaction of **HO-(PCL-OH)$_2$** ($M_{n,NMR}$ = 5,700 g mol^{-1}, 1.0 g, 175 μmol) with *exo*-NB-COOH (147 mg, 1.06 mmol), DMAP (195 mg, 159 mmol), and EDC (305 mg, 1.59 mmol) in CH_2Cl_2 (10 mL) to give **Pre$_{fig8}$-a** as a white solid (533 mg). Yield: 55.3%

$M_{n,NMR}$ = 6,200 g mol^{-1}, $M_{n,SEC}$ = 9,970 g mol^{-1} (THF), $Đ$ = 1.06

^{1}H NMR (400 MHz, $CDCl_3$): δ (ppm) 6.19-6.02 (m, -CH=CH- in norbornene ring), 4.32-3.77 (m, -OCO$(CH_2)_4$CH_2-), 3.08-2.95 (m, -CH-CH-CH$_2$O- in norbornene ring), 2.90 (s, -CH-CH-CH$_2$O- in norbornene ring), 2.53-2.06 (m, -OCOC$H_2(CH_2)_4$-), 2.00-1.83 (m, -

$OCO(CH_2)_2CH_2(CH_2)_2$-, bridge head -CH_2- in norbornene ring, *endo*-C*H*- of -CH-CH_2-CH-CH_2O-), 1.80-1.51 (m, -$OCOCH_2CH_2(CH_2)_3$-, -$OCO(CH_2)_3CH_2CH_2$-), 1.45-1.21 (-$OCO(CH_2)_2CH_2(CH_2)_2$-, -CCH_2CH_3), 1.01-0.79 (t, J = 7.50, -CCH_2CH_3)

Synthesis of 8-shaped PCL-a

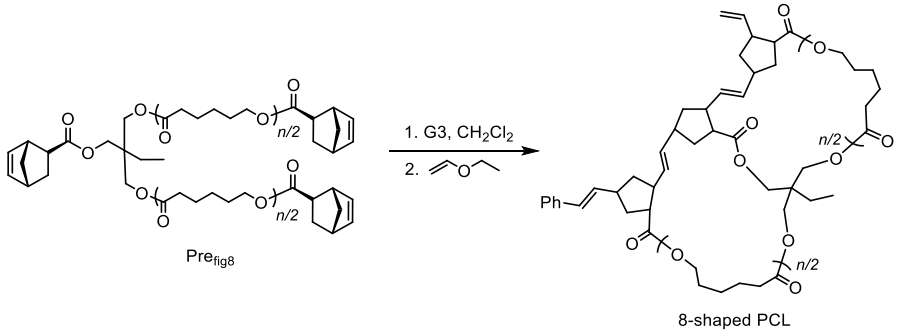

Method E was used for the ROMO of **Pre$_{fig8}$-a** ($M_{n,NMR}$ = 6,200 g mol^{-1}, 30.0 mg, 4.84 μmol, 170 μM in CH_2Cl_2) with G3 (25.7 mg, 29.0 μmol) in CH_2Cl_2 (240 mL) to give **8-shaped PCL-a** as a pale brown solid (27.8 mg). Yield: 91.0%

$M_{n,SEC}$ = 7,300 g mol^{-1} (THF), $Đ$ = 1.08

^{1}H NMR (400 MHz, $CDCl_3$): δ (ppm) 6.62-1.88 (br, alkenyl of poly(norbornene) backbone), 4.37-3.81 (m, -$OCO(CH_2)_4CH_2$-), 2.38-2.22 (m, -$OCOCH_2(CH_2)_4$-), 1.73-1.57 (m, -$OCOCH_2CH_2(CH_2)_3$-, -$OCO(CH_2)_3CH_2CH_2$-), 1.44-1.22 (m, -$OCO(CH_2)_2CH_2(CH_2)_2$-, -CCH_2CH_3), 0.90-0.82 (m, -CCH_2CH_3).

Synthesis of 2-(hydroxymethyl)-2-(((4-methoxybenzyl)oxy)methyl)propane-1,3-diol (I2)

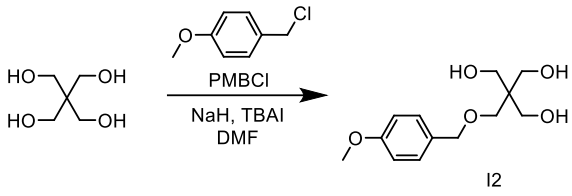

Method D was used for the protection of pentaerythritol (34.8 g, 255 mmol) with PMBCl (10.0 g, 63.9 mmol), NaH (3.84 g, 96 mmol; 60% in mineral oil), and TBAI (2.59 g, 7.01 mmol) in DMF (500 mL) to give **I2** as a white solid (11.1 g). Yield: 67.9%

^{1}H NMR (400 MHz, $CDCl_3$): δ (ppm) 7.25-7.15 (m, aromatic), 6.90-6.83 (m, aromatic), 4.41 (d, J = 12.8, -PhCH_2O-), 4.29-3.85 (m, -OCO$(CH_2)_4$CH_2-), 3.80 (d, J = 1.80, -OCH_3), 3.65 (t, J = 6.60, -CH_2OH), 3.42 (d, J = 18.7, -PhCH_2OCH_2-), 2.40-2.22 (m, -OCOC$H_2(CH_2)_4$-), 1.79-1.52 (m, -OCOCH_2C$H_2(CH_2)_3$-, -OCO$(CH_2)_3$CH_2CH_2-), 1.47-1.28 (-OCO$(CH_2)_2$C$H_2(CH_2)_2$-).

Synthesis of PMBO-(PCL-OH)$_3$

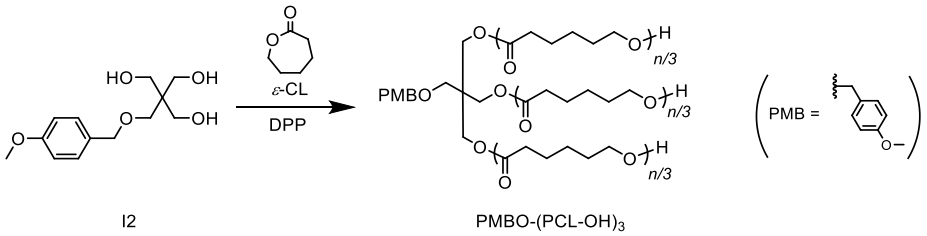

Method A was used for the polymerization of ε-CL (3.0 g, 26.3 mmol) with **I2** (135 mg, 525 μmol), and DPP (132 mg, 525 μmol) in toluene (20.2 mL) at r.t. for 2.7 h to give **PMBO-(PCL-OH)$_3$** as white solid (2.65 g). Yield: 88.3%

$M_{n,NMR}$ = 4,820 g mol^{-1}, $M_{n,SEC}$ = 8,190 g mol^{-1} (THF), $Đ$ = 1.08

^{1}H NMR (400 MHz, $CDCl_3$): δ (ppm) 7.25-7.15 (m, aromatic), 6.90-6.83 (m, aromatic), 4.41 (d, J = 12.8, -PhCH_2O-), 4.29-3.85 (m, -OCO$(CH_2)_4$CH_2-), 3.80 (d, J = 1.80, -OCH_3), 3.65 (t, J = 6.60, -CH_2OH), 3.42 (d, J = 18.7, -PhCH_2OCH_2-), 2.40-2.22 (m, -OCOC$H_2(CH_2)_4$-), 1.79-1.52 (m, -OCOCH_2C$H_2(CH_2)_3$-, -OCO$(CH_2)_3$CH_2CH_2-), 1.47-1.28 (m, -OCO$(CH_2)_2$C$H_2(CH_2)_2$-).

Synthesis of HO-(PCL-OH)$_3$

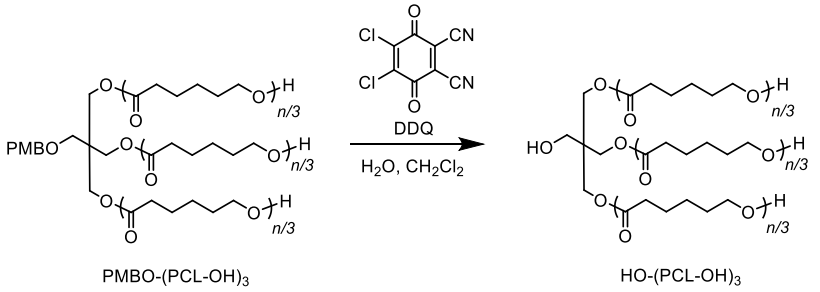

PMBO-(PCL-OH)$_3$ HO-(PCL-OH)$_3$

Method E was used for the deprotection reaction of **PMBO-(PCL-OH)$_3$** ($M_{n,NMR}$ = 4,820 g mol^{-1}, 2.0 g, 415 μmol) with DDQ (188 mg, 830 μmol) in H_2O/CH_2Cl_2 (1.50 mL, v/v = 2/1) to give **HO-(PCL-OH)$_3$** as white solid (1.17 g). Yield: 60.0%

$M_{n,NMR}$ = 5,350 g mol^{-1}, $M_{n,SEC}$ = 8,020 g mol^{-1} (THF), $Đ$ = 1.08

^{1}H NMR (400 MHz, $CDCl_3$): δ (ppm) 4.31-3.78 (m, -OCO(CH$_2$)$_4$C*H*$_2$-), 3.65 (t, J = 6.40, -OCO(CH$_2$)$_3$C*H*$_2$OH), 3.61-3.44 (m, -CC*H*$_2$OH,) 2.56-2.09 (m, -OCOC*H*$_2$(CH$_2$)$_4$-), 1.95-1.52 (m, -OCOCH$_2$C*H*$_2$(CH$_2$)$_3$-, -OCO(CH$_2$)$_3$C*H*$_2$CH$_2$-), 1.47-1.27 (m, -OCO(CH$_2$)$_2$C*H*$_2$(CH$_2$)$_2$-).

Synthesis of Pre$_{tre}$-a

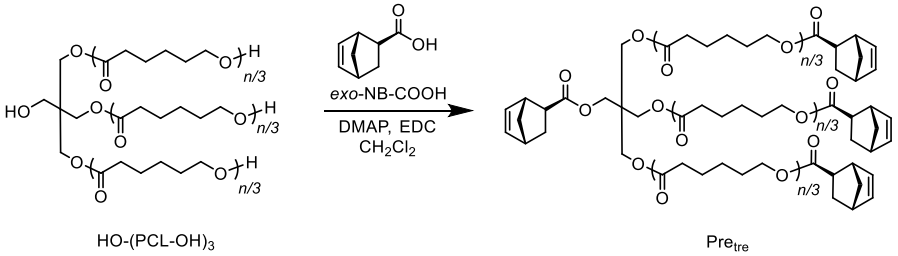

HO-(PCL-OH)$_3$ Pre$_{tre}$

Method B was used for the condensation reaction **of HO-(PCL-OH)$_3$** ($M_{n,NMR}$ = 5,350 g mol^{-1}, 1.0 g, 185 μmol) with *exo*-NB-COOH (204 mg, 1.48 mmol), DMAP (274 mg, 2.24 mmol), and EDC (430 mg, 2.24 mmol) in CH_2Cl_2 (10 mL) to give **Pre$_{tre}$-a** as a white solid (576 mg). Yield: 60.1%

$M_{n,NMR}$ = 6,160 g mol^{-1}, $M_{n,SEC}$ = 8,650 g mol^{-1} (THF), $Đ$ = 1.07

^{1}H NMR (400 MHz, $CDCl_3$): δ (ppm) 6.19-6.07 (m, -C*H*=C*H*- in norbornene ring), 4.18-4.00 (m, -OCO$(CH_2)_4$CH_2-), 3.05-2.98 (m, -C*H*-CH-CH_2O- in norbornene ring), 2.95-2.90 (s, -C*H*-CH-CH_2O- in norbornene ring), 2.43-2.25 (m, -OCOC$H_2(CH_2)_4$-), 1.78-1.56 (m, -OCOCH_2C$H_2(CH_2)_3$-, -OCO$(CH_2)_3$CH_2CH_2-), 1.48-1.31 (m, -OCO$(CH_2)_2$C$H_2(CH_2)_2$-).

Synthesis of trefoil-shaped PCL-a

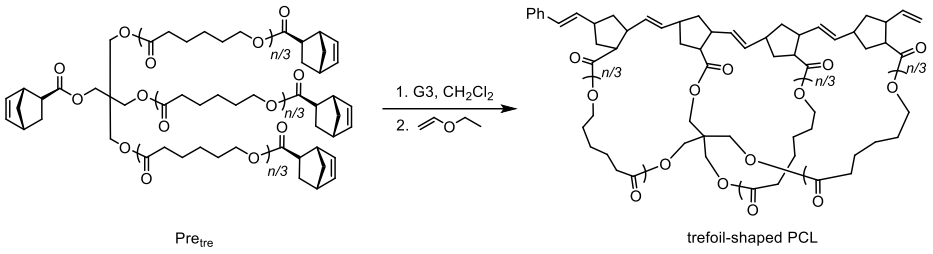

Method C was used for the ROMO of **Pre$_{tre}$-a** ($M_{n,NMR}$ = 6,160 g mol^{-1}, 30.0 mg, 4.92 μmol, 170 μM in CH_2Cl_2) with G3 (25.9 mg, 29.2 μmol) in CH_2Cl_2 (250 mL) to give **trefoil-shaped PCL-a** as a pale brown solid (27.7 mg). Yield: 90.0%

$M_{n,SEC}$ = 6,180 g mol^{-1} (THF), $Đ$ = 1.09

^{1}H NMR (400 MHz, $CDCl_3$): δ (ppm) 6.52-1.73 (br, alkenyl of poly(norbornene) backbone), 4.32-3.80 (m, -OCO$(CH_2)_4$CH_2-), 2.42-2.14 (m, -OCOC$H_2(CH_2)_4$-), 1.79-1.49 (m, -OCOCH_2C$H_2(CH_2)_3$-, -OCO$(CH_2)_3$CH_2CH_2-), 1.45-1.07 (m, -OCO$(CH_2)_2$C$H_2(CH_2)_2$-).

Synthesis of PMBO-(PCL-OH)$_4$

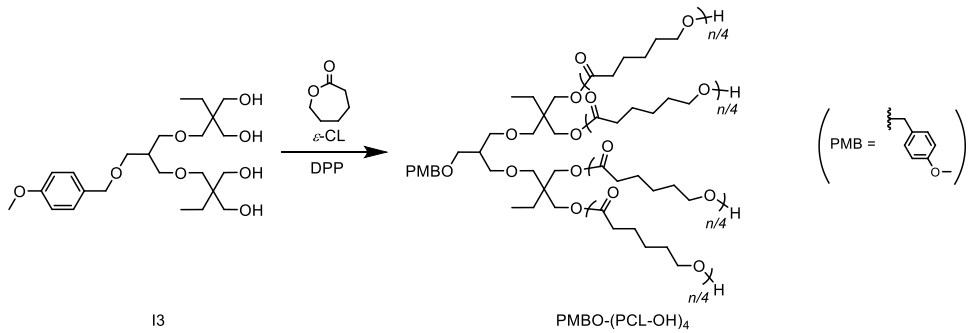

Method A was used for the polymerization of ε-CL (3.0 g, 26.3 mmol) with **I3** (241 mg, 525 μmol), and DPP (131 mg, 525 μmol) in toluene (20.2 mL) at r.t. for 3 h to give **PMBO-(PCL-OH)$_3$** as white solid (1.66 g). Yield: 66.3%

$M_{n,NMR}$ = 5,490 g mol^{-1}, $M_{n,SEC}$ = 9,240 g mol^{-1} (THF), $Đ$ = 1.04

^{1}H NMR (400 MHz, $CDCl_3$): δ (ppm) 7.23 (d, J = 8.70, aromatic), 6.87 (d, J = 8.20, aromatic), 4.39 (s, -PhCH_2O-), 4.13-4.00 (m, -OCO(CH$_2$)$_4$CH_2-), 3.97 (s, -CH_2OCO-), 3.80 (s, -OCH_3), 3.65 (t, J = 6.40, -CH_2OH), 3.44 (d, J = 5.90, -PhCH$_2$OCH_2-), 3.40 (d, J = 5.90, -CH$_2$OCH_2C(CH$_3$)-), 3.24 (s, -CH_2OCH$_2$C(CH$_3$)-), 2.39-2.20 (m, -OCOCH_2(CH$_2$)$_4$-), 1.71-1.54 (m, -OCOCH$_2$CH_2(CH$_2$)$_3$-, -OCO(CH$_2$)$_3$CH_2CH$_2$-), 1.49-1.31 (m, -OCO(CH$_2$)$_2$CH_2(CH$_2$)$_2$-) 0.95 (s, -C(CH_3)-).

Synthesis of HO-(PCL-OH)$_4$

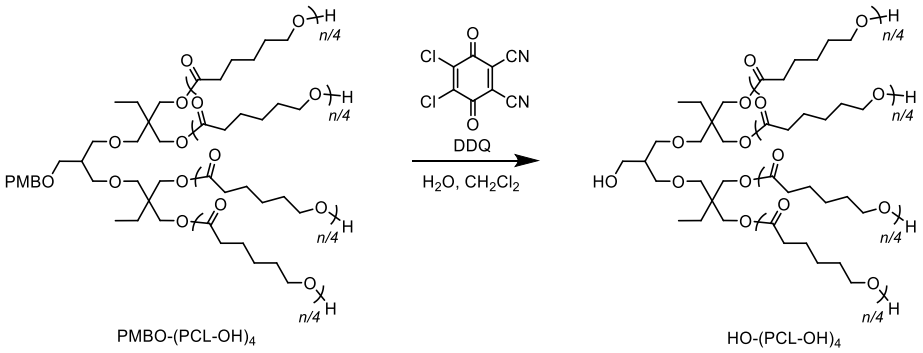

Method E was used for the deprotection reaction of **PMBO-(PCL-OH)$_4$** ($M_{n,NMR}$ = 5,490 g mol^{-1}, 1.5 g, 273 μmol) with DDQ (124 mg, 546 μmol) in H_2O/CH_2Cl_2 (1.50 mL, v/v = 2/1) to give **HO-(PCL-OH)$_4$** as white solid (691 mg). Yield: 47.3%

$M_{n,NMR}$ = 5,250 g mol^{-1}, $M_{n,SEC}$ = 9,110 g mol^{-1} (THF), $Đ$ = 1.05,

^{1}H NMR (400 MHz, $CDCl_3$): δ (ppm) 4.12-4.02 (m, -OCO(CH$_2$)$_4$CH_2-), 3.99 (s, -CH_2OCO-), 3.65 (t, J = 6.40, -CH_2OH), 3.48-3.40 (m, -PhCH$_2$OCH_2-, -CH$_2$OCH_2C(CH$_3$)-), 3.26 (s, -

C*H*$_2$OCH$_2$C(CH$_3$)-), 2.49-2.19 (m, -OCOC*H*$_2$(CH$_2$)$_4$-), 1.87-1.49 (m, -OCOCH$_2$C*H*$_2$(CH$_2$)$_3$-, -OCO(CH$_2$)$_3$C*H*$_2$CH$_2$-), 1.48-1.31 (m, -OCO(CH$_2$)$_2$C*H*$_2$(CH$_2$)$_2$-), 0.97 (s, -C(C*H*$_3$)-).

Synthesis of Pre$_{quatre}$-a

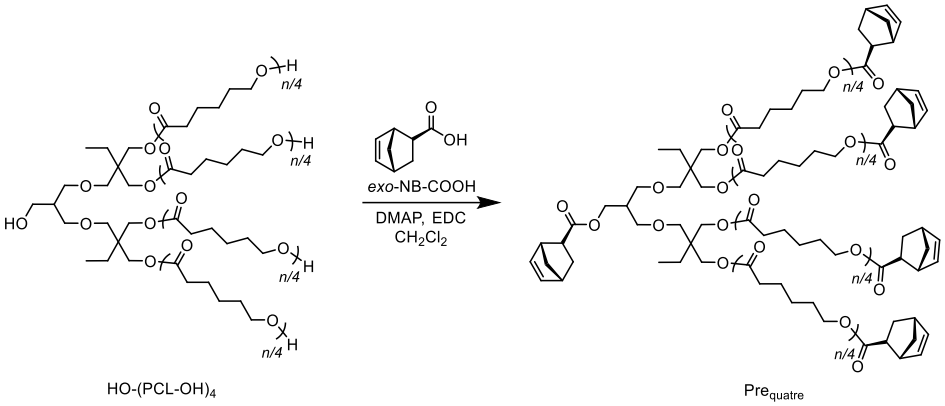

Method B was used for the condensation reaction of **HO-(PCL-OH)$_3$** ($M_{n,NMR}$ = 5,250 g mol^{-1}, 600 mg, 114 μmol) with *exo*-NB-COOH (156 mg, 1.14 mmol), DMAP (206 mg, 1.71 mmol), and EDC (329 mg, 1.71 mmol) in CH_2Cl_2 (6.0 mL) to give **Pre$_{quatre}$ -a** as a white solid (290 mg). Yield: 48.3%

$M_{n,NMR}$ = 6,620 g mol^{-1}, $M_{n,SEC}$ = 9,450 g mol^{-1} (THF), $Đ$ = 1.04,

^{1}H NMR (400 MHz, $CDCl_3$): δ (ppm) 6.22-6.03 (m, -C*H*=C*H*- in norbornene ring), 4.16-4.01 (m, -OCO(CH_2)$_4$C*H*$_2$-), 3.98 (s, -C*H*$_2$OCO-), 3.48-3.36 (m, -PhCH_2OC*H*$_2$-), 3.26 (s, CH_2OC*H*$_2$C(CH_3)-), 3.06-3.00 (m, -C*H*-CH-CH_2O- in norbornene ring), 2.92 (s, -C*H*-CH-CH_2O- in norbornene ring), 2.40-2.25 (m, -OCOC*H*$_2$(CH_2)$_4$-), 1.77-1.54 (m, -OCOCH_2C*H*$_2$(CH_2)$_3$-, -OCO(CH_2)$_3$C*H*$_2$$CH_2$-), 1.46-1.27 (m, -OCO($CH_2$)$_2$C*H*$_2$($CH_2$)$_2$-), 0.97 (s, -C(C*H*$_3$)-).

Synthesis of quatrefoil-shaped PCL-a

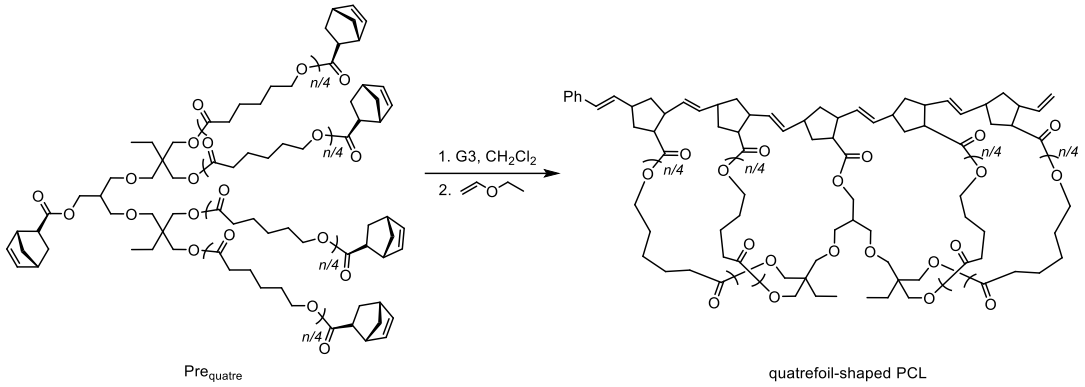

Method C was used for the ROMO of **Pre$_{quatre}$ -a** ($M_{n,NMR}$ = 6,620 g mol^{-1}, 30.0 mg, 4.55 μmol, 170 μM in CH_2Cl_2) with G3 (24.1 mg, 27.2 μmol) in CH_2Cl_2 (230 mL) to give **quatrefoil-shaped PCL-a** as a pale brown solid (27.4 mg). Yield: 89.7%

$M_{n,SEC}$ = 6,710 g mol^{-1} (THF), $Đ$ = 1.07

^{1}H NMR (400 MHz, $CDCl_3$): δ (ppm) 6.61-2.38 (br, alkenyl of poly(norbornene) backbone), 4.25-3.80 (m, -OCO$(CH_2)_4$CH_2-), 2.41-2.12 (m, -OCOC$H_2(CH_2)_4$-), 1.89-1.47 (m, -OCOCH$_2$C$H_2(CH_2)_3$-, -OCO$(CH_2)_3$CH_2CH$_2$-), 1.48-1.15 (m, -OCO$(CH_2)_2$C$H_2(CH_2)_2$-), 1.01-0.57 (s, -C(CH_3)-).

Functionalization of *spiro*-multicyclic polymers

The syntheses of the *α*-/*ω*-hydroxyl-functionalized trefoil-shaped PCLs (namely, **trefoil-shaped PCL-OH$^{\alpha}$** and **trefoil-shaped PCL-OH$^{\omega}$**; M.W. = ca. 6000) were carried out using 4-(hydroxymethyl)styrene or (*Z*)-2-butene-1,4-diol in one pot, respectively. The introduced hydroxyl group can be a versatile scaffold for post-polymerization modification, allowing access to the functionalized structures and higher-ordered architectures. Despite the complicated structure of the multicyclic polymer, both of end-functionalization approaches was readily achieved in high purity, as confirmed by SEC, ^{1}H NMR, and MALDI-TOF MS analyses. The synthetic procedures are as follows:

Synthesis of trefoil-shaped PCL-OH$^{\alpha}$

In a three-necked flask, G3 (12.9 mg, 14.6 μmol) and 4-(hydroxymethyl)styrene (22.2 mg, 165 μmol) was added to dry-CH_2Cl_2 (122 mL), and the solution was stirred for 1 h with Ar bubbling. Then, a solution of **Pre$_{tre}$-a** ($M_{n,NMR}$ = 6,160 g mol^{-1}, $M_{n,SEC}$ = 8,670, $Đ$ = 1.05, 15.0 mg, 2.44 μmol, 170 μM in CH_2Cl_2) was added dropwise to the G3 solution through the additional funnel over 20 min. After 5 min, the reaction was quenched by the addition of excess amount of ethyl vinyl ether. The metal residue and excess 4-(hydroxymethyl)styrene in the crude product were removed by preparative SEC (solvent, $CHCl_3$) to give **trefoil-shaped PCL-OH$^{\alpha}$** as a pale brown solid (14.1 mg). Yield: 91.6%

$M_{n,SEC}$ = 6,400 g mol^{-1} (THF), $Đ$ = 1.12

^{1}H NMR (400 MHz, $CDCl_3$): δ (ppm) 6.51-2.40 (br, alkenyl of poly(norbornene) backbone), 4.67 (s, -C*H*$_2$OH), 4.38-3.81 (m, -OCO(CH$_2$)$_4$C*H*$_2$-), 2.41-2.14 (m, -OCOC*H*$_2$(CH$_2$)$_4$-), 1.76-1.46 (m, -OCOCH$_2$C*H*$_2$(CH$_2$)$_3$-, -OCO(CH$_2$)$_3$C*H*$_2$CH$_2$-), 1.44-0.97 (m, -OCO(CH$_2$)$_2$C*H*$_2$(CH$_2$)$_2$-).

Synthesis of trefoil-shaped PCL-OH$^{\omega}$

In a three-necked flask, G3 (8.6 mg, 9.67 μmol) was added to a three-necked flask and dissolved in dry-CH_2Cl_2 (81.0 mL). Then, a solution of **Pre$_{tre}$-a** ($M_{n,NMR}$ = 6,160 g mol^{-1}, $M_{n,SEC}$ = 8,670, $Đ$ = 1.05, 10.0 mg, 1.62 μmol, 170 μM in CH_2Cl_2) was added dropwise to the G3 solution through the additional funnel over 30 min. After 5 min, *cis*-2-butene-1,4-diol (18.2 mg, 206 μmol) was added to the reaction mixture and the solution was stirred for 1.5 h. The reaction was quenched by the addition of excess amount of ethyl vinyl ether. The metal residue and

excess (*Z*)-2-butene-1,4-diol in the crude product were removed by preparative SEC (solvent, $CHCl_3$) to give **trefoil-shaped PCL-OH$^{\omega}$** as a pale brown solid (10.2 mg). Yield: 100%

$M_{n,SEC}$ = 6,290 g mol^{-1} (THF), $Đ$ = 1.13

^{1}H NMR (400 MHz, $CDCl_3$): δ (ppm) 6.49-2.41 (br, alkenyl of poly(norbornene) backbone), 4.33-3.90 (m, -OCO$(CH_2)_4$CH_2-, -CH_2OH), 2.39-2.21 (m, -OCOC$H_2(CH_2)_4$-), 1.74-1.48 (m, -OCOCH$_2$C$H_2(CH_2)_3$-, -OCO$(CH_2)_3$CH_2CH$_2$-), 1.45-1.16 (m, -OCO$(CH_2)_2$C$H_2(CH_2)_2$-).

Synthesis of PMBO-(PLLA-OH)$_3$

In a glovebox, **I3** (53.3 mg, 208 μmol) and L-LA (1.50 g, 10.4 mmol) were dissolved in dry-CH_2Cl_2 (21.0 mL). DBU (15.8 μL, 104 μmol) was then added to the CH_2Cl_2 solution to initiate the polymerization. After 7 min, the polymerization was quenched by the addition of excess amount of benzoic acid. The mixture was purified by reprecipitation from the CH_2Cl_2 solution to cold MeOH to give **PMBO-(PLLA-OH)$_3$** as a white solid (1.13 g). Yield: 86.9%

$M_{n,NMR}$ = 7,140 g mol^{-1}, $M_{n,SEC}$ = 10,800 g mol^{-1} (THF), $Đ$ = 1.04

^{1}H NMR (400 MHz, $CDCl_3$): δ (ppm) 7.18 (d, J = 8.2, aromatic), 6.86 (d, J = 8.7, aromatic), 5.38-5.00 (m, methine of PLLA backbone), 4.47-4.28 (m, -PhCH_2O-, -CH(CH$_3$)OH), 4.16 (q, J = 11.4, -C(CH_2O-)$_3$), 3.80 (s, -OCH_3), 3.34 (s, -CH_2C(CH$_2$O-)$_3$), 2.66 (m, -OH), 1.86-1.34 (m, methyl of PLLA backbone).

Synthesis of HO-(PLLA-OH)$_3$

Method E was used for the deprotection reaction of PMBO-(PLLA-OH)$_3$ ($M_{n,NMR}$ = 7,140 g mol^{-1}, 1.02 g, 143 μmol) with DDQ (65.5 mg, 289 μmol) in H_2O/CH_2Cl_2 (15 mL, v/v = 1/2) for 24 h. After the purification, the same procedure was performed again because the quantitative reaction was not found by ^{1}H NMR analysis of the product. After 24 h, the polymer

crude was purified by the reprecipitation twice from CH_2Cl_2 to cold methanol to give **HO-(PLLA-OH)$_3$** as white solid (443 mg). Yield: 44.3%

$M_{n,NMR}$ = 7,150 g mol^{-1}, $M_{n,SEC}$ = 10,900 g mol^{-1} (THF), $Đ$ = 1.04

^{1}H NMR (400 MHz, $CDCl_3$): δ (ppm) 5.40-5.01 (m, methine of PLLA backbone), 4.34 (m, methine of ω-chain end lactyl unit), 4.15 (s, -C(C*H*$_2$O-)$_3$), 3.49 (ddd, J = 32.0, 11.9, 6.6 Hz, -CC*H*$_2$OH), 2.75-2.59 (m, -CHCH$_3$O*H*), 1.81-1.35 (m, methyl of PLLA backbone).

Synthesis of NB-(PLLA-NB)$_3$

Method B was used for the condensation reaction of HO-(PLLA-OH)$_3$ ($M_{n,NMR}$ = 7,150 g mol^{-1}, 403 mg, 56.4 μmol) with *exo*-NB-COOH (64.5 mg, 467 mmol), DMAP (82.7 mg, 677 mmol), and EDC (135 mg, 706 mmol) in CH_2Cl_2 (4.0 mL) to give **NB-(PLLA-NB)$_3$** as a white solid (293 mg). Yield: 67.5%

$M_{n,NMR}$ = 8,050 g mol^{-1}, $M_{n,SEC}$ = 11,400 g mol^{-1} (THF), $Đ$ = 1.03

^{1}H NMR (400 MHz, $CDCl_3$): δ (ppm) 6.23-6.02 (m, -C*H*=C*H*- in norbornene ring), 5.41-4.91 (m, methine of PLLA backbone), 4.29-3.99 (m, -C*H*$_2$C(CH$_2$O-)$_3$, -C(C*H*$_2$O-)$_3$), 3.26-2.96 (m, -C*H*CHCO- in norbornene ring), 2.92 (s, -C*H*CH$_2$CHCO- in norbornene ring), 2.36-2.15 (m, -C*H*CO- in norbornene ring), 1.97 (m, *exo*-H of -C*H*$_2$- in norbornene ring), 1.74 (m, *endo*-H of -C*H*$_2$- in norbornene ring), 1.73-1.23 (m, methyl of PLLA backbone, bridge head -C*H*2- in norbornene ring).

Synthesis of trefoil-shaped PLLA

Method C was used for the ROMO of NB-(PLLA-NB)$_3$ ($M_{n,NMR}$ = 8,050 g mol^{-1}, 15.0 mg, 1.86 μmol, 170 μM in CH_2Cl_2) with G3 (9.9 mg, 11.2 μmol) in CH_2Cl_2 (93.0 mL) to give trefoil-shaped PLLA as a white solid (13.9 mg). Yield: 91.4%

$M_{n,SEC}$ = 7,700 g mol^{-1} (THF), $Đ$ = 1.09

^{1}H NMR (400 MHz, $CDCl_3$): δ (ppm) 6.47-1.34 (br, alkenyl of poly(norbornene) backbone), 5.43-4.77 (m, m, methine of PLLA backbone), 1.34-1.81 (m, methyl of PLLA backbone).

Synthesis of PMBO-(PEHGE-OH)$_3$

In a glovebox, **I3** (28.3 mg, 110 μmol) and EHGE (0.80 mL, 3.87 mmol) were dissolved in dry-toluene (1.3 mL). *t*-Bu-P_4 (138 μL of ~0.8 mol L^{-1} solution in *n*-hexane, 110 μmol) was then added to the toluene solution to initiate the polymerization. After 49 h, the polymerization was quenched by the addition of excess amount of benzoic acid. The product was purified by passing by a pad of alumina using dry-THF to give **PMBO-(PEHGE-OH)$_3$** as a colorless viscous liquid (472 mg). Yield: 63.0%

$M_{n,NMR}$ = 6,560 g mol^{-1}, $M_{n,SEC}$ = 7,170 g mol^{-1} (THF), $Đ$ = 1.04

^{1}H NMR (400 MHz, $CDCl_3$): δ (ppm) 7.20 (d, J = 8.5, aromatic), 6.84 (d, J = 8.5, aromatic), 4.37 (s, -PhCH_2O-), 3.92 (m, -OH), 3.78 (s, CH_3O-) 3.66-3.57 (m, -CH_2CH(CH_2-)O-), 3.57-3.35 (-CH_2CH(CH_2-)O-, -CH_2CH(CH_2-)O-, -C(CH_2O-)$_3$), 3.35-3.22 (m, -CH_2CH(CH_2OCH_2-)O-), 1.55-1.43 (m, methine of EHGE side chain), 1.42-1.19 (m, methylene of EHGE side chain), 0.99-0.76 (m, methyl of EHGE side chain).

Synthesis of HO-(PEHGE-OH)$_3$

Method E was used for the deprotection reaction of PMBO-(PEHGE-OH)$_3$ ($M_{n,NMR}$ = 6,540 g mol^{-1}, 428 mg, 65.4 μmol) with DDQ (30.0 mg, 132 μmol) in H_2O/CH_2Cl_2 (6.4 mL, v/v = 1/2) for 24 h. After 24 h, the reaction mixture was dried by Na_2SO_4 and the product was purified by passing by a pad of alumina using dry-THF to give **HO-(PEHGE-OH)$_3$** as a colorless viscous liquid (233 mg). Yield: 55.6%

$M_{n,NMR}$ = 6,910 g mol^{-1}, $M_{n,SEC}$ = 7,390 g mol^{-1} (THF), $Đ$ = 1.03

^{1}H NMR (400 MHz, $CDCl_3$): δ (ppm) 3.90 (m, -O*H*), 3.67-3.57 (m, -$CH_2CH(CH_2$-)O-), 3.57-3.37 (-$CH_2CH(CH_2$-)O-, -$CH_2CH(CH_2$-)O-, -$C(CH_2O$-$)_3$), 3.36-3.20 (m, -$CH_2CH(CH_2OCH_2$-)O-), 1.54-1.43 (m, methine of EHGE side chain), 1.42-1.18 (m, methylene of EHGE side chain), 1.05-0.74 (m, methyl of EHGE side chain).

Synthesis of NB-(PEHGE-NB)$_3$

Method B was used for the condensation reaction of HO-(PEHGE-OH)$_3$ ($M_{n,NMR}$ = 6,910 g mol^{-1}, 223 mg, 32.2 μmol) with *exo*-NB-COOH (35.8 mg, 259 mmol), DMAP (44.5 mg, 364 mmol), and EDC (76.5 mg, 399 mmol) in CH_2Cl_2 (2.2 mL) to give **NB-(PEHGE-NB)$_3$** as a pale yellow viscous liquid (172 mg). Yield: 71.4%

$M_{n,NMR}$ = 7,000 g mol^{-1}, $M_{n,SEC}$ = 7,690 g mol^{-1} (THF), $Đ$ = 1.03

^{1}H NMR (400 MHz, $CDCl_3$): δ (ppm) 6.22-6.00 (m, -C*H*=C*H*- in norbornene ring), 5.23-5.01 (m, methine of PEHGE backbone at the chain end), 4.09 (s, -COOCH_2-), 3.67-3.58 (m, -$CH_2CH(CH_2$-)O-), 3.57-3.36 (m, -$CH_2CH(CH_2$-)O-, -$CH_2CH(CH_2$-)O-, -$C(CH_2O$-$)_3$), 3.34-3.21 (m, -$CH_2CH(CH_2OCH_2$-)O-), 3.10-2.98 (m, -C*H*CHCO- in norbornene ring), 2.90 (s, -C*H*CH_2CHCO- in norbornene ring), 2.32-2.11 (m, -C*H*CO- in norbornene ring), 2.02-1.84 (m, *exo*-H of -CH_2- in norbornene ring), 1.54-1.42 (m, methine of EHGE side chain), 1.42-1.17 (m, methylene of EHGE side chain), 0.99-0.62 (m, methyl of EHGE side chain).

Synthesis of trefoil-shaped PEHGE

Method C was used for the ROMO of NB-(PEHGE-NB)$_3$ ($M_{n,NMR}$ = 7,000 g mol^{-1}, 10.0 mg, 1.43 μmol, 170 μM in CH_2Cl_2) with G3 (7.6 mg, 8.6 μmol) in CH_2Cl_2 (143 mL) to give trefoil-shaped PEHGE as a colorless viscous liquid (7.3 mg). Yield: 71.9%

$M_{n,SEC}$ = 6,320 g mol^{-1} (THF), $Đ$ = 1.05

^{1}H NMR (400 MHz, $CDCl_3$): δ (ppm) 6.54-1.82 (br, alkenyl of poly(norbornene) backbone), 3.68-3.58 (m, -$CH_2CH(CH_2$-)O-), 3.57-3.36 (m, -$CH_2CH(CH_2$-)O-, -$CH_2CH(CH_2$-)O-, -$C(CH_2O$-)$_3$), 3.35-3.19 (m, -$CH_2CH(CH_2OCH_2$-)O-), 1.55-1.43 (m, methine of EHGE side chain), 1.17-1.42 (m, methylene of EHGE side chain), 0.77-0.97 (m, methyl of EHGE side chain).

2.3 Results and Discussion

2.3.1 Construction of monocyclic polymer via intramolecular consecutive cyclization

As a model reaction system, the author initially optimized the reaction conditions for the intramolecular consecutive ROMO of an *α*,*ω*-dinorbornenyl end-functionalized linear PCL precursor, **Pre$_{ring}$-a**, to afford the corresponding monocyclic polymer **ring-a** (Scheme 1). The G3-mediated ROMO of **Pre$_{ring}$-a** (number-average molecular weight (M_n) estimated by ^{1}H NMR ($M_{n,NMR}$) = 5,510 g mol^{-1}, M_n estimated by SEC using PSt standards ($M_{n,SEC}$) = 9,790 g mol^{-1}, $Đ$ = 1.05; see also Table S2.1 and synthetic details in the Section 2.2.3) was conducted at high dilution (final polymer precursor concentration = 0.02 mM in CH_2Cl_2) to preferentially promote the desired intramolecular reaction rather than the undesired intermolecular one. To further minimize intermolecular coupling, the solution of **Pre$_{ring}$-a** was added dropwise to the stirred G3 solution in CH_2Cl_2 with varying [**Pre$_{ring}$-a**]$_0$/[G3]$_0$ ratios of 1/1, 1/2, 1/4, and 1/6. Notably, each reaction produced a soluble product, and ^{1}H NMR analysis suggested quantitative consumption of the norbornenyl group (Figure 2.2). The molecular weight distribution of the product varies significantly depending upon the [**Pre$_{ring}$-a**]$_0$/[G3]$_0$ ratio, as shown in Figure 2.3. The SEC traces of the products obtained at the [**Pre$_{ring}$-a**]$_0$/[G3]$_0$ ratios of 1/1, 1/2, and 1/4 exhibit two elution peak maxima in both higher and lower molecular weight regions with respect to that of **Pre$_{ring}$-a**, indicating the formation of intramolecular propagation and intermolecular cyclization products, respectively.[29] On the other hand, the product obtained at the [**Pre$_{ring}$-a**]$_0$/[G3]$_0$ ratio of 1/6 exhibits a narrowly dispersed unimodal peak at a lower molecular weight region that would be assignable to the intramolecularly constructed product **ring-a**, as reported previously.[30] The decrease in the apparent molecular weight after the ROMO with hydrodynamic volume change (0.75; calculated from the equation $M_{p,SEC(Prering)}/M_{p,SEC(ring)}$, where $M_{p,SEC}$ is the peak-top molecular weight; Figure S2.1) is consistent with the literature range of 0.71–0.83 for other monocyclic polymers possessing comparable molecular

weight.[31–33] Thus, successful cyclic structure formation is demonstrated for the synthesis of **ring-a** with suppressed intermolecular propagation. Moreover, the ^{1}H NMR and matrix-assisted laser desorption ionization time-of-flight (MALDI-TOF) mass spectra could be reasonably assigned to the expected chemical structure of **ring-a** (Figure 2.4). Hence, the author found that a $[precursor]_0/[G3]_0$ ratio of 1/6 in combination with a slow addition technique can selectively promote intramolecular ROMO.

Scheme 2.1. Synthesis of **ring-a** through intramolecular ring-opening metathesis oligomerization (ROMO) of *α*,*ω*-dinorbornenyl end-functionalized linear PCL.

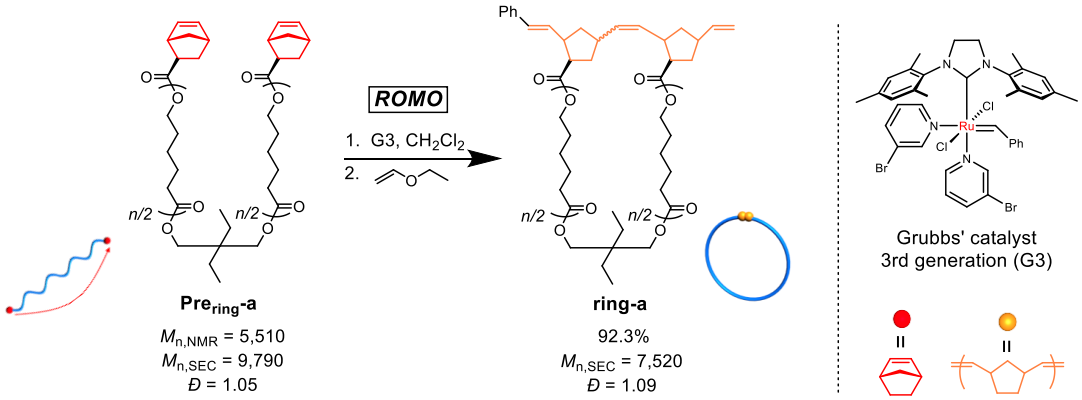

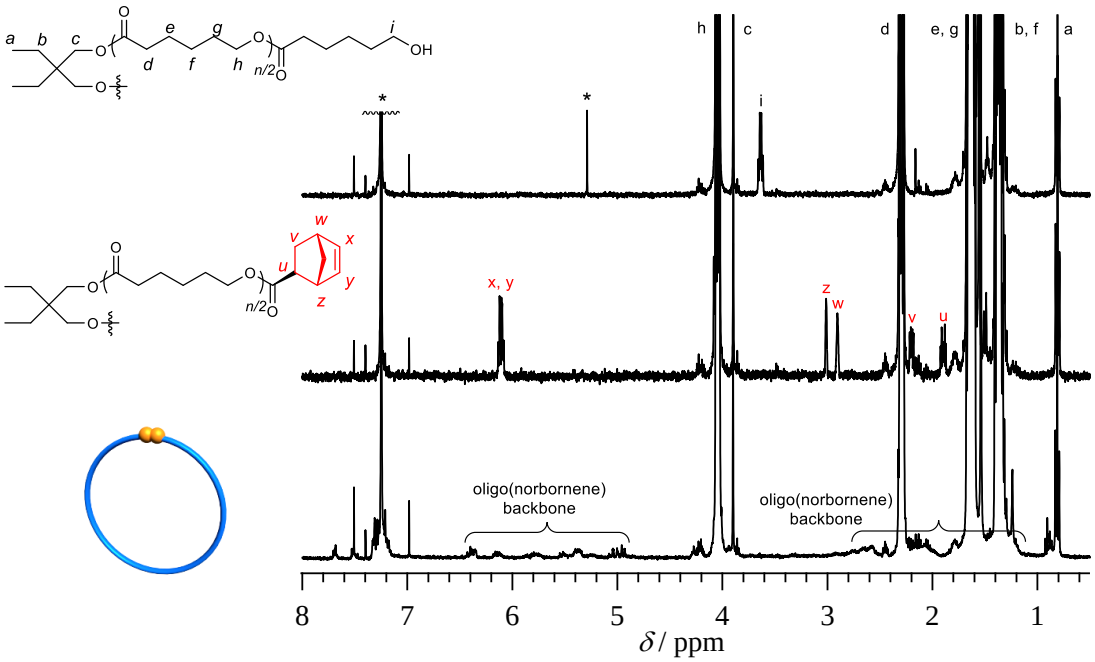

Figure 2.2. ^{1}H NMR spectra of **HO-PCL-OH-a** ($M_{n,NMR}$ = 4,890, $Đ$ = 1.06; upper), **Pre$_{ring}$-a** ($M_{n,NMR}$ = 5,510, $Đ$ =1.05; middle), and **ring-a** ($Đ$ = 1.09; lower) in $CDCl_3$. Asterisks show solvent signals.

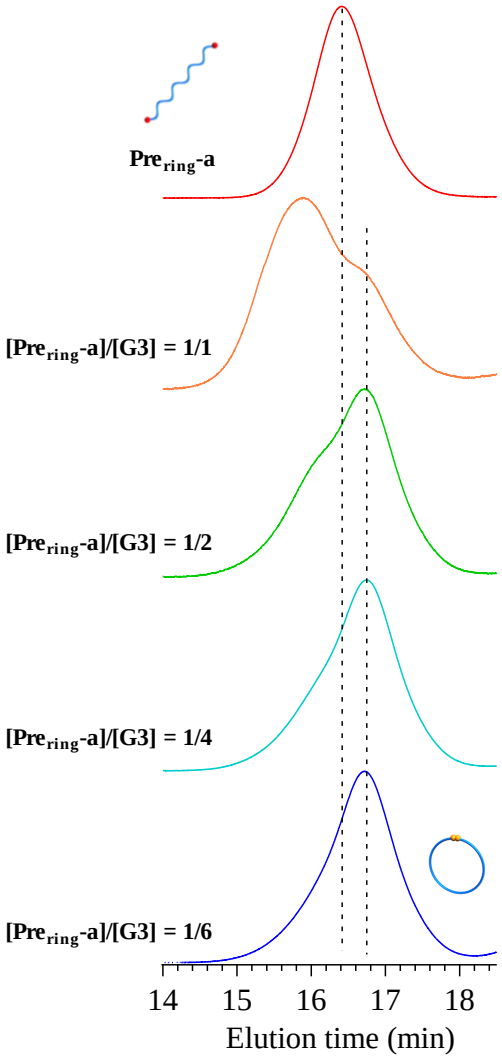

Figure 2.3. SEC traces of linear polymer precursor (**Pre$_{ring}$-a**) and ROMO product under various [**Pre$_{ring}$-a**]/[G3] ratio (RI detection; eluent, THF; flow rate, 1.0 mL min^{-1}).

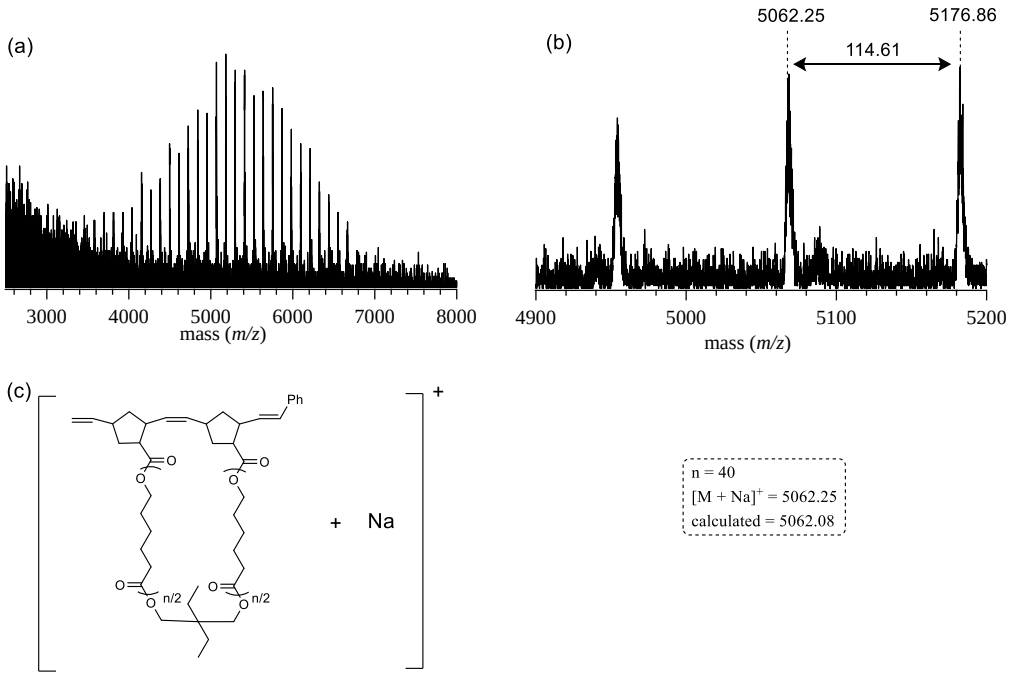

Figure 2.4. MALDI-TOF MS analysis of the obtained **ring-a**.

2.3.2 Synthesis of 8-shaped polymer via intramolecular consecutive cyclization

Next, for synthesis of an 8-shaped polymer, the author designed a PCL-based linear precursor with norbornenyl groups at each ω-chain end and chain center (**Pre$_{\mathbf{fig8}}$**; Scheme 2.2(a)). To introduce the norbornenyl groups at not only the chain ends but also the chain center, a diol initiator possessing a protected hydroxyl group was employed for the ε-caprolactone polymerization. The precursor **Pre$_{\mathbf{fig8}}$** (**Pre$_{\mathbf{fig8}}$-a**; $M_{n,NMR}$ = 6,200 g mol^{-1}, $M_{n,SEC}$ = 9,970 g mol^{-1}, $Đ$ = 1.06) was successfully synthesized by the ring-opening polymerization of ε-caprolactone using the initiator, followed by deprotection and condensation with (±)-*exo*-5-norbornene carboxylic acid (see Section 2.2.3 for the synthetic details).

Scheme 2.2. Programmed folding of linear, three-armed star, and four-armed star precursors with norbornenyl groups at the chain center and each end into 8- (a), trefoil- (b), and quatrefoil-shaped PCLs (c) through intramolecular ROMO.

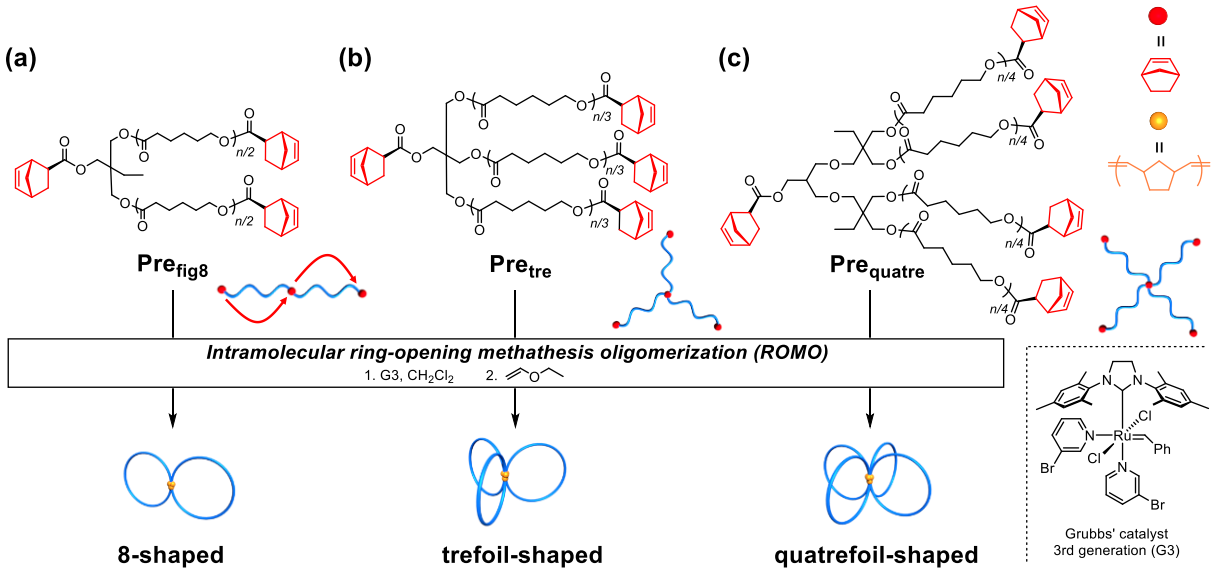

Subsequently, the intramolecular ROMO was carried out under highly diluted conditions in CH_2Cl_2 (final concentration = 0.02 mM) in the presence of excess Grubbs' 3rd generation catalyst ($[precursor]_0/[G3]$ = 1/6) with slow addition of the polymer precursor. After removing the catalyst residue, the product was obtained in high yield (91.0%).^{1}H NMR analysis of the obtained product revealed that signals arising from the *exo*-norbornenyl groups of the precursor completely disappeared, while new signals due to the oligonorbornene backbone appeared at 1.6–3.4 and 4.8–6.5 ppm (Figure 2.5). The SEC trace of the product showed a monomodal peak, and the elution peak was observed in a lower molecular weight region ($M_{n,SEC}$ = 7,340 g mol^{-1}, $Đ$ = 1.08) than that of the linear precursor (**Pre$_{fig8}$-a**; $M_{n,SEC}$ = 9,970 g mol^{-1}, $Đ$ = 1.06, Figure 2.6(a) and Figure S2.2). The dramatic shift in the SEC elution peak maximum indicates that intramolecular cyclization occurred to produce a hydrodynamically smaller polymer (*i.e.*, **8-shaped PCL-a**), rather than intermolecular side reactions. By comparing the SEC peak-top molecular weights of the precursors and cyclized polymers, the compaction parameter <*G*> was calculated as 0.67, which agrees with the reported value of <*G*> for 8-

shaped polymers of comparable molecular weights (<*G*> = 0.67–0.81; Table 2.1).[20–24] The matrix-assisted laser desorption/ionization-time of flight mass spectrometry (MALDI-TOF MS) spectrum of the obtained product showed two series of peaks with a regular *m*/*z* interval of 114.09, corresponding to the mass of the repeating ε-caprolactone unit (Figure 2.6(b)). The major series of peaks (denoted with ●) was assigned to the expected chemical structure of **8-shaped PCL-a**; for example, the peak at *m*/*z* = 5,184.84 agrees well with the calculated mass of the desired **8-shaped PCL-a** with a total degree of polymerization of 40 ($[M + Na]^+$ = 5,184.12). The minor series of peaks (denoted with ■) was assigned to cyclic or tadpole-shaped PCLs (calculated $[M + Na]^+$ = 5,174.11, *n* = 39) formed by reaction with two G3 molecules (Figure 2.7). The amount was determined to be 7.9% by peak deconvolution. Two topological isomers of cyclic- and tadpole-forms are expected to be produced by a side reaction, with the preferred isomer expected to have the tadpole topology due to the folding process being primarily directed by the spatial distance of crosslinking points.[25] Other possible byproducts (*e.g.*, linear PCL; calculated $[M + Na]^+$ = 5,278.17, *n* = 39) were not detected. Overall, successful folding into the 8-shaped topology (**8-shaped PCL-a**) was achieved by intramolecular ROMO of the linear precursor in a precise manner.

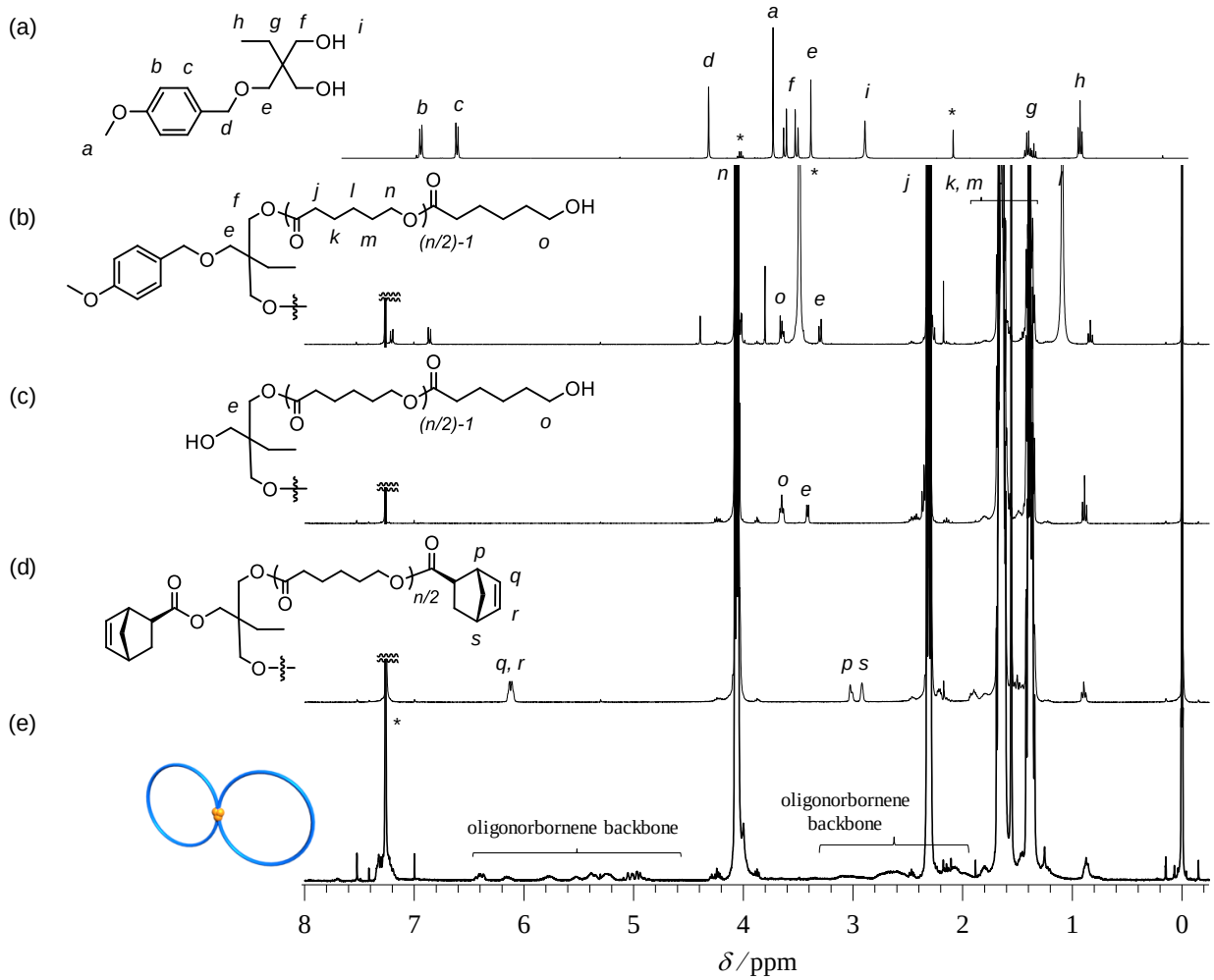

Figure 2.5. NMR spectra of (a) **I1**, (b) PMBO-(PCL-OH)$_2$, (c) HO-(PCL-OH)$_2$, (d) **Pre$_{fig8}$-a**, and (e) **8-shaped PCL-a** in $CDCl_3$ (400 MHz).

Table 2.1. Molecular characterization of *spiro*-multicyclic PCLs prepared by intramolecular ROMO.

Precursor	$M_{n,NMR(Pre)}$ [a]	Topology	$M_{n,SEC}$ [b]	$Đ$ [b]	M_p [c]	<G> [d]	D_h [e] (nm)	[η] [e] (mL g^{-1})	T_m [f] (°C)	X_{WAXD} [g] (%)
Pre$_{ring}$-a	5,510	**ring-a**	7,520	1.09	-	-	4.6	11.3	51.1	40.3
Pre$_{ring}$-b	7,720	**ring-b**	11,700	1.09	-	-	5.8	15.8	56.0	38.7
Pre$_{ring}$-c	10,300	**ring-c**	15,200	1.07	-	-	6.8	18.8	56.9	42.5
Pre$_{fig8}$-a	6,200	**8-shaped PCL-a**	7,340	1.08	7,140	0.67	4.2	9.5	53.8	41.8
Pre$_{fig8}$-b	8,900	**8-shaped PCL-b**	10,600	1.07	10,000	0.65	5.0	12.3	56.1	44.5
Pre$_{fig8}$-c	11,000	**8-shaped PCL-c**	13,200	1.08	11,900	0.63	5.6	14.9	57.7	50.6
Pre$_{tre}$-a	6,160	**trefoil-shaped PCL-a**	6,170	1.09	6,160	0.58	3.8	6.9	42.6	31.7
Pre$_{tre}$-b	9,700	**trefoil-shaped PCL-b**	9,790	1.08	9,010	0.54	4.8	11.3	52.8	42.8
Pre$_{tre}$-c	12,400	**trefoil-shaped PCL-c**	13,200	1.08	12,300	0.58	5.6	13.2	54.4	45.4
Pre$_{quatre}$-a	6,620	**quatrefoil-shaped PCL-a**	6,710	1.07	6,470	0.57	4.0	6.9	29.3	23.6
Pre$_{quatre}$-b	9,220	**quatrefoil-shaped PCL-b**	9,640	1.06	9,140	0.57	4.4	8.6	47.7	39.3
Pre$_{quatre}$-c	11,500	**quatrefoil-shaped PCL-c**	11,000	1.06	10,500	0.53	5.0	9.8	50.8	44.4

[a] The absolute molecular weight of the precursor ($M_{n,NMR(Pre)}$) estimated by ^{1}H NMR in $CDCl_3$ (400 MHz). [b] Determined by SEC in tetrahydrofuran (THF) using polystyrene (PS) standards (RI detection). [c] Peak-top molecular weight of the multicyclic polymer (M_p) estimated by SEC in THF using PS standards (refractive index (RI) detection). [d] <G> = $M_p/M_{n,NMR(Pre)}$, where M_p is the as a PS equivalent was converted into that of the PCL using a conversion coefficient of 0.58.[36] [e] Determined by SEC equipped with a viscometer in THF. [f] Determined by differential scanning calorimetry (DSC). [g] Determined by wide-angle X-ray diffraction (WAXD) through peak deconvolution.

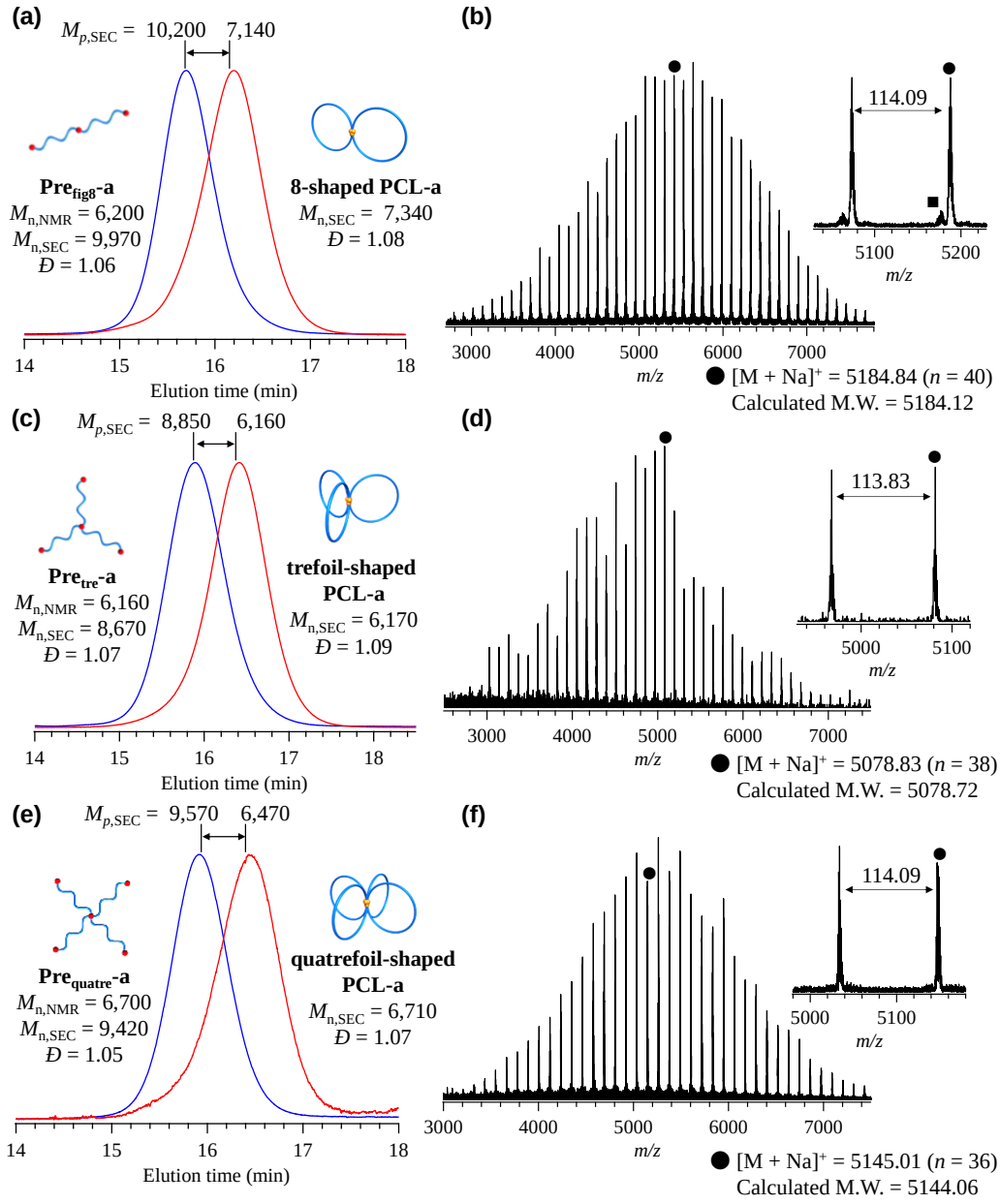

Figure 2.6 (a,c,e) SEC traces of the precursors (**Pre$_{fig8}$-a**, **Pre$_{tre}$ -a**, and **Pre$_{quatre}$-a**; blue curves) and the obtained *spiro*-multicyclic polymers (**8-shaped PCL-a**, **trefoil-shaped PCL-a**, and **quatrefoil-shaped PCL-a**; red curves) (RI detection; PS standards; eluent, THF). (b,d,f) MALDI-TOF MS spectra of **8-shaped PCL-a**, **trefoil-shaped PCL-a**, and **quatrefoil-shaped PCL-a** (reflector mode; *n* denotes number of monomer units).

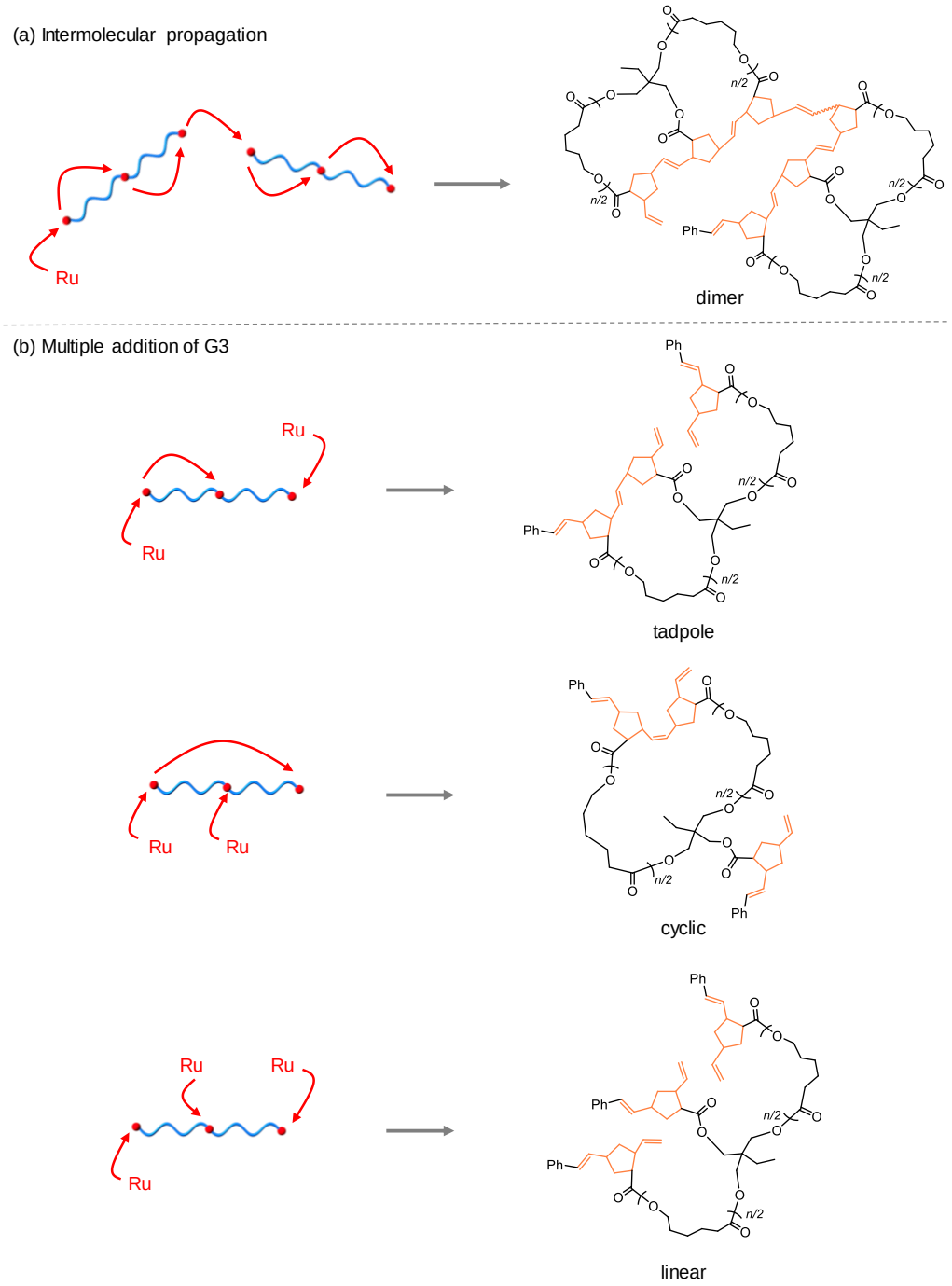

Figure 2.7. Schematic illustration of possible side reactions during the synthesis of **8-shaped PCL**: (a) oligomer formation by intermolecular propagation and (b) by-product formations through multiple addition of G3.

2.3.3 Construction of trefoil- and quatrefoil-shaped polymers

To further extend this strategy, intramolecular ROMO was applied to the synthesis of **trefoil-shaped PCL** and **quatrefoil-shaped PCL**s, where the number of cyclic units are three and four, respectively. For the synthesis of **trefoil-shaped PCL-a** and **quatrefoil-shaped PCL-a**, the well- defined three- and four-armed star-shaped PCLs bearing an *exo*-norbornenyl group at the chain center and each terminus (**Pre$_{tre}$-a** and **Pre$_{quatre}$ -a**; $M_{n,NMR}$ = ~6,500 g mol^{-1}) were subjected to ROMO conditions (Figure 2.6(c)–(f), Figures S2.3–S2.8, and Table 2.1). ^{1}H NMR analysis confirmed quantitative consumption of the *exo*-norbornenyl groups despite an increase in the number of groups in the precursors (Figures S2.4 and S2.7). Importantly, in both cases, the SEC elution peak clearly shifted to the lower molecular weight region while the peak shape remained monomodal with narrow dispersity ($Đ$ = 1.07–1.09; Figure 2.6(c), (e)). The estimated <G> values for **trefoil-shaped PCL-a** and **quatrefoil-shaped PCL-a** (0.57–0.58) were much lower than that of **8-shaped PCL-a** (0.67), confirming the much smaller volume. Notably, each MALDI-TOF MS spectrum showed only one series of peaks assignable to the expected structures of **trefoil-shaped PCL-a** and **quatrefoil-shaped PCL-a** (Figure 2.6(d), (f)). The SEC and MALDI-TOF MS analyses strongly support that ROMO proceeds in an intramolecular manner without side reactions regardless of the number of cyclic units. A question therefore arises with respect to the reaction order of the norbornenes. According to a recent report by Tezuka and co-workers, it can be reasonably expected that the norbornenes should react with those that are closer.[25]

2.3.4 Functionalization of topological polymers

Chain-end functionalization of topological polymers is essential to facilitate higher-order functions with a combination of diverse molecular designs. Typically, the α- and ω-chain ends of the polynorbornene backbone produced by ROMO can be readily transformed to the

desired reactive groups by using functional Ru initiators and end-capping agents, respectively.[26,27] Indeed, the *α*-/*ω*-end-functionalized trefoil-shaped PCLs with hydroxyl groups (namely, **trefoil-shaped PCL-OH$^{\alpha}$** and **trefoil-shaped PCL-OH$^{\omega}$**, respectively) were precisely synthesized while retaining narrow dispersity (*Đ* = 1.12–1.13, Scheme 2.3, Figures 2.8–2.11 and Figure S2.9). This allows facile access to surface-modified metal/semiconductor nanoparticles and substrates with topological polymers, which could be used to increase colloidal stability and to prepare bioinert and superlubricating coatings.[28–30]

Scheme 2.3. Synthetic pathways to **trefoil-shaped PCL-OH$^{\alpha}$** and **trefoil-shaped PCL-OH$^{\omega}$**.

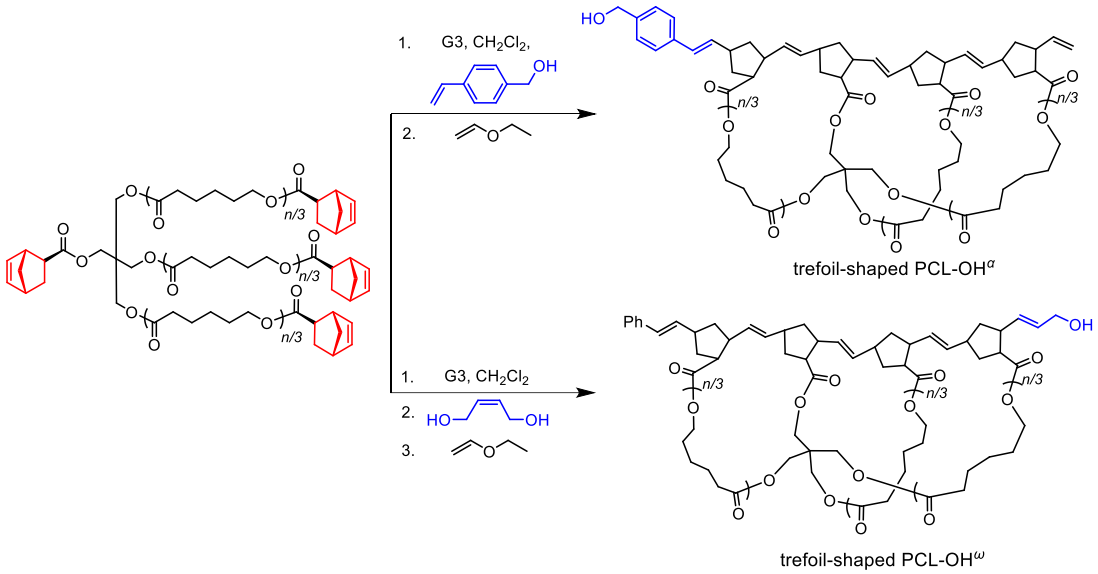

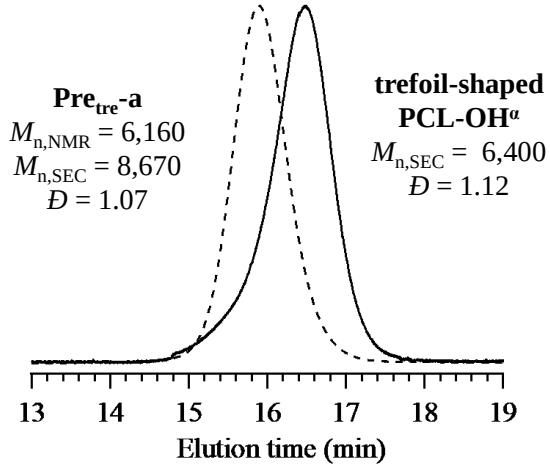

Figure 2.8. SEC traces of **Pre$_{tre}$-a** (dotted line), **trefoil-shaped PCL-OH$^{\alpha}$** (solid line).

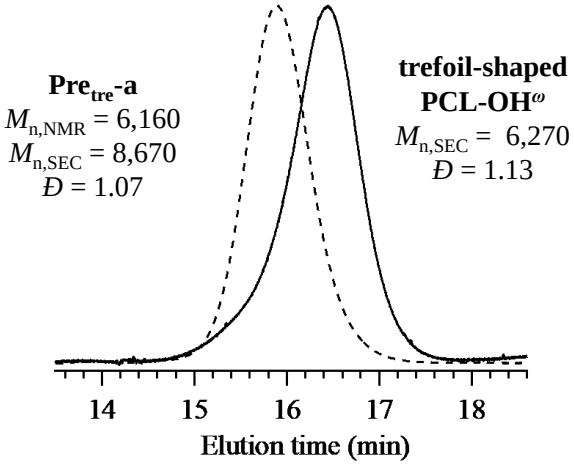

Figure 2.9. SEC traces of **Pre$_{tre}$-a** (dotted line), **trefoil-shaped PCL-OH$^{\omega}$** (solid line).

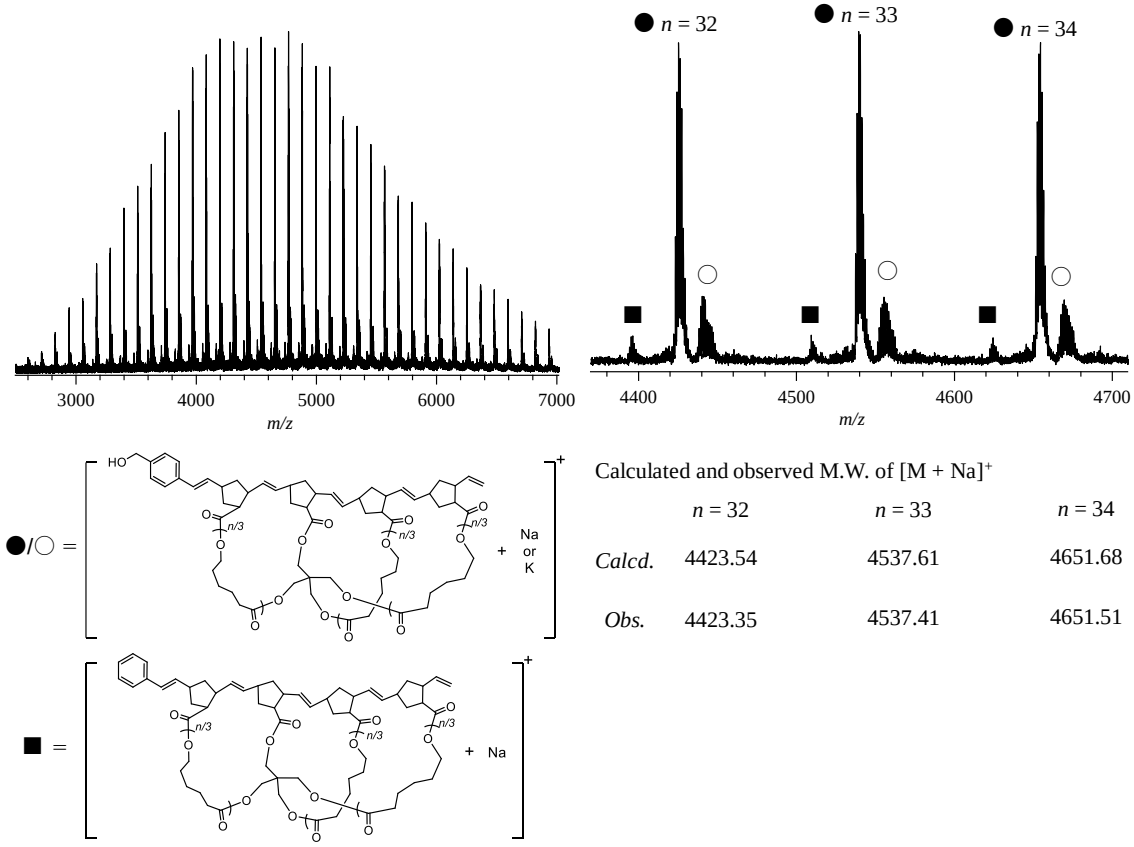

Calculated and observed M.W. of $[M + Na]^+$

	n = 32	*n* = 33	*n* = 34
Calcd.	4423.54	4537.61	4651.68
Obs.	4423.35	4537.41	4651.51

Figure 2.10. MALDI-TOF MS analysis of **trefoil-shaped PCL-OH$^{\alpha}$**.

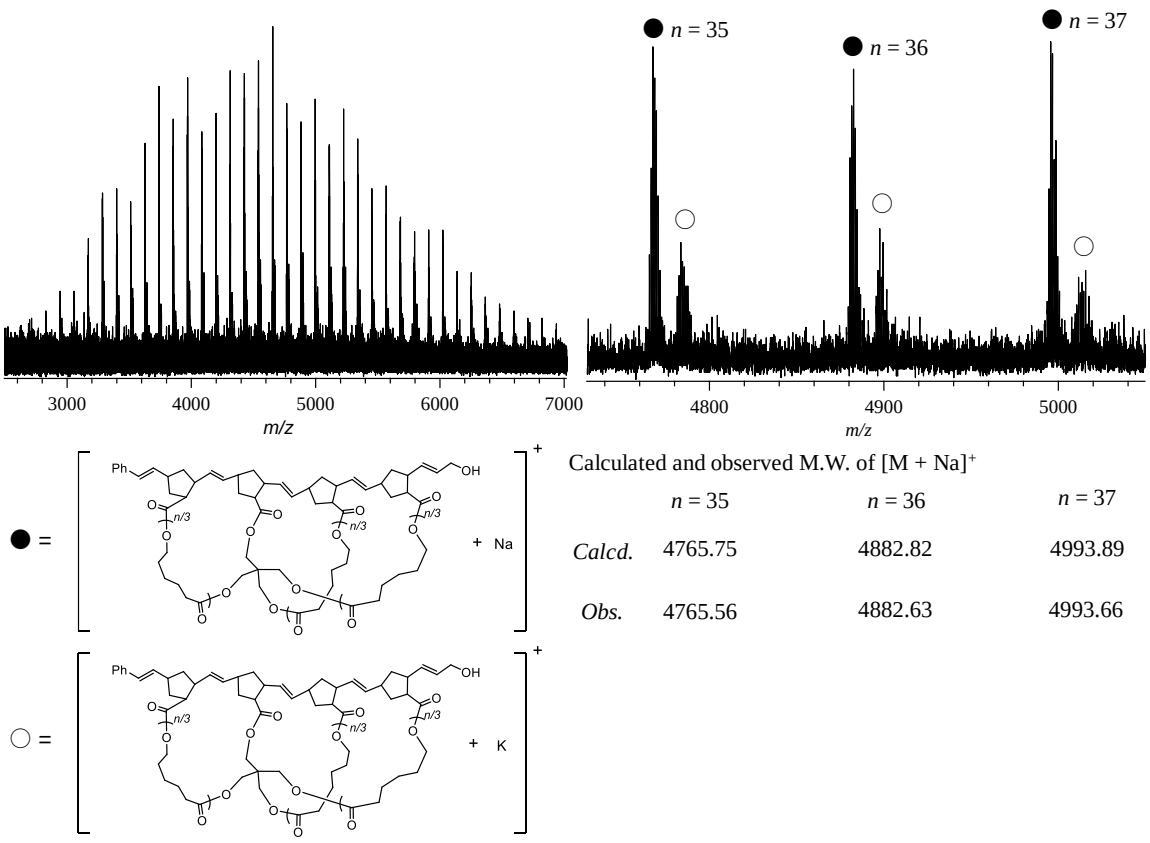

Figure 2.11. MALDI-TOF MS analysis of **trefoil-shaped PCL-OH$^{\omega}$**.

2.3.5 Size control of multicyclic polymers

For systematic characterization of the folded polymers, size control of the cyclic unit and control over the number of cyclic units is indispensable. By simply changing the degree of polymerization of the precursor, the molecular weight of each multicyclic (8-, trefoil-, and quatrefoil-shaped) polymer was successfully controlled from ~6,000 to 12,000 g mol^{-1} (Table 2.1). Note that the suffix on the name of each polymer sample represents its molecular weight (**-a** for ~6,000 g mol^{-1}, **-b** for ~9,000 g mol^{-1}, and **-c** for ~12,000 g mol^{-1}).

2.3.6 Applicability of intramolecular ROMO to diverse polymer species

Furthermore, to verify the applicability of intramolecular ROMO to other polymer backbones, the author applied this approach to the synthesis of *spiro*-multicyclic poly(L-lactide) (PLLA) and poly(2-ethylhexyl glycidyl ether) (PEHGE) (Scheme 2.4, Figures 2.12–2.16, and Table S2.5). Specifically, trefoil-shaped PLLA and PEHGE were synthesized by the ring-opening polymerization of the corresponding monomers with **I3** as the initiator using 1,8-diazabicyclo[5.4.0]-7-undecene (DBU) and *t*-Bu-P_4 catalysts,[31,32] respectively, followed by the deprotection reaction, installation of norbornene groups, and ROMO under the optimized conditions. The targeted folded structures were confirmed in both synthesized products through the comprehensive characterization by ^{1}H NMR, SEC (Figures 2.12 and 2.14), and MALDI-TOF MS, which suggested that the presented method is applicable for the synthesis of a broad range of polymer species.

Scheme S2.4. Synthetic pathways for *spiro*-multicyclic PLLA and PEHGE.

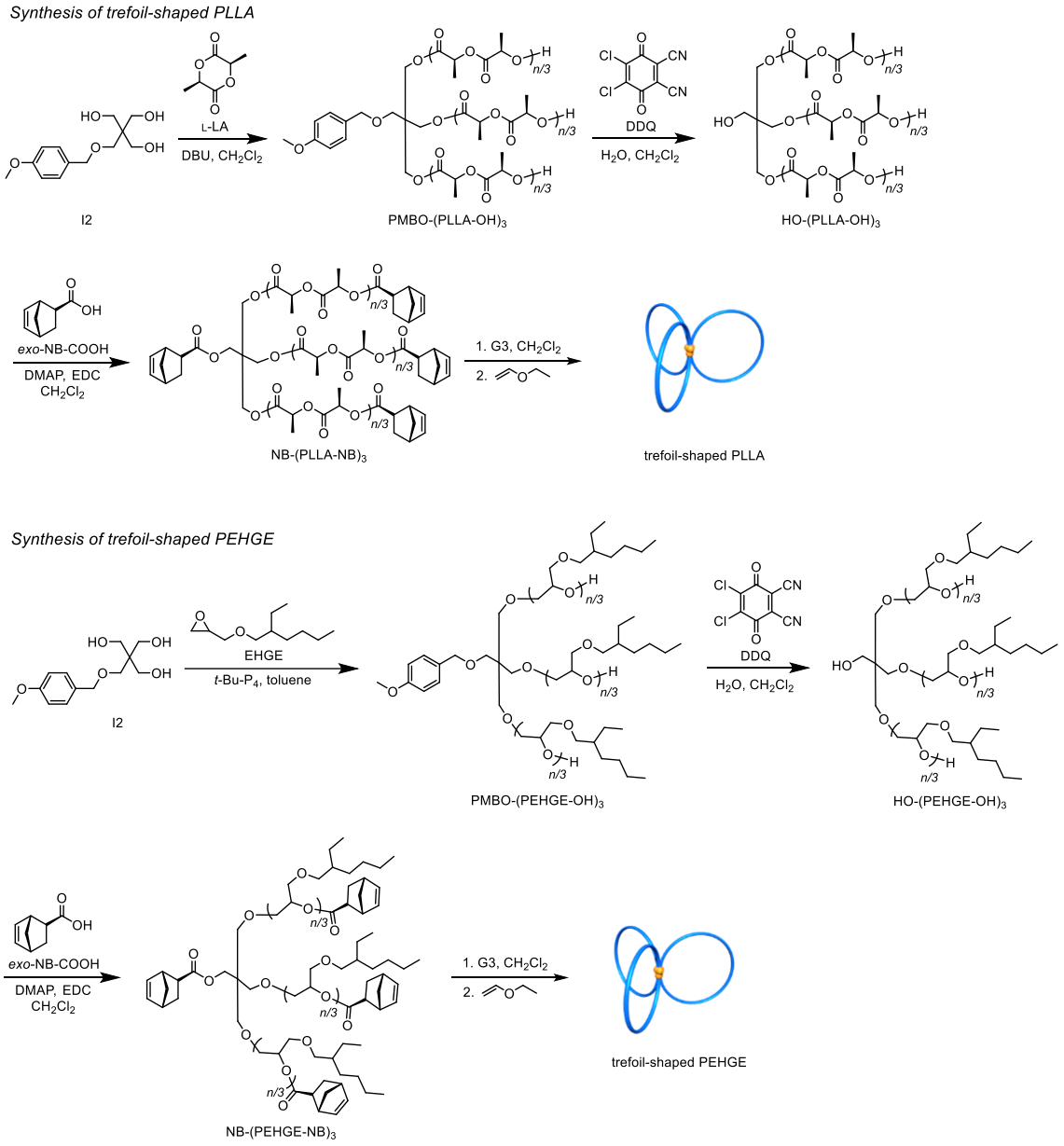

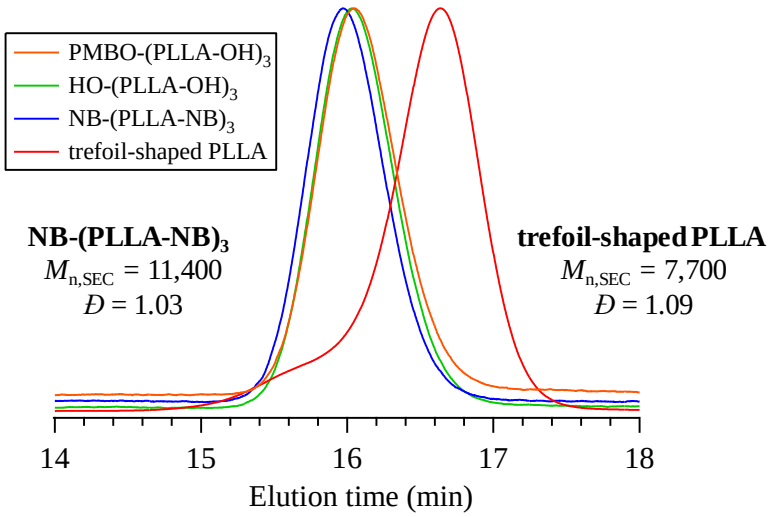

Figure 2.12. SEC traces of PMBO-(PLLA-OH)$_3$ (orange), HO-(PLLA-OH)$_3$ (green), NB-(PLLA-NB)$_3$ (blue) and trefoil-shaped PLLA (red). The amount of shoulder peak in trefoil-shaped PLLA was calculated to be ca. 17.0% by peak deconvolution.

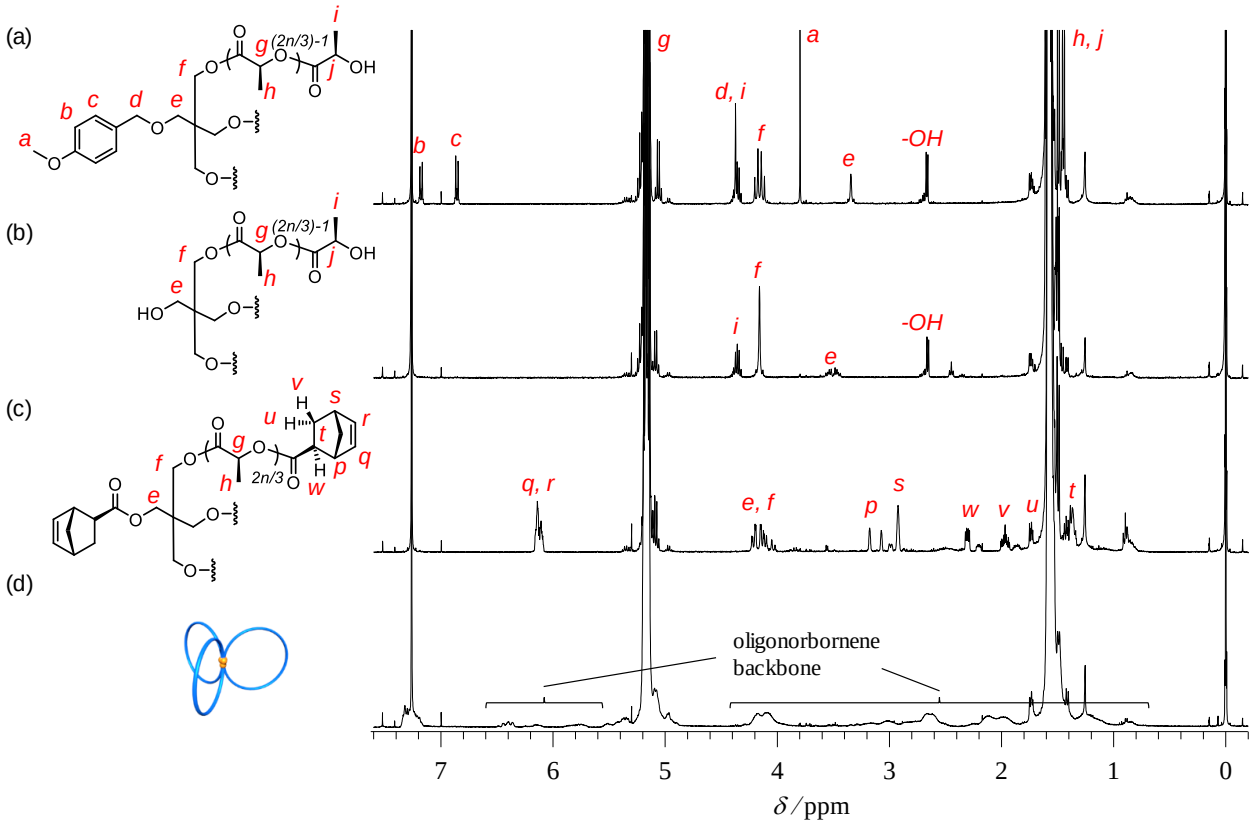

Figure 2.13. ^{1}H NMR spectra of (a) PMBO-(PLLA-OH)$_3$, (b) HO-(PLLA-OH)$_3$, (c) NB-(PLLA-NB)$_3$, and (d) trefoil-shaped PLLA in $CDCl_3$ (400 MHz).

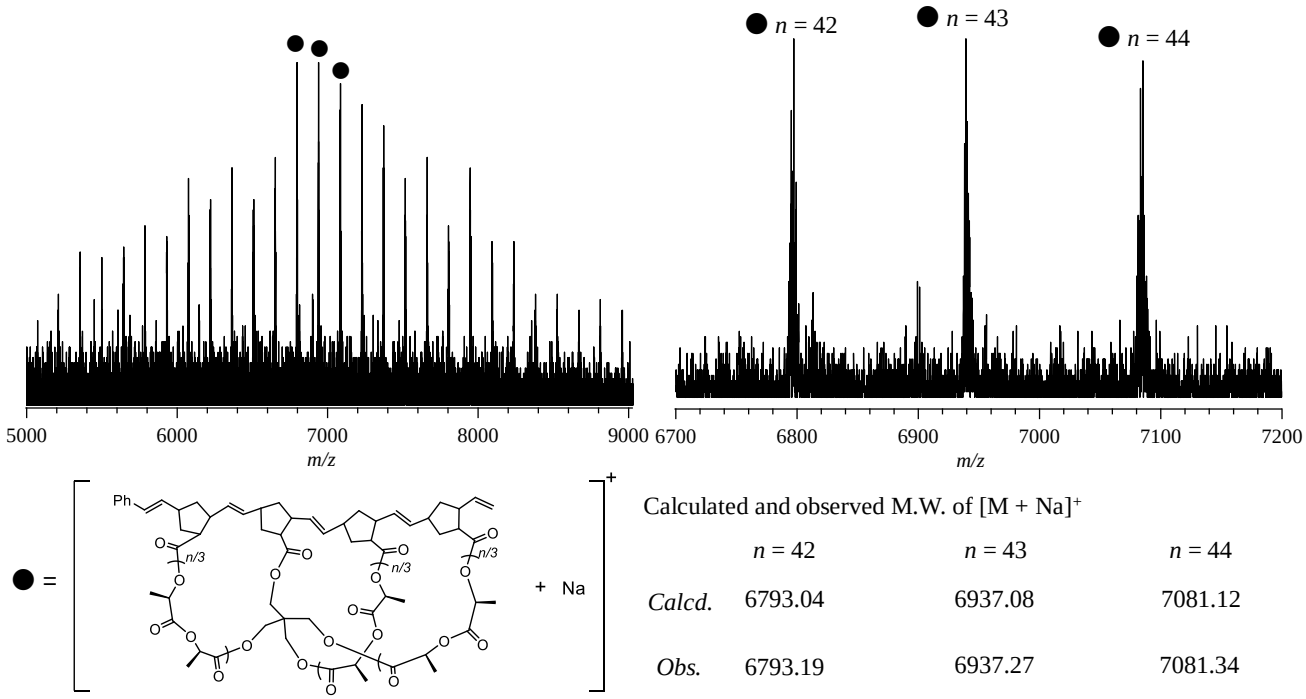

Calculated and observed M.W. of $[M + Na]^+$

	n = 42	n = 43	n = 44
Calcd.	6793.04	6937.08	7081.12
Obs.	6793.19	6937.27	7081.34

Figure 2.14. MALDI-TOF MS analysis of trefoil-shaped PLLA.

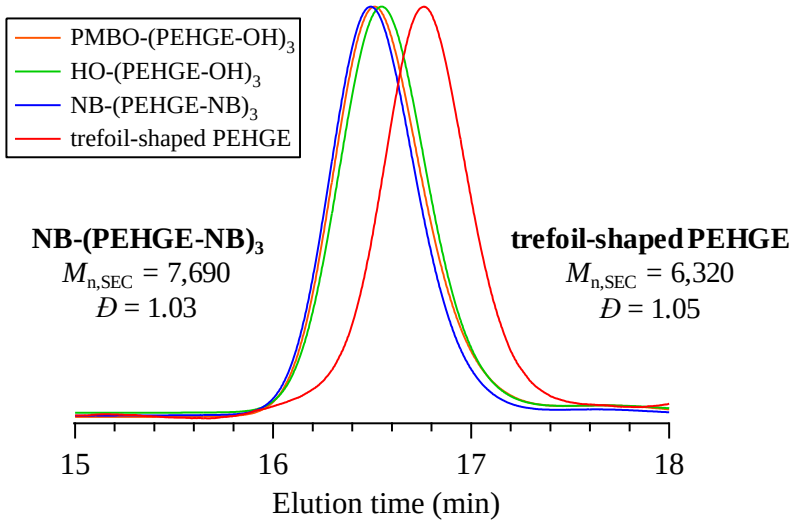

Figure 2.15. SEC traces of PMBO-(PEHGE-OH)$_3$ (orange), HO-(PEHGE-OH)$_3$ (green), NB-(PEHGE-NB)$_3$ (blue) and trefoil-shaped PEHGE (red).

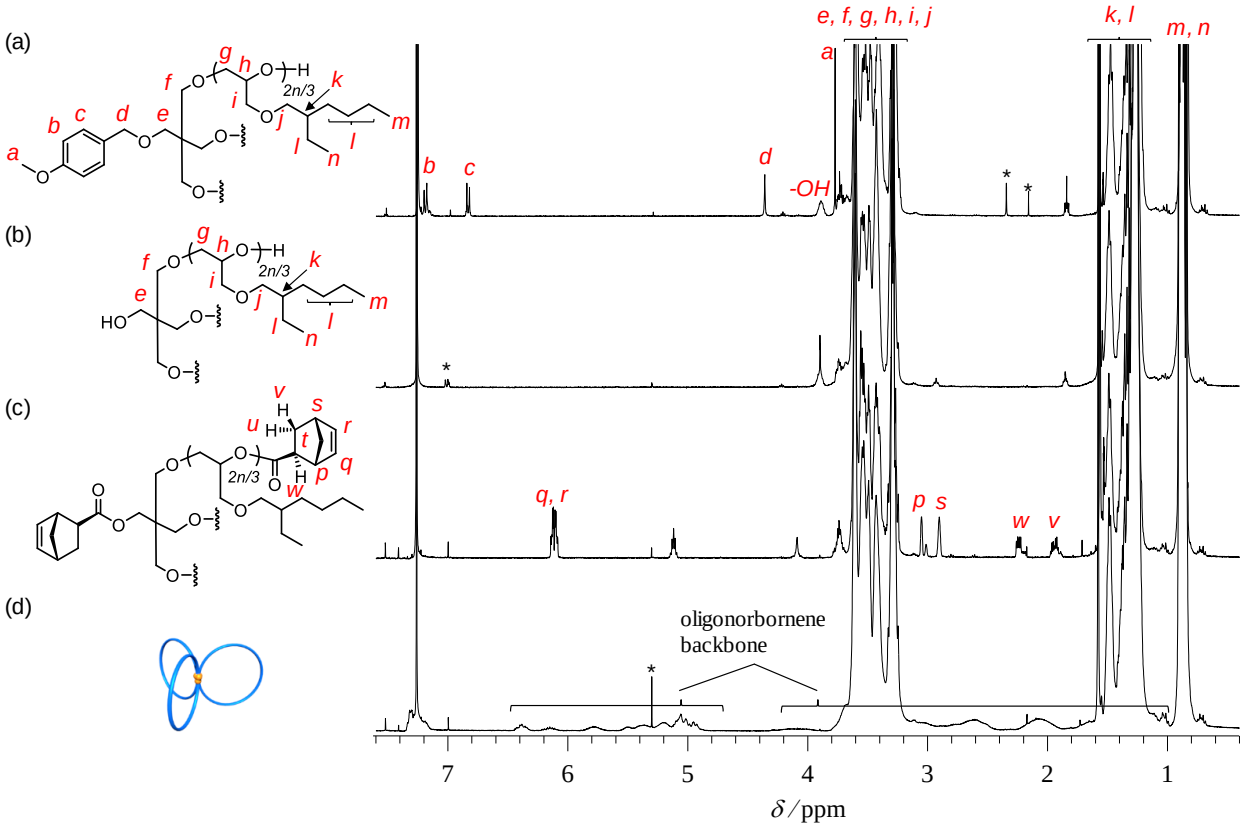

Figure S2.15. ^{1}H NMR spectra of (a) PMBO-(PEHGE-OH)$_3$, (b) HO-(PEHGE-OH)$_3$, (c) NB-(PEHGE-NB)$_3$, and (d) trefoil-shaped PEHGE in $CDCl_3$ (400 MHz).

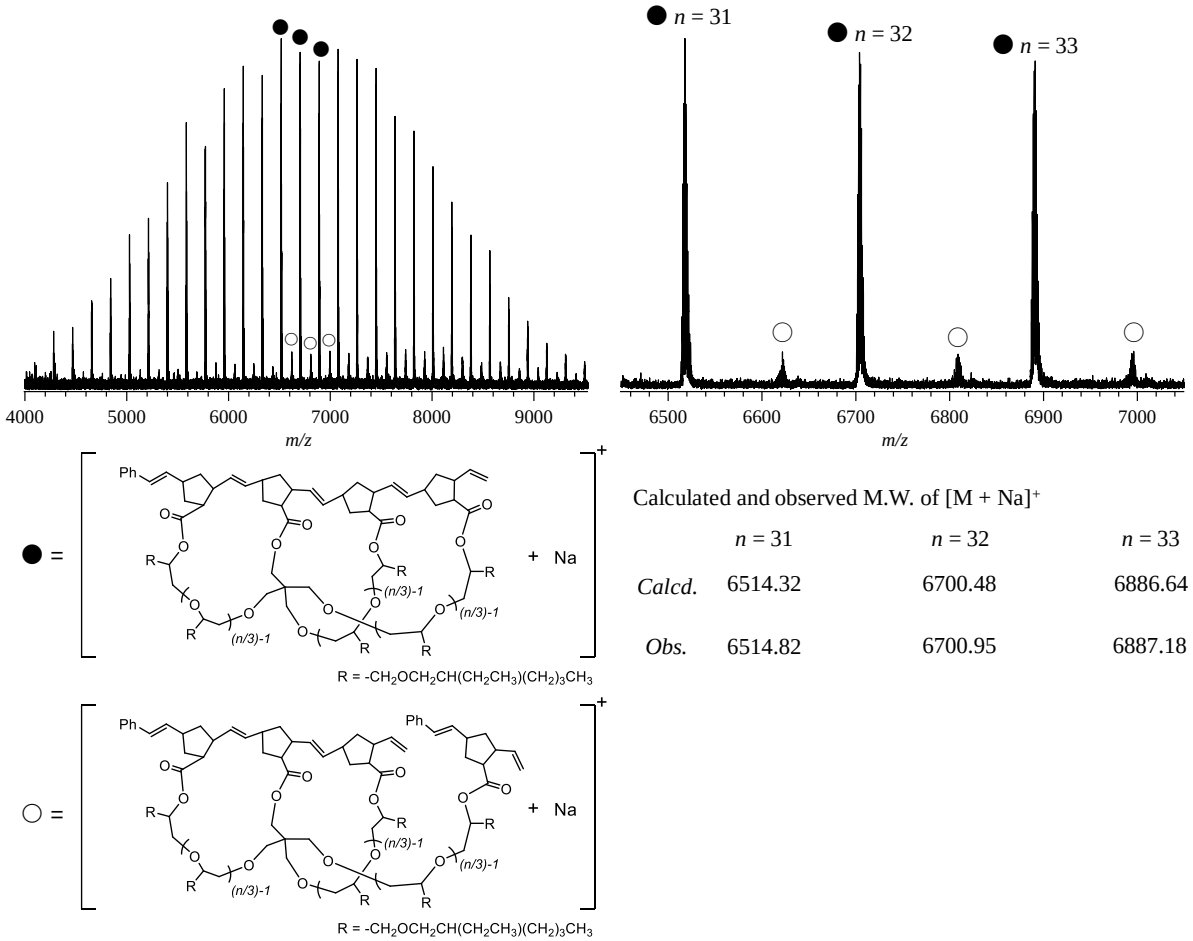

Figure 2.16. MALDI-TOF MS analysis of trefoil-shaped PEHGE. The amount of twin-head tadpole product was approximately calculated to be 11.4% by the ratio of integrated peak heights.

2.3.7 Programmed folding into *spiro*-multicyclic topologies via intramolecular ROMO under different conditions

Here, it is important to note that the present folding strategy affords a polymer with a predetermined topology, as opposed to the synthesis of SCNPs, in which the size and conformation of the resulting product are considerably affected by the solvent quality.[33] To provide a proof-of-concept of the programmed folding, the author performed intramolecular ROMO under different conditions that could affect the polymer chain dimension during the reaction (Figure 2.17). For example, to attain the complicated multicyclic folding of **quatrefoil-shaped PCL-a**, different solvents and/or elevated temperatures were used to determine whether

the folded structure of the resulting product is affected. Notably, the products obtained from the intramolecular ROMO of **Pre$_{quatre}$-a** in CH_2Cl_2/*n*-hexane showed exactly the same peak-top as **quatrefoil-shaped PCL-a** in the SEC, even in the case of *n*-hexane-rich media with up to 60% *n*-hexane (Figure 2.17(c)–(e)), indicating successful folding into the same architecture. By switching the solvent to toluene, successful formation of **quatrefoil-shaped PCL-a** was also observed upon heating (Figure 2.17(f), (g)). Thus, these results suggest that the precursor can be unambiguously folded into the predetermined topology.

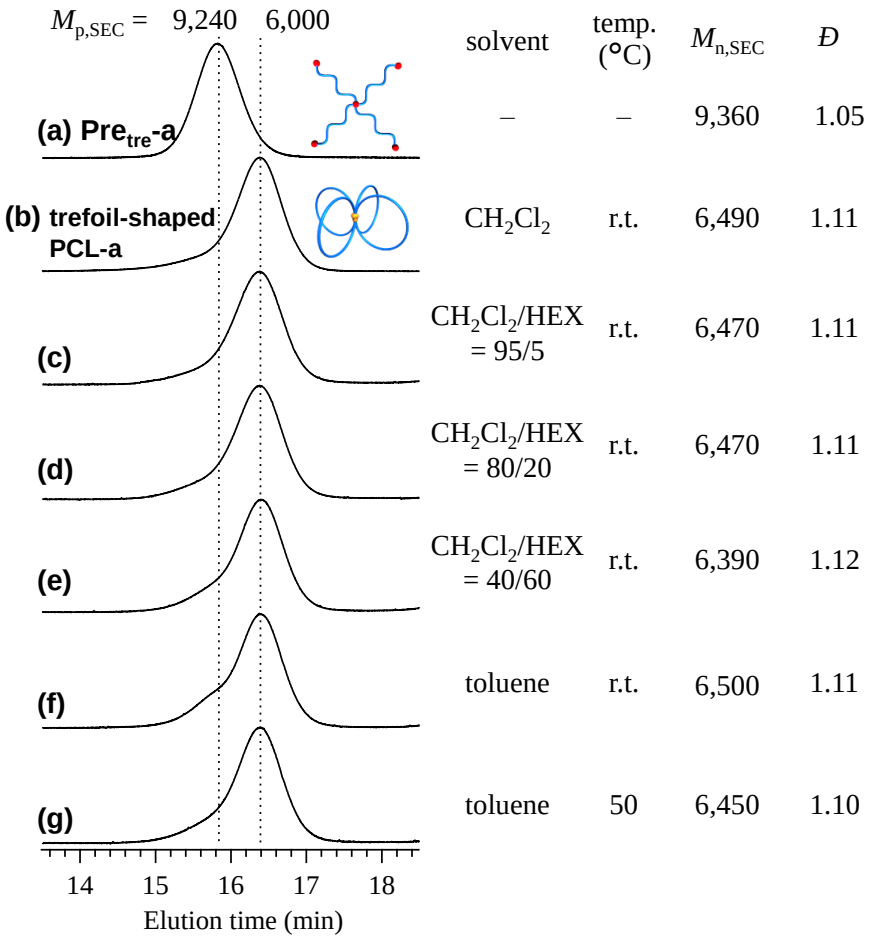

solvent	temp. (°C)	$M_{n,SEC}$	$Đ$
–	–	9,360	1.05
CH_2Cl_2	r.t.	6,490	1.11
CH_2Cl_2/HEX = 95/5	r.t.	6,470	1.11
CH_2Cl_2/HEX = 80/20	r.t.	6,470	1.11
CH_2Cl_2/HEX = 40/60	r.t.	6,390	1.12
toluene	r.t.	6,500	1.11
toluene	50	6,450	1.10

Figure 2.17. Programmed folding from **Pre$_{quatre}$-a** (a) into **quatrefoil-shaped PCL-a** (b) via intramolecular ROMO of the precursor with altered chain dimension induced using poor solvents (CH_2Cl_2/*n*-hexane (HEX); c–e) and variation of temperature in toluene (f–g).

2.3.8 Systematic investigation of structure–property relationships

Hydrodynamic diameter (D_h) and intrinsic viscosity ([η]), which are correlated to the polymer chain dimensions, are good measures to understand the folded polymer structure. To get information about the polymer chain dimensions, the obtained *spiro*-multicyclic PCLs and their related linear and cyclic counterparts were subjected to online SEC measurement combined with light scattering, viscosity, and reflective index detectors (SEC-MALS-Visco) in THF. Note that the previously synthesized linear and monocyclic counterparts with comparable molecular weights were subjected to these analyses for comparison.[34] As shown in Figure 2.18, both the D_h and [η] values decreased in the order of linear > cyclic > 8-shaped-PCL > trefoil-shaped-PCL > quatrefoil-shaped PCL when comparing the topologically different polymers with comparable molecular weights. This demonstrates that the polymer chain dimensions decrease with increasing number of cyclic units when the total molecular weight remains the same. Such a trend matches very well with the theoretically predicted one; the radius of gyration decreased in the same order as reported by Deguchi et al.[35] Interestingly, the aforementioned [η] values of *spiro*-multicyclic polymers were smaller than those of the topologically related cage-shaped PCLs (7.4–27.7 $mg \cdot mL^{-1}$ for cyclic, three-arm cage-shaped, and four-arm cage-shaped).[18] The *spiro*-multicyclic polymer is assumed to be a topological analog of the cage-shaped polymer, whereby an additional constraint at the focal point of the *spiro*-multicyclic polymer exists, further decreasing the chain dimension.

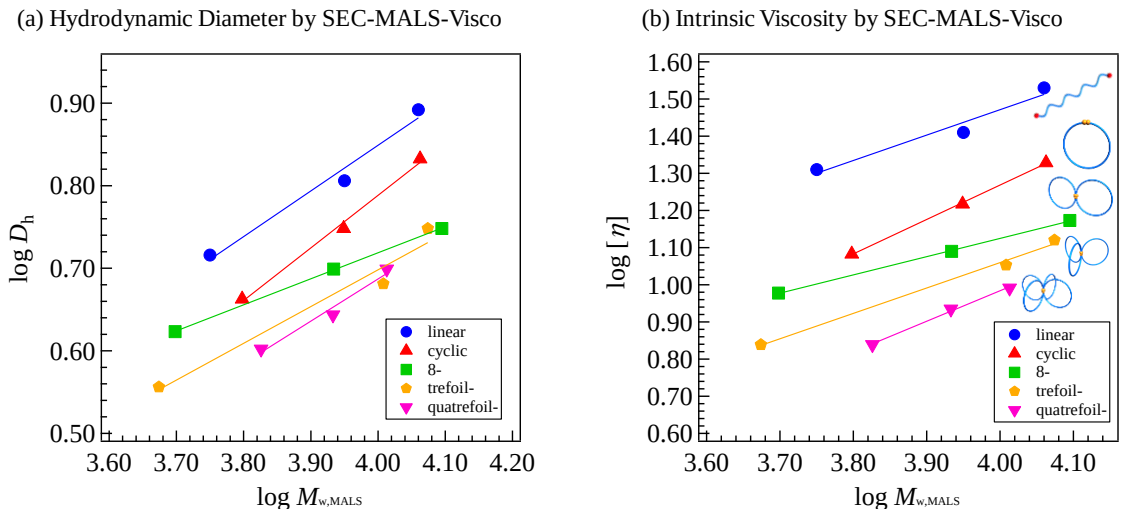

Figure 2.18. Double logarithmic plots of $M_{w,MALS}$ versus (a) D_h and (b) [η] for linear, monocyclic, 8-, trefoil-, and quatrefoil-shaped polymers (eluent, THF).

While the solution properties are important for understanding the folded structure, understanding the bulk state properties also provides new insight into topological effects. Initially, the author performed thermogravimetric analysis (TGA) for the *spiro*-multicyclic PCLs with $M_{n,NMR}$ of ~6,000 g mol^{-1} to examine the structure–thermal degradation relationship. The TGA results revealed a negligible difference in the degradation temperature (T_d) for 10% weight loss among the *spiro*-type multicyclic PCLs and the corresponding linear and cyclic counterparts (384–390 °C), which suggested that the polymer topology has no significant impact on the thermal degradation of PCL (See Figure S2.10 and Table S2.6). A similar conclusion was drawn in a previous report by Grayson, in which a cyclic PCL and its precursor were compared.[36] Among a number of cyclic polymers reported thus far, cyclic PCLs have been a target of investigation to understand the effect of cyclic topology on polymer crystallization behavior (*e.g.*, melting point, crystallite size, crystallinity, and crystallization kinetics). For example, Ree and Saalwächter groups reported the cyclic PCLs have higher melting point and crystallinity than their linear counterparts, albeit the reason remains unclear.[37–39] With a series of well-defined *spiro*-type PCLs in hand, the auth thus investigated the melting temperature

(T_m) and crystallinity (X_{WAXD}) using differential scanning calorimetry (DSC) and wide-angle X-ray diffraction (WAXD), respectively. Note that synthesized linear and monocyclic PCLs with comparable molecular weight were subjected to these analyses for comparison. Figure 2.19 shows the T_m and X_{WAXD} for each architecture, which seem to correlate with both the number of cyclic units and total molecular weight. The important finding here is that 8-shaped PCLs exhibit higher melting points and crystallinity than cyclic PCLs (Figure 2.19(a), (b)). More specifically, **8-shaped PCL-a** with molecular weight of ~6,000 g mol^{-1} exhibited dramatically enhanced T_m (53.8 °C) and X_{WAXD} (41.8%) compared with its linear and cyclic counterparts (T_m = 43.2–51.1 °C and X_{WAXD} = 35.2–40.3%). This can be explained by the topological confinement of the non-crystallizable segments (Figure 2.20). The non-crystallizable segments, such as the initiator moiety and oligonorbornene backbone in the cyclic PCL have mobility, which suppresses the ordered packing of the PCL chains, resulting in lesser crystallization ability. However, the initiator moiety and oligonorbornene backbone in the 8-shaped PCL are all constrained at the focal point, which successfully reduces the random placing of non-crystallizable segments, thus resulting in better crystallization ability. Further increase in the number of cyclic units in **trefoil-shaped PCL** and **quatrefoil-shaped PCL** apparently lowers the T_m and crystallinity. This can be attributed to suppressed molecular mobility and chain-packing ability due to strong constraints induced with increasing the number of arms. Small-angle X-ray scattering (SAXS) further supports this unique trend in lamellae thickness that appears to be correlated with T_m, while the long period (~12 nm) exhibits almost no change (see Note in SI and Figure S2.11), which is consistent with a previous report.[40] Compared to its counterparts, **8-shaped PCL-b** showed the longest lamellae thickness of 5.1 nm, which is approximately 25% of the theoretical extended length of 20 nm for each of its arms. This suggests that the *spiro*-type topological chain is likely further folded in the crystalline domain multiple times.

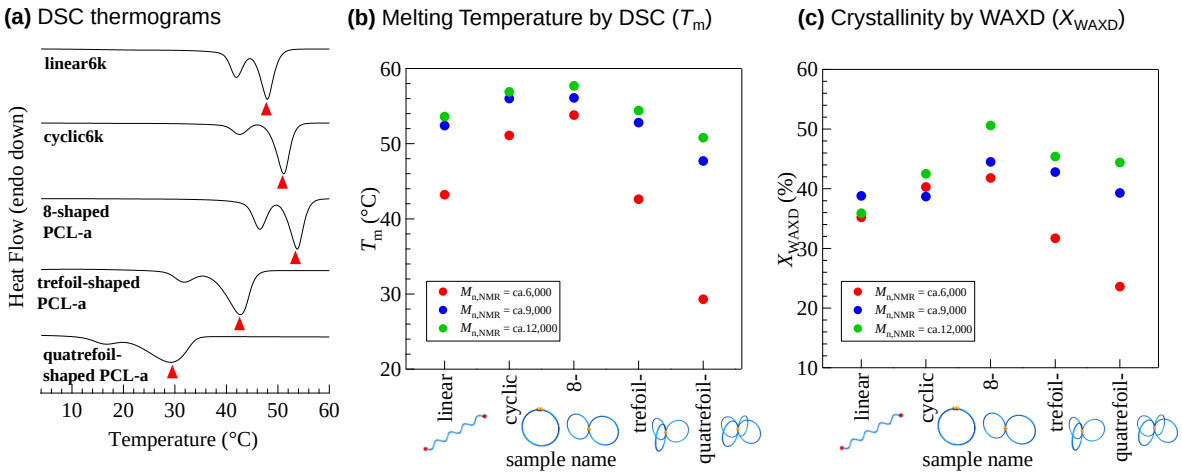

Figure 2.19. (a) DSC thermograms during the 2nd heating of the multicyclic polymers (**8-shaped PCL-a**, **trefoil-shaped PCL-a**, and **quatrefoil-shaped PCL-a**) and their counterparts with molecular weights of ~6,000 g mol^{-1}. The melting temperature (T_m) was determined as the peak-top of the transition marked with a triangle. (b and c) Plots of T_m and X_{WAXD} for the linear, monocyclic and multicyclic polymers (**8-shaped PCL**s, **trefoil-shaped PCL**s, and **quatrefoil-shaped PCL**s) with different molecular weights.

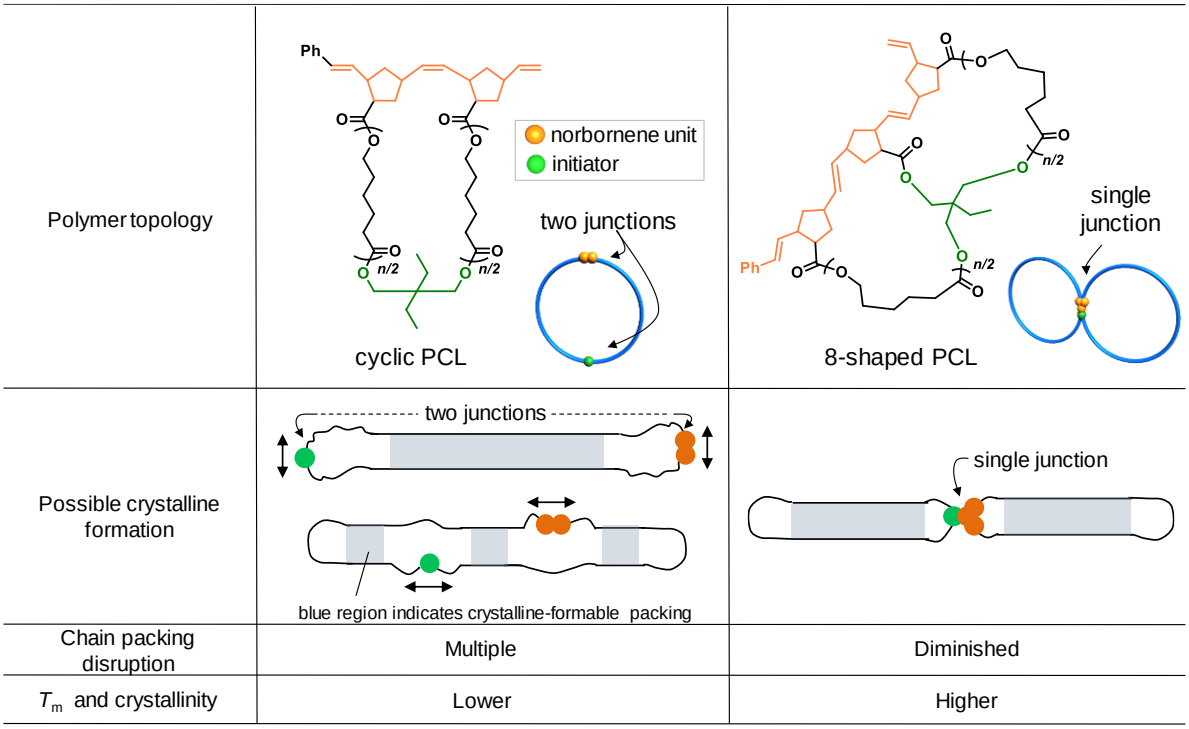

Figure 2.20. Illustration of proposed packing structure for the crystalline formation of cyclic PCL (left column) and **8-shaped PCL**s (right column).

2.4 Conclusion

The author has successfully established a robust and versatile synthetic strategy for *spiro*-multicyclic polymers based on the intramolecular consecutive ROMO of the highly reactive norbornenyl groups attached to linear and star-shaped polymer precursors with norbornenyl group at the chain center and each end. With the present strategy, diverse *spiro*-type multicyclic topologies with different amounts of cyclic units and total molecular weight were successfully constructed, demonstrating the versatility of this strategy as an effective means to synthesize topological polymers. Remarkably, this comprehensive study on the structure–property relationships of the folded PCLs revealed enhanced crystallization ability in the 8-shaped topology. Polymer folding into a *spiro*-type topology plays a crucial role in rendering higher-ordered functions to biomacromolecules. Furthermore, the results of this study can be applied to other polymer species for the development of bio-inspired materials with specific 3D nanostructures.

2.5 References

(1) Teif, V. B.; Bohinc, K. Condensed DNA: Condensing the Concepts. *Prog. Biophys. Mol. Biol.* **2011**, *105*, 208–222.

(2) Seeman, N. C. DNA in a Material World. *Nature* **2003**, *421*, 427–431.

(3) Craik, D. J. Seamless Proteins Tie Up Their Loose Ends. *Science.* **2006**, *311*, 1563–1564.

(4) Ouchi, M.; Badi, N.; Lutz, J. F.; Sawamoto, M. Single-Chain Technology Using Discrete Synthetic Macromolecules. *Nat. Chem.* **2011**, *3*, 917–924.

(5) Gonzalez-Burgos, M.; Latorre-Sanchez, A.; Pomposo, J. A. Advances in Single Chain Technology. *Chem. Soc. Rev.* **2015**, *44*, 6122–6142.

(6) Tezuka, Y. Topological Polymer Chemistry Designing Complex Macromolecular Graph Constructions. *Acc. Chem. Res.* **2017**, *50*, 2661–2672.

(7) Harth, E.; Van Horn, B.; Lee, V. Y.; Germack, D. S.; Gonzales, C. P.; Miller, R. D.; Hawker, C. J. A Facile Approach to Architecturally Defined Nanoparticles via Intramolecular Chain Collapse. *J. Am. Chem. Soc.* **2002**, *124*, 8653–8660.

(8) Foster, E. J.; Berda, E. B.; Meijer, E. W. Metastable Supramolecular Polymer Nanoparticles via Intramolecular Collapse of Single Polymer Chains. *J. Am. Chem. Soc.* **2009**, *131*, 6964–6966.

(9) Polymeropoulos, G.; Zapsas, G.; Ntetsikas, K.; Bilalis, P.; Gnanou, Y.; Hadjichristidis, N. 50th Anniversary Perspective: Polymers with Complex Architectures. *Macromolecules* **2017**, *50*, 1253–1290.

(10) Laurent, B. A.; Grayson, S. M. Synthetic Approaches for the Preparation of Cyclic Polymers. *Chem. Soc. Rev.* **2009**, *38*, 2202–2213.

(11) Zhang, K.; Lackey, M. A.; Cui, J.; Tew, G. N. Gels Based on Cyclic Polymers. *J. Am. Chem. Soc.* **2011**, *133*, 4140–4148.

(12) Honda, S.; Yamamoto, T.; Tezuka, Y. Topology-Directed Control on Thermal Stability: Micelles Formed from Linear and Cyclized Amphiphilic Block Copolymers. *J. Am. Chem. Soc.* **2010**, *132*, 10251–10253.

(13) Yamamoto, T.; Tezuka, Y. Topological Polymer Chemistry: A Cyclic Approach toward Novel Polymer Properties and Functions. *Polym. Chem.* **2011**, *2*, 1930–1941.

(14) Oike, H.; Imaizumi, H.; Mouri, T.; Yoshioka, Y.; Uchibori, A.; Tezuka, Y. Designing Unusual Polymer Topologies by Electrostatic Self-Assembly and Covalent Fixation. *J. Am. Chem. Soc.* **2000**, *122*, 9592–9599.

(15) Hossain, M. D.; Reid, J. C.; Lu, D.; Jia, Z.; Searles, D. J.; Monteiro, M. J. Influence of Constraints within a Cyclic Polymer on Solution Properties. *Biomacromolecules* **2018**, *19*, 616–625.

(16) Pipertzis, A.; Hossain, M. D.; Monteiro, M. J.; Floudas, G. Segmental Dynamics in Multicyclic Polystyrenes. *Macromolecules* **2018**, *51*, 1488–1497.

(17) Choi, T. L.; Grubbs, R. H. Controlled Living Ring-Opening-Metathesis Polymerization by a Fast-Initiating Ruthenium Catalyst. *Angew. Chem. Int. Ed.* **2003**, *42*, 1743–1746.

(18) Satoh, Y.; Matsuno, H.; Yamamoto, T.; Tajima, K.; Isono, T.; Satoh, T. Synthesis of Well-Defined Three- and Four-Armed Cage-Shaped Polymers via "Topological Conversion" from Trefoil- and Quatrefoil-Shaped Polymers. *Macromolecules* **2017**, *50*, 97–106.

(19) Saha, B.; Choudhury, N.; Seal, S.; Ruidas, B.; De, P. Aromatic Nitrogen Mustard-Based Autofluorescent Amphiphilic Brush Copolymer as PH-Responsive Drug Delivery Vehicle. *Biomacromolecules* **2019**, *20*, 546–557.

(20) Ko, Y. S.; Yamamoto, T.; Tezuka, Y. Click Construction of Spiro- and Bridged-Quatrefoil Polymer Topologies with Kyklo-Telechelics Having an Azide Group. *Macromol. Rapid Commun.* **2014**, *35*, 412–416.

(21) Schmidt, B. V. K. J.; Fechler, N.; Falkenhagen, J.; Lutz, J. F. Controlled Folding of Synthetic Polymer Chains through the Formation of Positionable Covalent Bridges. *Nat. Chem.* **2011**, *3*, 234–238.

(22) Isono, T.; Kamoshida, K.; Satoh, Y.; Takaoka, T.; Sato, S. I.; Satoh, T.; Kakuchi, T. Synthesis of Star- and Figure-Eight-Shaped Polyethers by t -Bu-P 4-Catalyzed Ring-Opening Polymerization of Butylene Oxide. *Macromolecules* **2013**, *46*, 3841–3849.

(23) Oike, H.; Hamada, M.; Eguchi, S.; Danda, Y.; Tezuka, Y. Novel Synthesis of Single- and Double-Cyclic Polystyrenes by Electrostatic Self-Assembly and Covalent Fixation with Telechelics Having Cyclic Ammonium Salt Groups. *Macromolecules* **2001**, *34*, 2776–2782.

(24) Antonietti, M.; Folsch, K. J. Synthesis and Characterization of "Eight-Shaped" Polystyrene. *Makromol. Chem., Rapid Commun.* **1988**, *9*, 423–430.

(25) Kyoda, K.; Yamamoto, T.; Tezuka, Y. Programmed Polymer Folding with Periodically Positioned Tetrafunctional Telechelic Precursors by Cyclic Ammonium Salt Units as Nodal Points. *J. Am. Chem. Soc.* **2019**, *141*, 7526–7536.

(26) Hilf, S.; Kilbinger, A. F. M. Functional End Groups for Polymers Prepared Using Ring-Opening Metathesis Polymerization. *Nat. Chem.* **2009**, *1*, 537–546.

(27) Bielawski, C. W.; Benitez, D.; Morita, T.; Grubbs, R. H. Synthesis of End-Functionalized Poly(norbornene)s via Ring-Opening Metathesis Polymerization. *Macromolecules* **2001**, *34*, 8610–8618.

(28) Morgese, G.; Shirmardi Shaghasemi, B.; Causin, V.; Zenobi-Wong, M.; Ramakrishna, S. N.; Reimhult, E.; Benetti, E. M. Next-Generation Polymer Shells for Inorganic Nanoparticles Are Highly Compact, Ultra-Dense, and Long-Lasting Cyclic Brushes. *Angew. Chem. Int. Ed.* **2017**, *56*, 4507–4511.

(29) Ramakrishna, S. N.; Morgese, G.; Zenobi-Wong, M.; Benetti, E. M. Comblike Polymers with Topologically Different Side Chains for Surface Modification: Assembly Process

and Interfacial Physicochemical Properties. *Macromolecules* **2019**, *52*, 1632–1641.

(30) Morgese, G.; Cavalli, E.; Rosenboom, J. G.; Zenobi-Wong, M.; Benetti, E. M. Cyclic Polymer Grafts That Lubricate and Protect Damaged Cartilage. *Angew. Chem. Int. Ed.* **2018**, *57* (6), 1621–1626. https://doi.org/10.1002/anie.201712534.

(31) Brown, H. A.; De Crisci, A. G.; Hedrick, J. L.; Waymouth, R. M. Amidine-Mediated Zwitterionic Polymerization of Lactide. *ACS Macro Lett.* **2012**, *1* (9), 1113–1115.

(32) Misaka, H.; Tamura, E.; Makiguchi, K.; Kamoshida, K.; Sakai, R.; Satoh, T.; Kakuchi, T. Synthesis of End-Functionalized Polyethers by Phosphazene Base-Catalyzed Ring-Opening Polymerization of 1,2-Butylene Oxide and Glycidyl Ether. *J. Polym. Sci. Part*

(33) Watanabe, K.; Tanaka, R.; Takada, K.; Kim, M. J.; Lee, J. S.; Tajima, K.; Isono, T.; Satoh, T. Intramolecular Olefin Metathesis as a Robust Tool to Synthesize Single-Chain Nanoparticles in a Size-Controlled Manner. *Polym. Chem.* **2016**, *7*, 4782–4792.

(34) Mato, Y.; Honda, K.; Tajima, K.; Yamamoto, T.; Isono, T.; Satoh, T. A Versatile Synthetic Strategy for Macromolecular Cages: Intramolecular Consecutive Cyclization of Star-Shaped Polymers. *Chem. Sci.* **2019**, *10*, 440–446.

(35) Uehara, E.; Deguchi, T. Mean-Square Radius of Gyration and the Hydrodynamic Radius for Topological Polymers Expressed with Graphs Evaluated by the Method of Quaternions Revisited. *React. Funct. Polym.* **2018**, *133*, 93–102.

(36) Hoskins, J. N.; Grayson, S. M. Synthesis and Degradation Behavior of Cyclic Poly(ε-Caprolactone). *Macromolecules* **2009**, *42*, 6406–6413.

(37) Shin, E. J.; Jeong, W.; Brown, H. A.; Koo, B. J.; Hedrick, J. L.; Waymouth, R. M. Crystallization of Cyclic Polymers: Synthesis and Crystallization Behavior of High Molecular Weight Cyclic Poly(ε-Caprolactone)S. *Macromolecules* **2011**, *44*, 2773–2779.

(38) Schäler, K.; Ostas, E.; Schröter, K.; Thurn-Albrecht, T.; Binder, W. H.; Saalwächter, K. Influence of Chain Topology on Polymer Dynamics and Crystallization. Investigation of Linear and Cyclic Poly(ε-Caprolactone)s by 1H Solid-State NMR Methods. *Macromolecules* **2011**, *44*, 2743–2754.

(39) Li, X.; Ryu, W.; Kim, H.; Ree, M. Precise Synthesis, Properties, and Structures of Cyclic Poly(ε-Caprolactone)s. **2018**, *10*, 577.

(40) Takizawa, K.; Tang, C.; Hawker, C. J. Molecularly Defined Caprolactone Oligomers and Polymers: Synthesis and Characterization. *J. Am. Chem. Soc.* **2008**, *130*, 1718–1726.

(41) Strobl, G. R.; Schneider, M. Direct Evaluation of the Electron Density Correlation Function of Partially Crystalline Polymers. *J. Polym. Sci. Part A-2, Polym. Phys.* **1980**, *18*, 1343–1359.

(42) Isono, T.; Miyachi, K.; Satoh, Y.; Nakamura, R.; Zhang, Y.; Otsuka, I.; Tajima, K.; Kakuchi, T.; Borsali, R.; Satoh, T. Self-Assembly of Maltoheptaose-Block-Polycaprolactone Copolymers: Carbohydrate-Decorated Nanoparticles with Tunable

Morphology and Size in Aqueous Media. *Macromolecules* **2016**, *49*, 4178–4194.

2.6 Supporting Information

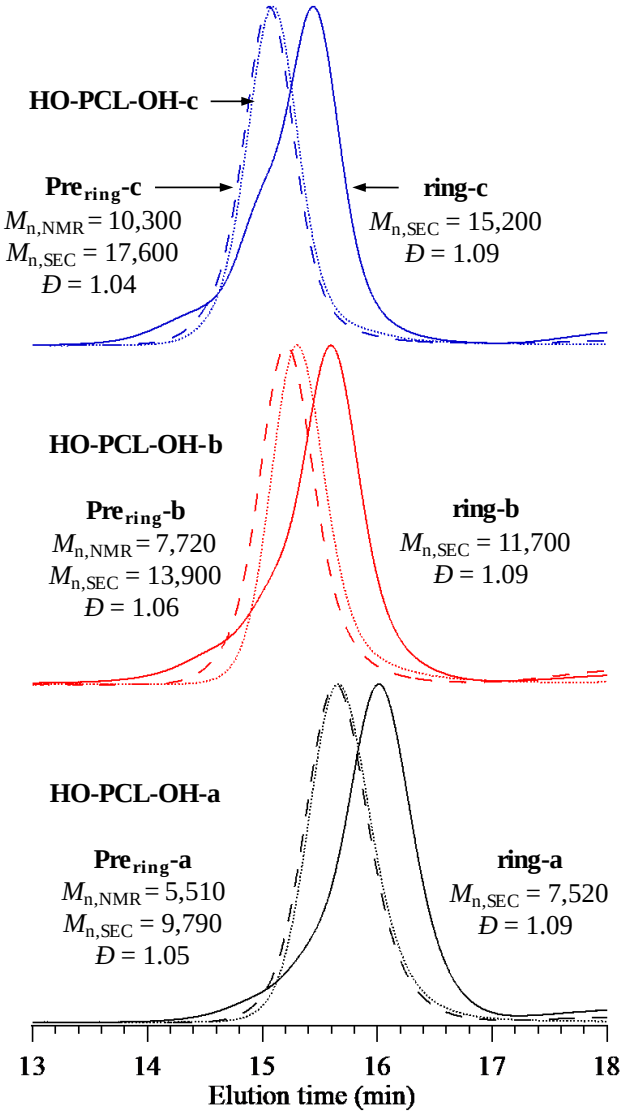

Figure S2.1. SEC traces of **HO-PCL-OH**s (dashed line), **Pre$_{ring}$**s (dotted line), and **ring**s (solid line) with different molecular weight.

Table S2.1. Molecular characterization of cyclic PCLs (**ring**) and their precursors

Sample	$M_{n,NMR}$ [a]	$M_{n,SEC}$ [b]	$M_{w,MALS}$ [c]	$Đ$ [b]	yield (%)	D_h [c] (nm)	$[\eta]$ [c] (mL g^{-1})	T_m [d] (°C)	X_{WAXD} [e] (%)	L_{ac} [f] (nm)	L_c/L_{ac} [f] (%)
HO-PCL-OH-a	4,890	9,620	-	1.06	65.3	-	-	-	-	-	-
Pre_{ring}-a	5,510	9,790	5,590	1.05	61.0	5.2	17.5	43.2	35.2	11.1	39.7
ring-a	-	7,520	6,280	1.09	92.3	4.6	11.3	51.1	40.3	11.0	38.5
HO-PCL-OH-b	7,480	13,400	-	1.05	73.3	-	-	-	-	-	-
Pre_{ring}-b	7,720	13,900	8,040	1.06	72.6	6.4	22.4	52.4	38.8	11.1	41.7
ring-b	-	11,700	8,900	1.09	92.3	5.8	15.8	56.0	38.7	11.0	43.1
HO-PCL-OH-c	10,800	17,300	-	1.05	86.0	-	-	-	-	-	-
Pre_{ring}-c	10,300	17,600	11,500	1.04	87.0	7.4	27.7	53.6	35.9	11.2	40.4
ring-c	-	15,200	11,600	1.07	91.6	6.8	18.8	56.9	42.5	N.D.[g]	N.D.[g]

[a] Determined by ^{1}H NMR. [b] Determined by SEC in THF using PSt standards. [c] Determined by SEC-MALS-Visco in THF. $D_h = 2\ R_h = 2(3V_h/4\pi)^{1/3}$; V_h is hydrodynamic volume. V_h was calculated by Einstein–Simha equation ($V_h = M_{w,MALS}[\eta]/2.5N_A$; N_A: Avogadro's number). [d] Determined from a melting peak of the DSC curve. [e] Determined by WAXD at r.t. [f] Determined by SAXS at r.t. [g] Not determined.

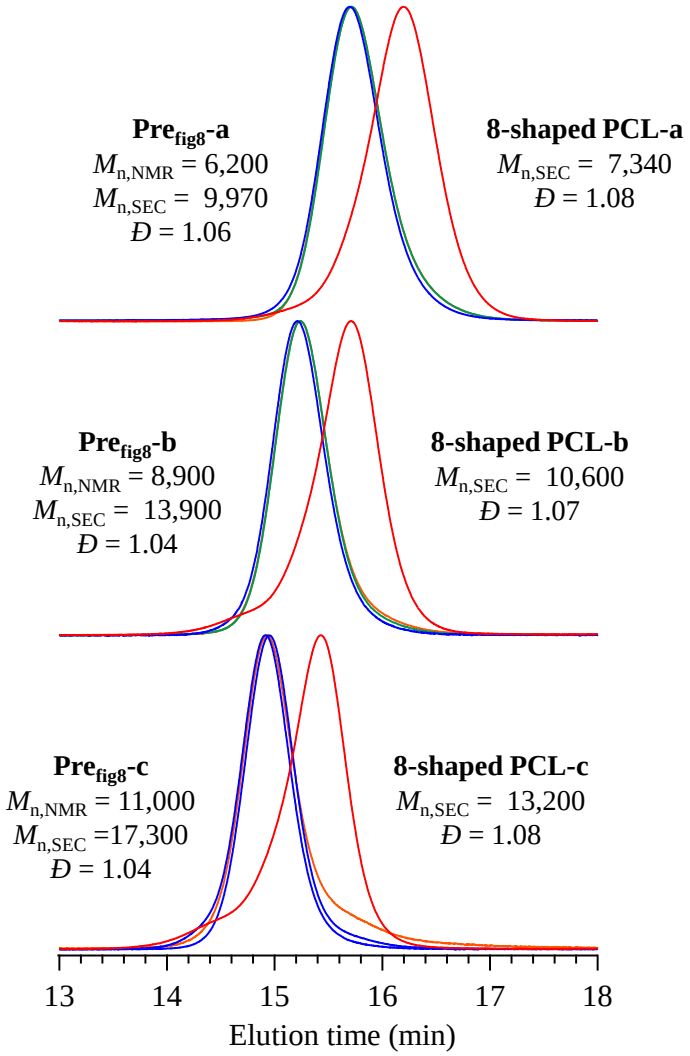

Figure S2.2 SEC traces of PMBO-(PCL-OH)$_2$s (orange), HO-(PCL-OH)$_2$s (green), **Pre$_{fig8}$**s (blue) and **8-shaped PCL**s (red) with different molecular weight.

Table S2.2. Molecular characterization of **8-shaped PCL** s and their precursors

Sample	$M_{n,NMR}$ [a]	$M_{n,SEC}$ [b]	$M_{w,MALS}$ [c]	$Đ$ [b]	yield (%)	D_h [c] (nm)	$[\eta]$ [c] (mL g^{-1})	T_m [d] (°C)	X_{WAXD} [e] (%)
PMBO-(PCL-OH)$_2$-a	5,670	9,640	-	1.06	89.3	-	-	-	-
HO-(PCL-OH)$_2$-a	5,650	9,690	-	1.06	52.0	-	-	-	-
Pre$_{fig8}$-a	6,200	9,970	6,210	1.06	55.3	5.0	18.3	47.9	45.1
8-shaped PCL-a	-	7,340	5,190	1.08	91.0	4.2	9.5	53.8	41.8
PMBO-(PCL-OH)$_2$-b	8,000	13,400	-	1.04	88.1	-	-	-	-
HO-(PCL-OH)$_2$-b	7,900	13,500	-	1.04	64.4	-	-	-	-
Pre$_{fig8}$-b	8,900	13,900	6,940	1.04	76.2	5.8	22.1	51.4	45.2
8-shaped PCL-b	-	10,600	8,770	1.07	89.7	5.0	12.3	56.1	44.5
PMBO-(PCL-OH)$_2$-c	10,600	15,700	-	1.07	63.3	-	-	-	-
HO-(PCL-OH)$_2$-c	10,600	16,600	-	1.04	81.8	-	-	-	-
Pre$_{fig8}$-c	11,000	17,300	9,810	1.04	70.0	6.6	26.5	52.8	40.3
8-shaped PCL-c	-	13,200	12,700	1.08	86.7	5.6	14.9	57.7	50.6

[a] Determined by ^{1}H NMR. [b] Determined by SEC in THF using PSt standards. [c] Determined by SEC-MALS-Visco in THF. [d] Determined from a melting peak of the DSC curve. [e] Determined by WAXD at r.t..

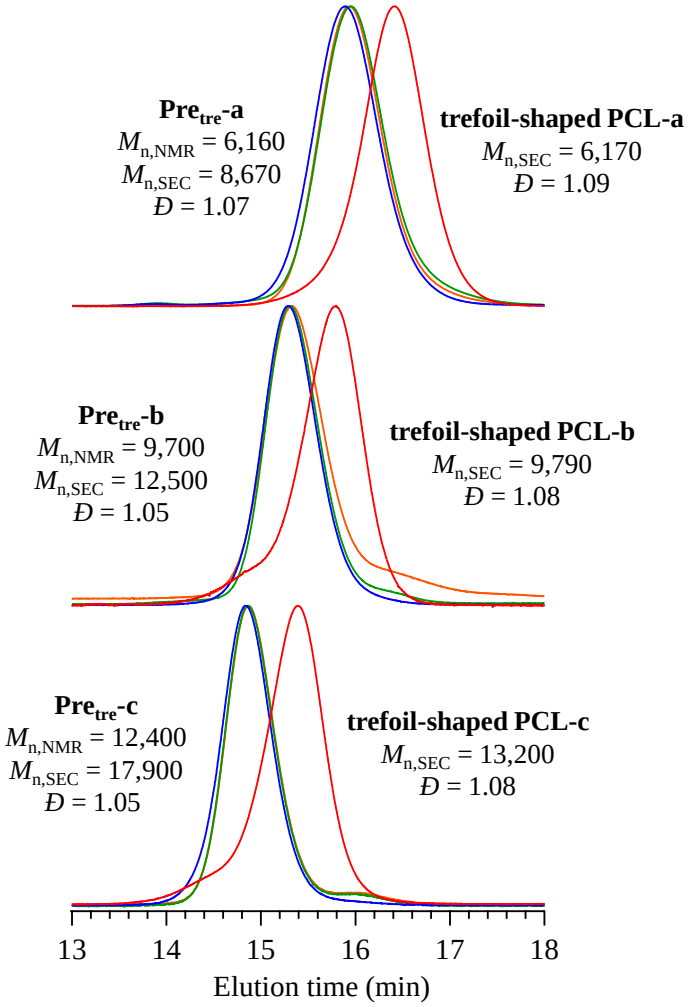

Figure S2.3. SEC traces of PMBO-(PCL-OH)$_3$s (orange), HO-(PCL-OH)$_3$s (green), **Pre$_{fig8}$s** (blue) and **trefoil-shaped PCL**s (red) with different molecular weight.

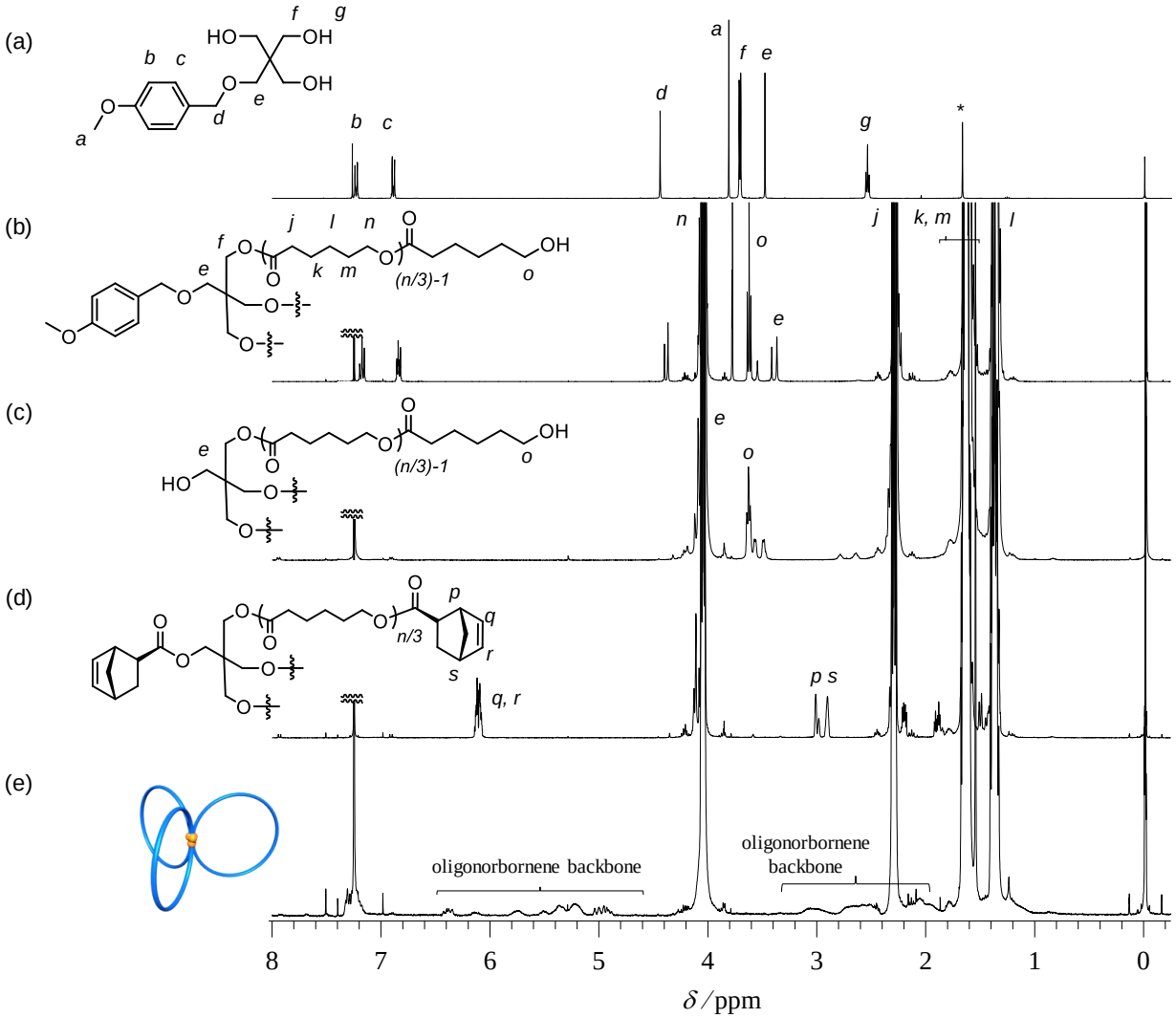

Figure S2.4. ^{1}H NMR spectra of (a) **I2**, (b) PMBO-(PCL-OH)$_3$, (c) HO-(PCL-OH)$_3$, (d) **Pre$_{tre}$-a**, and (e) **trefoil-shaped PCL-a** in $CDCl_3$ (400 MHz).

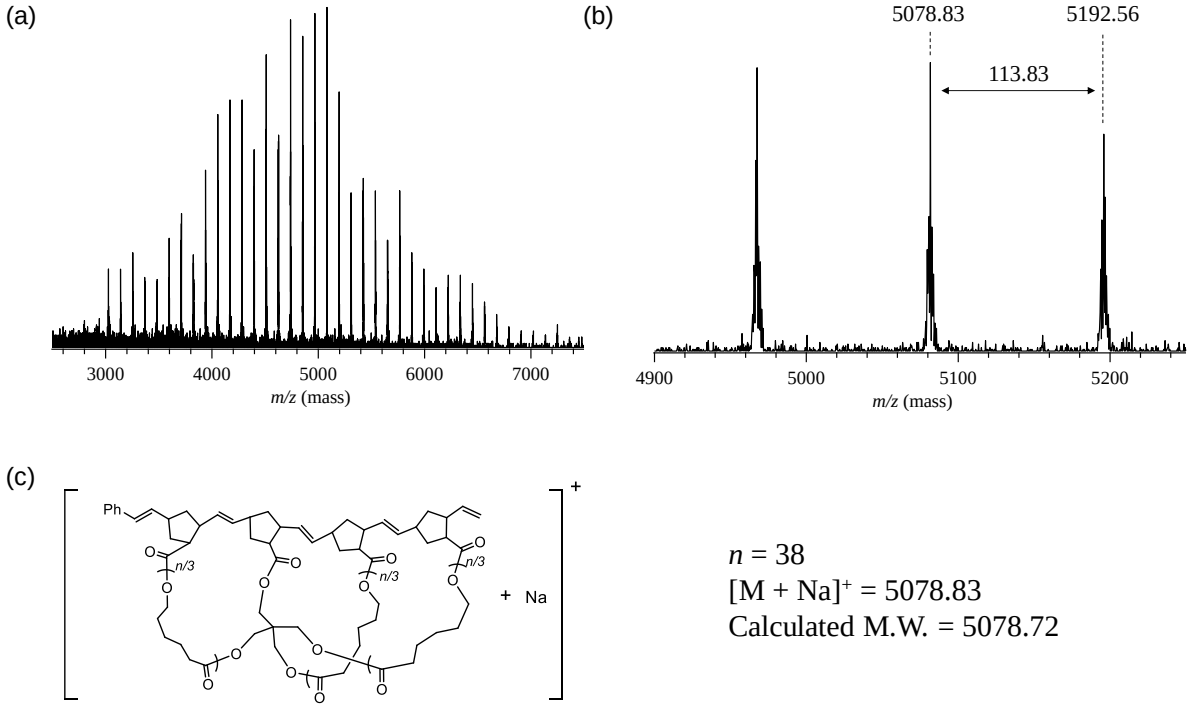

Figure S2.5. MALDI-TOF MS analysis of **trefoil-shaped PCL-a**.

Table S2.3 Molecular characterization of **trefoil-shaped PCL**s and their precursors

Sample	$M_{n,NMR}$ [a]	$M_{n,SEC}$ [b]	$M_{w,MALS}$ [c]	$Đ$ [b]	yield (%)	D_h [c] (nm)	$[\eta]$ [c] (mL g^{-1})	T_m [d] (°C)	X_{WAXD} [e] (%)
PMBO-(PCL-OH)$_3$-a	4,820	8,190	-	1.08	88.3	-	-	-	-
HO-(PCL-OH)$_3$-a	5,350	8,020	-	1.09	60.0	-	-	-	-
Pre$_{tre}$-a	6,160	8,670	5,330	1.07	60.1	4.4	14.3	42.6	39.3
trefoil-shaped PCL-a	-	6,170	4,820	1.09	90.0	3.6	6.9	42.6	31.7
PMBO-(PCL-OH)$_3$-b	8,830	11,200	-	1.09	89.1	-	-	-	-
HO-(PCL-OH)$_3$-b	10,700	12,100	-	1.06	72.8	-	-	-	-
Pre$_{tre}$-b	9,700	12,500	8,380	1.05	73.7	5.8	20.6	48.8	44.0
trefoil-shaped PCL-b	-	9,790	10,400	1.08	64.7	4.8	11.3	52.8	42.8
PMBO-(PCL-OH)$_3$-c	12,700	16,700	-	1.06	80.0	-	-	-	-
HO-(PCL-OH)$_3$-c	12,300	16,800	-	1.06	88.2	-	-	-	-
Pre$_{tre}$-c	12,400	17,900	10,300	1.05	77.5	6.8	24.9	50.9	46.3
trefoil-shaped PCL-c	-	13,200	12,100	1.08	91.2	5.6	13.2	54.4	45.4

[a] Determined by ^{1}H NMR. [b] Determined by SEC in THF using PSt standards. [c] Determined by SEC-MALS-Visco in THF. [d] Determined from a melting peak of the DSC curve. [e] Determined by WAXD at r.t..

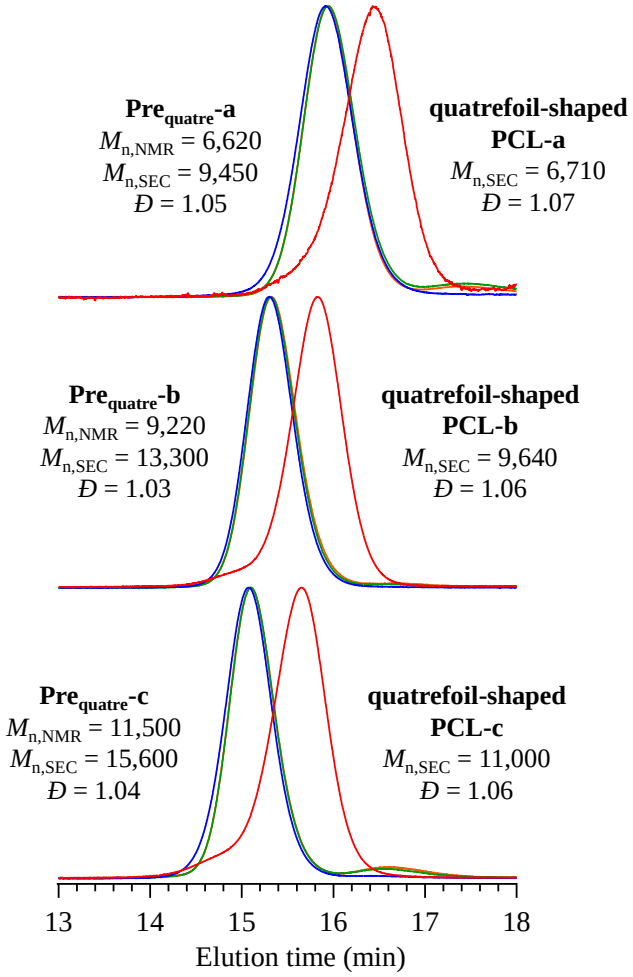

Figure S2.6. SEC traces of PMBO-(PCL-OH)$_4$s (orange), HO-(PCL-OH)$_4$s (green), **Pre$_{quatre}$s** (blue) and **quatrefoil-shaped PCL**s (red) with different molecular weight.

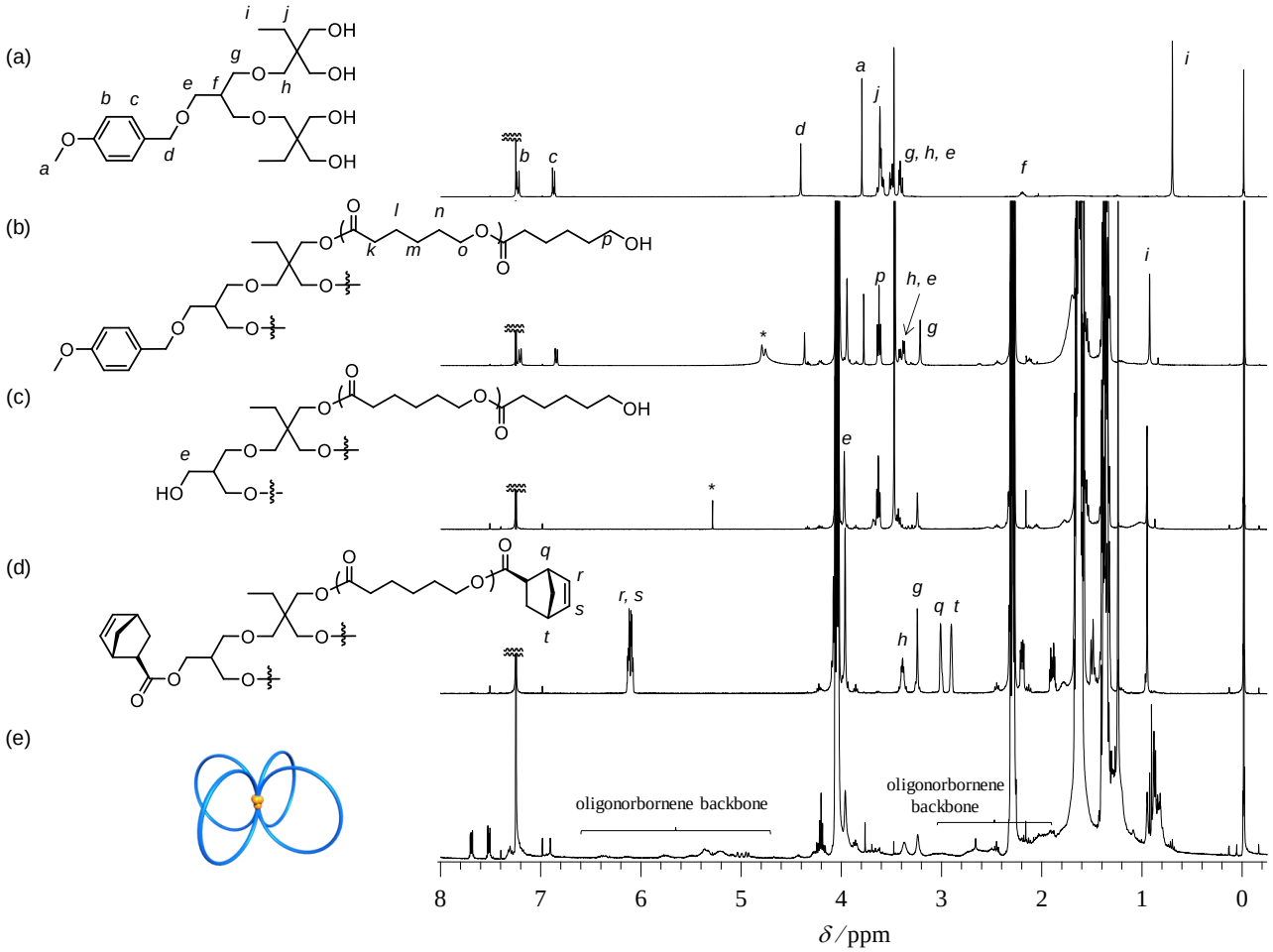

Figure S2.7. ^{1}H NMR spectra of (a) **I3**, (b) PMBO-(PCL-OH)$_4$, (c) HO-(PCL-OH)$_4$, (d) **Pre$_{quatre}$-a**, and (e) **quatrefoil-shaped PCL-a** in $CDCl_3$ (400 MHz).

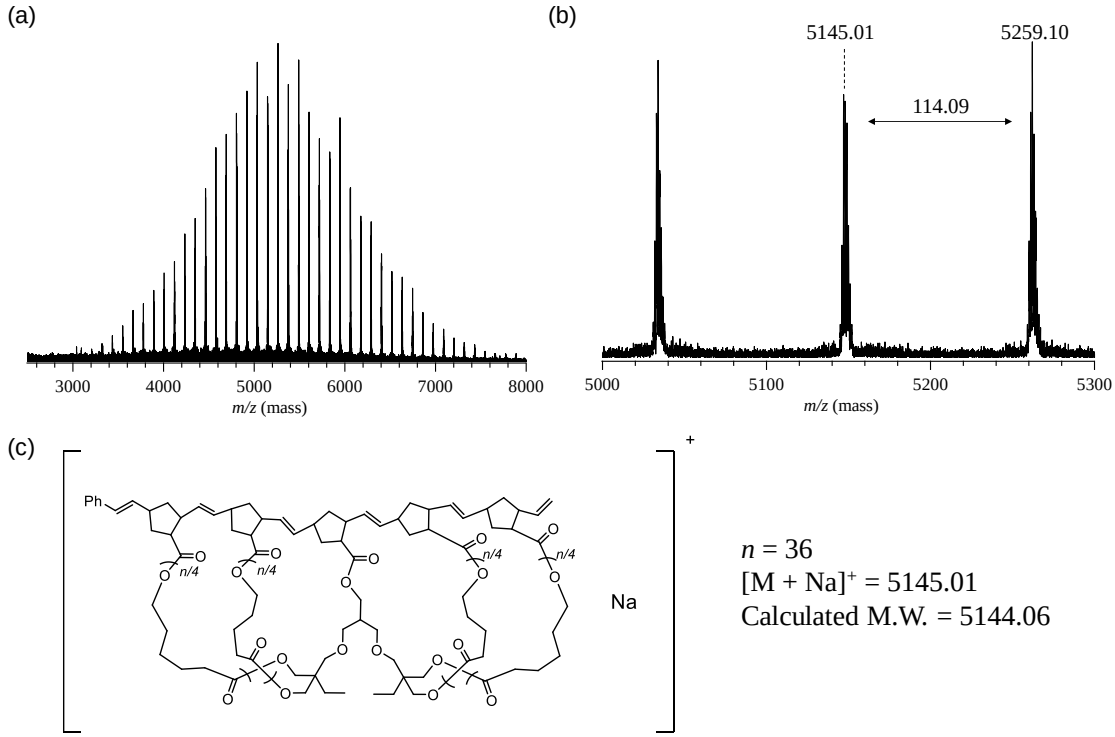

Figure 2.8. MALDI-TOF MS analysis of **quatrefoil-shaped PCL-a**.

Table S2.4. Molecular characterization of **quatrefoil-shaped PCL**s and their precursors

Sample	$M_{n,NMR}$ [a]	$M_{n,SEC}$ [b]	$M_{w,MALS}$ [c]	$Đ$ [b]	yield (%)	D_h [c] (nm)	$[\eta]$ [c] (mL g^{-1})	T_m [d] (°C)	X_{WAXD} [e] (%)
PMBO-(PCL-OH)$_4$-a	5,490	9,240	-	1.04	66.3	-	-	-	-
HO-(PCL-OH)$_4$-a	5,250	9,110	-	1.05	47.3	-	-	-	-
Pre$_{quatre}$-a	6,620	9,450	6,380	1.05	48.3	4.6	13.6	38.0	34.4
quatrefoil-shaped PCL-a	-	6,710	6,900	1.07	89.7	4.0	6.9	29.3	23.6
PMBO-(PCL-OH)$_4$-b	9,930	12,900	-	1.04	76.0	-	-	-	-
HO-(PCL-OH)$_4$-b	8,800	13,000	-	1.03	73.4	-	-	-	-
Pre$_{quatre}$-b	9,220	13,300	8,340	1.03	67.5	5.6	17.6	45.2	40.7
quatrefoil-shaped PCL-b	-	9,640	8,740	1.06	89.3	4.4	8.6	47.7	39.3
PMBO-(PCL-OH)$_4$-c	11,200	15,200	-	1.03	77.3	-	-	-	-
HO-(PCL-OH)$_4$-c	10,900	15,200	-	1.03	69.4	-	-	-	-
Pre$_{quatre}$-c	11,500	15,600	10,000	1.04	64.1	6.0	19.9	47.0	43.4
quatrefoil-shaped PCL-c	-	11,000	10,400	1.06	85.3	5.0	9.8	50.8	44.4

[a] Determined by ^{1}H NMR. [b] Determined by SEC in THF using PSt standards. [c] Determined by SEC-MALS-Visco in THF. [d] Determined from a melting peak of the DSC curve. [e] Determined by WAXD at r.t..

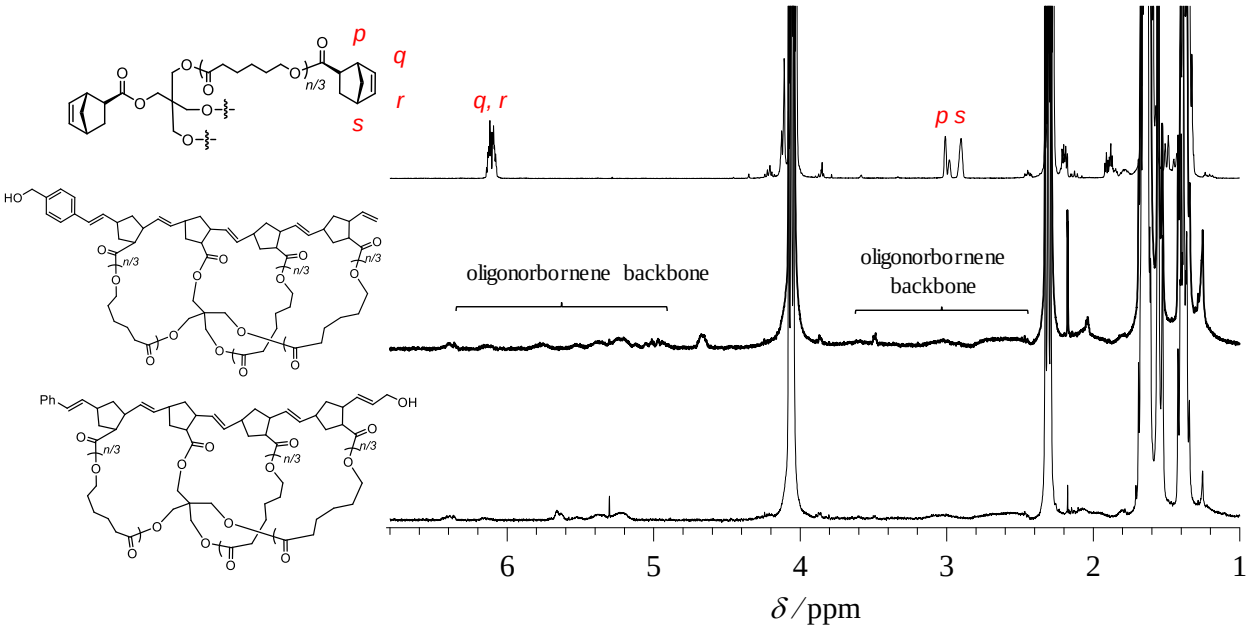

Figure S2.9. ^{1}H NMR spectra of **Pre$_{tre}$-a** (upper), (b) **trefoil-shaped PCL-OH$^{\alpha}$** (middle), and **trefoil-shaped PCL-OH$^{\omega}$** (lower) in $CDCl_3$ (400 MHz).

Table S2.5. Molecular characterization of trefoil-shaped PLLA, trefoil-shaped PEHGE and their precursors

Sample	$M_{n,NMR}$ [a] (g mol^{-1})	$M_{n,SEC}$ [b] (g mol^{-1})	$Đ$ [b]	yield (%)
PMBO-(PLLA-OH)$_3$	7,140	10,800	1.04	86.9
HO-(PLLA-OH)$_3$	7,150	10,900	1.04	44.3
NB-(PLLA-NB)$_3$	8,050	11,400	1.03	67.5
trefoil-shaped PLLA	-	7,700	1.09	91.4
PMBO-(PEHGE-OH)$_3$	6,560	7,490	1.03	63.0
HO-(PEHGE-OH)$_3$	6,910	7,390	1.03	55.6
NB-(PEHGE-NB)$_3$	7,000	7,690	1.03	71.4
trefoil-shaped PEHGE	-	6,320	1.05	71.9

[a] Determined by ^{1}H NMR. [b] Determined by SEC in THF using PSt standards.

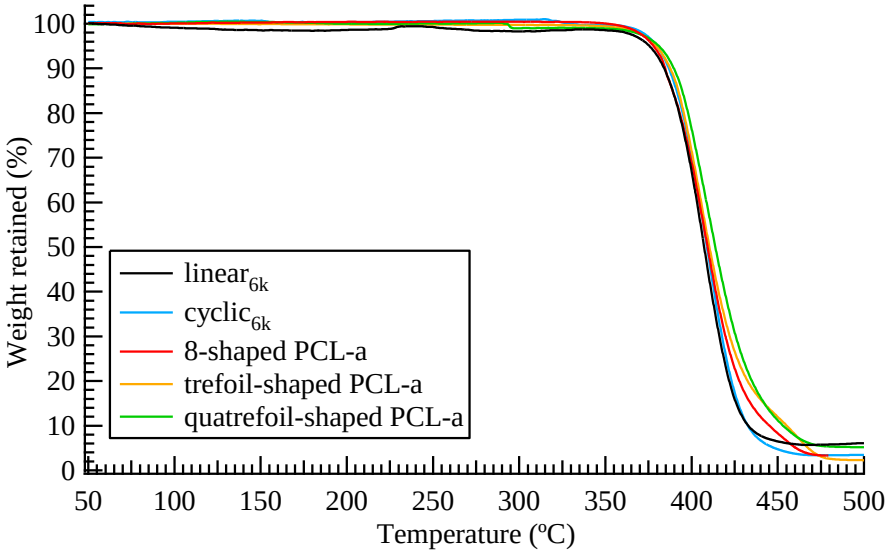

Figure S2.10. TGA result of *spiro*-multicyclic PCLs and their linear and cyclic counterparts obtained under Ar atmosphere (total MW; ~6000 g mol^{-1}, heating rate; 10 °C min^{-1}).

Table S2.6 Thermal degradation properties of *spiro*-multicyclic polymers and their linear and cyclic counterparts

Sample	$M_{n,NMR\ (precursor)}$ (g mol^{-1})	T_d (°C) [a]
linear$_{6k}$	6,540	384
cyclic$_{6k}$	6,540	387
8-shaped PCL-a	6,200	389
trefoil-shaped PCL-a	6,160	388
quatrefoil-shaped PCL-a	6,620	390

[a] 10% degradation temperature (T_d) was determined by TGA.

Note 1. SAXS analysis

To further elucidate the topological effect on bulk properties of semicrystalline polymers, SAXS experiments was carried out for the *spiro*-multicyclic PCLs (**8-shaped PCL-b**, **trefoil-shaped PCL-b**, and **quatrefoil-shaped PCL-b**) and their linear and cyclic

counterparts (**linear$_{9k}$** and **cyclic$_{9k}$**) with molecular weight of ca. 9000. With respect to the SAXS analysis, the thicknesses of crystalline domain (*d*) were estimated by following equation:

$d = 2\pi/q^*$

where the q^* is primary scattering vector from the SAXS profiles as summarized in Figure S2.11. Moreover, the crystalline lamellae thickness was determined by correlation function analysis according to the report using SasView.[41] The theoretical chain length of **8-shaped PCL-b** per arm was calculated as 0.735 nm × (((MW$_{\textbf{8-shaped PCL-b}}$ – (MW$_{NB}$ × 4 + MW$_{ini}$)) ÷ 4), where 0.735 nm is the molecular length of a PCL repeating unit,[42] MW$_{\textbf{8-shaped PCL-b}}$ is $M_{n,NMR}$ of **8-shaped PCL-b**, MW$_{NB}$ is the molecular weight of oligonorbornene backbone, and MW$_{ini}$ is the molecular weight of initiator.

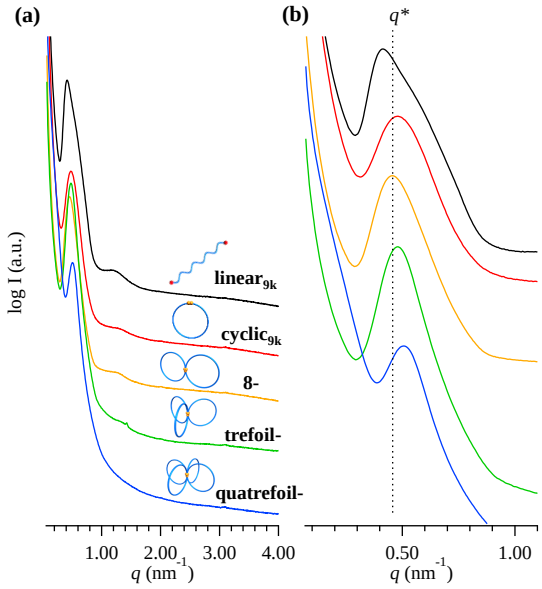

sample	SAXS peak analysis		Correlation function analysis	
	q^* (nm^{-1})	*d* (nm)	lamellae thickness (nm)	*d* (nm)
linear$_{9k}$	0.405	15.5	4.6	11.1
cyclic$_{9k}$	0.486	12.9	4.8	11.0
8-shaped PCL-b	0.456	13.8	5.1	11.8
trefoil-shaped PCL-b	0.476	13.2	4.8	11.7
quatrefoil-shaped PCL-b	0.507	12.4	4.8	11.7

Figure S2.11. (a) SAXS profiles of *spiro*-multicyclic PCLs (**8-shaped PCL-b**, **trefoil-shaped PCL-b**, and **quatrefoil-shaped PCL -b**) and their counterparts (**linear$_{9k}$** and **cyclic$_{9k}$**) (bulk sample; SDD = 1.5 m). (b) expanded SAXS profiles for the determination of q^* and *d*, that shows obvious change of **8-shaped PCL-b** compared to the topological counterparts.

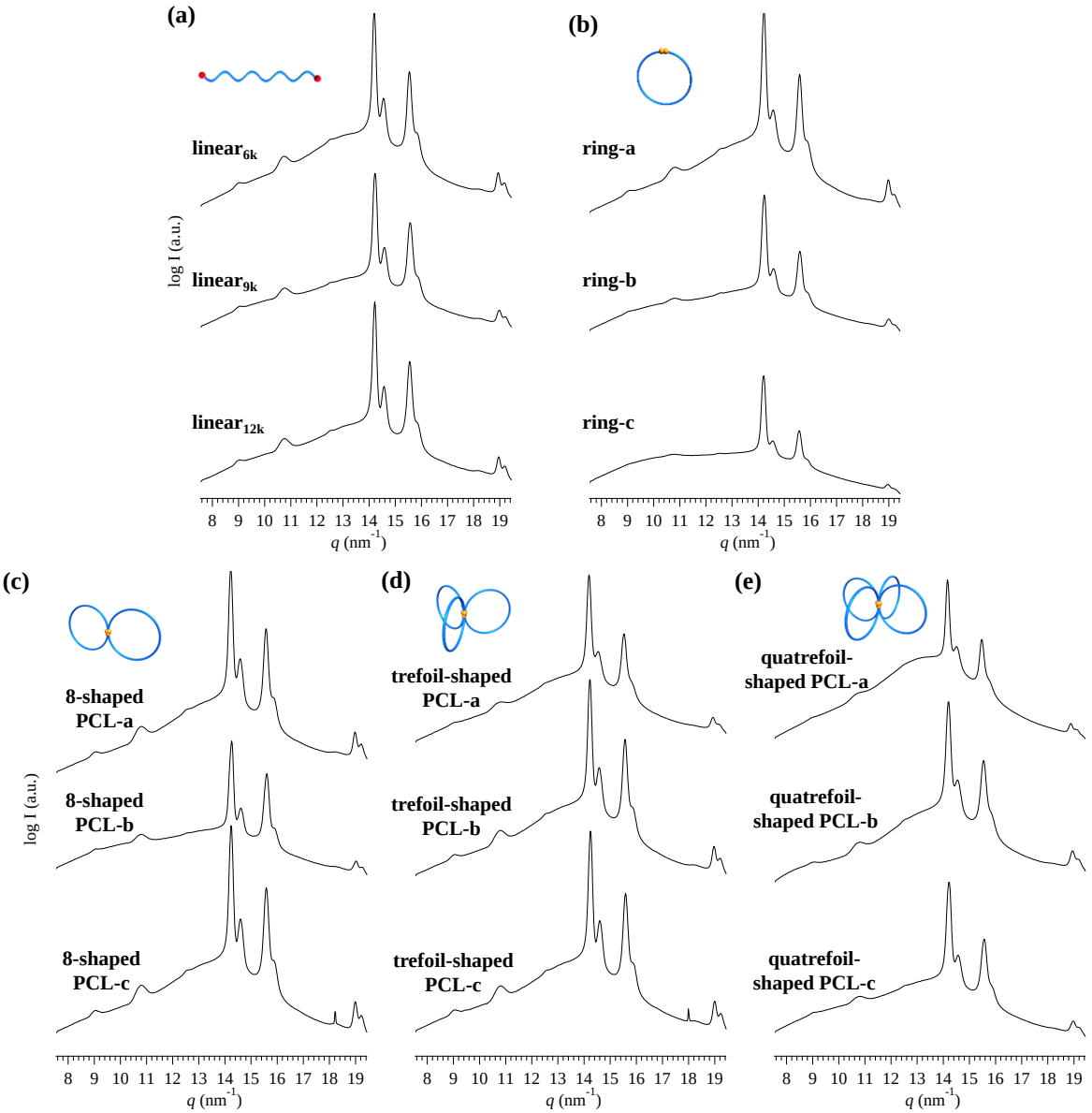

Figure S2.12. WAXD profiles of (a) linear, (b) cyclic, (c) 8-shaped (**8-shaped PCL**s), (d) trefoil-shaped (**trefoil-shaped PCL**s), and (e) quatrefoil-shaped PCLs (**quatrefoil-shaped PCL**s) with different molecular weight.

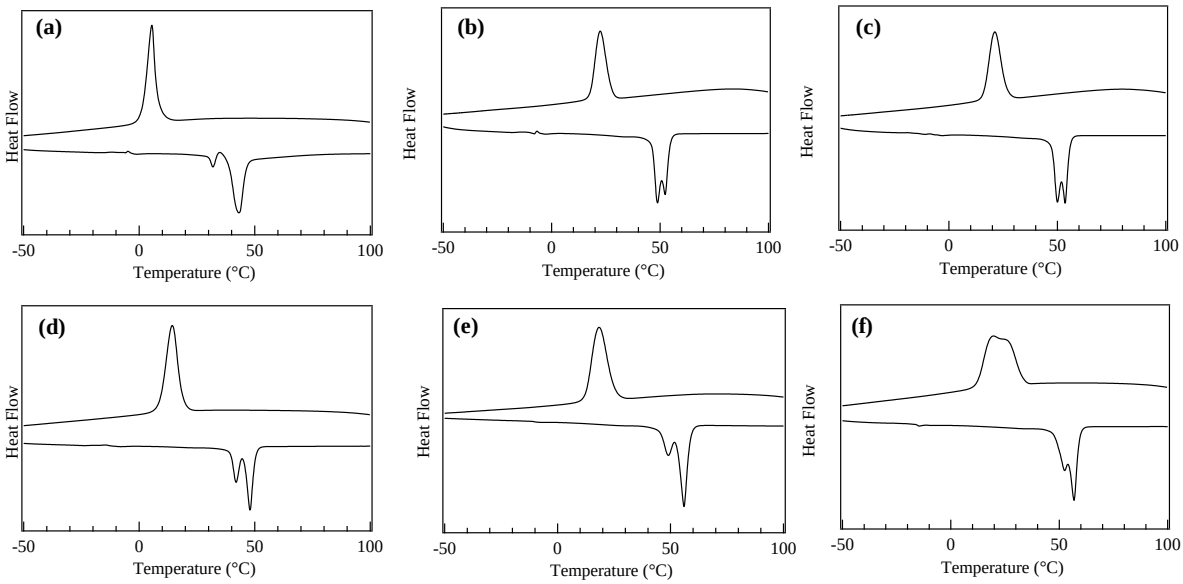

Figure S2.13. DSC thermograms of (a) linear$_{6k}$, (b) linear$_{9k}$, (c) linear$_{12k}$, (d) cyclic$_{6k}$, (e) cyclic$_{9k}$, and (f) cyclic$_{12k}$.

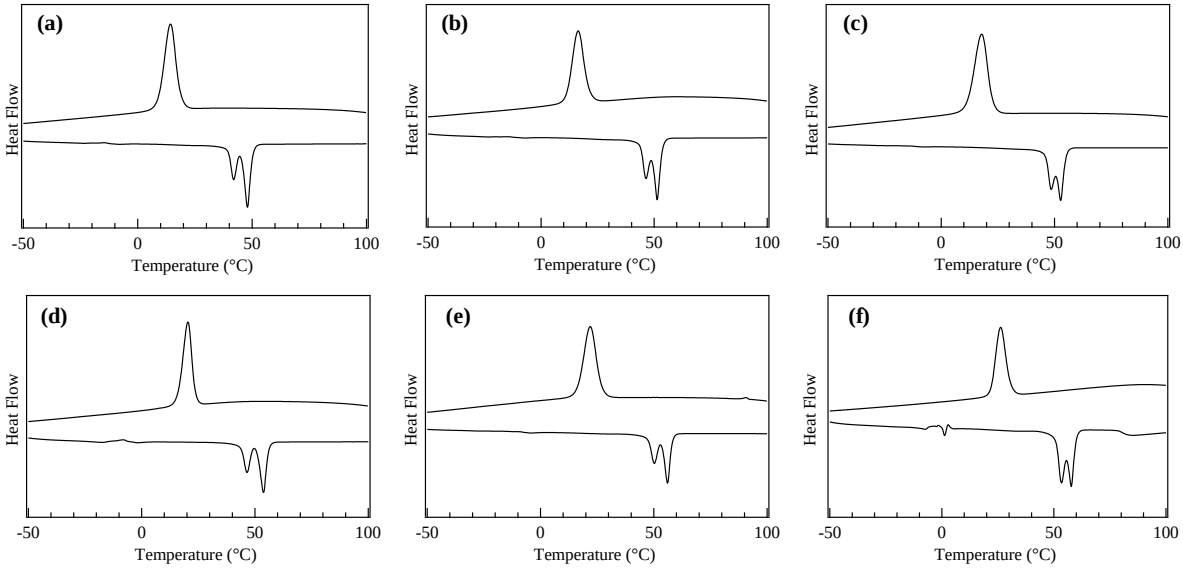

Figure S2.14. DSC thermograms of (a) **Pre$_{fig8}$-a**, (b) **Pre$_{fig8}$-b**, (c) **Pre$_{fig8}$-c**, (d) **8-shaped PCL-a**, (e) **8-shaped PCL-b**, and (f) **8-shaped PCL-c**.

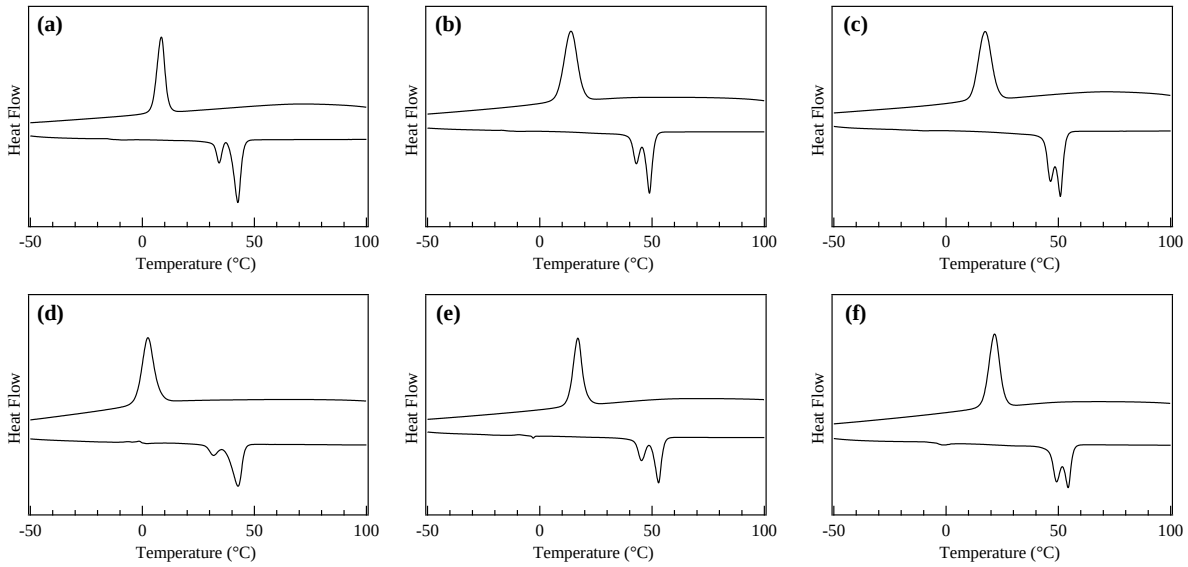

Figure S2.15. DSC thermograms of (a) **Pre$_{tre}$-a**, (b) **Pre$_{tre}$-b**, (c) **Pre$_{tre}$-c**, (d) **trefoil-shaped PCL-a**, (e) **trefoil-shaped PCL-b**, and (f) **trefoil-shaped PCL-c**.

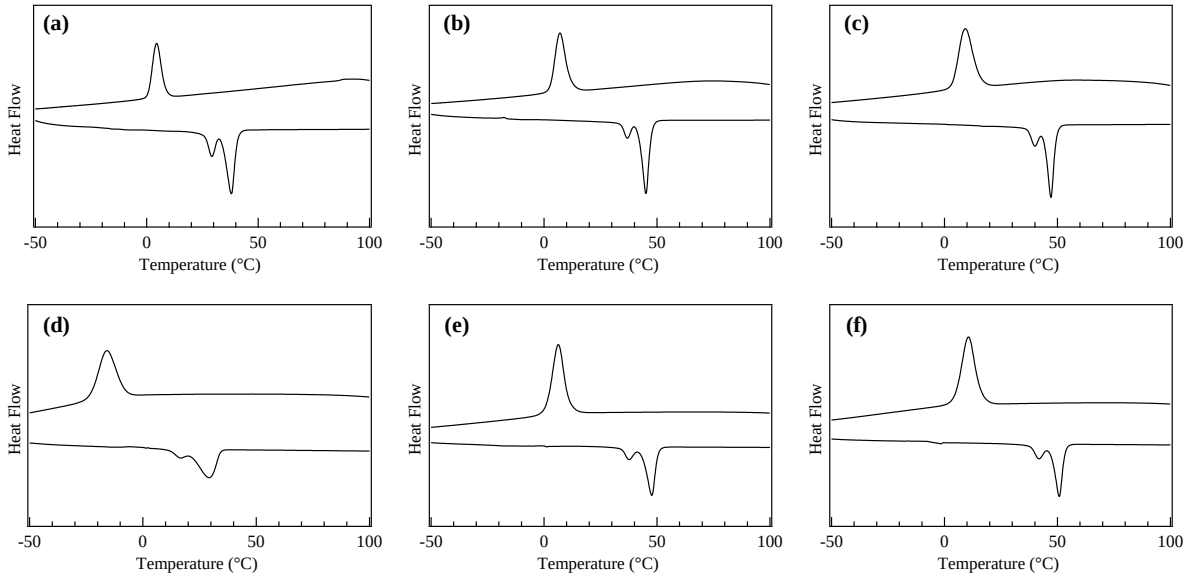

Figure S2.16. DSC thermograms of (a) **Pre$_{quatre}$-a**, (b) **Pre$_{quatre}$-b**, (c) **Pre$_{quatre}$-c**, (d) **quatrefoil-shaped PCL-a**, (e) **quatrefoil-shaped PCL-b**, and (f) **quatrefoil-shaped PCL-c**.

Chapter 3

Systematic Synthesis of Cage-shaped Polymers via Intramolecular Consecutive Cyclization

3.1 Introduction

Molecular cages have drawn attention as intriguing chemical research subjects because of their structural uniqueness, featuring three-dimensional cavities inside their molecular frameworks.[1–4] Owing to such distinctive architectures, cage molecules have been utilized for a diverse range of applications, such as nanocapsules for relatively large molecules,[5,6] templates for the size-controlled synthesis of metal nanoparticles,[7] and nanoflasks for catalytic reactions.[8,9] Cage molecules can be constructed by either the formation of covalent bonds or self-assembly through non-covalent bonding interactions. A number of small organic cages such as cryptands have been synthesized mainly by the former approach.[10,11] On the other hand, the latter approach has recently proven to be a powerful means to construct giant cages such as DNA and protein cages as well as 3D metallocages with molecular size ranges of 1–50 nm.[12–15] Remarkably, the robustness of the self-assembly approach has enabled the creation of novel cage molecules possessing various sizes, topologies, and functionalities.[1,16] However, the non-covalent bonding interactions are highly sensitive to external conditions, so that the self-assembled cages are relatively fragile upon exposure to chemical/physical stimuli including pH, temperature, and solvent polarity. To further extend the possible applications of cage molecules, a novel covalent-bond-forming strategy for the systematic synthesis of cage molecules with tunable functionality and controllable cavity size is highly desired.

To achieve this goal, the author envisioned the use of synthetic polymers as building blocks for the cage-shaped framework. A major advantage of a synthetic polymer is that a cage molecule of a targeted size can be readily synthesized by simply tuning its degree of polymerization. Moreover, the author anticipated that the choice of comonomers and their sequence would endow the cage molecules with vast functional utility such as molecular recognition ability, external stimuli responsiveness, and the capability to self-assemble into higher-ordered structures.[17–20] However, only limited efforts have been made thus far to prepare

macromolecular cages, and therefore, a general synthetic strategy remains lacking. To date, macromolecular cages composed of up to six arms have been reported by the groups of Tezuka and Paik, Satoh, and more recently, Zhang, as described in Section 1.3.[21–24] Although each synthesis produced well-defined macromolecular cages, the laborious and multistep natures of these conventional syntheses present a practical limitation to the systematic synthesis of macromolecular cages with arm numbers greater than seven. Consequently, the structures and properties of macromolecular cages, especially with respect to the molecular weight and arm number, have never been systematically studied. To achieve the systematic synthesis of macromolecular cages with varying arm numbers, the author envisioned that the intramolecular consecutive cyclization method established in Chapter 2 could effectively facilitate to construct a series of multi-ring cage system with various arm numbers and ring sizes. As shown in Figure 3.1, intramolecular ring-opening metathesis oligomerization (ROMO) of star-shaped polymers bearing a polymerizable group at each chain end would enable the systematic synthesis of macromolecular cages.

Here, in this chapter, the author describes the systematic synthesis of macromolecular cages with varied arm numbers and ring size via intramolecular ROMO of the end-norbornenyl-functionalized star-shaped PCL precursors. Firstly, the three-, four-, six-, and eight-armed star-shaped PCL precursors were prepared in two steps: the ring-opening polymerization of ε-caprolactone using polyol initiators and subsequent end-norbornenyl-functionalization. The established intramolecular ROMO of the star-shaped precursors successfully afforded the desired cage-shaped PCL in sufficient yields with high purity. It is notable that the intramolecular consecutive cyclization enabled the facile yet precise synthesis of six and eight-armed cage-shaped polymers, while conventional syntheses present a practical limitation to the synthesis of macromolecular cages with grater arm numbers. With a series of cage-PCLs, the polymer properties associated with a cage-shaped architecture have systematically evaluated

for the first time, which revealed that the hydrodynamic diameter, viscosity, and crystallization behavior of macromolecular cages are strongly affected by the arm number and arm length.

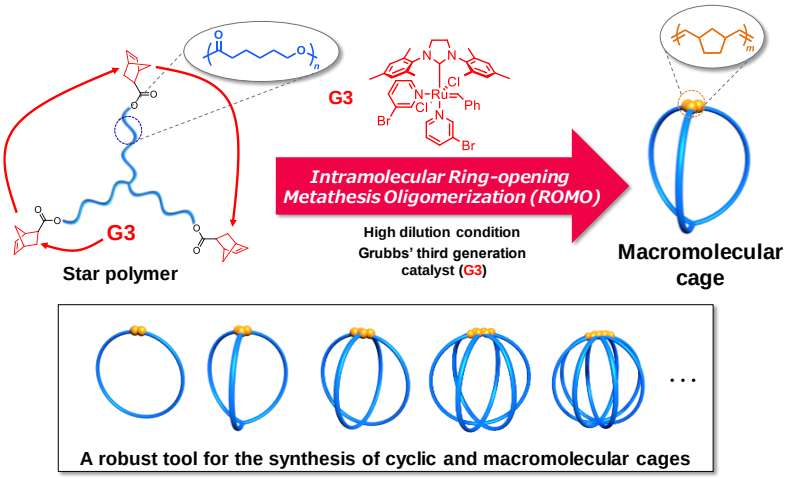

Figure. 3.1 Schematic illustration of the synthetic strategy for macromolecular cages through intramolecular consecutive ROMO mediated by G3.

3.2 Experimental Section

3.2.1 Materials

Grubbs' catalyst 3rd generation (G3)[25] and 5-(hydroxymethyl)-2,2,5-trimethyl-1,3-dioxane (HTMD)[26] were prepared according to previously reported method. Amberlyst® A21 (Organo Co., Ltd), *N*,*N*-dimethyl-4-aminopyridine (DMAP; Tokyo Chemical Industry Co., Ltd. (TCI), >99.0%), 1-ethyl-3-(3-(dimethylamino)-propyl)carbodiimide hydrochloride (EDC; TCI, >98.0%), ethyl vinyl ether (TCI, >98.0%), (±)-*exo*-5-norbornenecarboxylic acid (*exo*-NB-COOH; Aldrich, 97%), sodium iodide (NaI; Wako Pure Chemical Industry Co. Ltd., >99.5%), and 2, 5-dihydroxybenzoic acid (DHB; Sigma-Aldrich, >98.0%) were used as received. ε-Caprolactone (ε-CL; TCI, >99%) was purified by distillation over CaH_2 under reduced pressure and stored in the glovebox. Diphenyl phosphate (DPP; TCI, >99.0%), 2,2-diethyl-1,3-propanol (TCI, >98.0%), trimethylolpropane (TCI, >98.0%), pentaerythritol (TCI, >98.0%), and dipentaerythritol (TCI, >98.0%) were purified by azeotropic distillation with dry toluene and stored in the glovebox.

3.2.2 Instruments

The polymerization experiments were carried out in an MBRAUN stainless steel glovebox equipped with a gas purification system (molecular sieves and copper catalyst) in a dry argon atmosphere (H_2O, O_2<0.1 ppm). The moisture and oxygen contents in the glovebox were monitored by an MB-MO-SE 1 moisture sensor and an MB-OX-SE 1 oxygen sensor, respectively. Dry toluene (>99.5%; water content, <0.001%, Kanto Chemical Co., Inc.) used for the polymerization was purified by passing through an MBRAUN solvent purification system (MB SPS COMPACT) consisting of a column of activated alumina and a column with activated copper catalyst. The ^{1}H (400 MHz) and ^{13}C nuclear magnetic resonance (NMR)s (100 MHz) spectra were recorded using a JEOL JNM-ECS400 instrument at room temperature in

$CDCl_3$ or methanol-d_4. The size exclusion chromatography (SEC) was performed at 40 °C in THF (flow rate, 1.0 mL min^{-1}) using a Shodex GPC-101 gel permeation chromatography system (Shodex DU-2130 dual pump, Shodex RI-71-S reflective index detector, and Shodex ERC-3125SN degasser) equipped with a Shodex KF-G guard column (4.6 mm × 10 mm; particle size, 8 μm) and two Shodex KF-804L columns (linear, 8 mm × 300 mm). The number-average molecular weight ($M_{n,SEC}$) and the dispersity ($Đ$) of the polymers were calculated on the basis of polystyrene calibrations. The absolute molecular weights ($M_{w,MALS}$) of the samples of macromolecular cages and their star-shaped polymer precursors were determined by SEC with multiangle light scattering detection (SEC-MALS-Visco) in THF (flow rate, 1.0 mL min^{-1}) at 40 °C using an Agilent 1100 series instrument equipped with a DG 1100 degasser, a Shodex KF-G guard column (4.6 mm × 10 mm; particle size, 8 μm), a Shodex KF-800D solvent-peak separation column (linear, 8.0 mm × 100 mm; particle size, 10μm), two Shodex KF-805L columns (linear, 8.0 mm × 300 mm; exclusion limit, 4.0×10^6; particle size, 10 μm), a DAWN 8+ multiangle laser light scattering detector (Wyatt Technology), an Optilab rEX refractive index detector (Wyatt Technology), and a Viscostar viscosity detector (Wyatt Technology). The preparative SEC for Grubbs' catalyst removal was performed at r.t. in CH_3Cl (flow rate, 3.5 mL min^{-1}) using LC-9201 liquid chromatography system (Japan Analytical Industry Co. Ltd.) equipped with a BG-12 degasser, a PI-50 pump, a RI-50S RI detector, a JAIGEL-H-P guard column (8 mm × 40 mm; Japan Analytical Industry Co. Ltd.), and a Shodex K-2004 column (linear, 20.0 mm × 300 mm; exclusion limit, 1.4×10^4; particle size, 7 μm). The matrix-assisted laser desorption ionization time-of-flight mass spectrometry (MALDI-TOF MS) of the obtained polymers was performed using an Applied Biosystems Voyager-DE STR-H equipped with a 337 nm nitrogen laser (3 ns pulse width). Two hundred shots were accumulated for the spectra at a 20 kV acceleration voltage in the reflector mode and calibrated using PSt as the internal standard. Samples for the MALDI-TOF MS were prepared as follows: (i) the polymer sample

(1.0 mg) and DHB (2.0 mg) as a matrix were dissolved in THF (3.0 mL). (ii) Then, the solution was added to the THF solution of cationic agent (NaI; 1.0 mg mL^{-1}, 1.0 mL). (iii) The mixed solution was dropped to a sample plate. The thermal properties of the polymer samples were measured from −50 to 100 °C during the second heating by a Bruker AXS DSC 3100 differential scanning calorimeter under a nitrogen atmosphere with the heating rate of 10 °C min^{-1} and cooling rate 20 °C min^{-1}. Synchrotron small-angle X-ray scattering (SAXS) and wide-angle X-ray diffraction (WAXD) measurements of the obtained macromolecular cages and their precursors were performed with an X-ray beam of 1.5Å at the BL-6A in the Photon Factory (Tsukuba, Japan). The 2D SAXS and WAXD profiles were obtained with a Pilatus 1M and 100K detectors, respectively, which were circularly averaged to produce the 1D plots of log *I* (intensity) and *q* (scattering vector). The *q* value was calibrated using a silver behenate. The powder sample of the polymer was put into a Hilgenberg lindemann glass capillary (1.5 mm × 80 mm), which was annealed at 100 °C for 1 h in a pre-heated oven to erase a thermal history and then cooled to room temperature.

3.2.3 Synthetic details

Synthesis of three-armed star-shaped PCL (*s*-(PCL-OH)$_3$)

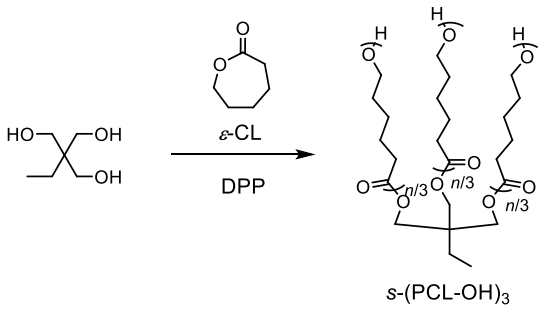

A typical procedure for the polymerization is as follows (method A): Under Ar atmosphere, ε-CL (3.00 g, 26.3 mmol), trimethylolpropane (70.0 mg, 526 μmol), and DPP (6.6 mg, 26 μmol) were placed in a reaction vessel. The reaction mixture was stirred at 80 °C for

2.5 h. The polymerization was quenched by the addition of Amberlyst® A21. The polymer crude was purified by the reprecipitation from CH_2Cl_2 into cold methanol to give ***s*-(PCL-OH)$_3$-a** as a white solid. Yield: 77.5%.

^{1}H NMR (400 MHz, $CDCl_3$): δ (ppm) 3.98-4.09 (m, $CH_3CH_2CCH_2$–, –OCO$(CH_2)_4CH_2$–), 3.63 (q, J = 6.00, -CH_2OH), 2.30 (m, –OCO$CH_2(CH_2)_4$–), 1.55-1.68 (m, –OCO$CH_2CH_2(CH_2)_3$–, –OCO$(CH_2)_3CH_2CH_2$–), 1.32-1.44 (m, CH_3CH_2–, –OCO$(CH_2)_2CH_2(CH_2)_2$–), 0.87 (t, J = 15.2, CH_3CH_2–). $M_{n,NMR}$ = 5,530 g mol^{-1} ($CDCl_3$), $M_{n,SEC}$ = 9,440 g mol^{-1} (THF), $Đ$ = 1.07.

Synthesis of ω-norbornenyl end-functionalized three-armed star-shaped PCL (Pre$_3$)

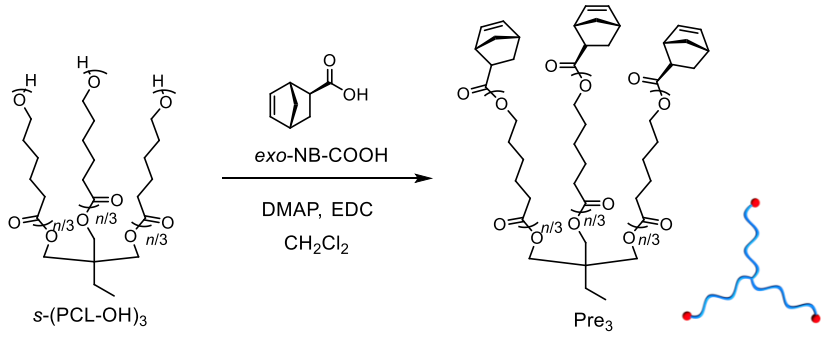

A typical procedure for the condensation reaction is as follows (method B): In a Schlenk flask, ***s*-(PCL-OH)$_3$-a** ($M_{n,NMR}$ = 5,530 g mol^{-1}, 1.00 g, 181 μmol), *exo*-NB-COOH (150 mg, 1.08 mmol), DMAP (199 mg, 1.66 μmol), and EDC (199 mg, 1.66 μmol) were dissolved in CH_2Cl_2 (10 mL) and the mixture was stirred at r.t. for 24 h. The polymer crude was purified by reprecipitation from CH_2Cl_2 into cold methanol to give **Pre$_3$-a** as a white solid. Yield: 58.6%.

^{1}H NMR (400 MHz, $CDCl_3$): δ (ppm) 6.11 (m, –C*H*=C*H*– in norbornene ring), 4.08-3.97 (m, $CH_3CH_2CCH_2$–, –OCO$(CH_2)_4CH_2$–), 3.01 (s, –C*H*–CH–CH_2O– in norbornene ring), 2.90 (s, –C*H*–CH_2–CH–CH_2O– in norbornene ring), 2.29 (m, –OCO$CH_2(CH_2)_4$–), 2.20 (m, –CH–CH_2–C*H*–CH2O– in norbornene ring), 1.89 (m, *exo*–C*H*– of CH–CH_2–CH–CH_2O– in

norbornene ring), 1.58-1.66 (m, –OCOCH$_2$C*H*$_2$(CH$_2$)$_3$–, –OCO(CH$_2$)$_3$C*H*$_2$CH$_2$–), 1.33-1.41 (m, CH$_3$C*H*$_2$-, –OCO(CH$_2$)$_2$C*H*$_2$(CH$_2$)$_2$–, bridge head –CH$_2$– in norbornene ring, *endo*-C*H*– of –CH–C*H*$_2$–CH–CH$_2$O–), 0.87 (t, J = 15.2, *C*H$_3$CH$_2$–). $M_{n,NMR}$ = 6,000 g mol^{-1} (CDCl$_3$), $M_{n,SEC}$ = 9,810 g mol^{-1} (THF), $Đ$ = 1.05.

Synthesis of three-armed macromolecular cage (cage$_3$) via intramolecular ROMO

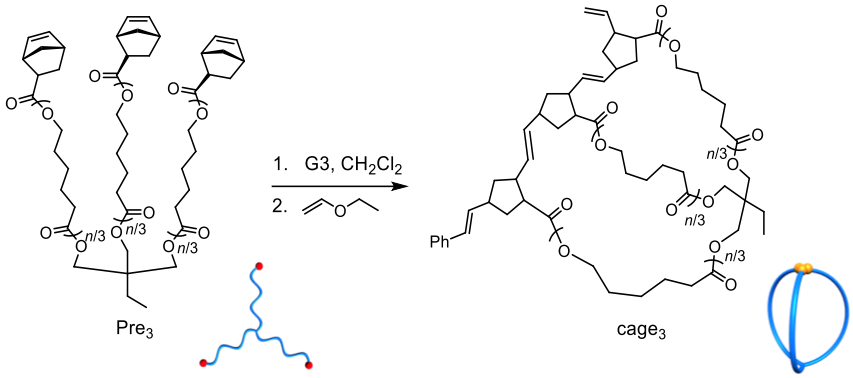

A typical procedure for the intramolecular ring-opening metathesis oligomerization is as follows (method C): G3 (26.6 mg, 30.0 μmol) was added to a three-necked flask and dissolved in deggased-CH$_2$Cl$_2$ (230 mL). Then, a solution of **Pre$_3$-a** ($M_{n,NMR}$ = 6,000 g mol^{-1}, 30.0 mg, 5.00 μmol, 170 μM in CH$_2$Cl$_2$) was added dropwise to the G3 solution through the additional funnel over 30 min. After 10 min, the reaction was quenched by the addition of excess ethyl vinyl ether. The metal residue in the crude product was removed by preparative SEC (solvent, CH$_3$Cl) to give **cage$_3$-a** as a pale brown solid. Yield: 92.3%.

^{1}H NMR (400 MHz, CDCl$_3$): δ (ppm) 7.70, 7.54 (Aromatic), 7.70-4.80 (br, alkenyl of poly(norbornene) backbone), 4.08-3.97 (m, CH$_3$CH$_2$CC*H*$_2$–, –OCO(CH$_2$)$_4$C*H*$_2$–), 2.79-1.10 (br, cyclopentane ring of poly(norbornene) backbone), 2.29 (m, –OCOC*H*$_2$(CH$_2$)$_4$–), 1.66-1.58 (m, –OCOCH$_2$C*H*$_2$(CH$_2$)$_3$–, –OCO(CH$_2$)$_3$C*H*$_2$CH$_2$–), 1.41-1.33 (m, CH$_3$C*H*$_2$–, –OCO(CH$_2$)$_2$C*H*$_2$(CH$_2$)$_2$–), 0.87 (t, J = 15.2, *C*H$_3$CH$_2$–). $M_{n,SEC}$ = 6,770 g mol^{-1} (THF), $Đ$ = 1.09.

Synthesis of four-armed star-shaped PCL (*s*-(PCL-OH)$_4$)

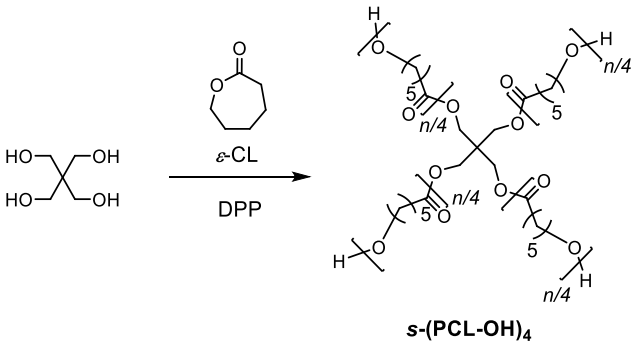

***s*-(PCL-OH)$_4$**

Method A was used for the polymerization of ε-CL (3.00 g, 26.3 mmol), pentaerythritol (70.0 mg, 526 μmol) and DPP (6.6 mg, 26 μmol) at 80 °C for 1.8 h to give ***s*-(PCL-OH)$_4$-a** as a white solid. Yield: 82.9%. ^{1}H NMR (400 MHz, $CDCl_3$): δ (ppm) 4.33-3.82 (m, –OCO(CH$_2$)$_4$C*H*$_2$–), 3.72-3.56 (m, –C*H*$_2$OH), 2.54-2.08 (–OCOC*H*$_2$(CH$_2$)$_4$–), 1.86-1.53 (–OCOCH$_2$C*H*$_2$(CH$_2$)$_3$-, –OCO(CH$_2$)$_3$C*H*$_2$CH$_2$–), 1.50-1.17 (m, –OCO(CH$_2$)$_2$C*H*$_2$(CH$_2$)$_2$–). $M_{n,NMR}$ = 5,970 g mol^{-1} ($CDCl_3$), $M_{n,SEC}$ = 9,900 g mol^{-1} (THF), $Đ$ = 1.06.

Synthesis of ω-norbornenyl end-functionalized four-armed star-shaped PCL (Pre$_4$)

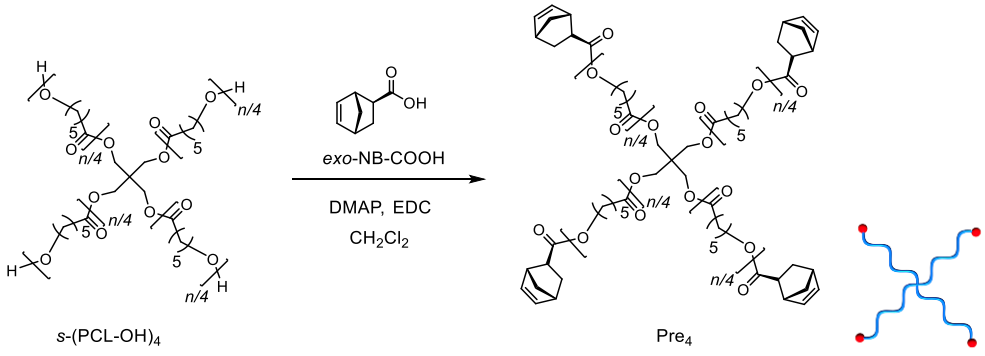

s-(PCL-OH)$_4$ Pre$_4$

Method B was used for the reaction of ***s*-(PCL-OH)$_4$-a** ($M_{n,NMR}$ = 5,970 g mol^{-1}, 1.00 g, 168 μmol) with *exo*-NB-COOH (185 mg, 1.34 mmol) in the presence of DMAP (245 mg, 2.01 μmol), EDC (385 mg, 2.01 mmol) in CH_2Cl_2 (10 mL) to give **Pre$_4$-a** as a white solid. Yield: 66.0%. ^{1}H NMR (400 MHz, $CDCl_3$): δ (ppm) 6.12 (m, –C*H*=C*H*– in norbornene ring),

4.31-3.82 (m, –OCO(CH$_2$)$_4$C*H*$_2$–), 3.02 (s, –C*H*–CH–CH$_2$O– in norbornene ring), 2.92 (s, –C*H*–CH$_2$–CH–CH$_2$O– in norbornene ring), 2.54-2.08 (m, –OCOC*H*$_2$(CH$_2$)$_4$–), 1.96-1.87 (m, –OCO(CH$_2$)$_2$C*H*$_2$(CH$_2$)$_2$–, bridge head –CH$_2$– in norbornene ring, *endo*-C*H*– of –CH–C*H*$_2$–CH–CH$_2$O–), 1.74-1.47 (m, –OCOCH$_2$C*H*$_2$(CH$_2$)$_3$–, –OCO(CH$_2$)$_3$C*H*$_2$CH$_2$–), 1.46-1.22 (m, –OCO(CH$_2$)$_2$C*H*$_2$(CH$_2$)$_2$–). $M_{n,NMR}$ = 5,990 g mol^{-1} (CDCl$_3$), $M_{n,SEC}$ = 9,100 g mol^{-1} (THF), $Đ$ = 1.05.

Synthesis of four-armed macromolecular cage (cage$_4$) via intramolecular ROMO

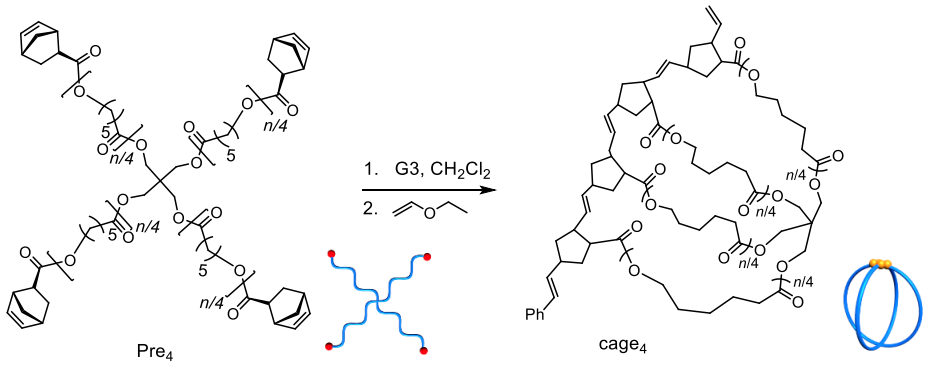

Method C was used for the ROMO of **Pre$_4$-a** ($M_{n,NMR}$ = 5,990 g mol^{-1}, 30.0 mg, 5.01 μmol, 170 μM in CH$_2$Cl$_2$) with G3 (26.6 mg, 30.0 μmol) in CH$_2$Cl$_2$ (230 mL) to give **cage$_4$-a** as a pale brown solid. Yield: 85.0%. ^{1}H NMR (400 MHz, CDCl$_3$): δ (ppm) 7.70, 7.54 (Aromatic), 6.51-4.90 (br, alkenyl of oligo(norbornene) backbone), 4.29-3.86 (m, –OCO(CH$_2$)$_4$C*H*$_2$–), 3.20-1.83 (br, cyclopentane ring of oligo(norbornene) backbone), 2.43-2.20 (m, –OCOC*H*$_2$(CH$_2$)$_4$–), 1.82-1.49 (m, –OCOCH$_2$C*H*$_2$(CH$_2$)$_3$–, –OCO(CH$_2$)$_3$C*H*$_2$CH$_2$–), 1.45-1.19 (m, –OCO(CH$_2$)$_2$C*H*$_2$(CH$_2$)$_2$–). $M_{n,SEC}$ = 6,290 g mol^{-1} (THF), $Đ$ = 1.08.

Synthesis of six-armed star-shaped PCL (*s*-(PCL-OH)$_6$)

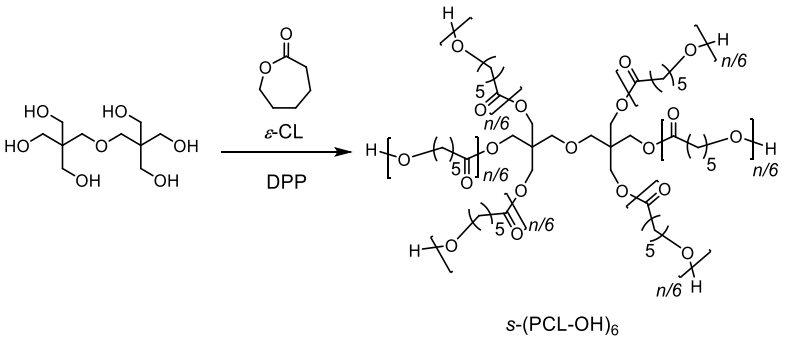

Method A was used for the polymerization of ε-CL (3.00 g, 26.3 mmol), dipentaerythritol (134 mg, 526 μmol) and DPP (6.6 mg, 26 μmol) at 80 °C for 35 min to give ***s*-(PCL-OH)$_6$-a** as a white solid. Yield: 72.0%. ^{1}H NMR (400 MHz, $CDCl_3$): δ (ppm) 4.26-3.91 (m, –OCO(CH$_2$)$_4$C*H*$_2$–, –OC*H*$_2$C(CH$_2$O-)$_3$), 3.70-3.59 (m, –C*H*$_2$OH), 3.38 (d, J = 11.0, –OCH$_2$C(C*H*$_2$O–)$_3$), 2.51-2.19 (–OCOC*H*$_2$(CH$_2$)$_4$–), 1.86-1.48 (–OCOCH$_2$C*H*$_2$(CH$_2$)$_3$–, –OCO(CH$_2$)$_3$C*H*$_2$CH$_2$–), 1.46-1.20 (m, –OCO(CH$_2$)$_2$C*H*$_2$(CH$_2$)$_2$–). $M_{n,NMR}$ = 5,300 g mol^{-1} ($CDCl_3$), $M_{n,SEC}$ = 7,000 g mol^{-1} (THF), $Đ$ = 1.09.

Synthesis of *ω*-norbornenyl end-functionalized six-armed star-shaped PCL (Pre$_6$)

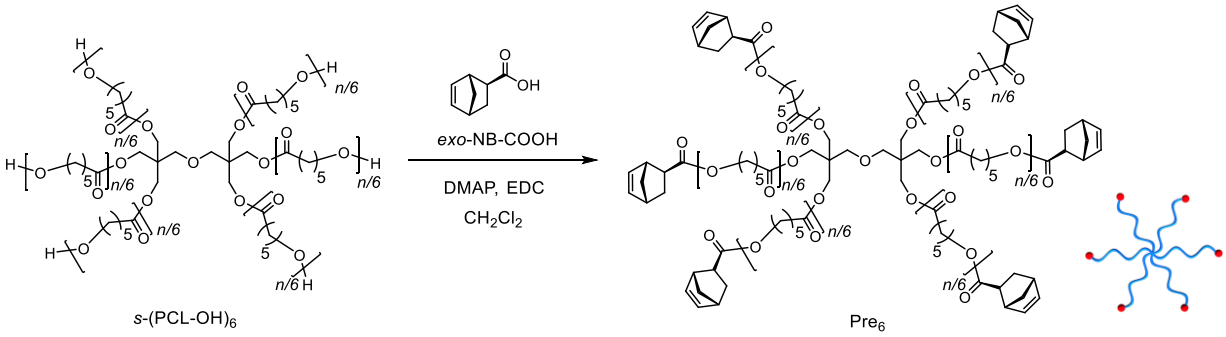

Method B was used for the reaction of ***s*-(PCL-OH)$_4$-a** ($M_{n,NMR}$ = 5,300 g mol^{-1}, 1.00 g, 189 μmol) with *exo*-NB-COOH (313 mg, 2.26 mmol) in the presence of DMAP (415 mg, 3.39 mmol), EDC (650 mg, 3.39 mmol) in CH_2Cl_2 (10 mL) to give **Pre$_6$-a** as a white solid. Yield: 41.0%. ^{1}H NMR (400 MHz, $CDCl_3$): δ (ppm) 6.12 (m, –C*H*=C*H*– in norbornene ring), 4.31-3.85 (m, –OCO(CH$_2$)$_4$C*H*$_2$–, –OC*H*$_2$C(CH$_2$O–)$_3$), 3.09-2.97 (br, –OCH$_2$C(C*H*$_2$O–)$_3$),

3.03 (s, –C*H*–CH–CH_2O– in norbornene ring), 2.92 (s, ––C*H*–CH_2–CH–CH_2O– in norbornene ring), 2.54-2.13 (m, –OCOCH_2(CH_2)$_4$–), 1.96-1.87 (m, –OCO(CH_2)$_2$CH_2(CH_2)$_2$–, bridge head –CH_2– in norbornene ring, *endo*-C*H*– of –CH–CH_2–CH–CH_2O–), 1.77-1.54 (m, –OCOCH_2CH_2(CH_2)$_3$–, –OCO(CH_2)$_3$C$H_2$$CH_2$–), 1.48-1.18 (m, –OCO($CH_2$)$_2CH_2$($CH_2$)$_2$–). $M_{n,NMR}$ = 6,030 g mol^{-1} ($CDCl_3$), $M_{n,SEC}$ = 7,760 g mol^{-1} (THF), $Đ$ = 1.06.

Synthesis of six-armed macromolecular cage (cage$_6$) via intramolecular ROMO

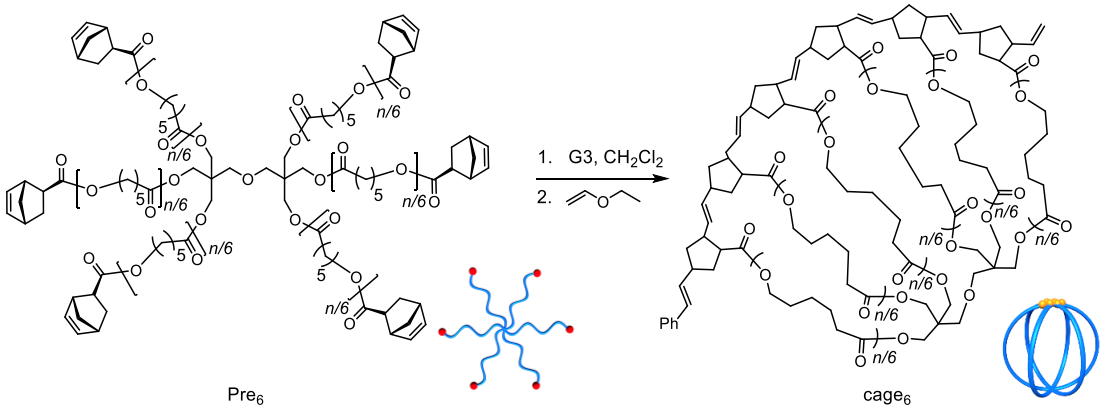

Method C was used for the ROMO of **Pre$_6$-a** ($M_{n,NMR}$ = 6,030 g mol^{-1}, 30.0 mg, 4.98 μmol, 170 μM in CH_2Cl_2) with G3 (26.4 mg, 29.9 μmol) in CH_2Cl_2 (230 mL) to give **cage$_6$-a** as a pale brown viscous liquid. Yield: 91.0%. ^{1}H NMR (400 MHz, $CDCl_3$): δ (ppm) 7.70, 7.55 (Aromatic), 6.56-4.84 (br, alkenyl of oligo(norbornene) backbone), 4.37-3.72 (m, –OCO(CH_2)$_4$CH_2–, –OCH_2C(CH_2O–)$_3$), 3.58-3.24 (br, –OCH_2C(CH_2O–)$_3$), 3.23-1.85 (br, cyclopentane ring of oligo(norbornene) backbone), 2.40-2.20 (m, –OCOCH_2(CH_2)$_4$–), 1.81-1.50 (m, –OCOCH_2CH_2(CH_2)$_3$–, –OCO(CH_2)$_3$C$H_2$$CH_2$–), 1.51-1.14 (m, –OCO($CH_2$)$_2CH_2$($CH_2$)$_2$–). $M_{n,SEC}$ = 5,100 g mol^{-1} (THF), $Đ$ = 1.08.

Synthesis of 5,5'-(((2,2-bis(((2,2,5-trimethyl-1,3-dioxan-5-yl)methoxy)methyl)propane-1,3-diyl)bis(oxy))bis(methylene))bis(2,2,5-trimethyl-1,3-dioxane) (1)

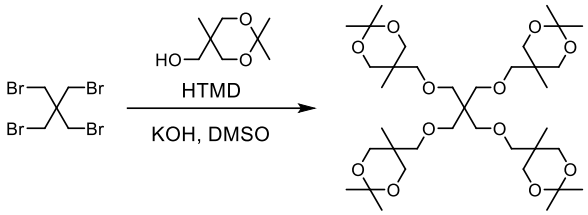

1

HTMD (7.98 g, 49.8 mmol) was added to a stirred solution of KOH (14.0 g, 249 mmol) pentaerythritol tetrabromide (3.87 g, 9.96 mmol) in DMSO (100 mL), and then the solution was stirred at 60 °C for 1 days. After removing the solvent by evaporation, the obtained residue was dissolved in ether and washed with brine. The organic layer was dried over anhydrous Na_2SO_4, filtrated, and then concentrated. The residue was purified by silica gel column chromatography (AcOEt/*n*-hexane = 3/7, R_f = 0.30) to give **1** as a white solid. Yield: 79.3 %. ^{1}H NMR (400 MHz, $CDCl_3$): δ(ppm) 3.81-3.64 (m, 2H, –CCH$_3$(CH_2O)$_2$C–), 3.60-3.47 (m, 2H, –CCH$_3$(CH_2O)$_2$C–), 3.45-3.36 (m, 2H, –CH$_2$OCH_2C–), 3.31 (s, 2H, –CH_2OCH$_2$C–), 1.40 (d, 6H, J = 12.1, –C(CH_3)$_2$), 0.89 (s, 3H, –CCH_3). ^{13}C NMR (100 MHz, $CDCl_3$): 97.9 (–C(*C*H$_2$)$_2$), 74.4, 70.6, 66.8, 34.7, 25.7, 22.1 (–*C*(CH$_2$–)$_4$), 18.7 (–C*C*H$_3$). HRMS (FD): *m/z* calcd for $C_{37}H_{69}O_{12}$: 705.4789 $[M+H]^+$; found: 705.4776.

Synthesis of 2,2'-(((2,2-bis((3-hydroxy-2-(hydroxymethyl)-2-methylpropoxy)methyl) propane-1,3-diyl)bis(oxy))bis(methylene))bis(2-methylpropane-1,3-diol) (2)

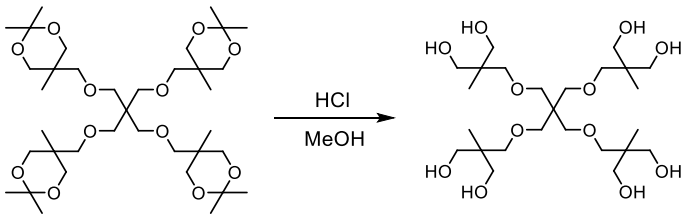

1 **2**

1 (10.2 g, 14.5 mmol) was added to a mixed solvent of MeOH (120 mL) and

concentrated hydrochloric acid (5.0 mL), and then the solution was stirred at r.t. for 14 h. After removing the solvent by evaporation, the obtained residue was dried over by a vacuum oven at 150 ºC to give **2** as a white solid. Yield: 90.9 %. ^{1}H NMR (400 MHz, methanol-d_4): δ (ppm) 4.88 (s, 2H, –CCH$_3$(CH$_2$O*H*)$_2$), 3.46 (s, 4H, –CCH$_3$(C*H*$_2$OH)$_2$), 3.39 (s, 2H, –CH$_2$OC*H*$_2$C–), 3.28 (s, 2H, –C*H*$_2$OCH$_2$C–), 0.87 (s, 3H, –CC*H*$_3$(CH$_2$OH)$_2$). ^{13}C NMR (100 MHz, methanol-d_4): 74.2 (–C(*C*H$_2$OH)$_2$), 70.5 (–*C*CH$_3$(CH$_2$OH)$_2$), 65.2 (–CH$_2$O*C*H$_2$C–), 45.9 (–*C*H$_2$OCH$_2$C–), 41.3 (–*C*(CH$_2$–)$_4$), 15.9 (–C*C*H$_3$). HRMS (ESI, in methanol solution): *m/z* calcd for C$_{25}$H$_{52}$O$_{12}$Na: 567.3351 [M+Na]$^+$; found: 567.3353.

Synthesis of eight-armed star-shaped PCL (*s*-(PCL-OH)$_8$)

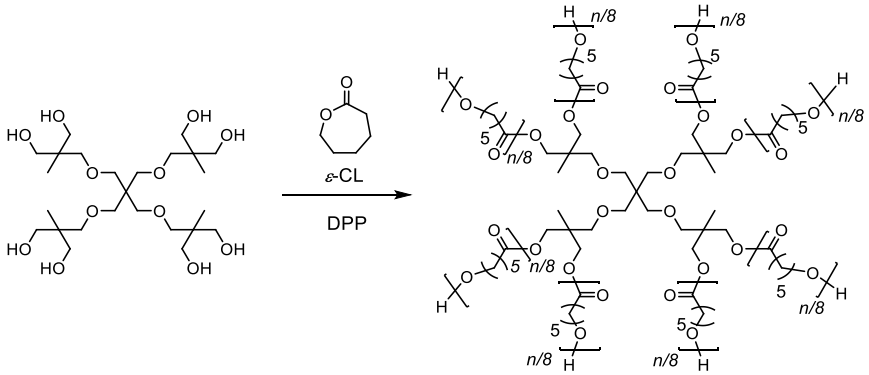

2 *s*-(PCL-OH)$_8$

Method A was used for the polymerization of ε-CL (3.00 g, 26.3 mmol) with **2** (286 mg, 525 μmol) and DPP (6.58 mg, 26.3 μmol) at 80 °C for 35 min to give ***s*-(PCL-OH)$_8$-a** as a white solid. Yield: 93.0%. ^{1}H NMR (400 MHz, CDCl$_3$): δ (ppm) 4.15-4.01 (m, –OCO(CH$_2$)$_4$C*H*$_2$–), 3.97 (s, –CC*H*$_2$O–), 3.65 (q, J = 5.8, –C*H*$_2$OH), 3.31 (s, C(C*H*$_2$OCH$_2$–)$_4$), 3.22 (s, C(CH$_2$OC*H*$_2$–)$_4$), 2.41-2.24 (m, –OCOC*H*$_2$(CH$_2$)$_4$–), 1.75-1.52 (m, –OCOCH$_2$C*H*$_2$(CH$_2$)$_3$–, –OCO(CH$_2$)$_3$C*H*$_2$CH$_2$–), 1.49-1.29 (m, –OCO(CH$_2$)$_2$C*H*$_2$(CH$_2$)$_2$–), 0.96, 0.87 (rotamers, –CC*H*$_3$). $M_{n,NMR}$ = 5,970 g mol^{-1} (CDCl$_3$), $M_{n,SEC}$ = 8,400 g mol^{-1} (THF), $Đ$ = 1.04.

Synthesis of *ω*-norbornenyl end-functionalized eight-armed star-shaped PCL (Pre$_8$)

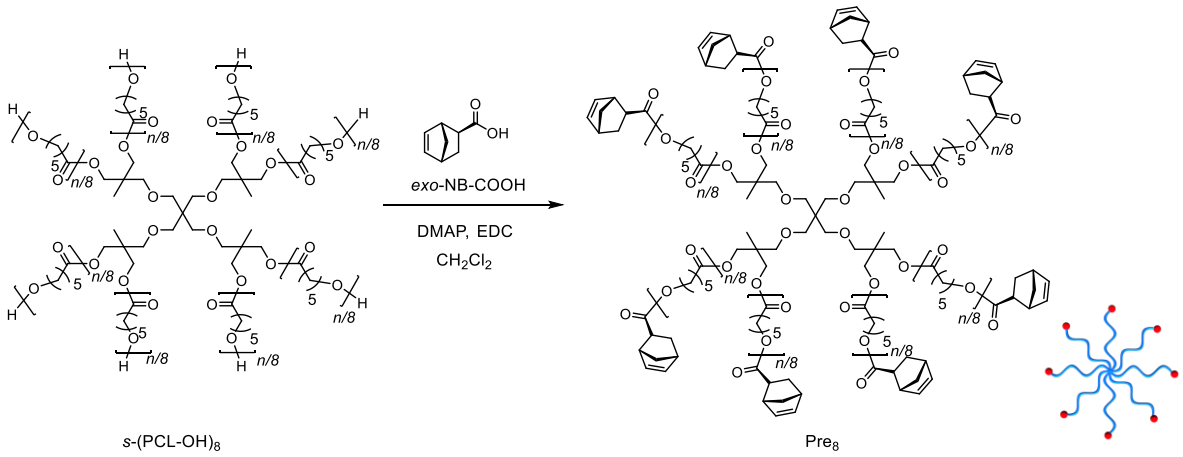

Method B was used for the reaction of ***s*-(PCL-OH)$_8$-a** ($M_{n,NMR}$ = 5,970 g mol^{-1}, 1.00 g, 168 μmol) with *exo*-NB-COOH (370 mg, 2.68 mmol) in the presence of DMAP (491 mg, 4.02 μmol), EDC (770 mg, 4.02 mmol) in CH_2Cl_2 (10 mL) to give **Pre$_8$-a** as a white solid. Yield: 92.1%. ^{1}H NMR (400 MHz, $CDCl_3$): δ (ppm) 6.12 (m, –C*H*=C*H*– in norbornene ring), 4.19-4.01 (m, –OCO(CH$_2$)$_4$C*H*$_2$–), 3.97 (s, –CC*H*$_2$O–), 3.32 (s, C(C*H*$_2$OCH$_2$–)$_4$), 3.22 (s, C(CH$_2$OC*H*$_2$–)$_4$), 3.03 (s, –C*H*–CH$_2$–CH–CH$_2$O– in norbornene ring), 2.92 (s, –C*H*–CH–CH$_2$O– in norbornene ring), 2.54-2.25 (m, –OCOC*H*$_2$(CH$_2$)$_4$–), 1.97-1.85 (m, H$_3$C*H*$_2$–, –OCO(CH$_2$)$_2$C*H*$_2$(CH$_2$)$_2$–, bridge head –CH$_2$– in norbornene ring, *endo*-C*H*– of –CH–C*H*$_2$–CH–CH$_2$O–), 1.81-1.48 (m, –OCOCH$_2$C*H*$_2$(CH$_2$)$_3$–, –OCO(CH$_2$)$_3$C*H*$_2$CH$_2$–), 1.47-1.21 (m, –OCO(CH$_2$)$_2$C*H*$_2$(CH$_2$)$_2$–), 0.92 (rotamers, –CC*H*$_3$). $M_{n,NMR}$ = 7,300 g mol^{-1} ($CDCl_3$), $M_{n,SEC}$ = 8,930 g mol^{-1} (THF), $Đ$ = 1.04

Synthesis of eight-armed macromolecular cage (cage$_8$) via intramolecular ROMO

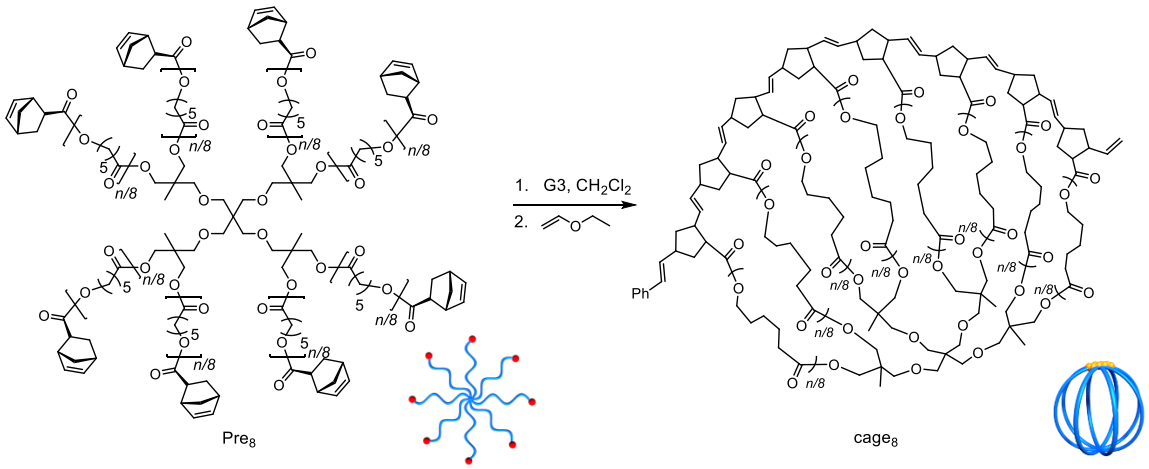

Method C was used for the ROMO of **Pre$_8$-a** ($M_{n,NMR}$ = 7,300 g mol^{-1}, 30.0 mg, 4.11 μmol, 170 μM in CH_2Cl_2) with G3 (21.8 mg, 24.7 μmol) in CH_2Cl_2 (230 mL) to give **cage$_8$-a** as a pale brown viscous liquid. Yield: 98.3%. ^{1}H NMR (400 MHz, $CDCl_3$): δ (ppm) 7.70, 7.53 (Aromatic), 6.57-4.52 (br, alkenyl of poly(norbornene) backbone), 4.16-4.01 (m, –OCO(CH$_2$)$_4$C*H*$_2$–), 3.97 (s, –CC*H*$_2$O–), 3.40-3.16 (m, C(C*H*$_2$OCH$_2$–)$_4$, C(CH$_2$OC*H*$_2$–)$_4$), 3.15-1.75 (br, cyclopentane ring of poly(norbornene) backbone), 2.41-2.21 (m, –OCOC*H*$_2$(CH$_2$)$_4$–), 1.80-1.51 (m, –OCOCH$_2$C*H*$_2$(CH$_2$)$_3$–, –OCO(CH$_2$)$_3$C*H*$_2$CH$_2$–), 1.52-1.05 (m, –OCO(CH$_2$)$_2$C*H*$_2$(CH$_2$)$_2$–), 1.04-0.74 (m, –CC*H*$_3$). $M_{n,SEC}$ = 6,400 g mol^{-1} (THF), $Đ$ = 1.06

3.3 Results and Discussion

3.3.1 Synthesis of three-armed cage-shaped PCL via intramolecular consecutive cyclization

The author synthesized the three-armed star-shaped PCL bearing a norbornenyl group at each end, **Pre$_3$-a** ($M_{n,NMR}$ = 6,000 g mol^{-1}, $M_{n,SEC}$ = 9,810 g mol^{-1}, $Đ$ = 1.05), which is subject to the intramolecular ring-opening metathesis oligomerization (ROMO) to give the corresponding three-armed macromolecular cage, **cage$_3$-a** (Scheme 3.1). The preparation of **Pre$_3$-a** is successfully achieved in two steps: (i) diphenyl phosphate (DPP)-catalyzed ring-opening polymerization of ε-CL using a commercially available triol initiator with the [ε-CL]$_0$/[initiator]$_0$ ratio of 50/1 and (ii) subsequent condensation reaction with excess (±)-*exo*-5-norbornene carboxylic acid (see Synthetic details in Section 3.2.3 for more information). ^{1}H NMR spectrum of the product clearly shows the signals attributed to the norbornenyl groups, indicating quantitative introduction of norbornenyl groups to each polymer end (Figures 3.2(a) and S3.1). SEC traces of the obtained product retained monomodal even after the condensation reaction (Figure S3.2).

Scheme 3.1. Synthesis of three-armed **cage$_3$-a** through intramolecular ring-opening metathesis oligomerization (ROMO) of corresponding PCLs with a reactive norbornenyl group at each chain end

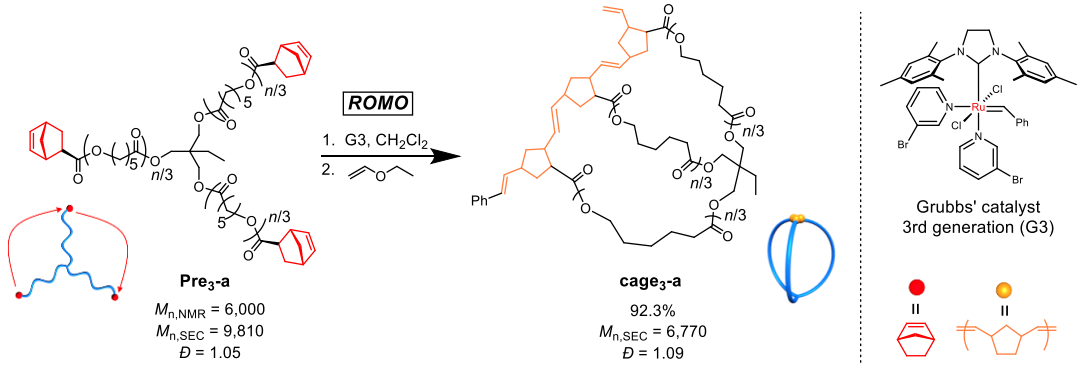

With the optimized reaction conditions in Chapter 2 ($[\text{precursor}]_0/[\text{G3}]_0$ = 1/6; $[\text{precursor}]_0$ = 0.02 mM) in hand, the intramolecular consecutive ROMO of **Pre$_3$-a**, was carried out to give **cage$_3$-a** (Scheme 3.1). In the ^{1}H NMR spectrum of the product, no signals due to the norbornenyl group are detected, whereas signals attributable to the oligonorbornene backbone are observed near 1.05–3.25 and 4.95–6.60 ppm (Figure 3.2(a)). Although the ^{1}H NMR analysis revealed the completion of the reaction, several possible side reactions such as intermolecular polymerization and the multiple addition of G3 were also considered (Figure S3.3(a)). To exclude the possibilities of such side reactions, SEC and MALDI TOF-MS analyses were performed to further verify the detailed structure of the product. The SEC trace of the obtained product is significantly shifted to the lower molecular region ($M_{\text{n,SEC}}$ = 6,770 g mol^{-1}, $Đ$ = 1.09) as compared to **Pre$_3$-a** ($M_{\text{n,SEC}}$ = 9,810 g mol^{-1}), implying the formation of the desired cage-shaped product with a smaller hydrodynamic volume (Figures 3.2(b) and S3.2).

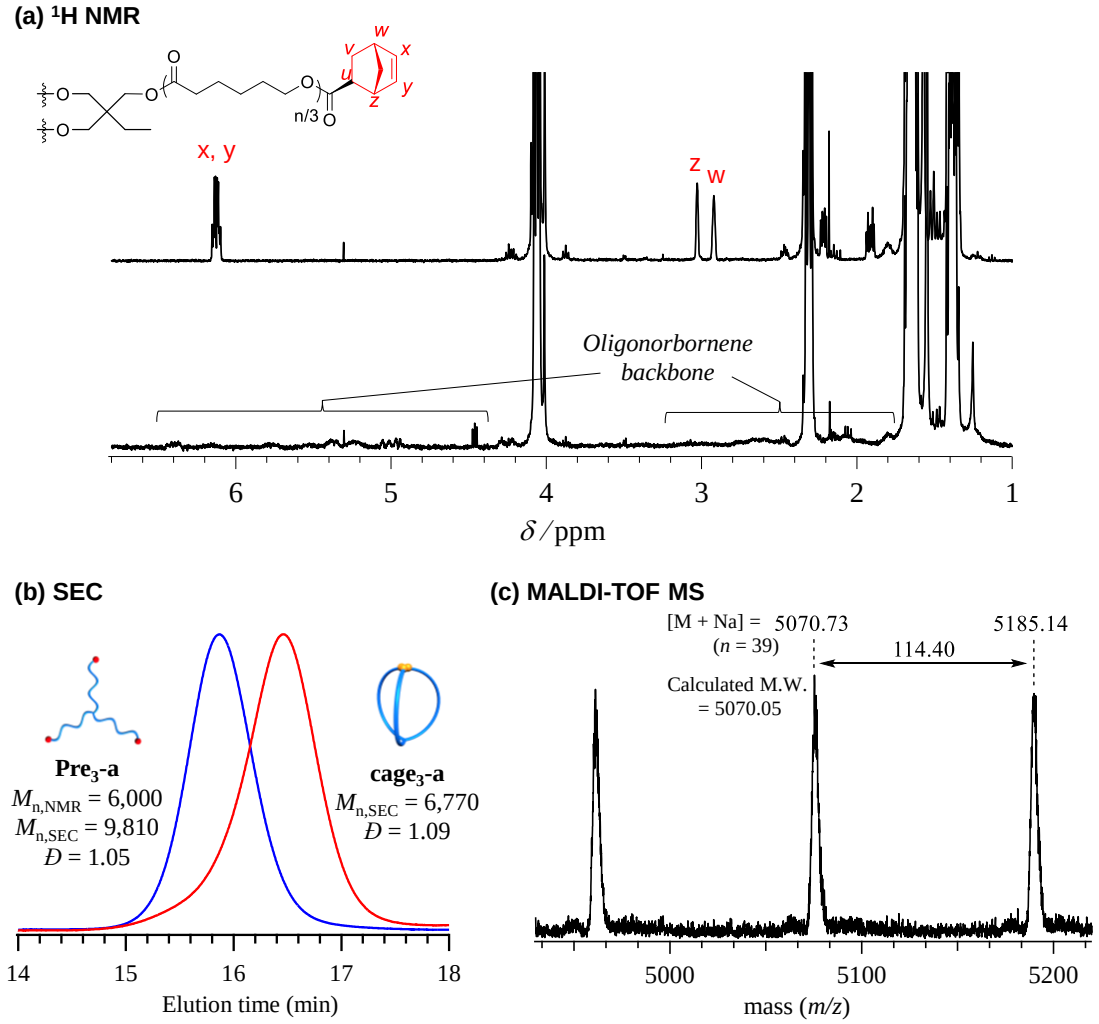

Figure 3.2. Structural analysis of three-armed macromolecular cage (**cage$_3$-a**). (a) ^{1}H NMR spectra of **Pre$_3$-a** (upper) and **cage$_3$-a** (lower). (b) SEC traces of **Pre$_3$-a** ($M_{n,NMR}$ = 6,000 g mol^{-1}, $M_{n,SEC}$ = 9,810 g mol^{-1}, $Đ$ = 1.05; blue line) and **cage$_3$-a** (before purification by preparative SEC; $M_{n,SEC}$ = 6,770 g mol^{-1}, $Đ$ = 1.09; red line) synthesized by intramolecular ROMO. (c) Expanded MALDI-TOF MS spectrum of **cage$_3$-a** ranging from 4500 to 5200 Da.

Furthermore, the monomodal elution peak is retained after the reaction, suggesting that the intermolecular reaction is highly suppressed. Although small higher molecular weight shoulder, perhaps due to the dimer and trimer formed via the intermolecular propagation, was observed in the SEC trace, the purity of the desired product was calculated to be higher than 90% based on the elution peak area. Moreover, the MALDI-TOF mass spectrum shows only one set of peaks with a regular interval of 114.40 Da corresponding to the ε-CL monomer unit,

which is a good indication that multiple G3 addition did not occur (Figures 3.2c and S3.4). Specifically, peaks due to possible multiple G3 adducts, such as the tadpole- (for example $[M + Na]^+$ = 5059.97 Da, n = 38) and star-shaped polymers(for example $[M + Na]^+$ = 5165.03 Da, n = 38, Figure S3.3), are not detected. In addition, an observed peak at *m/z* 5070.73Da agrees with the calculated mass for the desired **cage$_3$-a** with a degree of polymerization of 39 ($[M + Na]^+$ = 5070.05 Da, n = 39). Overall, these data strongly confirm that the intramolecular consecutive ROMO using G3 produces **cage$_3$-a** with sufficient purity.

3.3.2 Synthesis of four-, six-, and eight-armed cage-shaped PCL via intramolecular consecutive cyclization

The optimized ROMO reaction condition was also applicable to four-, six-, and eight-armed star-shaped PCLs bearing a norbornene at each chain end (**Pre$_4$-a, Pre$_6$-a**, and **Pre$_8$-a**), which afforded the corresponding cage-shaped PCLs with varied arm numbers (**cage$_4$-a**, **cage$_6$-a,** and **cage$_8$-a**, respectively) in good yields, typically in the range of 80–97% (Figure 3.3, Tables S2-4). Each product was fully characterized by SEC, ^{1}H NMR, and MALDI-TOF MS, which confirmed the successful synthesis of the macromolecular cages (Figures S3.5-3.14). It is worth noting that narrowly-dispersed macromolecular cages ($Đ$ = 1.06–1.09) were obtained without obvious side reactions, despite the increases in the arm-numbers of the precursors. Although some of the obtained macromolecular cages showed high molecular shoulders in their SEC traces, the purity was calculated to be more than 89%, according to the SEC elution peak area. These results suggest that G3-mediated intramolecular ROMO proceeds in preference to the addition of a second G3 to other norbornenyl groups in the same molecule, preventing the formation of possible by-products such as the tadpole-shaped product. In addition, the author has succeeded in controlling the molecular weight of a series of macromolecular cages in an $M_{n,NMR}$ range of ~6,000–12,000 g mol^{-1} (Table 3.1) by simply employing star-shaped PCLs

with different molecular weights. Hence, the author has established a versatile yet robust synthetic strategy for macromolecular cages based on the intramolecular ROMO that enables the production of a series of macromolecular cages with controlled molecular weights and arm numbers.

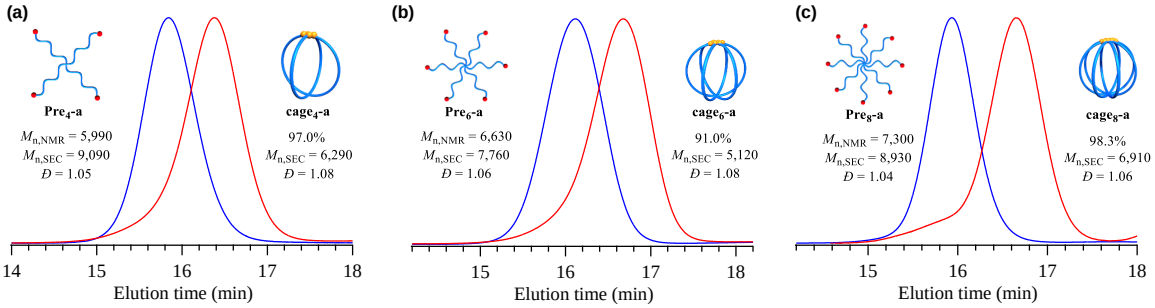

Figure 3.3. SEC traces for (a) four-, (b) six-, and (c) eight-armed star-shaped precursors (blue; **Pre$_4$-a**, **Pre$_6$-a**, and **Pre$_8$-a**, respectively) and the macromolecular cages constructed via intramolecular ROMO (red; **cage$_4$-a**, **cage$_6$-a**, and **cage$_8$-a**, respectively).

Table 3.1 Molecular characteristics of cyclic polymers and macromolecular cages obtained by intramolecular ROMO

Macromolecular cage	$M_{n,SEC}$ [b]	$M_{p,MALS}$[c]	$Đ$ [b]	D_h [c] (nm)	Yield (%)
ring-a	7,520	6,280	1.09	4.6	92.3
ring-b	11,700	8,890	1.09	5.8	92.3
ring-c	15,200	11,600	1.09	6.8	91.6
cage$_3$-a	6,770	7,550	1.09	4.4	92.3
cage$_3$-b	9,360	9,370	1.09	5.0	80.0
cage$_3$-c	11,500	10,200	1.09	5.6	84.0
cage$_4$-a	6,290	7,420	1.08	4.2	97.0
cage$_4$-b	9,590	9,840	1.08	5.0	94.0
cage$_4$-c	10,700	11,800	1.08	5.6	91.0
cage$_6$-a	5,120	7,950	1.08	3.8	91.0
cage$_6$-b	8,570	10,900	1.09	5.0	98.7
cage$_6$-c	10,700	12,800	1.07	5.2	91.2
cage$_8$-a	6,910	8,180	1.06	3.8	98.3
cage$_8$-b	9,130	10,300	1.08	4.6	97.7
cage$_8$-c	12,000	14,300	1.06	5.6	84.7

[a] Determined by SEC in THF using PSt standards. [b] Weight-average absolute molecular weight ($M_{w,MALS}$) was estimated by SEC-MALS-Visco in THF. [c] Weight-average hydrodynamic diameter (D_h) was determined through SEC-MALS-Visco measurement in THF by the following equations: $D_h = 2\,R_h = 2(3V_h/4\pi)^{1/3}$ where V_h (hydrodynamic volume) was calculated by Einstein–Simha equation ($V_h = M_{w,MALS}[\eta]/2.5N_A$, where N_A is Avogadro's number).

3.3.3 Systematic investigation of structure–property relationships

Owing to the lack of a universal synthetic strategy, the polymer properties associated with a cage-shaped architecture have never been systematically evaluated, although a comprehensive structural study has been attempted for monocyclic PCLs.[27] With a series of macromolecular cages with varied arm numbers and molecular weights in hand, the author initially investigated the weight-average hydrodynamic diameters (D_h) and the weight-average intrinsic viscosities ([η]) in THF by employing triple-detection SEC consisting of multiangle light scattering, viscosity, and refractive index detectors (SEC-MALS-Visco). The D_h values of

the macromolecular cages are in the range of 3.8–6.8 nm, as summarized in Table 3.1 and Figure 3.4a (see also Figure S3.15). The D_h value is dependent on both the arm number and total molecular weight. Figure 4b shows double-logarithmic plots of the $M_{W,MALS}$ versus $[\eta]$ for the prepared linear and monocyclic PCLs as well as macromolecular cages, which clearly indicate a linear relationship between the viscosity and molecular weight. More importantly, the $[\eta]$ values for the macromolecular cages (5.4–14.1 mg mL^{-1}) are apparently lower than the corresponding precursors (11.1–22.0 mg mL^{-1}; Tables S3.1–S3.4 and Figure S3.16), despite their comparable molecular weights. In addition, the $[\eta]$ values of the macromolecular cages further decrease with the increasing arm number. A similar trend was observed in a series of multicyclic polymer.[28,29] These solution state studies demonstrate that the increase in the arm number or decrease in the molecular weight of the macromolecular cage results in a lower hydrodynamic volume, which supports the possibility of controlling the inner cavity size.

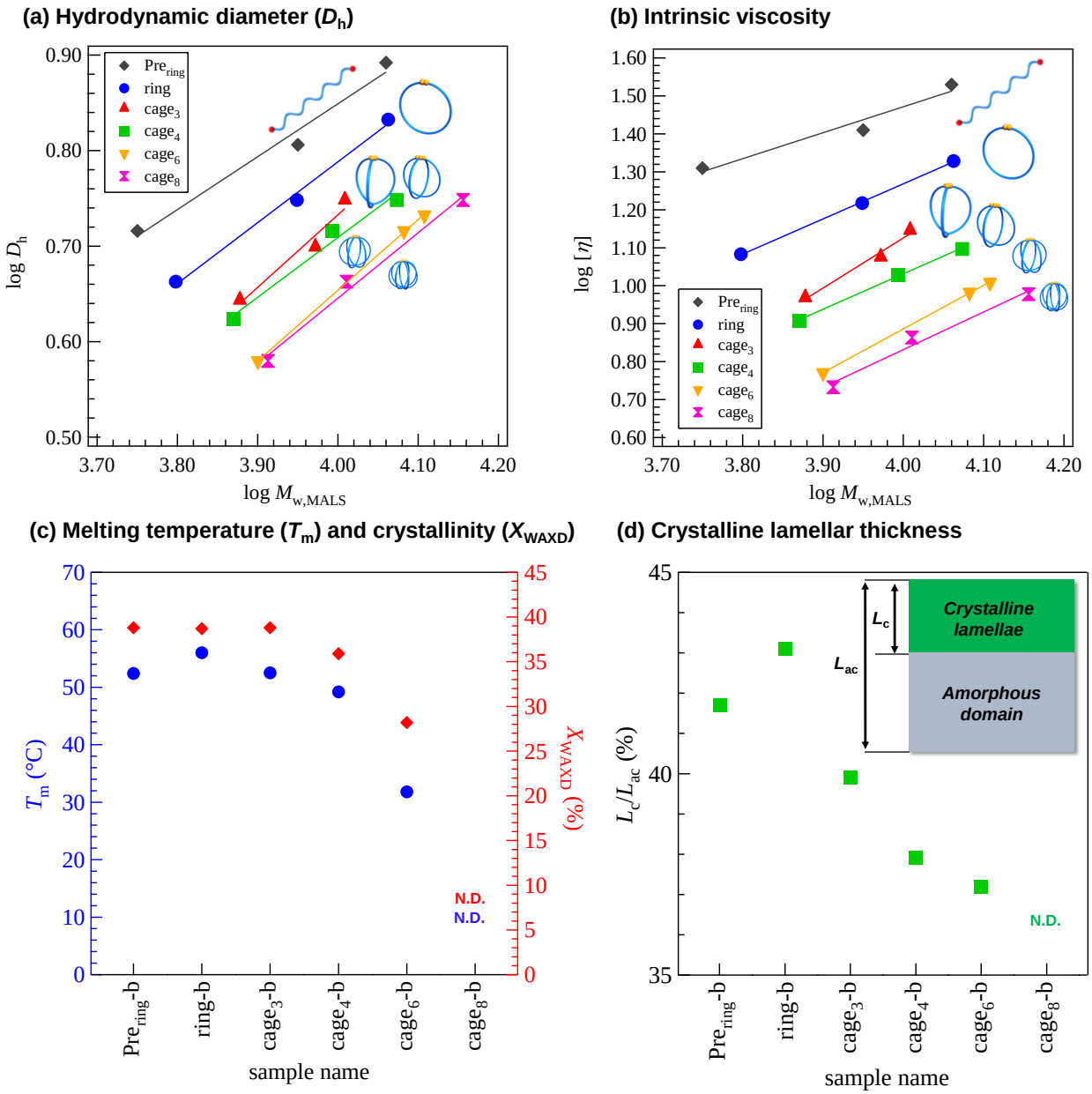

Figure 3.4. Structure-property relationships in macromolecular cage systems. (Panels a and b) Double logarithmic plots of $M_{w,MALS}$ versus D_h and [η] for linear (**Pre$_{ring}$**), monocyclic (**ring**) (eluent, THF). (Panels c and d) Plots of T_m (blue), X_{WAXD} (red), and (d) L_c/L_{ac} (green) versus arm numbers of linear, monocyclic polymers, and macromolecular cages (all the samples had $M_{n,NMR}$ of ca. 9,000 g mol^{-1}; from left to right, **Pre$_{ring}$-b**, **ring-b**, **cage$_3$-b**, **cage$_4$-b**, **cage$_6$-b**, and **cage$_8$-b**). The inset in panel d illustrates the model structure of the long period of the PCL crystal which consists of a crystalline lamellar and an amorphous domain with thicknesses of L_c and L_{ac}, respectively. The T_m and L_c/L_{ac} for **cage$_8$-b** were not determined (N.D.) due to its poor crystallinity.

Since PCL is a typical semicrystalline polymer, its solid state properties are also of particular interest. Thus, melting temperature (T_m), crystallinity (X_{WAXD}), and the lamellar thickness in the PCL crystal long period, were then examined by differential scanning calorimetry (DSC), wide-angle X-ray diffraction (WAXD), and small-angle X-ray scattering (SAXS) measurements, respectively. Note that a series of samples discussed in Figure 3.4(c) and 3.4(d) had $M_{n,NMR}$ of ca. 9,000 g mol^{-1}and thus their arm lengths are reduced with the increasing arm number. The T_m value of the **ring-b** (56.0 °C) is found to be slightly higher than the linear counterpart **Pre$_{ring}$-b** (52.4 °C). Ree and Saalwächter groups also reported a similar trend when compared among linear and ring PCLs.[27,30] In contrast, T_m and X_{WAXD} values of macromolecular cages apparently decrease with the increasing arm number. For example, the T_m and X_{WAXD} of **cage$_6$-b** are determined to be 31.8 °C and 28.2%, respectively, which are apparently lower than those of **ring-b** (56.0 °C and 38.7%, respectively) and **cage$_3$-b** (52.5°C and 38.8%, respectively) (see also Figures S3.17 and S3.18). On the other hand, **cage$_8$-b** is found to hardly crystallize. These results implied the distinctive difference in crystallization behaviors between the single cyclic polymer and macromolecular cages. Increase in arm number causes decrease in chain mobility and chain packing ability as well as reduction in each arm length, resulting in less or no crystalline formation in the macromolecular cages (Figure S3.19).[31,32] To further gain an insight into the crystallization behaviors, SAXS analysis was performed on the PCL samples, which provided information about the crystalline lamellar layer formation in crystalline-amorphous two-phase systems (Figures S3.20–3.24). Based on the correlation function analysis of the SAXS profiles,[33] the author estimated the ratio of the crystalline lamellae thickness (L_c) and long period (L_{ac}), i.e., L_c/L_{ac} (Figure 4d). The L_c/L_{ac} values of the macromolecular cages decrease with increasing arm number, whereas no significant change is observed in their L_{ac} (see Tables S3.1–S3.4). In a similar manner with the T_m and X_{WAXD} values, significant decrease in the lamellae thickness (37.2–43.1% and N.D.) is

observed with the increasing arm number, which also can be considered due to the suppressed molecular mobility and diminished chain-packing ability. The increased L_c/L_{ac} value in **ring-b**, as compared to the liner counterpart, seems to be correlated with its increased T_m value. It is also worth noting that the T_m, X_{WAXD}, and L_c/L_{ac} of the macromolecular cages tend to be lower than those of the star-shaped precursors, despite their equivalent arm length. This suggests that one additional junction point to construct the cage-shaped architecture bring about significant impact on the solid state properties. The difference in the crystallization behaviors among the macromolecular cages and the corresponding star-shaped precursors is more pronounced when the arm number is increased. For example, low molecular weight macromolecular cages having six- and eight-arms (**cage$_6$- a** and **cage$_8$-a**; $M_{n,NMR}$ = ca. 6,000 g mol^{-1}) do not show any evidence of crystallization from the WAXD analysis (Figures S3.25–S3.29), while their star-shaped precursors displayed distinct scattering peaks corresponding to the PCL crystal structure (Figures S3.23, S3.24, S3.28, S3.29). Interestingly, **cage$_8$-b** ($M_{n,NMR}$ = 9,530 g mol^{-1}) with degree of polymerization of each arm of around eight is still amorphous, despite the fact that linear caprolactone tetramer can be crystallized.[34] This demonstrates a cage-shaped topological effects on the solid state properties.

3.4 Conclusion

In this study, the author has successfully demonstrated the synthesis of macromolecular cages with desired arm numbers and sizes based on the intramolecular consecutive ROMO of the highly reactive norbornenyl groups attached to star-shaped polymer precursors. It is notable that the intramolecular ROMO enabled the facile yet precise synthesis of six and eight-armed cage-shaped polymers, while conventional syntheses present a practical limitation to the systematic synthesis of macromolecular cages with arm numbers greater than seven. In addition, the author was able to systematically evaluate the polymer properties associated with the cage-shaped architecture, which revealed that the hydrodynamic diameter, viscosity, and crystallization behavior of macromolecular cages are strongly affected by the arm number and arm length. The synthetic strategy proposed in this study should be applicable to a wide range of polymer backbones, enabling access to macromolecular cages with unique structures and functions that will open new avenues for research in supramolecular chemistry and the material sciences.

3.5 References

(1) Cook, T. R.; Stang, P. J. Recent Developments in the Preparation and Chemistry of Metallacycles and Metallacages via Coordination. *Chem. Rev.* **2015**, *115*, 7001–7045.

(2) Zhang, D.; Martinez, A.; Dutasta, J. P. Emergence of Hemicryptophanes: From Synthesis to Applications for Recognition, Molecular Machines, and Supramolecular Catalysis. *Chem. Rev.* **2017**, *117*, 4900–4942.

(3) Durot, S.; Taesch, J.; Heitz, V. Multiporphyrinic Cages: Architectures and Functions. *Chem. Rev.* **2014**, *114*, 8542–8578.

(4) Jutz, G.; Van Rijn, P.; Santos Miranda, B.; Böker, A. Ferritin: A Versatile Building Block for Bionanotechnology. *Chem. Rev.* **2015**, *115*, 1653–1701.

(5) Juul, S.; Iacovelli, F.; Falconi, M.; Kragh, S. L.; Christensen, B.; Frøhlich, R.; Franch, O.; Kristoffersen, E. L.; Stougaard, M.; Leong, K. W.; Ho, Y. P.; Sørensen, E. S.; Birkedal, V.; Desideri, A.; Knudsen, B. R. Temperature-Controlled Encapsulation and Release of an Active Enzyme in the Cavity of a Self-Assembled DNA Nanocage. *ACS Nano* **2013**, *7*, 9724–9734.

(6) Erben, C. M.; Goodman, R. P.; Turberfield, A. J. Single-Molecule Protein Encapsulation in a Rigid DNA Cage. *Angew. Chem. Int. Ed.* **2006**, *45*, 7414–7417.

(7) McCaffrey, R.; Long, H.; Jin, Y.; Sanders, A.; Park, W.; Zhang, W. Template Synthesis of Gold Nanoparticles with an Organic Molecular Cage. *J. Am. Chem. Soc.* **2014**, *136*, 1782–1785.

(8) Ueda, Y.; Ito, H.; Fujita, D.; Fujita, M. Permeable Self-Assembled Molecular Containers for Catalyst Isolation Enabling Two-Step Cascade Reactions. *J. Am. Chem. Soc.* **2017**, *13*, 6090–6093.

(9) Yoshizawa, M.; Klosterman, J. K.; Fujita, M. Functional Molecular Flasks: New Properties and Reactions within Discrete, Self-Assembled Hosts. *Angew. Chem. Int. Ed.* **2009**, *48* (19), 3418–3438.

(10) Lehn, J. M. Cryptates: Inclusion Complexes of Macropolycyclic Receptor Molecules. *Pure Appl. Chem.* **1978**, *50* (9–10), 871–892. https://doi.org/10.1351/pac197850090871.

(11) Mastalerz, M. Shape-Persistent Organic Cage Compounds by Dynamic Covalent Bond Formation. *Angew. Chem. Int. Ed.* **2010**, *49*, 5042–5053.

(12) Edwardson, T. G. W.; Carneiro, K. M. M.; McLaughlin, C. K.; Serpell, C. J.; Sleiman, H. F. Site-Specific Positioning of Dendritic Alkyl Chains on DNA Cages Enables Their Geometry-Dependent Self-Assembly. *Nat. Chem.* **2013**, *5*, 868–875.

(13) Lai, Y. T.; Cascio, D.; Yeates, T. O. Structure of a 16-Nm Cage Designed by Using Protein Oligomers. *Science* **2012**, *336*, 1129.

(14) Yavuz, M. S.; Cheng, Y.; Chen, J.; Cobley, C. M.; Zhang, Q.; Rycenga, M.; Xie, J.; Kim, C.; Song, K. H.; Schwartz, A. G.; Wang, L. V.; Xia, Y. Gold Nanocages Covered by Smart

Polymers for Controlled Release with Near-Infrared Light. *Nat. Mater.* **2009**, *8*, 935–939.

(15) Fujita, D.; Ueda, Y.; Sato, S.; Mizuno, N.; Kumasaka, T.; Fujita, M. Self-Assembly of Tetravalent Goldberg Polyhedra from 144 Small Components. *Nature* **2016**, *540*, 563–566.

(16) Cook, T. R.; Zheng, Y. R.; Stang, P. J. Metal-Organic Frameworks and Self-Assembled Supramolecular Coordination Complexes: Comparing and Contrasting the Design, Synthesis, and Functionality of Metal-Organic Materials. *Chem. Rev.* **2013**, *113*, 734–777.

(17) Bo, Z.; Feng, W.; Shengyi, D.; Feihe, H. Polymers Constructed By Crown Ether-Based Molecular Recognition. *Chem. Soc. Rev.* **2012**, *41*, 1621–1636.

(18) Polymeropoulos, G.; Zapsas, G.; Ntetsikas, K.; Bilalis, P.; Gnanou, Y.; Hadjichristidis, N. 50th Anniversary Perspective: Polymers with Complex Architectures. *Macromolecules* **2017**, *50*, 1253–1290.

(19) Bates, C. M.; Bates, F. S. 50th Anniversary Perspective: Block Polymers-Pure Potential. *Macromolecules* **2017**, *50* (1), 3–22. https://doi.org/10.1021/acs.macromol.6b02355.

(20) Poelma, J. E.; Ono, K.; Miyajima, D.; Aida, T.; Satoh, K.; Hawker, C. J. Cyclic Block Copolymers for Controlling Feature Sizes in Block Copolymer Lithography. *ACS Nano* **2012**, *6*, 10845–10854.

(21) Jeong, J.; Kim, K.; Lee, R.; Lee, S.; Kim, H.; Jung, H.; Kadir, M. A.; Jang, Y.; Jeon, H. B.; Matyjaszewski, K.; Chang, T.; Paik, H. J. Preparation and Analysis of Bicyclic Polystyrene. *Macromolecules* **2014**, *47*, 3791–3796.

(22) Tezuka, Y.; Tsuchitani, A.; Yoshioka, Y.; Oike, H. Synthesis of θ-Shaped Poly(THF) by Electrostatic Self-Assembly and Covalent Fixation with Three-Armed Star Telechelics Having Cyclic Ammonium Salt Groups. *Macromolecules* **2003**, *36*, 65–70.

(23) Tezuka, Y.; Fujiyama, K. Construction of Polymeric ??-Graph: A Doubly Fused Tricyclic Topology. *J. Am. Chem. Soc.* **2005**, *127*, 6266–6270.

(24) Satoh, Y.; Matsuno, H.; Yamamoto, T.; Tajima, K.; Isono, T.; Satoh, T. Synthesis of Well-Defined Three- and Four-Armed Cage-Shaped Polymers via “Topological Conversion” from Trefoil- and Quatrefoil-Shaped Polymers. *Macromolecules* **2017**, *50*, 97–106.

(25) Choi, T. L.; Grubbs, R. H. Controlled Living Ring-Opening-Metathesis Polymerization by a Fast-Initiating Ruthenium Catalyst. *Angew. Chem. Int. Ed.* **2003**, *42*, 1743–1746.

(26) Ouchi, M.; Inoue, Y.; Wada, K.; Iketani, S. I.; Hakushi, T.; Weber, E. Molecular Design of Crown Ethers. 4.1,2Syntheses and Selective Cation Binding of 16-Crown-5 and 19-Crown-6 Lariats. *J. Org. Chem.* **1987**, *52*, 2420–2427.

(27) Li, X.; Ryu, W.; Kim, H.; Ree, M. Precise Synthesis, Properties, and Structures of Cyclic Poly(ε-caprolactone)s. **2018**, *10*, 577.

(28) Pipertzis, A.; Hossain, M. D.; Monteiro, M. J.; Floudas, G. Segmental Dynamics in

Multicyclic Polystyrenes. *Macromolecules* **2018**, *51*, 1488–1497.

(29) Hossain, M. D.; Reid, J. C.; Lu, D.; Jia, Z.; Searles, D. J.; Monteiro, M. J. Influence of Constraints within a Cyclic Polymer on Solution Properties. *Biomacromolecules* **2018**, *19*, 616–625.

(30) Schäler, K.; Ostas, E.; Schröter, K.; Thurn-Albrecht, T.; Binder, W. H.; Saalwächter, K. Influence of Chain Topology on Polymer Dynamics and Crystallization. Investigation of Linear and Cyclic Poly(ε-Caprolactone)s by 1H Solid-State NMR Methods. *Macromolecules* **2011**, *44*, 2743–2754.

(31) Wang, J. L.; Dong, C. M. Physical Properties, Crystallization Kinetics, and Spherulitic Growth of Well-Defined Poly(ε -Caprolactone)s with Different Arms. *Polymer* **2006**, *47*, 3218–3228.

(32) Tezuka, Y.; Ohtsuka, T.; Adachi, K.; Komiya, R.; Ohno, N.; Okui, N. A Defect-Free Ring Polymer: Size-Controlled Cyclic Poly(Tetrahydrofuran) Consisting Exclusively of the Monomer Unit. *Macromol. Rapid Commun.* **2008**, *29*, 1237–1241.

(33) Goderis, B.; Reynaers, H.; Koch, M. H. J.; Mathot, V. B. F. Use of SAXS and Linear Correlation Functions for the Determination of the Crystallinity and Morphology of Semi- Crystalline Polymers . Application to Linear Polyethylene. *Polymer* **1999**, *1*, 1715–1738.

(34) Takizawa, K.; Tang, C.; Hawker, C. J. Molecularly Defined Caprolactone Oligomers and Polymers: Synthesis and Characterization. *J. Am. Chem. Soc.* **2008**, *130*, 1718–1726.

(35) Strobl, G. R.; Schneider, M. Direct Evaluation of the Electron Density Correlation Function of Partially Crystalline Polymers. *J. Polym. Sci. Part A-2, Polym. Phys.* **1980**, *18*, 1343–1359.

3.6 Supporting Information

Additional results

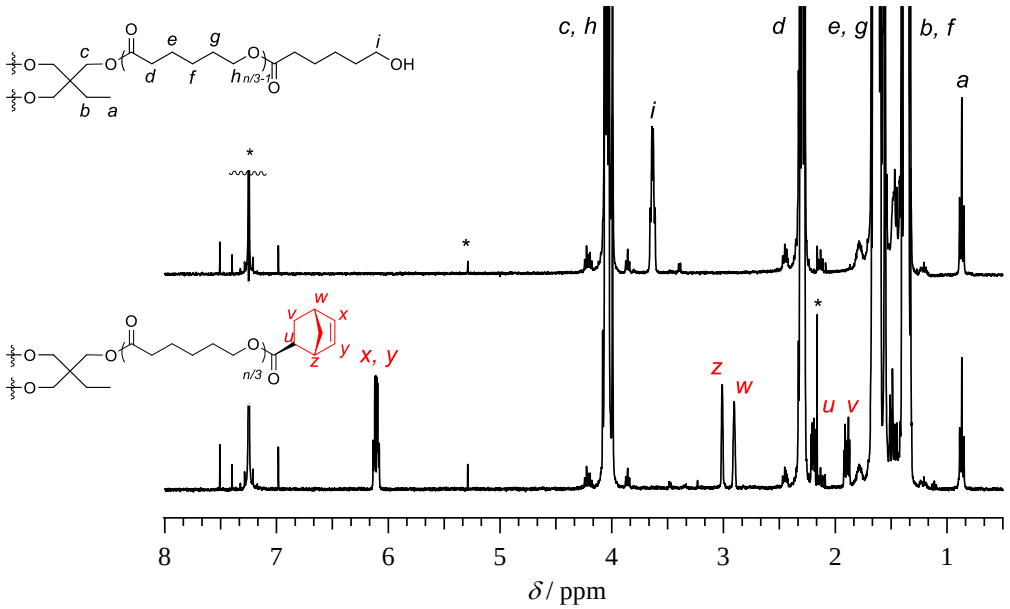

Figure S3.1. ^{1}H NMR spectra of *s*-(PCL-OH)$_3$-a ($M_{n,NMR}$ = 5,530, $Đ$ = 1.07; upper) and **Pre$_3$-a** ($M_{n,NMR}$ = 6,000, $Đ$ = 1.05; lower) in $CDCl_3$. Asterisks show solvent signals.

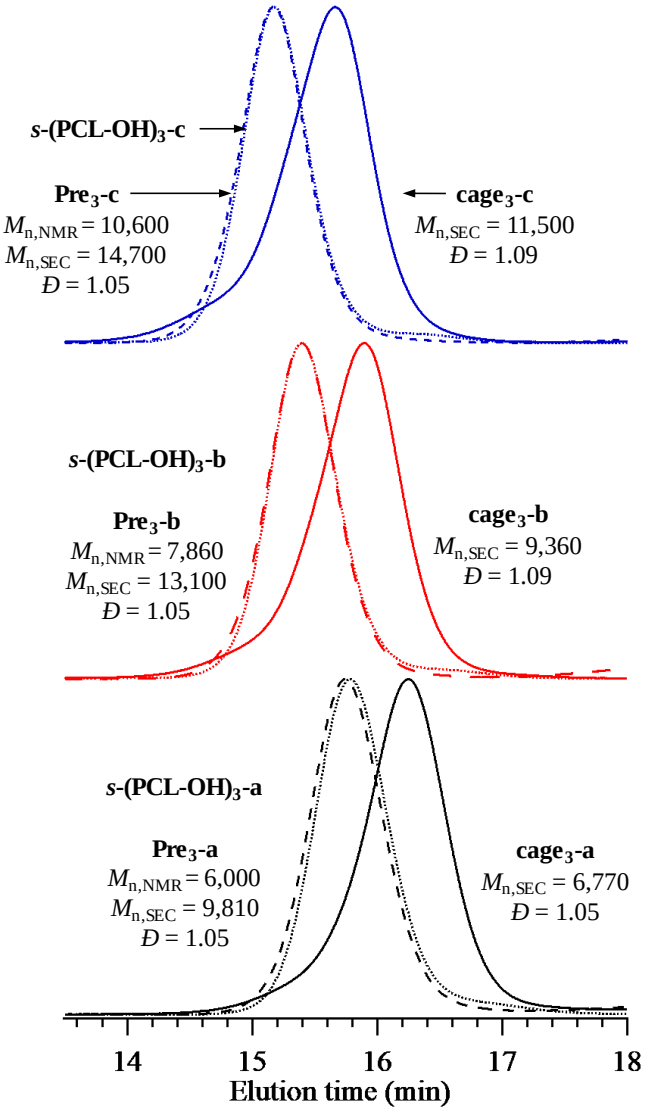

Figure S3.2. SEC traces of ***s*-(PCL-OH)3**s (dashed line), **Pre3**s (dotted line), and **cage3**s (solid line) with different molecular weight.

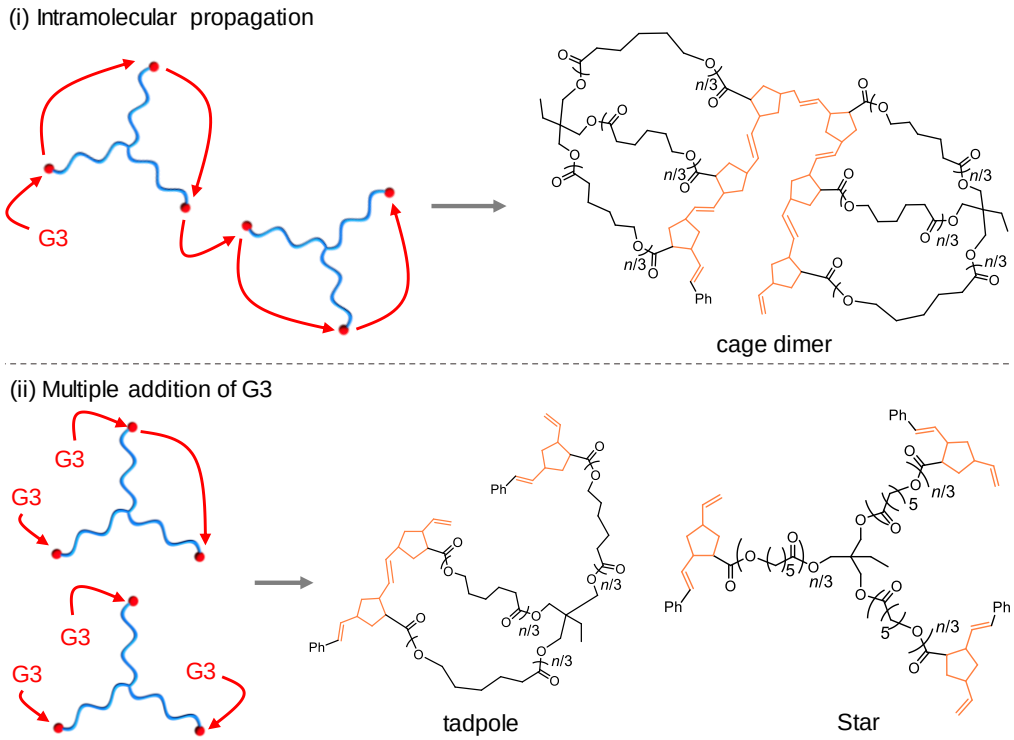

Figure S3.3. Schematic illustration of possible side reactions during the synthesis of **cage3-a**: (i) oligomer formation through intermolecular propagation and (ii) acyclic by-product formation through multiple addition of G3.

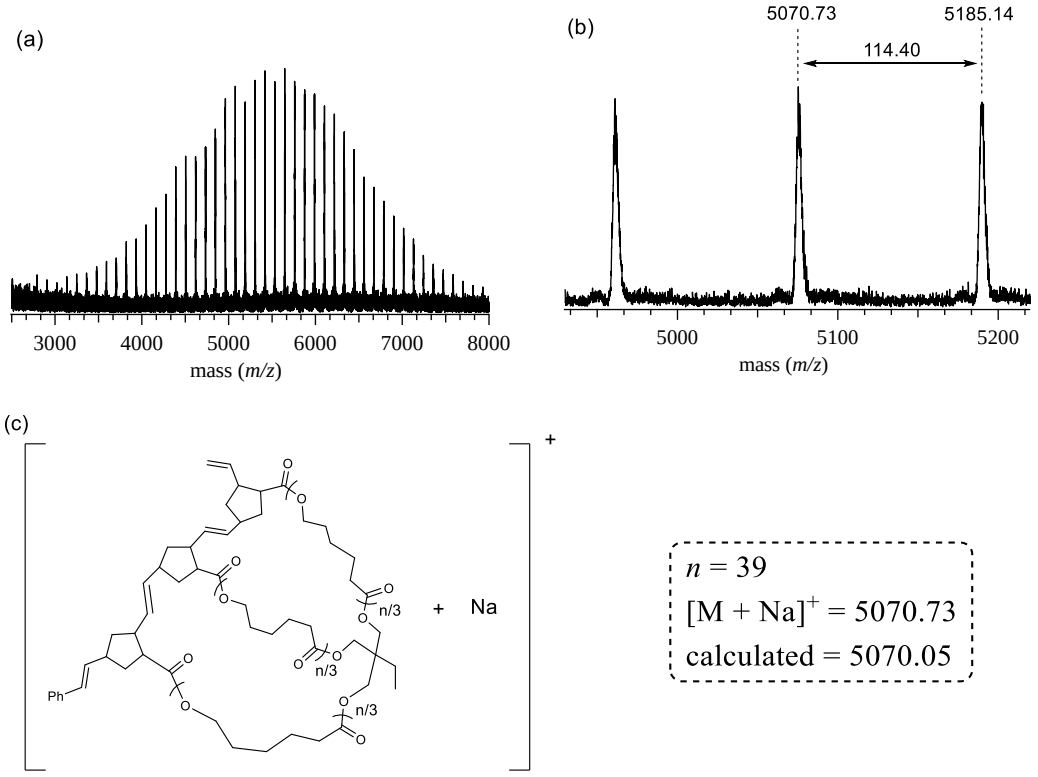

Figure S3.4. MALDI-TOF MS analysis of the obtained **cage$_3$-a**

Table S3.1. Molecular characterization of three-armed macromolecular cages (**cage$_3$**) and their precursors

Sample	$M_{n,NMR}$ [a]	$M_{n,SEC}$ [b]	$M_{w,MALS}$ [c]	$Đ$ [b]	yield (%)	D_h [c] (nm)	$[\eta]$ [c] (mL g^{-1})	T_m [d] (°C)	X_{WAXD} [e] (%)	L_{ac} [f] (nm)	L_c/L_{ac} [f] (%)
s-(PCL-OH)$_3$-a	5,530	9,440	-	1.07	77.5	-	-	-	-	-	-
Pre$_3$-a	6,000	9,810	5,900	1.05	63.2	4.8	16.3	44.5	36.8	12.3	37.1
cage$_3$-a	-	6,770	7,550	1.09	92.3	4.4	9.1	46.3	33.9	10.8	38.2
s-(PCL-OH)$_3$-b	7,730	12,100	-	1.07	82.2	-	-	-	-	-	-
Pre$_3$-b	7,860	13,100	8,060	1.05	79.5	6.0	19.6	38.4	39.5	12.5	38.5
cage$_3$-b	-	9,360	9,370	1.09	80.0	5.0	11.8	52.5	38.8	11.2	39.9
s-(PCL-OH)$_3$-c	9,390	14,600	-	1.06	75.6	-	-	-	-	-	-
Pre$_3$-c	10,600	14,700	9,680	1.05	39.0	6.8	22.0	49.9	38.7	11.2	40.0
cage$_3$-c	-	11,500	10,200	1.09	84.0	5.6	14.1	54.3	40.6	11.4	40.3

.

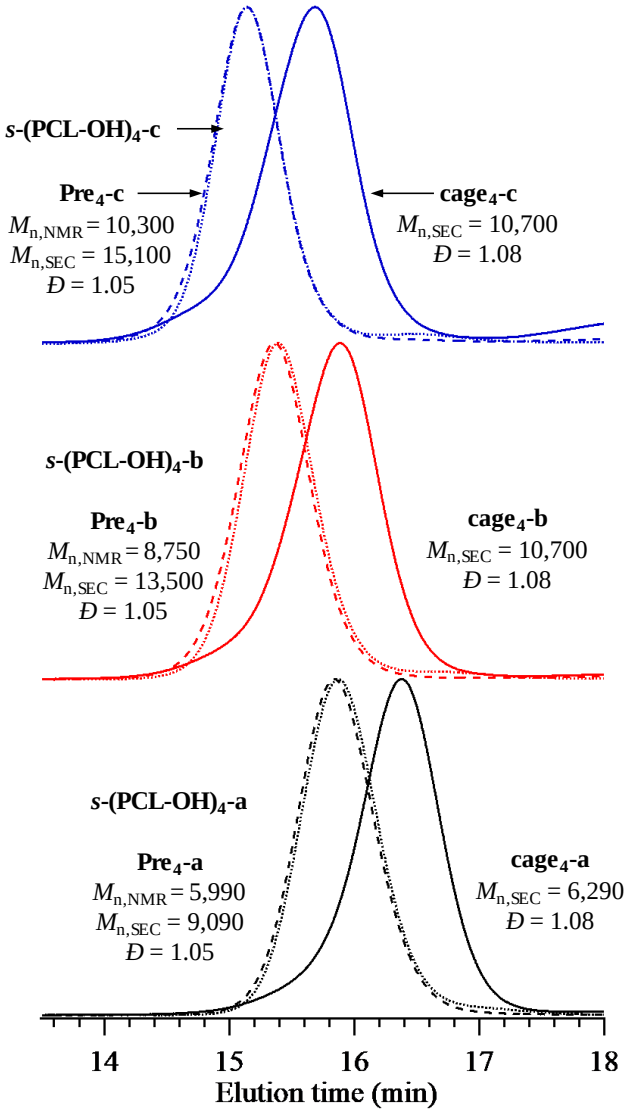

Figure S3.5. SEC traces of ***s*-(PCL-OH)$_4$s** (dashed line), **Pre$_4$s** (dotted line), and **cage$_4$s** (solid line) with different molecular weight.

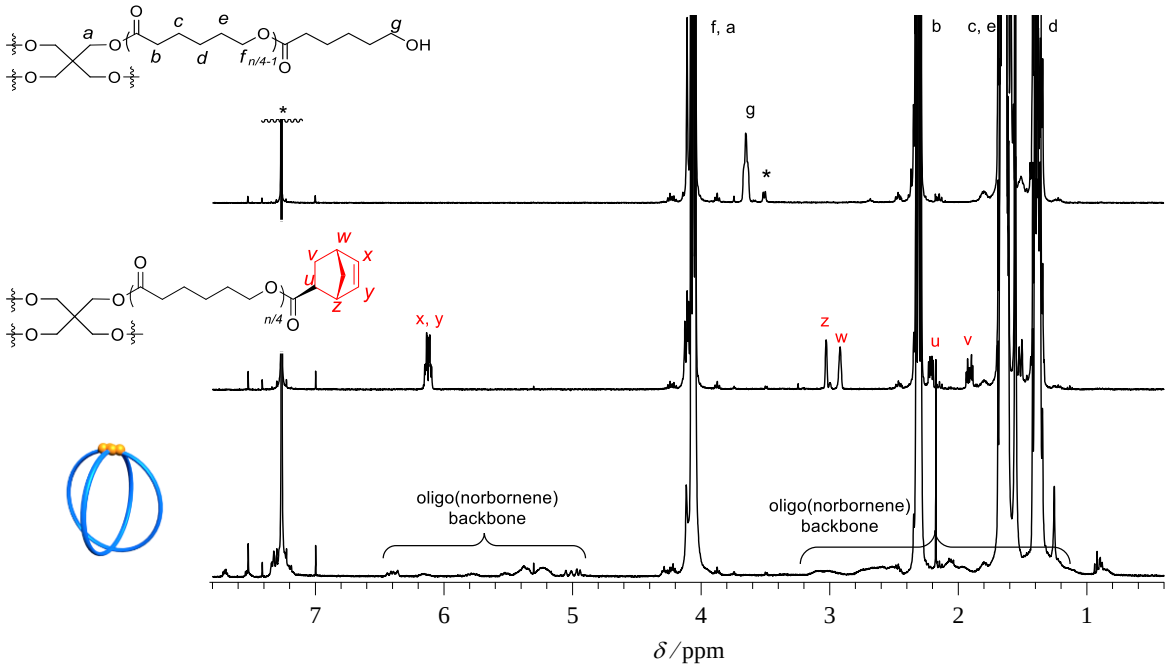

Figure S3.6. ^{1}H NMR spectra of ***s*-(PCL-OH)$_4$-a** ($M_{n,NMR}$ = 5,970, $Đ$ = 1.06; upper), **Pre$_4$-a** ($M_{n,NMR}$ = 5,990, $Đ$ = 1.05; middle), and **cage$_4$-a** ($Đ$ = 1.08; lower) in $CDCl_3$. Asterisks show solvent signals.

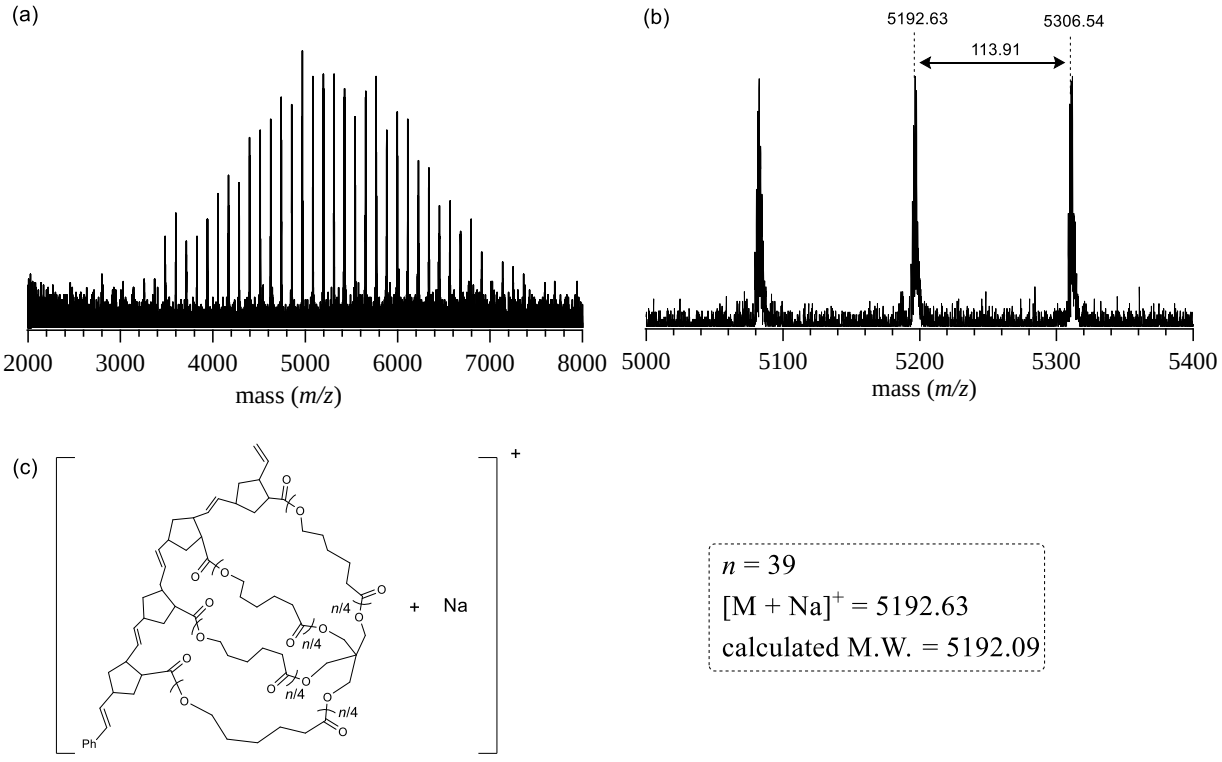

Figure S3.7. MALDI-TOF MS analysis of the obtained **cage$_4$-a**.

Table S3.2. Molecular characterization of four-armed macromolecular cages (**cage$_4$**) and their precursors

Sample	$M_{n,NMR}$ [a]	$M_{n,SEC}$ [b]	$M_{w,MALS}$ [c]	$Đ$ [b]	yield (%)	D_h [c] (nm)	$[\eta]$ [c] (mL g^{-1})	T_m [d] (°C)	X_{WAXD} [e] (%)	L_{ac} [f] (nm)	L_c/L_{ac} [f] (%)
s-(PCL-OH)$_4$-a	5,970	9,290	-	1.06	82.9	-	-	-	-	-	-
Pre$_4$-a	5,990	9,090	6,210	1.05	63.2	5.0	15.4	40.0	31.7	12.3	37.2
cage$_4$-a	-	6,290	7,420	1.08	97.0	4.2	7.4	38.0	32.4	11.1	37.2
s-(PCL-OH)$_4$-b	8,740	12,700	-	1.06	82.3	-	-	-	-	-	-
Pre$_4$-b	8,750	13,500	8,820	1.05	79.5	6.0	19.0	46.0	42.8	12.1	38.3
cage$_4$-b	-	9,590	9,840	1.08	94.0	5.0	10.8	45.2	35.9	11.0	37.9
s-(PCL-OH)$_4$-c	10,400	15,200	-	1.05	84.5	-	-	-	-	-	-
Pre$_4$-c	10,300	15,100	10,100	1.05	39.0	6.6	21.9	48.4	36.2	11.1	40.1
cage$_4$-c	-	10,700	11,800	1.08	91.0	5.6	12.0	47.0	34.4	11.0	38.6

[a] Determined by ^{1}H NMR. [b] Determined by SEC in THF using PSt standards. [c] Determined by SEC-MALS-Visco in THF. $D_h = 2\ R_h = 2(3V_h/4\pi)^{1/3}$; V_h is hydrodynamic volume. V_h was calculated by Einstein–Simha equation ($V_h = M_{w,MALS}[\eta]/2.5N_A$; N_A: Avogadro's number).[d] Determined from a melting peak of the DSC curve. [e] Determined by WAXD at r.t. [f] Determined by SAXS at r.t.

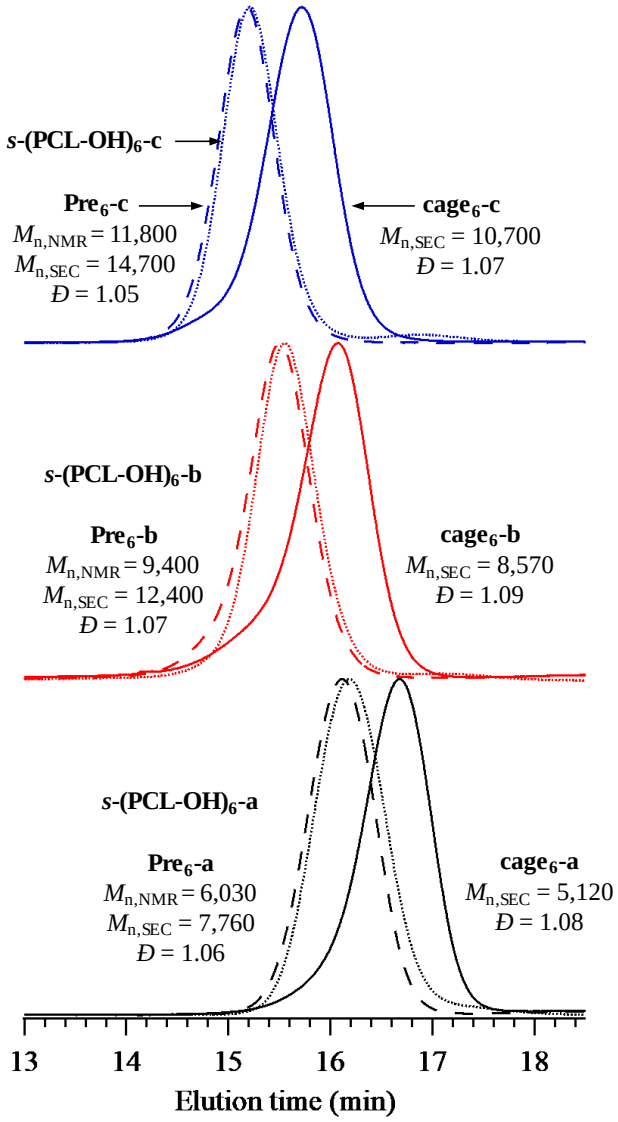

Figure S3.8. SEC traces of ***s*-(PCL-OH)$_6$s** (dashed line), **Pre$_6$s** (dotted line), and **cage$_6$s** (solid line) with different molecular weight.

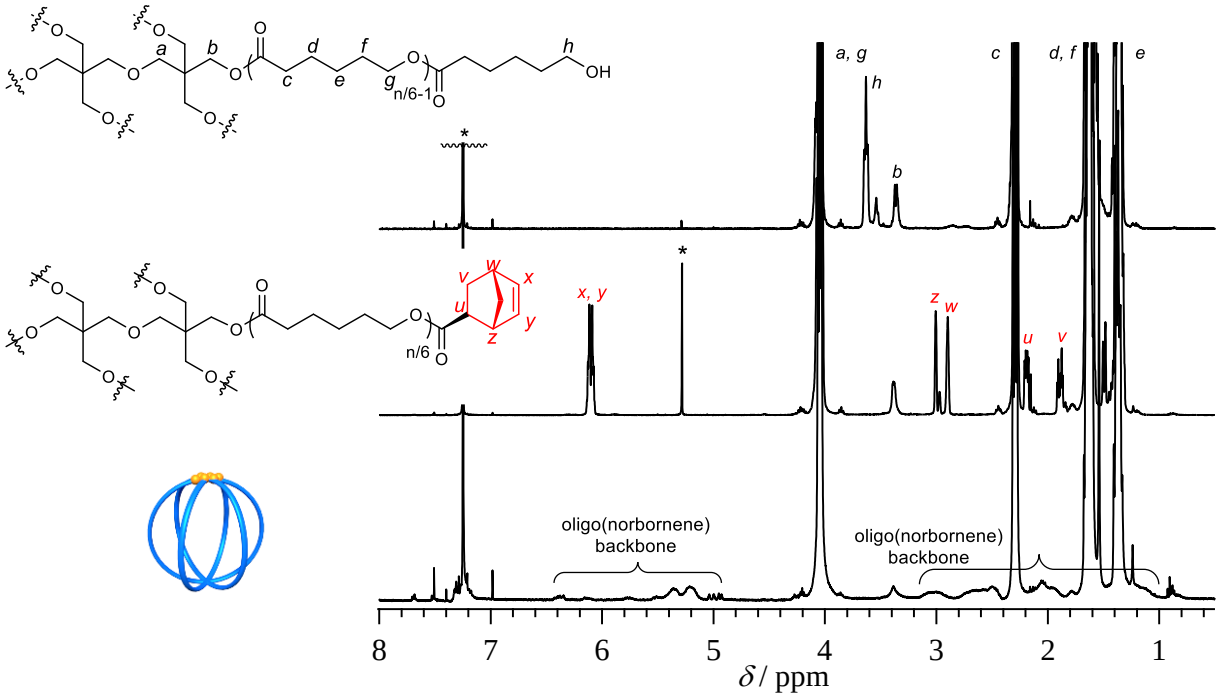

Figure S3.9. ^{1}H NMR spectra of ***s*-(PCL-OH)$_6$-a** ($M_{n,NMR}$ = 5,300, $Đ$ = 1.09; upper), **Pre$_6$-a** ($M_{n,NMR}$ = 6,030, $Đ$ = 1.06; middle), and **cage$_6$-a** ($Đ$ = 1.08; lower) in $CDCl_3$. Asterisks show solvent signals.

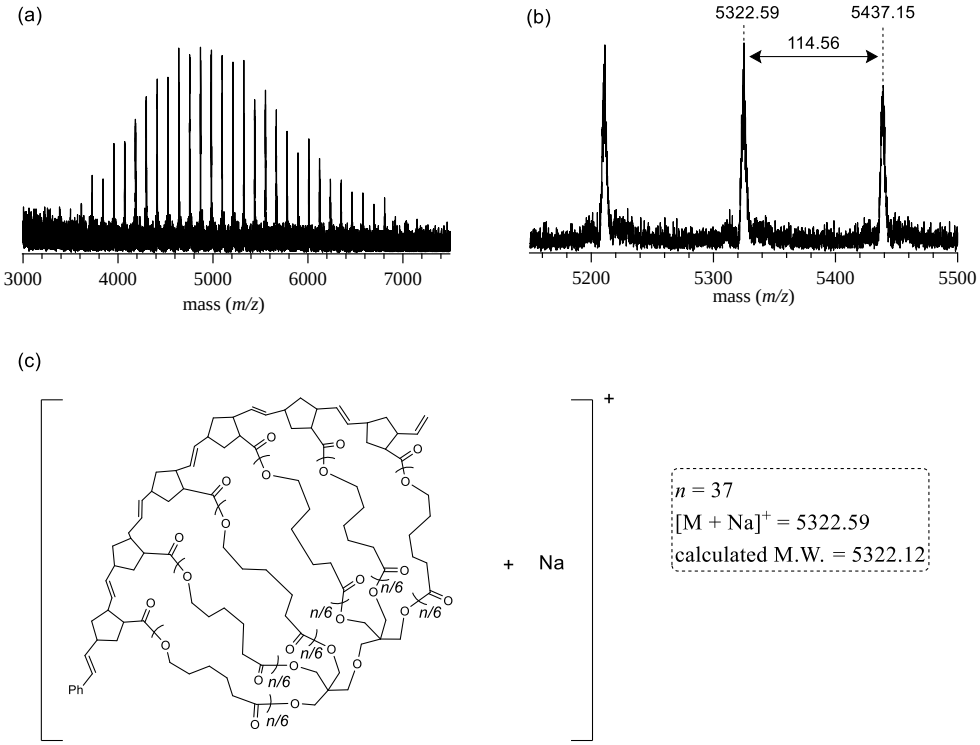

Figure S3.10. MALDI-TOF MS analysis of the obtained **cage$_6$-a**.

Table S3.3. Molecular characterization of six-armed macromolecular cages (**cage$_6$**) and their precursors

Sample	$M_{n,NMR}$ [a]	$M_{n,SEC}$ [b]	$M_{w,MALS}$ [c]	$Đ$ [b]	yield (%)	D_h [c] (nm)	$[\eta]$ [c] (mL g^{-1})	T_m [d] (°C)	X_{WAXD} [e] (%)	L_{ac} [f] (nm)	L_c/L_{ac} [f] (%)
s-(PCL-OH)$_6$-a	5,300	7,000	-	1.09	72.0	-	-	-	-	-	-
Pre$_6$-a	6,030	7,760	6,000	1.06	41.1	4.4	11.7	26.4	11.9	N.D.[g]	N.D.[g]
cage$_6$-a	-	5,120	7,950	1.08	91.0	3.8	5.6	N.D.[g]	N.D.[g]	N.D.[g]	N.D.[g]
s-(PCL-OH)$_6$-b	7,760	11,600	-	1.06	67.8	-	-	-	-	-	-
Pre$_6$-b	9,400	12,400	8,880	1.07	49.8	5.6	15.7	39.6	25.7	12.6	38.9
cage$_6$-b	-	8,570	10,900	1.09	98.7	5.0	9.1	31.8	28.2	12.5	37.2
s-(PCL-OH)$_6$-c	10,700	14,400	-	1.04	85.1	-	-	-	-	-	-
Pre$_6$-c	11,800	14,700	11,900	1.05	48.0	6.2	17.5	42.2	33.0	12.6	37.3
cage$_6$-c	-	10,700	12,800	1.07	91.2	5.2	9.8	40.5	29.9	12.5	37.4

[a] Determined by ^{1}H NMR. [b] Determined by SEC in THF using PSt standards. [c] Determined by SEC-MALS-Visco in THF. $D_h = 2\ R_h = 2(3V_h/4\pi)^{1/3}$; V_h is hydrodynamic volume. V_h was calculated by Einstein–Simha equation ($V_h = M_{w,MALS}[\eta]/2.5N_A$; N_A: Avogadro's number).[d] Determined from a melting peak of the DSC curve. [e] Determined by WAXD at r.t. [f] Determined by SAXS at r.t. [g] Not determined.

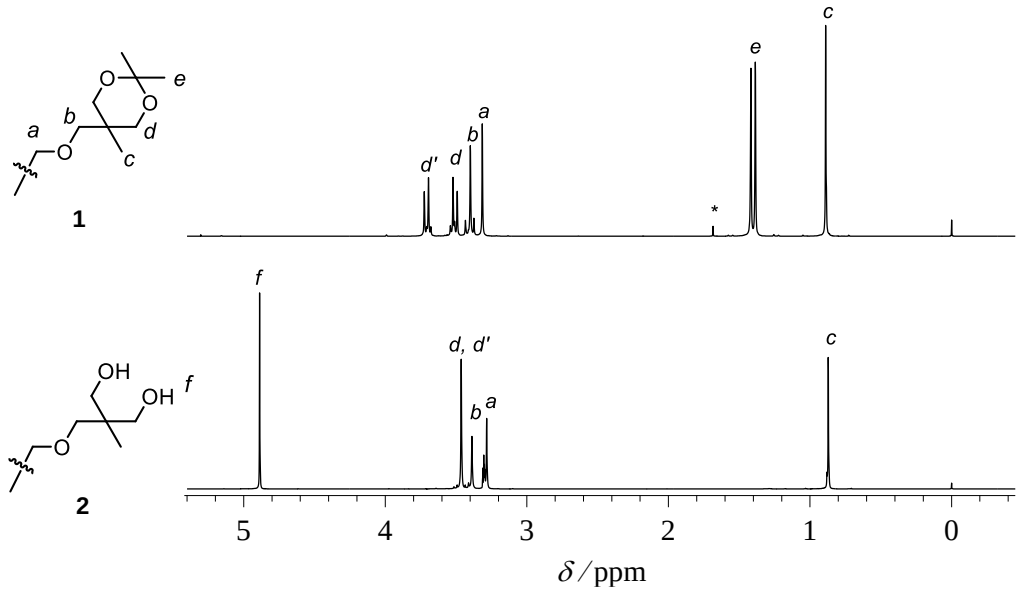

Figure S3.11. ^{1}H NMR spectra of **1** (upper) and **2** (lower).

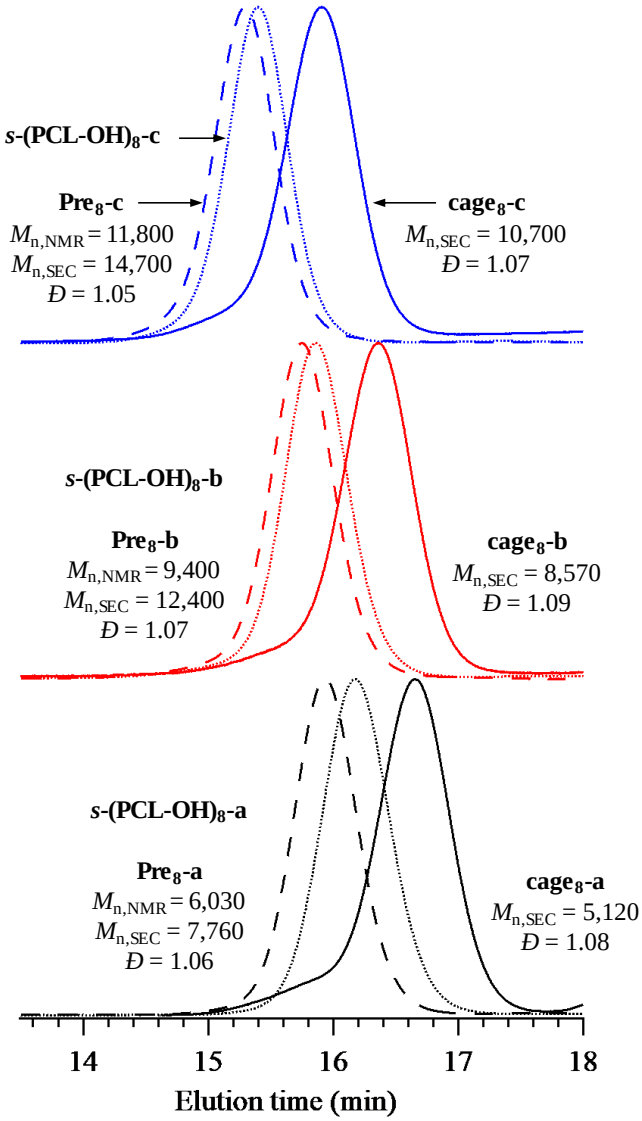

Figure S3.12. SEC traces of ***s*-(PCL-OH)$_8$s** (dashed line), **Pre$_8$s** (dotted line), and **cage$_8$s** (solid line) with different molecular weight.

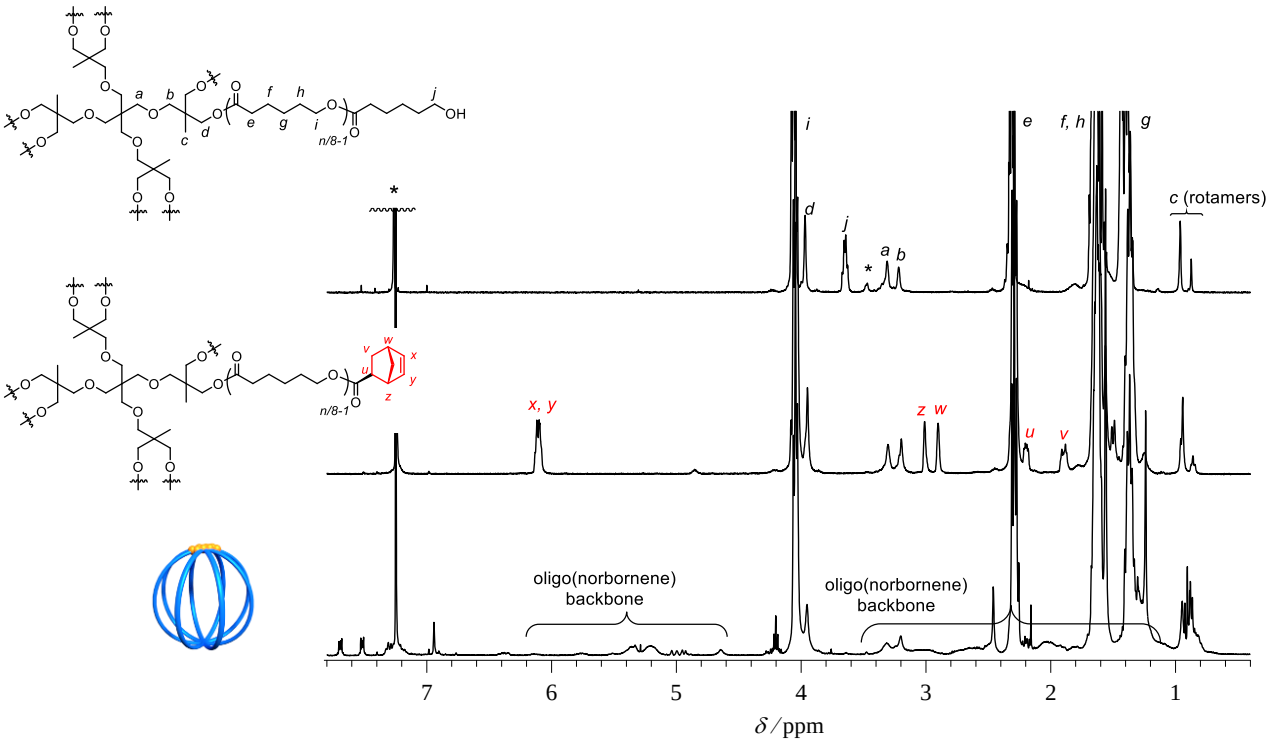

Figure S3.13. ^{1}H NMR spectra of ***s*-(PCL-OH)$_8$-a** ($M_{n,NMR}$ = 5,970, $Đ$ = 1.04; upper), **Pre$_8$-a** ($M_{n,NMR}$ = 7,300, $Đ$ = 1.04; middle), and **cage$_8$-a** ($Đ$ = 1.06; lower) in $CDCl_3$. Asterisks show solvent signals.

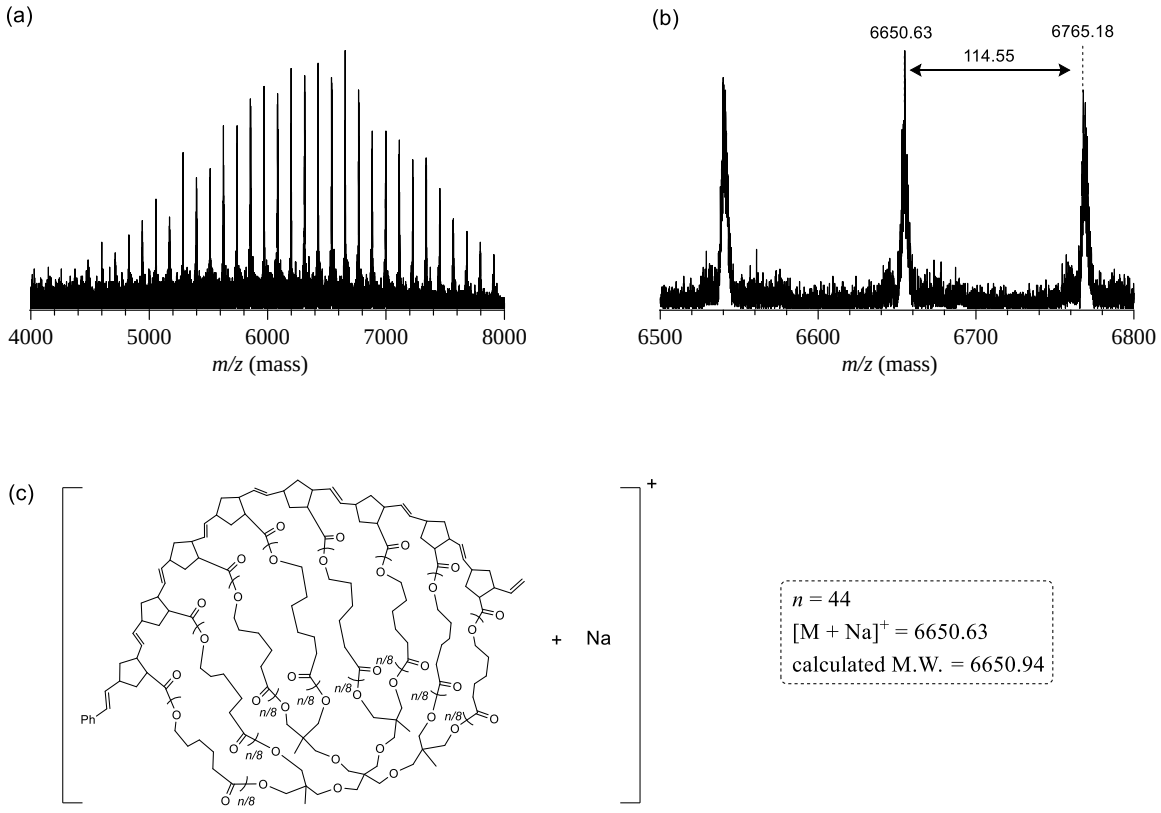

Figure S3.14. MALDI-TOF MS analysis of the obtained **cages-a**.

Table S3.4. Molecular characterization of eight-armed macromolecular cages (**cages**) and their precursors

Sample	$M_{n,NMR}$ [a]	$M_{n,SEC}$ [b]	$M_{w,MALS}$ [c]	$Đ$ [b]	yield (%)	D_h [c] (nm)	$[\eta]$ [c] (mL g^{-1})	T_m [d] (°C)	X_{WAXD} [e] (%)	L_{ac} [f] (nm)	L_c/L_{ac} [f] (%)
s-(PCL-OH)$_8$-a	5,970	8,400	-	1.04	93.0	-	-	-	-	-	-
Pre$_8$-a	7,300	8,930	7,230	1.04	92.1	4.6	11.1	19.8	N.D.[g]	N.D.[g]	N.D.[g]
cage$_8$-a	-	6,400	8,180	1.06	98.3	3.8	5.4	N.D.	N.D.[g]	N.D.[g]	N.D.[g]
s-(PCL-OH)$_8$-b	8,000	10,500	-	1.04	88.5	-	-		-	-	-
Pre$_8$-b	9,530	11,100	9,280	1.05	72.6	5.4	14.1	38.2	19.5	14.1	38.9
cage$_8$-b	-	8,100	10,300	1.08	97.7	4.6	7.3	N.D.[g]	2.7	N.D.[g]	N.D.[g]
s-(PCL-OH)$_8$-c	11,400	14,600	-	1.04	83.7	-	-		-	-	-
Pre$_8$-c	13,100	15,200	12,800	1.05	64.9	6.6	17.1	42.6	29.2	12.6	37.2
cage$_8$-c	-	11,100	14,300	1.06	84.7	5.6	9.5	31.9	23.3	12.5	37.9

[a] Determined by ^{1}H NMR. [b] Determined by SEC in THF using PSt standards. [c] Determined by SEC-MALS-Visco in THF. $D_h = 2\ R_h = 2(3V_h/4\pi)^{1/3}$; V_h is hydrodynamic volume. V_h was

calculated by Einstein–Simha equation ($V_h = M_{w,MALS}[\eta]/2.5N_A$; N_A: Avogadro's number). [d] Determined from a melting peak of the DSC curve. [e] Determined by WAXD at r.t. [f] Determined by SAXS at r.t. [g] Not determined.

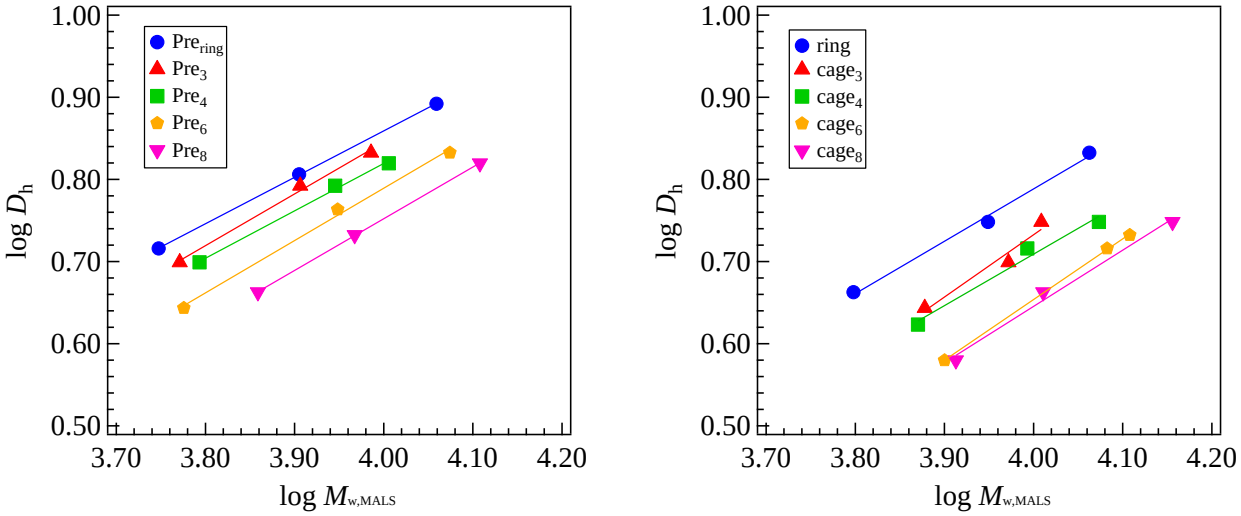

Figure S3.15. Plots of $M_{w,MALS}$ versus D_h for the precursors (**Pre$_{ring}$**, **Pre$_3$**, **Pre$_4$**, **Pre$_6$**, and **Pre$_8$**; left) and the cyclic polymers and macromolecular cages (**ring**, **cage$_3$**, **cage$_4$**, **cage$_6$**, and **cage$_8$**; right).

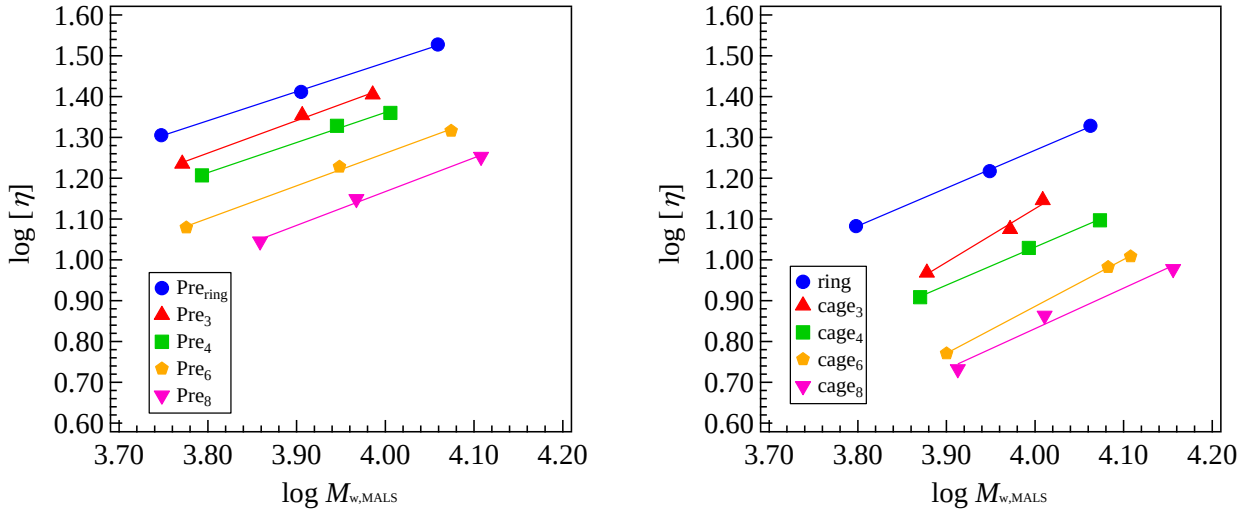

Figure S3.16. Plots of $M_{w,MALS}$ versus [η] for the precursors (**Pre$_{ring}$**, **Pre$_3$**, **Pre$_4$**, **Pre$_6$**, and **Pre$_8$**; left) and the cyclic polymers and macromolecular cages (**ring**, **cage$_3$**, **cage$_4$**, **cage$_6$**, and **cage$_8$**; right).

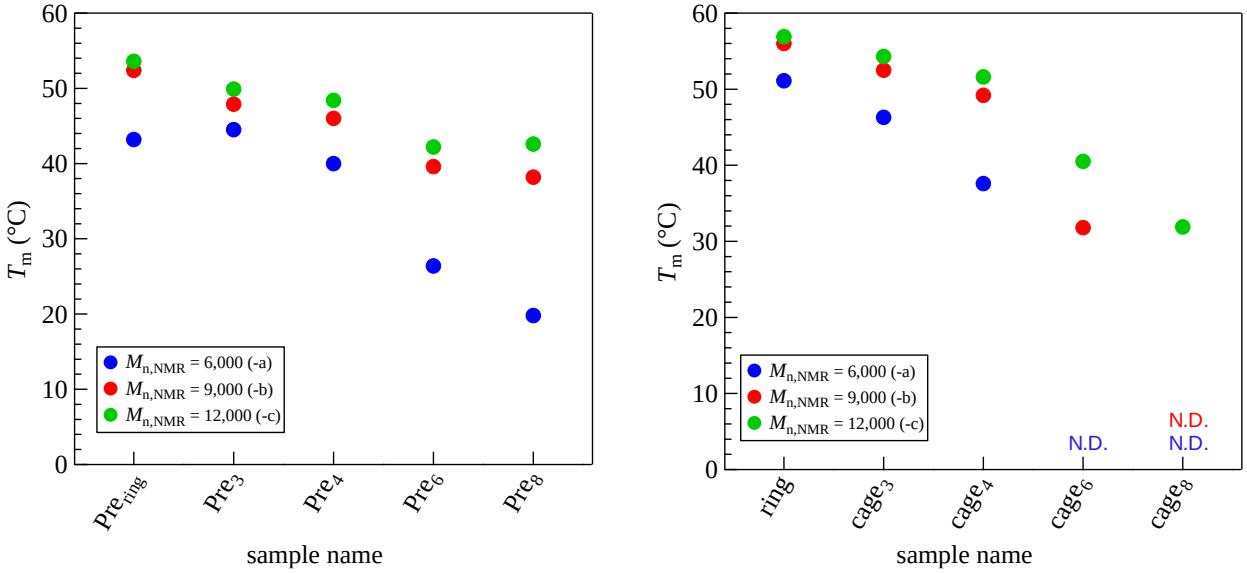

Figure S3.17. Plots of arm numbers versus melting temperature (T_m) for the precursors (**Pre$_{ring}$**, **Pre$_3$**, **Pre$_4$**, **Pre$_6$**, and **Pre$_8$**; left) and the cyclic polymers and macromolecular cages (**ring**, **cage$_3$**, **cage$_4$**, **cage$_6$**, and **cage$_8$**; right) with varying molecular weight (blue, samples with $M_{n,NMR}$ of ca. 6,000; red, samples with $M_{n,NMR}$ of ca. 9,000; green, samples with $M_{n,NMR}$ of ca. 12,000).

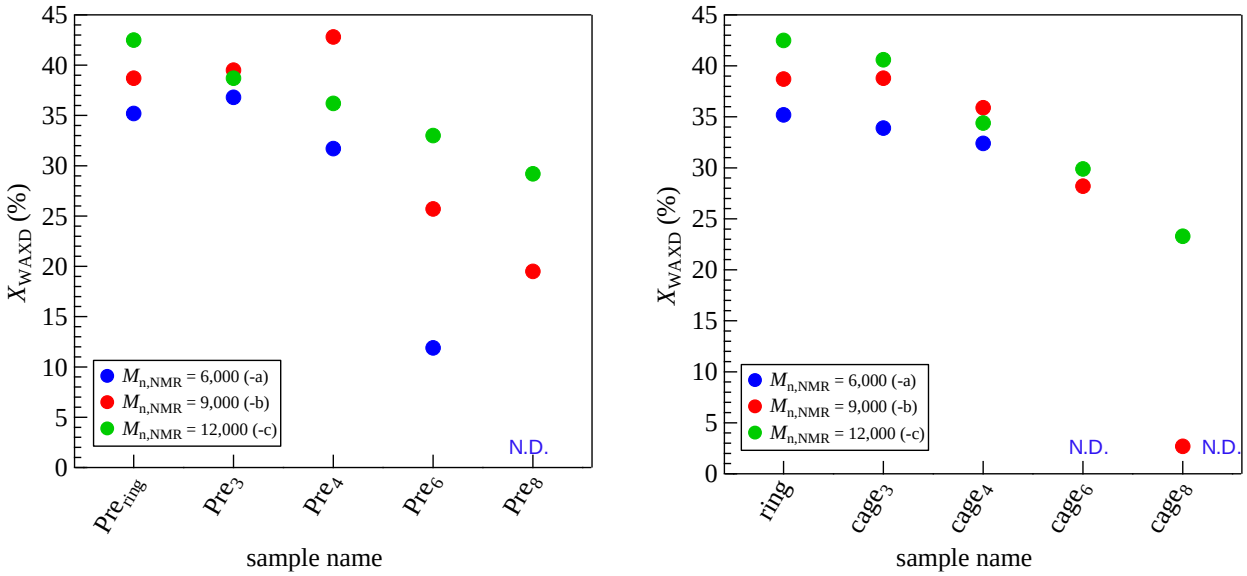

Figure S3.18. Plots of arm numbers versus crystallinity (X_{WAXD}) for the precursors (**Pre$_{ring}$**, **Pre$_3$**, **Pre$_4$**, **Pre$_6$**, and **Pre$_8$**; left) and the cyclic polymers and macromolecular cages (**ring** and

cage$_3$, **cage$_4$**, **cage$_6$**, and **cage$_8$**; right) with varying molecular weight (blue: samples with $M_{n,NMR}$ of ca. 6,000; red, samples with $M_{n,NMR}$ of ca. 9,000; green, samples with $M_{n,NMR}$ of ca. 12,000).

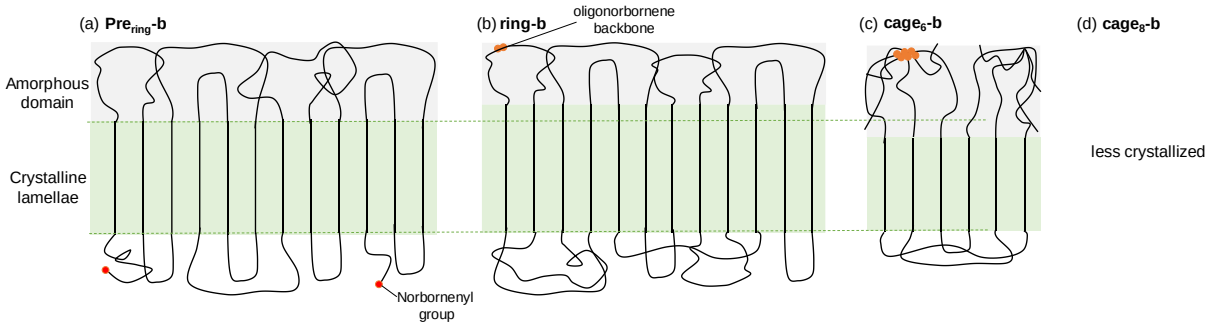

Figure S3.19. Representative possible crystalline lamellae formation of (a) **Pre$_{ring}$-b**, (b) **ring-b**, (c) **cage$_6$-b**, and (d) **cage$_8$-b** with different lamella thickness, indicated as green domains.

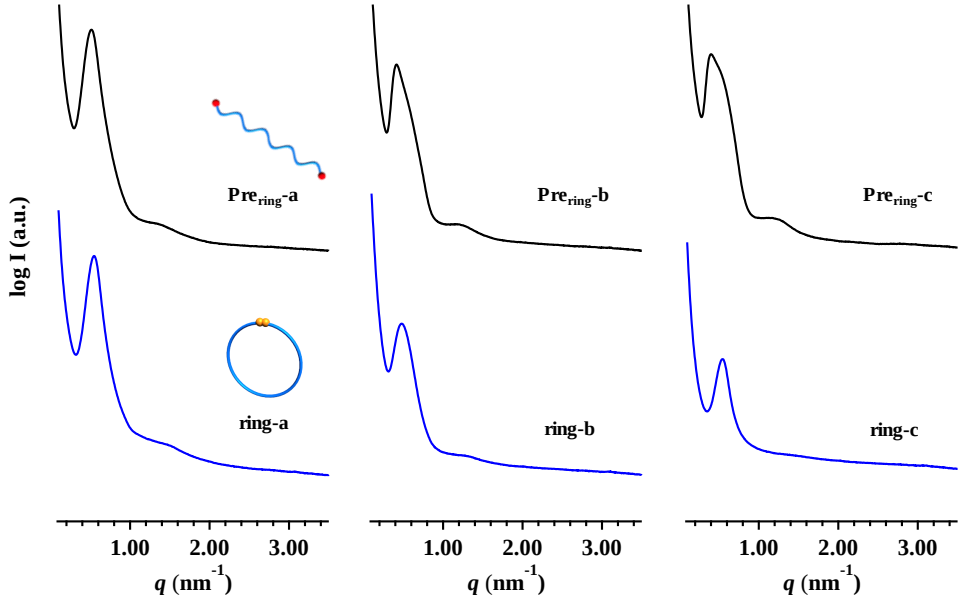

Figure S3.20. SAXS profiles of the obtained cyclic polymers (**ring**s; blue) and their precursors (**Pre$_{ring}$**s; black) at ambient temperature.

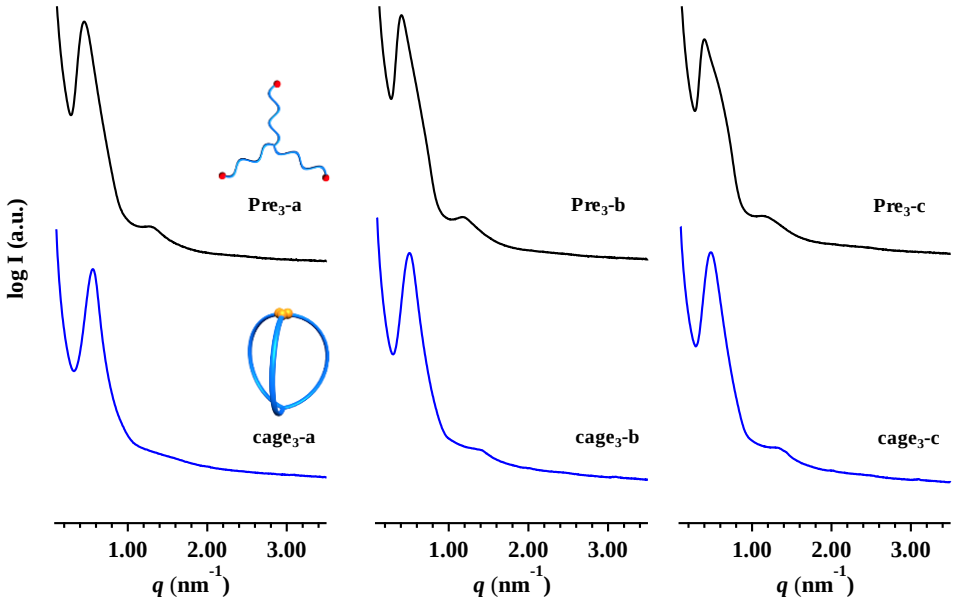

Figure S3.21. SAXS profiles of the obtained three-armed macromolecular cages (**cage**3s; blue) and their precursors (**Pre**3s; black) at ambient temperature.

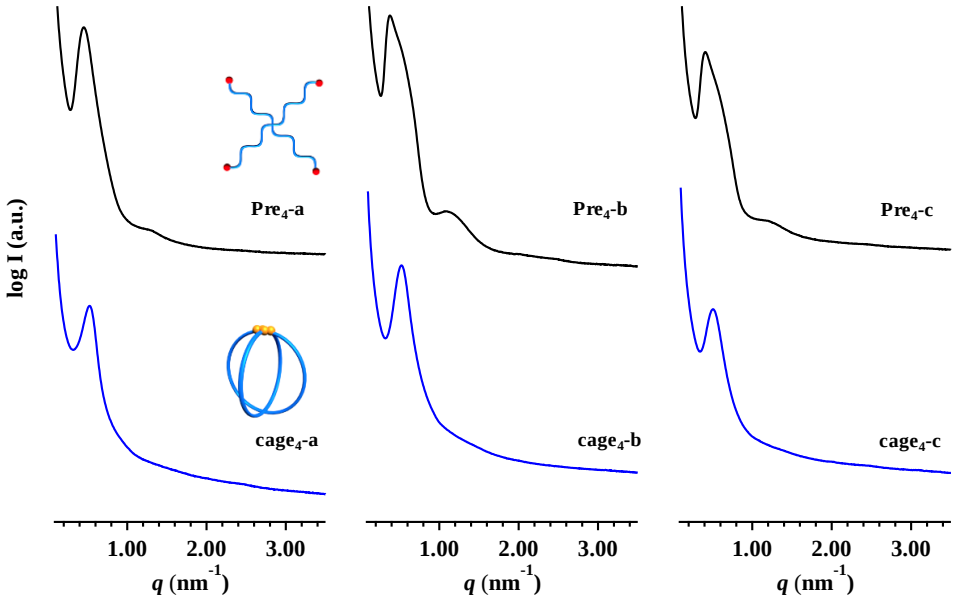

Figure S3.22. SAXS profiles of the obtained four-armed macromolecular cages (**cage**4s; blue) and their precursors (**Pre**4s; black) at ambient temperature.

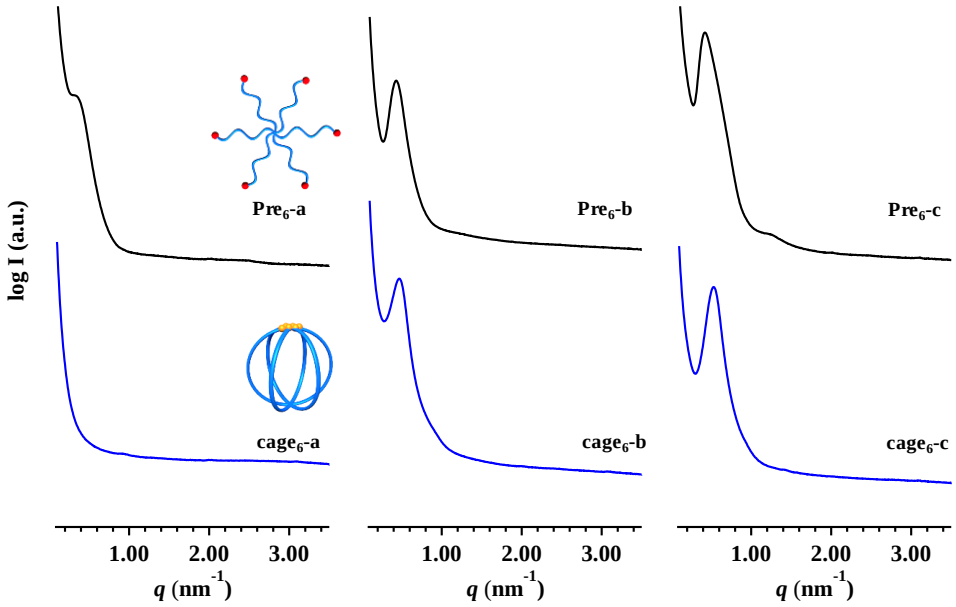

Figure S3.23. SAXS profiles of the obtained six-armed macromolecular cages (**cage$_6$**s; blue) and their precursors (**Pre$_6$**s; black) at ambient temperature.

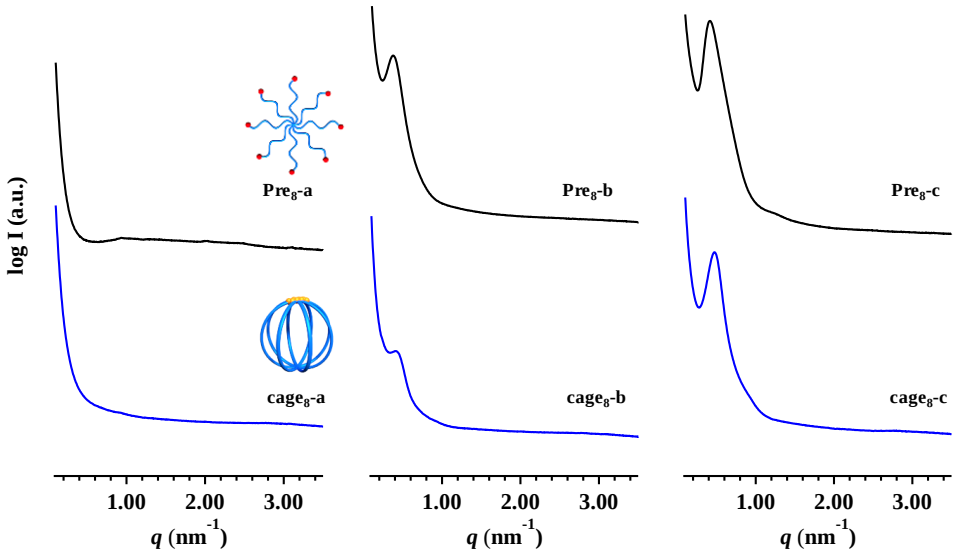

Figure S3.24. SAXS profiles of the obtained eight-armed macromolecular cages (**cage$_8$**s; blue) and their precursors (**Pre$_8$**s; black) at ambient temperature.

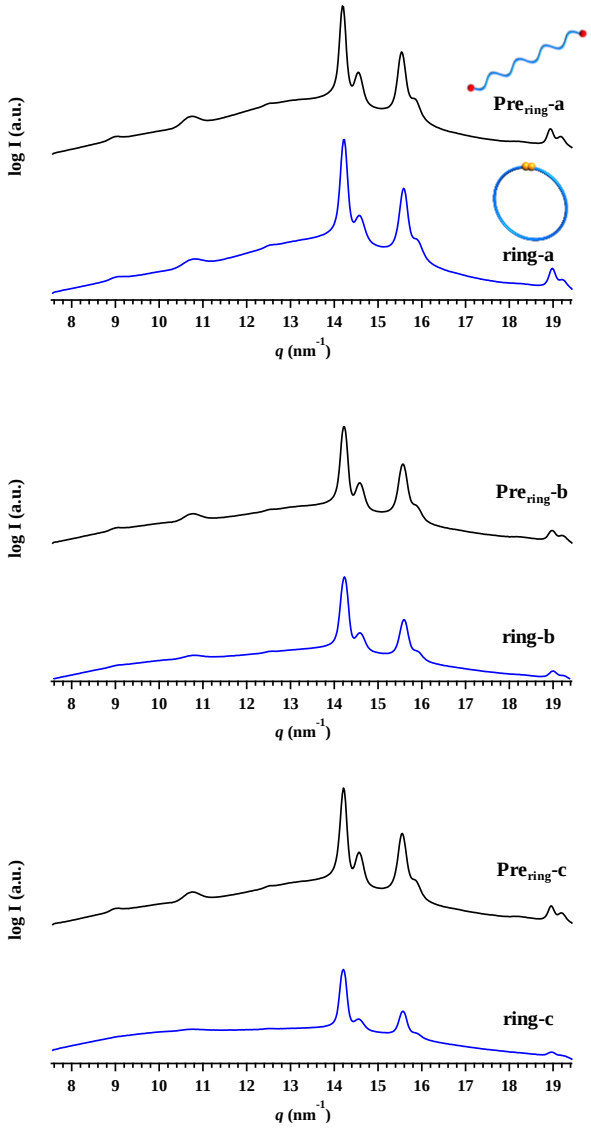

Figure S3.25. WAXD profiles of the obtained cyclic polymers (**ring**s; blue) and their precursors (**Pre$_{ring}$**s; black) at ambient temperature.

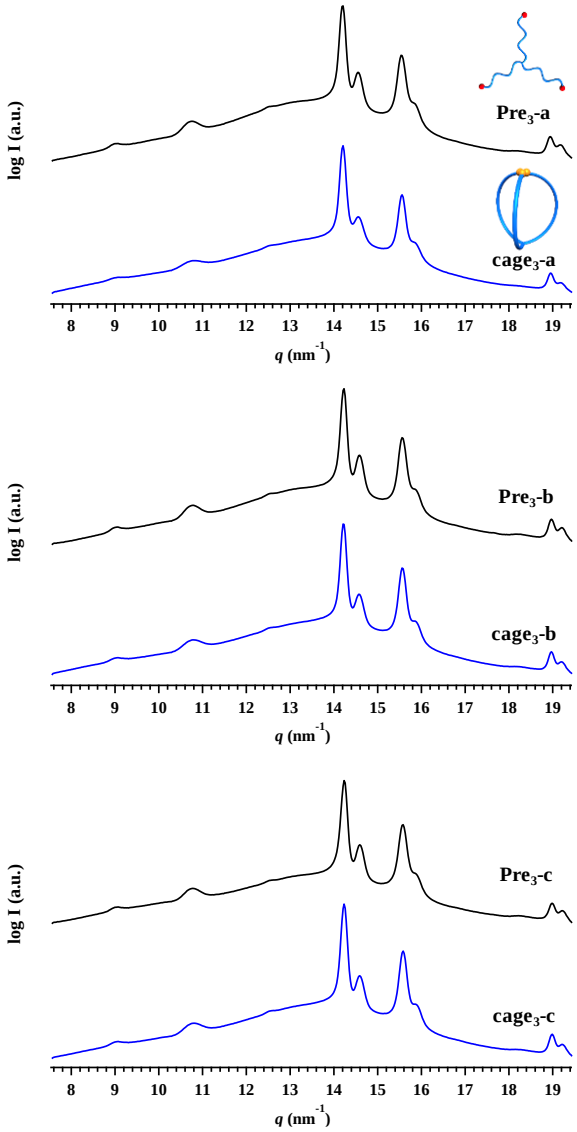

Figure S3.26. WAXD profiles of the obtained three-armed macromolecular cages (**cage**$_3$s; blue) and their precursors (**Pre**$_3$s; black) at ambient temperature.

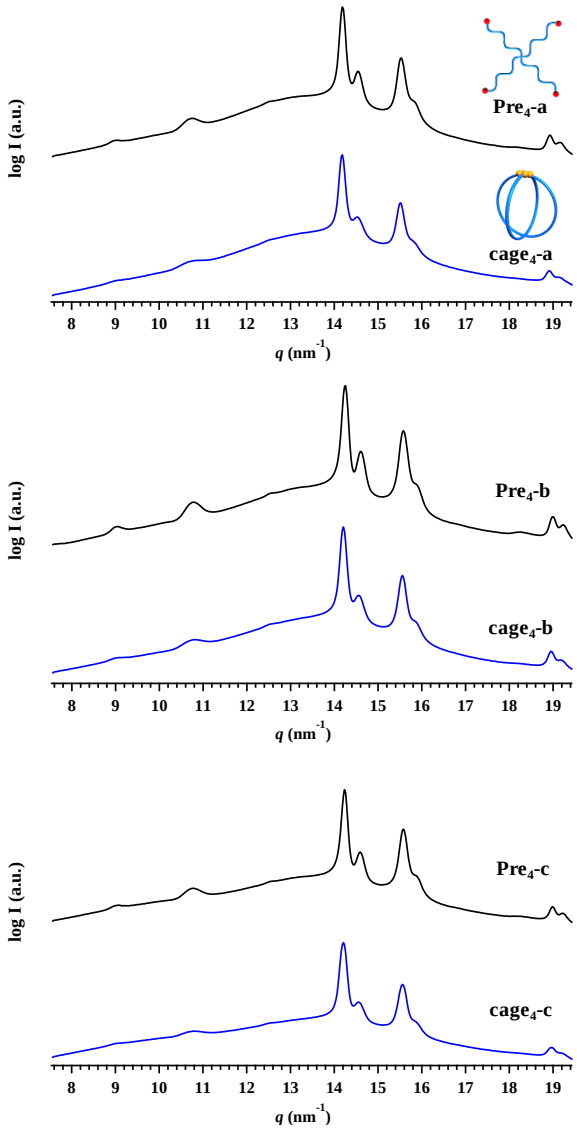

Figure S3.27. WAXD profiles of the obtained four-armed macromolecular cages (**cage**$_4$s; blue) and their precursors (**Pre**$_4$s; black) at ambient temperature.

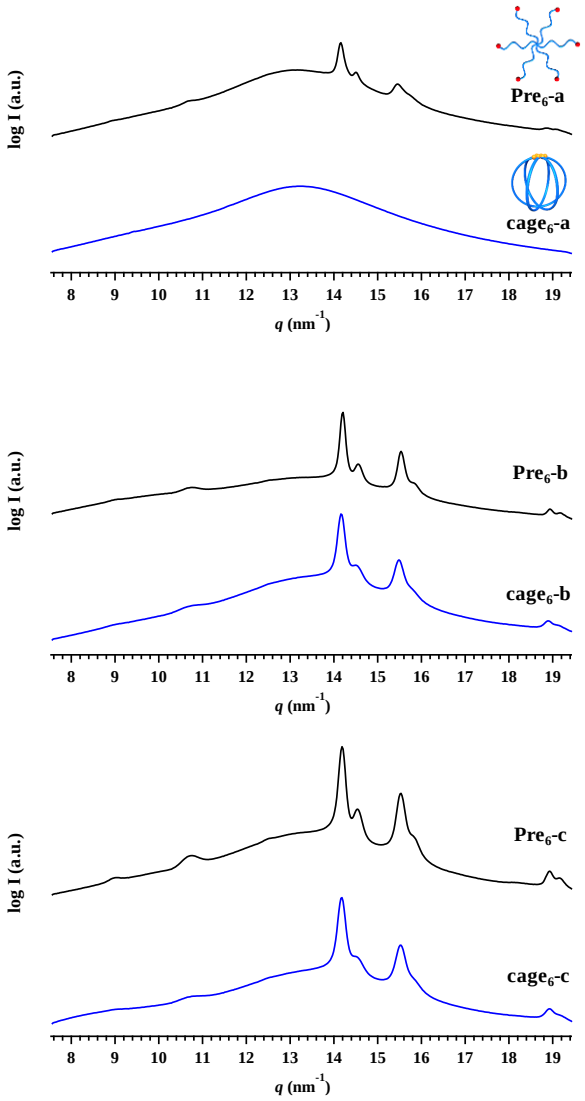

Figure S3.28. WAXD profiles of the obtained six-armed macromolecular cages (**cage$_6$**s; blue) and their precursors (**Pre$_6$**s; black) at ambient temperature.

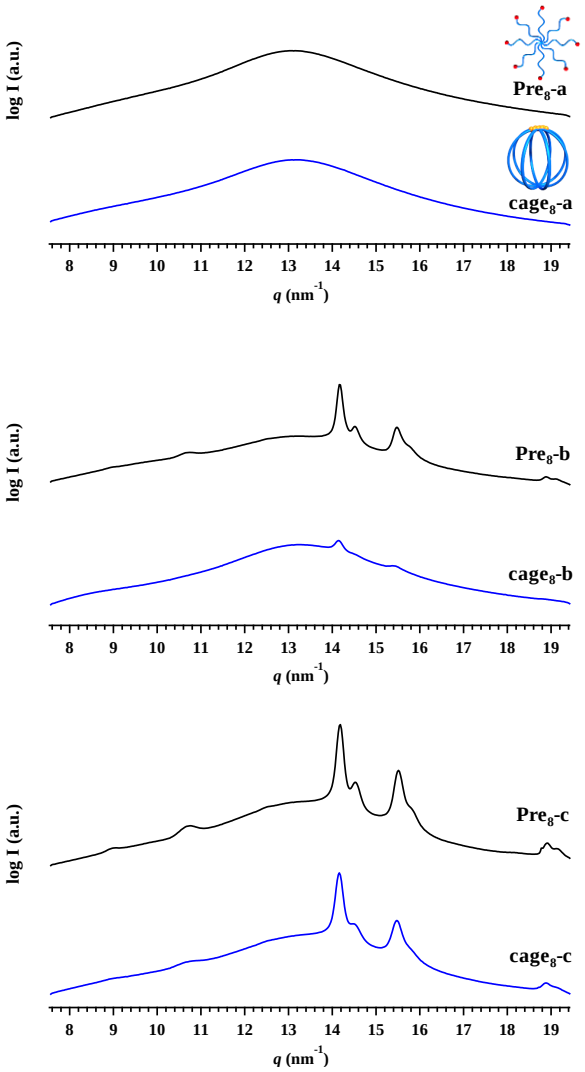

Figure S3.29. WAXD profiles of the obtained eight-armed macromolecular cages (**cages**; blue) and their precursors (**Pres**; black) at ambient temperature.

Note. Long period estimation by correlation function analysis

The lamellar thickness (L_c) and the long period (L_{ac}) of the PCL crystal were estimated by correlation function analysis of the SAXS profiles of the samples, in accordance with previously reported method[35] using a following equation:

$$\gamma(z) = \frac{1}{Q^*}\int_0^\infty I(q)q^2\cos(qz)dq$$

where Q^* is the scattering invariant. The L_c were assigned to the z value of intersection point of linear fitting and horizontal line drew from the first peak as seen in Figure S3.30, because the crystallinity (X_{WAXD}) of all polymer samples were lower than 50%.

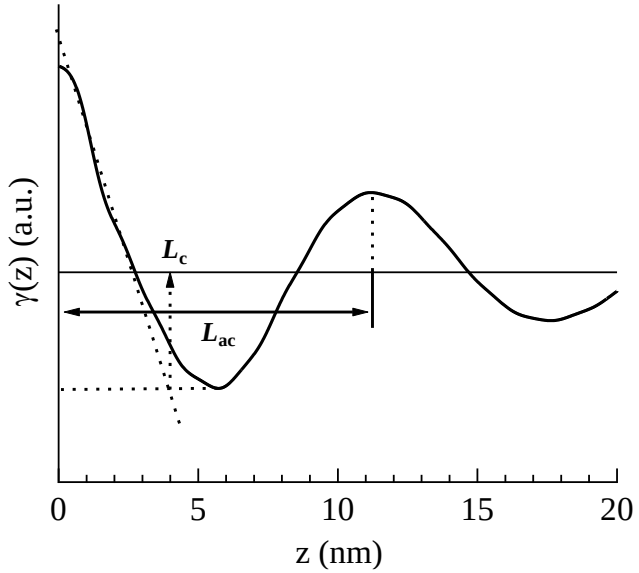

Figure S3.30. Correlation function analysis of the SAXS profile for **cage$_3$-b**.

Chapter 4

Synthesis of Graft Polymers with Densely-arrayed Cage-shaped Side Chains via Cyclopolymerization of Star-shaped Macromonomers

4.1 Introduction

Polymer chain topology is one of the important structural variables for designing polymeric materials possessing sophisticated functions, as mentioned Section 1.1.[1] The cyclic topology has attracted particular interest owing to its higher density,[2] smaller hydrodynamic volume,[3] and superior optical properties[4] compared to its linear counterparts having the same composition and molecular weight, which stems from the lack of chain-ends. Advances in polymer chemistry have made it possible to synthesize not only monocyclic polymers but also polymers possessing complicated cyclic topologies. Consequently, experimental and theoretical studies on how these intriguing topologies affect the properties and functions of the polymers have recently attracted considerable interest.[5–8]

As a result, significant efforts have been devoted to the development of functional materials and interfaces by integrating cyclic polymer chains. Examples include viscoelastically augmented gels prepared by chemical crosslinking of a cyclic polymer[9] and thermostable micelles formed by the self-assembly of cyclic block copolymers.[10] Cyclic-chain grafting onto diverse surfaces or interfaces, such as bulk metals,[11–14] metal nanoparticles,[15,16] and damaged cartilage[17,18], have been discovered as highly efficient means to improve the colloidal stability of metallic nanoparticles and enhance the bioinertness and lubricating properties of biomaterials. The Benetti group has demonstrated that graft polymers (*i.e.*, bottlebrush polymer) fabricated using macrocyclic poly(2-alkyl-2-oxazoline) side-chains can be used as surface modifiers to impart biomaterials with superior lubricating abilities and antifouling natures.[19] These intriguing properties arise from the suppressed chain entanglement in cyclic polymers, which is further enhanced by the denser packing of the polymer chains due to the graft-polymer-like architecture. Therefore, it is of particular interest to synthesize unique graft polymers (GPs) carrying various cyclic topological polymer side-chains possessing tunable grafting densities, which could further expand their potential applications as surface modifiers. The cage-shaped

topology is particularly interesting for functional surface/interface applications because of its diminished chain entanglement and molecular dimensions compared to its monocyclic counterparts. In addition, the three-dimensional structure of the cage-shaped framework may serve as a platform for novel supramolecular nanomaterial applications, as inspired by cryptands.[20] Therefore, graft polymers with densely arrayed cage-shaped side-chains (*cage*-GPs, Figure 4.1) are intriguing synthetic targets.

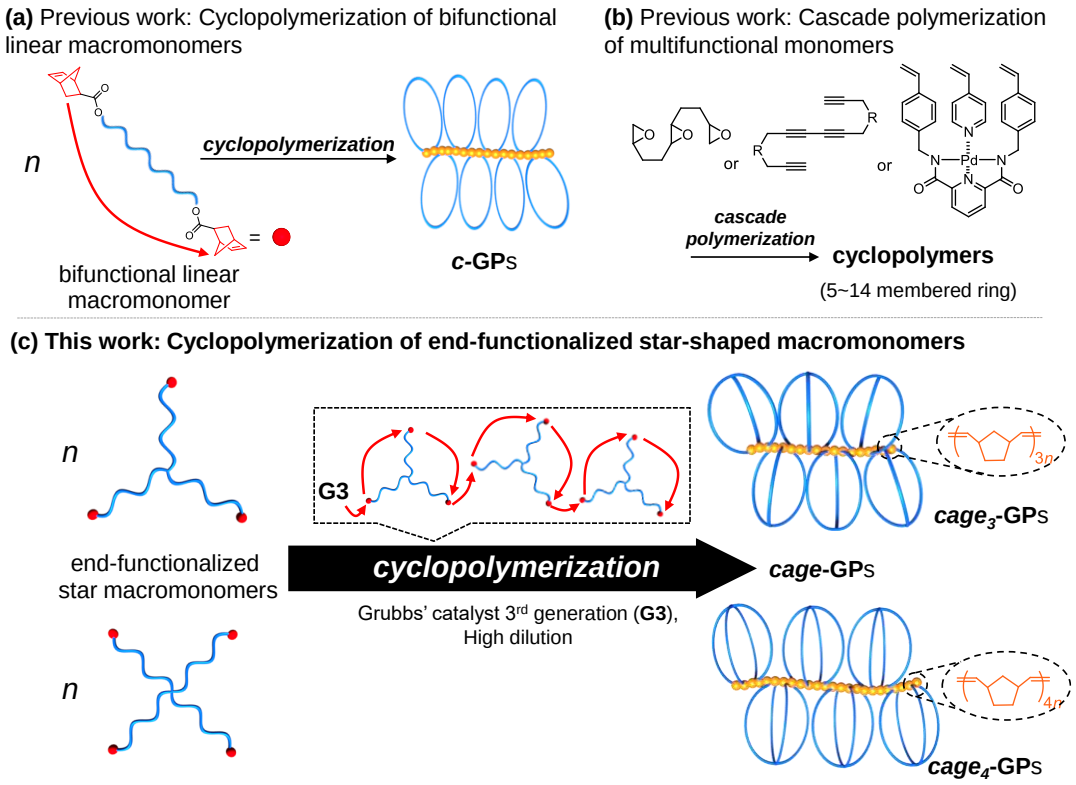

Figure 4.1. Schematic of cyclopolymerization strategies for constructing architecturally unique polymers. (a) Cyclopolymerization of linear bifunctional macromonomers to produce cyclic GPs (*c*-GPs). (b) Cascade polymerization of multifunctional monomers to produce corresponding cyclopolymers having small rings. (c) Cyclopolymerization of norbornenyl-end-functionalized star-shaped macromonomers to synthesize *cage*-GPs.

Generally, graft polymers can be synthesized by three different methods[21]: (i) grafting from, (ii) grafting onto, and (iii) grafting through. Approach (i) is applicable solely to the

synthesis of graft polymers possessing linear side-chains and is therefore impossible to apply to *cage*-GP synthesis. Approach (ii) may be applied to the construction of *cage*-GPs by grafting a separately prepared cage-shaped macromolecule onto a reactive polymer backbone. This is probably feasible because some researchers have reported the synthesis of GPs possessing monocyclic side-chains (*c*-GPs) by the grafting onto method.[19,22–24] However, the necessity of preparing cage-shaped macromolecules containing a reactive functional group is a major hurdle in the way of realizing this approach. Furthermore, this strategy inherently produces poorly-defined *cage*-GPs because the quantitative grafting of bulky polymeric chains is challenging. Approach (iii) is advantageous over the other two approaches in its ability to precisely construct well-defined *cage*-GPs. However, this approach also requires the preparation of cage-shaped macromonomers.

Satoh et al. recently established a robust synthetic pathway to *c*-GPs without using cyclic macromonomers: the cyclopolymerization of *α*,*ω*-norbornenyl-functionalized bifunctional linear macromonomers produces well-defined multicyclic polymers through ring-opening metathesis polymerization (ROMP) using Grubbs' third generation catalyst (G3) (Figure 4.1(a)).[25,26] The cyclopolymerization is facilitated by the significantly quicker intramolecular cyclization compared to the intermolecular propagation under highly diluted conditions. The author envisioned that extending this approach would directly yield the corresponding *cage*-GPs from star-shaped macromonomers containing polymerizable groups at each chain-end. A few examples of the cascade cyclopolymerization of specially designed multifunctional monomers (*e.g.*, trivinyl,[27] tetrayne,[28] and triepoxide[29]) have been reported previously (Figure 4.1b). However, such multifunctional monomers all have a low molecular degree of freedom. Consequently, they exclusively produce small-ringed cyclopolymers (up to 14-membered rings[27]). Therefore, the establishment of the cyclopolymerization of star-shaped macromonomers to construct a large topological unit is of significant fundamental interest.

Furthermore, generating mechanistic insights into cyclopolymerization may provide elementary yet crucial knowledge to expand the ROMP-based syntheses of a variety of architecturally complex macromolecules.

In this chapter, the author reports a facile and versatile synthesis of graft polymers carrying three- and four-armed cage-shaped polymer side-chains through the cyclopolymerization of three- and four-armed star-shaped macromonomers, respectively, that bear a norbornenyl group at each chain-end (Figure 4.1(c)). Note that poly(ε-caprolactone) (PCL) was also employed for same reason as of Chapters 2 and 3.[30] Employing this synthetic approach, the author have successfully synthesized a series of *cage*-GPs containing different numbers of cage-shaped grafted PCL units (*cage*-GPCLs), together with GPCLs containing linear and cyclic side-chains as reference samples, which facilitated a systematic study on the structure-property relationships (*i.e.*, melting temperature, crystallinity, viscosity, and hydrodynamic diameter) of topological GPCLs in the bulk as well as solution states. Additionally, the versatility of the proposed synthetic approach was further confirmed by applying it to other macromonomers consisting of poly(trimethylene carbonate), polylactide, and poly(ethylene oxide).

4.2 Experimental Section

4.2.1 Materials

Macromonomers (NB-PCL-NB, *s*-(PCL-NB)$_3$, and *s*-(PCL-NB)$_4$) and monomeric PCL samples (PCL-NB, *c*-PCL, *cage*$_3$-PCL, and *cage*$_4$-PCL) were prepared according to the reported papers.[1,2] Grubbs' catalyst 3rd generation (G3) was prepared according to the previously reported method.[3] Amberlyst® A21 (Organo Co., Ltd.), *N*,*N*-dimethyl-4-aminopyridine (DMAP; Tokyo Chemical Industry Co., Ltd. (TCI), >99.0%), 1-ethyl-3-(3-(dimethylamino)-propyl)carbodiimide hydrochloride (EDC; TCI, >98.0%), ethyl vinyl ether (TCI, >98.0%), (±)-*exo*-5-norbornenecarboxylic acid (*exo*-NB-COOH; Aldrich, 97%), sodium methoxide (NaOMe; 1 mol L^{-1} in methanol, Kanto Chemical Co., Inc.), Dowex® 50WX2 hydrogen form (Aldrich, 50-100 mesh), sodium iodide (NaI; Wako Pure Chemical Industry Co. Ltd., >99.5%), 2,5-dihydroxybenzoic acid (DHB; Sigma-Aldrich, >98.0%), dithranol (Fluka, >98%), sodium trifluoroacetate (ACROS Organics, 97%), CH_2Cl_2 (Junsei Chemical Co., Ltd., >99.0%), diethyl ether (Kanto Chemical Co., Inc., >99%), methanol (MeOH; Kanto Chemical Co., Inc., >99.5%), and dry-CH_2Cl_2 (Kanto Chemical Co., Inc., >99.5%, water content, <0.001%) were used as received. Dry-toluene (Kanto Chemical Co., Inc., >99.5%, water content, <0.001%) was further purified by an MBRAUN MB SPS Compact solvent purification system equipped with a MB-KOL-C and a MB-KOL-A columns, which were directly used for reactions. ε-Caprolactone (ε-CL; TCI, >99%), 1-butanol (Wako Pure Chemical Industry Co. Ltd., >99.0%), and tin(II) ethylhexanoate (Aldrich, 95%) were purified by distillation over CaH_2 under reduced pressure and stored in the glovebox. L-Lactide (TCI, >98.0%) was purified twice by recrystallization using dry toluene and stored in the glovebox. Trimethylene carbonate was kindly received from Mitsubishi Chemical Co., Ltd and purified by recrystallization using dry tetrahydrofuran and diethyl ether, followed by kept in the glovebox. 1,3,5-trihydroxymethylbenzene (TCI, >95%), pentaerythritol (TCI, >98.0%), and diphenyl phosphate

(DPP; TCI, >99.0%) were purified by azeotropic distillation with dry-toluene and stored in the glovebox. Four-armed star-shaped poly(ethylene glycol) with a hydroxyl group at each chain end (4-Arm PEG-OH 5k Da, namely *s*-(PEG-OH)$_4$; MW = 5,160 g mol^{-1}, dispersity = 1.03, >99.9%) was purchased from Creative PEGWorks and purified by reprecipitation from CH_2Cl_2 to cold diethyl ether before use.

4.2.2 Instruments

The polymerization experiments were carried out in an MBRAUN stainless steel glovebox equipped with a gas purification system (molecular sieves and copper catalyst) in a dry argon atmosphere (H_2O, O_2<0.1 ppm). The moisture and oxygen contents in the glovebox were monitored by an MB-MO-SE 1 moisture sensor and an MB-OX-SE 1 oxygen sensor, respectively. The ^{1}H NMR (400 MHz) spectra were recorded using a JEOL JNM-ECS400 instrument at room temperature in $CDCl_3$. The size exclusion chromatography (SEC) was performed at 40 °C in THF (flow rate, 1.0 mL min^{-1}) using a Shodex GPC-101 gel permeation chromatography system (Shodex DU-2130 dual pump, Shodex RI-71-S reflective index detector, and Shodex ERC-3125SN degasser) equipped with a Shodex KF-G guard column (4.6 mm × 10 mm; particle size, 8 μm) and two Shodex KF-804L columns (linear, 8 mm × 300 mm) or Jasco high-performance liquid chromatography system (PU-3 980 Intelligent HPLC Pump, CO-2065 Plus Intelligent Column Oven, RI-2031 Plus Intelligent RI Detector, and DG-2080-53 Degasser) equipped with a Shodex KF-G guard column (4.6 mm × 10 mm; particle size, 8 μm) and two Shodex KF-804L columns (linear; particle size 7 μm; 8.0 mm × 300 mm; exclusion limit, 4 × 10^4) or in DMF (flow rate, 0.6 mL min^{-1}; containing 0.01 mol L^{-1} LiCl) using a JASCO HPLC system (PU-980 Intelligent HPLC Pump, CO-965 Column Oven, RI-930 Intelligent RI Detector, and DG-2080-53 Degasser) equipped with a Shodex KD-G guard column (4.6 mm × 10 mm; particle size, 8 μm), a Shodex Asahipak GF-310 HQ column (linear;

particle size, 5 μm; 7.5 mm × 300 mm; exclusion limit, 4×10^4) and a Shodex Asahipak GF-7 M HQ column (linear; particle size, 9 μm; 7.5 mm × 300 mm; exclusion limit, 1.0×10^7). The number-average molecular weight ($M_{n,SEC}$) and the dispersity ($Đ$) of the polymers were calculated on the basis of polystyrene calibrations. The absolute number-averaged and weight-averaged molecular weights ($M_{n,MALS}$ and $M_{w,MALS}$, respectively) of the samples were determined by SEC with multiangle light scattering detection (SEC-MALS-Visco) in THF (flow rate, 1.0 mL min^{-1}) at 40 °C using an Agilent 1100 series instrument equipped with a DG 1100 degasser, a Shodex KF-G guard column (4.6 mm × 10 mm; particle size, 8 μm), a Shodex KF-800D solvent-peak separation column (linear, 8.0 mm × 100 mm; particle size, 10μm), two Shodex KF-805L columns (linear, 8.0 mm × 300 mm; exclusion limit, 4.0×10^6; particle size, 10 μm), a DAWN 8+ multiangle laser light scattering detector (Wyatt Technology), an Optilab rEX refractive index detector (Wyatt Technology), and a Viscostar viscosity detector (Wyatt Technology). The preparative SEC for Grubbs' catalyst removal was performed at r.t. in $CHCl_3$ (flow rate, 3.5 and 10 mL min^{-1}) using LC-9201 liquid chromatography system (Japan Analytical Industry Co. Ltd.) equipped with a BG-12 degasser, a PI-50 pump, a RI-50S RI detector, a JAIGEL-H-P guard column (8 mm × 40 mm; Japan Analytical Industry Co. Ltd.), and a Shodex K-2004 column (linear, 20.0 mm × 300 mm; exclusion limit, 1.4×10^4; particle size, 7 μm) or LaboACE LC-7080 liquid chromatography system (Japan Analytical Industry Co. Ltd.) equipped with a JAIGEL-HR-P guard column (8 mm × 40 mm; Japan Analytical Industry Co. Ltd.) and JAIGEL-4HR (20 mm × 600 mm; exclusion limit, 5×10^5; Japan Analytical Industry Co. Ltd.).

Matrix-assisted laser desorption ionization time-of-flight mass spectrometry (MALDI-TOF MS). MALDI-TOF MS of the obtained polymers was performed using an Applied Biosystems Voyager-DE STR-H equipped with a 337 nm nitrogen laser (3 ns pulse width). Two hundred shots were accumulated for the spectra at a 20 kV acceleration voltage in

the reflector or linear mode and calibrated using PSt as the internal standard. PCL samples for the MALDI-TOF MS were prepared as follows: (i) the THF solution of polymer sample (4.0 mg mL^{-1}) and the THF solution of matrix (DHB; 60 mg mL^{-1}) were mixed at a volume ratio of 1:1. (ii) Then, the sample plate was spotted by the THF solution of cationic agent (NaI; 1.0 mg mL^{-1}, 1.0 μL), followed by the mixed solution (1.0 μL). The methanolyzed polynorbornene sample was prepared by depositing a mixture (1.0 μL) of polymer (10 mg mL^{-1}, 100 μL in THF), matrix (dithranol; 20 mg mL^{-1}, 20 μL in THF), and cationic agent (sodium trifluoroacetate; 20 mg mL^{-1}, 20 μL in MeOH).

Differential Scanning Calorimetry (DSC). DSC analysis was carried out on a DSC7000X (Hitachi High-Tech Corporation) calibrated with the indium and tin standards. The system was purged with nitrogen gas at a flow rate of 50 mL min^{-1}. All analyses were performed by utilizing 3−7 mg of samples in hermetically sealed aluminum pans. The isothermal crystallization studies to determine the equilibrium melting temperature ($T_m°$) were carried out according to the Hoffman–Weeks extrapolation method.[4] The samples were heated on a hot plate (EYELA VOM-1000) from room temperature to 100 °C and kept at 100 °C for 5 min under vacuum to eliminate thermal history. Then, the samples were cooled down rapidly to a constant crystallization temperature (T_c; 0–40 °C) using a cooling plate (AS ONE SCP-85). At that temperature, the samples were held for adequate time (more than 40 h). After the isothermal steps, the samples were immediately immersed in liquid N_2 to quit the crystallization and heated again up to 100 °C at the heating rate of 10 °C min^{-1} to record the melting temperature (T_m). The determined T_m values for the isothermally crystallized samples were plotted against T_cs, and their linear extrapolation to the line of $T_m = T_c$ gave $T_m°$ as the intersection.

Small-angle X-ray scattering (SAXS) and wide-angle X-ray diffraction (WAXD) analysis. Synchrotron SAXS and WAXD measurements of the obtained polymers were performed with an X-ray beam of a wavelength (λ) of 1.500 Å at the BL-6A in the Photon

Factory of KEK (Tsukuba, Japan). The 2D SAXS and WAXD patterns were obtained with PILATUS3 1M and PILATUS 100K detectors, respectively, which were circularly averaged to produce the 1D plots of I (scattering intensity with an arbitrary unit) and q [scattering vector; $q = 4\pi \sin\theta / \lambda$, where θ is a half of scattering angle (2θ)]. The q value was calibrated using silver behenate. The samples were heated on a hot plate (EYELA VOM-1000) from room temperature to 100 °C and kept at 100 °C for 5 min under vacuum to eliminate thermal history. Then, the samples were cooled down rapidly to 30 °C and held for 48 h using a cooling plate (AS ONE SCP-85). The obtained powder sample was sandwiched by two pieces of Kapton tapes with a spacer of a stainless washer, which was applied for the measurement. The crystallinity (X_{WAXD}) was determined by the peak separation of WAXD profile. The lamellae thickness (l_c), amorphous layer thickness (l_a), and long period (L_p) were evaluated by the correlation function analysis of SAXS profile as follows: Each SAXS curve was converted to the normalized one-dimensional correlation function [$\gamma(r)$]:[5]

$$\gamma(r) = \frac{\int_0^\infty q^2 I(q)\cos(qr)\mathrm{d}q}{\int_0^\infty q^2 I(q)\mathrm{d}q}$$

where r is the correlation length (nm). Integral calculations were executed for $0 \le q \le q_{\mathrm{cutoff}}$, where q_{cutoff} is the scattering vector at which the calculated value of $q^2I(q)$ became a sufficiently small value. $I(q)$ in a relatively low q range ($0 \le q \le$ 0.2–0.4 nm^{-1}) was calculated according to the Guinier law[6] and $I(q)$ in a relatively high q range ($q >$ 1.1–1.6 nm^{-1}) was determined on the basis of the Porod law.[6] Based on the lamellar two-phase model, l_c, l_a, and L_p were determined from $\gamma(r)$ by the method of Strobl and Schneider.[7]

4.2.3 Synthetic details

Synthesis of PCL-OH

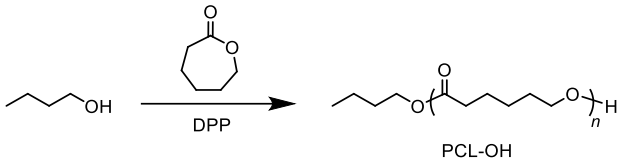

In the glovebox, ε-CL (4.00 g, 35.0 mmol), 1-butanol (173 mg, 2.34 mmol), and DPP (53.4 mg, 213 μmol) were added to a reaction vessel. The reaction mixture was stirred at 80 °C for 18 min. The polymerization was quenched by the addition of Amberlyst® A21. The polymer crude was purified by the reprecipitation from CH_2Cl_2 into cold MeOH to give **PCL-OH** as a white solid (2.48 g). Yield: 70.2%

$M_{n,NMR}$ = 1,790 g mol^{-1}, $M_{n,SEC}$ = 2,810 g mol^{-1} (THF), $Đ$ = 1.11

^{1}H NMR (400 MHz, $CDCl_3$): δ (ppm) 4.10-4.03 (m, -OCO$(CH_2)_4$CH_2-), 3.67 (q, 2H, J = 6.10, -CH_2OH), 2.37-2.26 (m, -OCOC$H_2(CH_2)_4$-), 1.75-1.54 (m, -OCOCH$_2$C$H_2(CH_2)_3$-, -OCO$(CH_2)_3$CH_2CH$_2$-), 1.50-1.30 (m, -OCO$(CH_2)_2$C$H_2(CH_2)_2$-, -CH_2CH$_2$CH$_2$CH$_3$, -CH$_2$CH_2CH$_2$CH$_3$, -CH$_2$CH$_2$CH_2CH$_3$), 0.94 (t, 3H, J =7.30, -CH_3).

Synthesis of PCL-NB

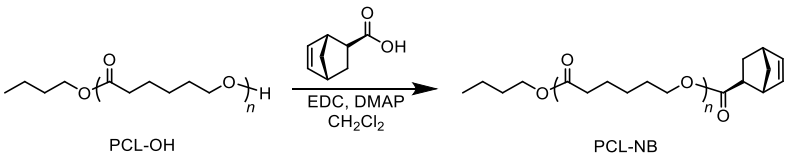

A typical procedure for the condensation reaction is as follows (Method A): In a Schlenk flask, **PCL-OH** ($M_{n,NMR}$ = 1,790 g mol^{-1}, 2.20 g, 1.22 mmol), *exo*-NB-COOH (340 mg, 2.46 mmol), EDC (708 mg, 3.69 mmol), and DMAP (450 mg, 3.68 mmol) were dissolved in dry CH_2Cl_2 (22.0 mL) and the mixture was stirred at r.t. for 24 h. The polymer crude was purified by reprecipitation twice from CH_2Cl_2 into cold MeOH to give **PCL-NB** as a white solid (1.57 g). Yield: 66.2%

$M_{n,NMR}$ = 2,040 g mol^{-1}, $M_{n,SEC}$ = 2,970 g mol^{-1} (THF), $Đ$ = 1.12

^{1}H NMR (400 MHz, $CDCl_3$): δ (ppm) 6.23-6.07 (m, -C*H*=C*H*- in norbornene ring), 4.17-3.99 (m, -OCO(CH_2)$_4$C*H*$_2$-), 3.03 (s, -C*H*-CH-COO- in norbornene ring), 2.92 (s, -C*H*-CH_2-CH-COO- in norbornene ring), 2.39-2.25 (m, -OCOC*H*$_2$(CH_2)$_4$-), 2.25-2.19 (m, *endo*-CH- of -CH-CH_2-CH-CH_2O-), 1.95-1.88 (m, -C*H*$_2$-CH-COO- in norbornene ring), 1.77-1.54 (m, -OCOCH_2C*H*$_2$(CH_2)$_3$-, -OCO(CH_2)$_3$C*H*$_2$CH_2-), 1.47-1.32 (m, -OCO(CH_2)$_2$C*H*$_2$(CH_2)$_2$-, -C*H*$_2$CH_2CH_2CH_3, -CH_2C*H*$_2$CH_2CH_3, -CH_2CH_2C*H*$_2$CH_3), 0.94 (t, 3H, J = 7.3, -C*H*$_3$).

Synthesis of *l*-GPCL

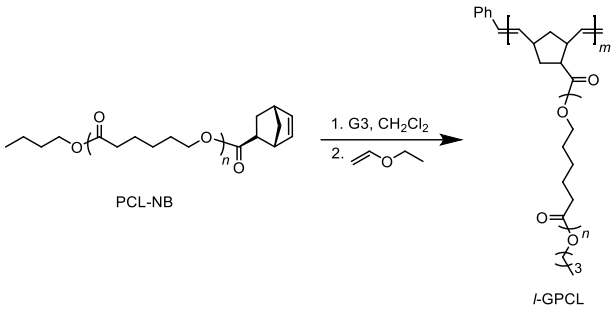

In a vial, a stock solution of G3 (163 μL as a 20 mmol L^{-1} solution in dry-CH_2Cl_2, 3.26 μmol) was added to a stirred solution of **PCL-NB** ($M_{n,NMR}$ = 2,040 g mol^{-1}, 100 mg, 49.0 μmol) in dry-CH_2Cl_2 (4.9 mL) under an argon atmosphere. After 10 min, ethyl vinyl ether was added to reacting mixture to terminate the ROMP. The mixture was purified by reprecipitation from CH_2Cl_2 into cold MeOH to give ***l*-GPCL** as a pale brown solid (73.6 mg). Yield: 73.5%

$M_{n,SEC}$ = 29,600 g mol^{-1} (THF), $Đ$ = 1.06

^{1}H NMR (400 MHz, $CDCl_3$): δ (ppm) 5.65-4.87 (br, alkenyl of poly(norbornene) backbone), 4.39-3.74 (m, -OCO(CH_2)$_4$C*H*$_2$-), 3.28-1.07 (br, cyclopentane ring of poly(norbornene) backbone), 2.45-2.14 (m, -OCOC*H*$_2$(CH_2)$_4$-), 1.83-1.49 (m, -OCOCH_2C*H*$_2$(CH_2)$_3$-, -OCO(CH_2)$_3$C*H*$_2$CH_2-), 1.46-1.24 (m, -OCO(CH_2)$_2$C*H*$_2$(CH_2)$_2$-, -C*H*$_2$CH_2CH_2CH_3, -CH_2C*H*$_2$CH_2CH_3, -CH_2CH_2C*H*$_2$CH_3), 0.94 (t, 3H, J = 7.3, -C*H*$_3$).

Synthesis of *c*-GPCL

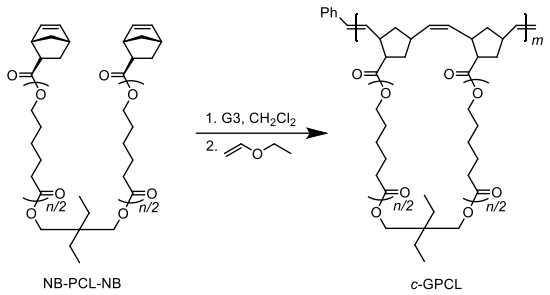

A typical procedure for the cyclopolymerization is as follows (method B): In a three-necked flask, a stock solution of G3 (521 μL as a 4.0 mM solution in dry-CH_2Cl_2, 2.08 μmol) was quickly added to a stirred mixture of **NB-PCL-NB** ($M_{n,NMR}$ = 3,200 g mol^{-1}, 50.0 mg, 15.6 μmol) in dry-CH_2Cl_2 (78.1 mL) under an argon atmosphere at room temperature. After 60 min, excess amount of ethyl vinyl ether was added to the mixture to terminate the reaction. The metal residue in the crude product was removed by preparative SEC (solvent, $CHCl_3$) to give ***c*-GPCL** as a pale brown solid (49.7 mg). Yield: 99.1%

$M_{n,SEC}$ = 23,700 g mol^{-1} (THF), $Đ$ = 1.14

^{1}H NMR (400 MHz, $CDCl_3$): δ (ppm) 6.70-4.85 (br, alkenyl of poly(norbornene) backbone), 4.16-3.77 (m, -OCO$(CH_2)_4$CH_2-), 3.88 (s, $(CH_3CH_2)_2$C-), 3.42-1.73 (br, cyclopentane ring of poly(norbornene) backbone), 2.40-2.19 (m, -OCOC$H_2(CH_2)_4$-), 1.76-1.51 (m, -OCOCH_2C$H_2(CH_2)_3$-, -OCO$(CH_2)_3$CH_2CH_2-), 1.48-1.20 (m, CH_3CH_2-, -OCO$(CH_2)_2$C$H_2(CH_2)_2$-), 0.97 (s, -CH_3).

Synthesis of *cage$_3$*-GPCL

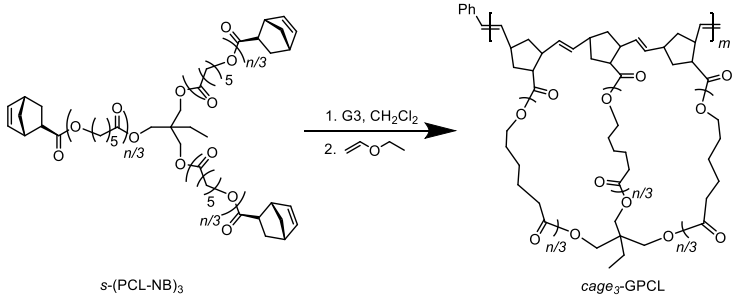

Method B was used for the cyclopolymerization of ***s*-(PCL-NB)$_3$** ($M_{n,NMR}$ = 4,700 g mol^{-1}, 50.0 mg, 10.6 μmol) with G3 (532 μL as a 4.0 mM solution in dry-CH_2Cl_2, 2.13 μmol) in dry-CH_2Cl_2 (106 mL) for 2 h to give ***cage$_3$*-GPCL** as a pale brown solid (49.7 mg). Yield: 98.9%

$M_{n,SEC}$ = 18,200 g mol^{-1} (THF), $Đ$ = 1.17

^{1}H NMR (400 MHz, $CDCl_3$): δ (ppm) 6.54-4.79 (br, alkenyl of poly(norbornene) backbone), 4.39-3.73 (m, -OCO(CH$_2$)$_4$C*H*$_2$-), 3.23-0.95 (br, cyclopentane ring of poly(norbornene) backbone), 2.39-2.18 (m, -OCOC*H*$_2$(CH$_2$)$_4$-), 1.74-1.50 (m, -OCOCH$_2$C*H*$_2$(CH$_2$)$_3$-, -OCO(CH$_2$)$_3$C*H*$_2$CH$_2$-), 1.49-1.28 (m, CH$_3$C(C*H*$_2$-)$_3$, -OCO(CH$_2$)$_2$C*H*$_2$(CH$_2$)$_2$-), 0.67-0.95 (m, -C*H*$_3$).

Synthesis of *cage$_4$*-GPCL

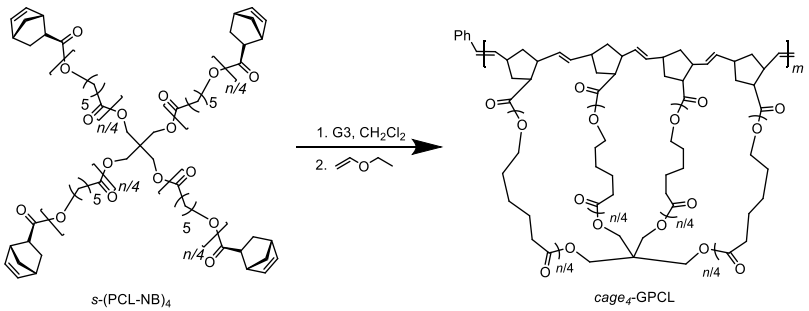

Method B was used for the cyclopolymerization of ***s*-(PCL-NB)$_4$** ($M_{n,NMR}$ = 6,000 g mol^{-1}, 50.0 mg, 8.35 μmol) with G3 (556 μL as a 4.0 mM solution in dry-CH_2Cl_2, 2.22 μmol)

in dry-CH_2Cl_2 (41.7 mL) for 90 min to give ***cage*$_4$-GPCL** as a pale brown solid (49.5 mg). Yield: 98.8%

$M_{n,SEC}$ = 24,000 g mol^{-1} (THF), $Đ$ = 1.27

^{1}H NMR (400 MHz, $CDCl_3$): δ (ppm) 6.58-4.79 (br, alkenyl of poly(norbornene) backbone), 4.42-3.75 (m, -OCO(CH_2)$_4$CH_2-), 3.24-1.04 (br, cyclopentane ring of poly(norbornene) backbone), 2.42-2.21 (m, -OCOCH_2(CH_2)$_4$-), 1.83-1.51 (m, -OCOCH$_2$CH_2(CH_2)$_3$-, -OCO(CH_2)$_3$CH_2CH$_2$-), 1.50-1.29 (m, C(CH_2-)$_4$, -OCO(CH_2)$_2$CH_2(CH_2)$_2$-).

Methanolysis of *cage*$_3$-GPCL

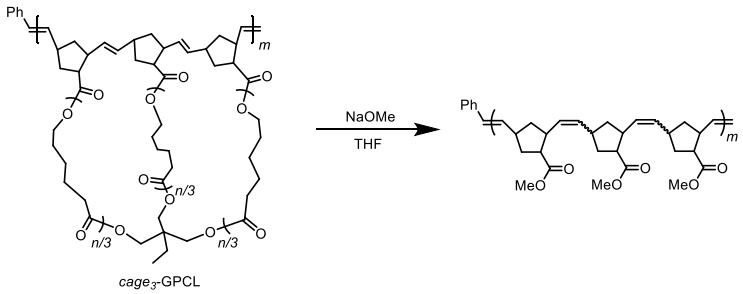

In a vial, NaOMe (870 μL as 1 M solution in MeOH, 870 μmol) was added to the solution of *cage*$_3$-GP (M_n = 47,000, calculated by the following equation: ($M_{n,NMR}$ of *s*-(PCL-NB)$_3$; 4,700) × ([*s*-(PCL-NB)$_3$]$_0$/[G3]$_0$; 10), 98.1 mg, 2.09 μmol) in dry-THF (3.3 mL), and then the solution was stirred at r.t. for 24 h. The Dowex® 50WX2 and water were added to the reaction mixture to let it neutralize. The crude product was evaporated and purified by the preparative SEC (eluent; $CHCl_3$) to give poly(methyl norbornenecarboxylate) as a pale brown solid (2.9 mg). Yield: 27.4%

Synthesis of *cage*-GPs with diverse polymer backbones

Scheme S4.1. Synthetic pathways to (a) *cage*$_3$-GPLLA, (b) *cage*$_4$-GPLLA, (c) *cage*$_3$-GPTMC, and (d) *cage*$_4$-GPEG

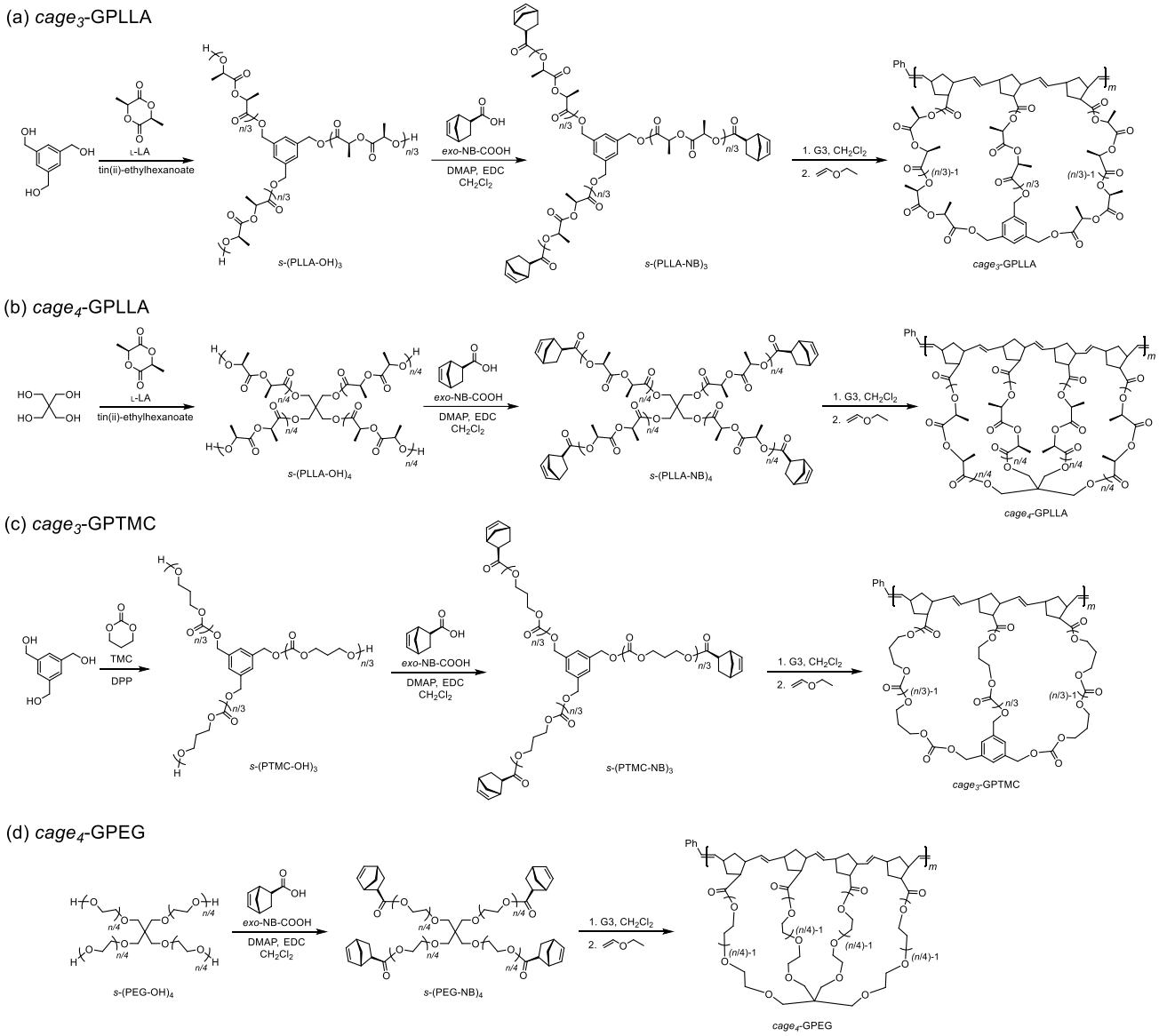

Synthesis of *s*-(PLLA-OH)$_3$

A typical procedure for the ring-opening polymerization is as follows (Method C): In the glovebox, L-lactide (1.00 g, 8.76 mmol), 1,3,5-trihydroxymethylbenzene (29.2 mg, 173 μmol), and tin(II) ethylhexanoate (7.4 μL as 0.1 mol L^{-1} solution in toluene, 0.74 μmol) were placed in a reaction vessel. The reaction mixture was stirred at 120 °C for 8.6 h. The

polymerization was quenched by the addition of excess amount of CH_2Cl_2. The polymer crude was purified by the reprecipitation from CH_2Cl_2 into cold MeOH to give ***s*-(PLLA-OH)$_3$** as a white solid (811 mg). Yield: 78.8%

$M_{n,NMR}$ = 6,770 g mol^{-1}, $M_{n,SEC}$ = 9,510 g mol^{-1} (THF), $Đ$ = 1.13

^{1}H NMR (400 MHz, $CDCl_3$): δ (ppm) 7.25 (s, aromatic), 5.29-5.06 (m, methine of PLLA backbone, -C*H*$_2$O-), 4.44-4.27 (m, -C*H*(CH$_3$)OH), 2.77-2.55 (m, -O*H*), 1.86-1.37 (m, methyl of PLLA backbone).

Synthesis of *s*-(PLLA-NB)$_3$

Method A was used for the condensation reaction of *s*-(PLLA-OH)$_3$ ($M_{n,NMR}$ = 6,770 g mol^{-1}, 745 mg, 110 μmol) with *exo*-NB-COOH (100 mg, 724 μmol), EDC (184 mg, 960 μmol), and DMAP (118 mg, 965 μmol) in CH_2Cl_2 (7.5 mL). The polymer crude was purified by reprecipitation twice from CH_2Cl_2 into cold MeOH followed by the removal of remaining impurities using preparative SEC (solvent, $CHCl_3$) to give ***s*-(PLLA-NB)$_3$** as a white solid (489 mg). Yield: 61.9%

$M_{n,NMR}$ = 7,910 g mol^{-1}, $M_{n,SEC}$ = 9,580 g mol^{-1} (THF), $Đ$ = 1.13

^{1}H NMR (400 MHz, $CDCl_3$): δ (ppm) 7.25 (s, aromatic), 6.21-6.06 (-C*H*=C*H*- in norbornene ring), 5.25-5.04 (m, methine of PLLA backbone, -C*H*$_2$O-), 3.18-3.05 (m, -C*H*-CH-CH$_2$O- in norbornene ring), 2.92 (s, -C*H*-CH-CH$_2$O- in norbornene ring), 2.44-2.24 (m, -C*H*CO- in norbornene ring), 2.10-1.91 (m, *exo*-H of -C*H*$_2$- in norbornene ring), 1.70-1.48 (m, methyl of PLLA backbone, *endo*-H of -C*H*$_2$- in norbornene ring), 1.46-1.31 (m, bridge head -C*H*$_2$- in norbornene ring).

Synthesis of *cage*$_3$-GPLLA

Method B was used for the cyclopolymerization of ***s*-(PLLA-NB)$_3$** ($M_{n,NMR}$ = 7,910 g

mol^{-1}, 51.0 mg, 6.45 μmol) with G3 (79.0 μL as a 8.0 mmol L^{-1} solution in dry-CH_2Cl_2, 0.632 μmol) in dry-CH_2Cl_2 (31.6 mL) for 40 min to give ***cage*$_3$-GPLLA** as a pale brown solid (48.9 mg). Yield: 95.9%

$M_{n,SEC}$ = 51,100 g mol^{-1} (THF), $Đ$ = 1.45

^{1}H NMR (400 MHz, $CDCl_3$): δ (ppm) 5.69-0.59 (br, alkenyl of poly(norbornene) backbone), 5.27-4.94 (m, methine of PLLA backbone), 1.76-1.37 (m, methyl of PLLA backbone).

Synthesis of *s*-(PLLA-OH)$_4$

Method C was used for the polymerization of L-lactide (1.00 g, 8.76 mmol) with pentaerythritol (23.6 mg, 173 μmol), and tin(ii)-ethylhexanoate (7.4 μL as 0.1 mol L^{-1} solution in toluene, 0.74 μmol) at 120 °C for 10 h to give ***s*-(PLLA-OH)$_4$** as a white solid (754 mg). Yield: 73.7%

$M_{n,NMR}$ = 5,500 g mol^{-1}, $M_{n,SEC}$ = 8,800 g mol^{-1} (THF), $Đ$ = 1.13

^{1}H NMR (400 MHz, $CDCl_3$): δ (ppm) 5.32-5.00 (m, methine of PLLA backbone), 4.46-4.28 (m, -C*H*(CH_3)OH), 4.27-3.99 (m, -C*H*$_2$O-), 2.67 (s,-O*H*), 1.83-1.37 (m, methyl of PLLA backbone).

Synthesis of *s*-(PLLA-NB)$_4$

Method A was used for the condensation reaction of *s*-(PLLA-OH)$_4$ ($M_{n,NMR}$ = 5,500 g mol^{-1}, 707 mg, 129 μmol) with *exo*-NB-COOH (141 mg, 1.02 mmol), EDC (296 mg, 1.54 mmol), and DMAP (177 mg, 1.45 mmol) in CH_2Cl_2 (7.0 mL). The polymer crude was purified by reprecipitation twice from CH_2Cl_2 into cold MeOH followed by the removal of remaining impurities using preparative SEC (solvent, $CHCl_3$) to give ***s*-(PLLA-NB)$_4$** as a white solid (445 mg). Yield: 57.0%

$M_{n,NMR}$ = 6,760 g mol^{-1}, $M_{n,SEC}$ = 8,290 g mol^{-1} (THF), $Đ$ = 1.18

^{1}H NMR (400 MHz, $CDCl_3$): δ (ppm) 6.23-6.05 (m, -C*H*=C*H*- in norbornene ring), 5.27-4.99 (m, methine of PLLA backbone), 4.22-4.01 (m, -CH_2O-), 3.24-3.03 (m, -C*H*CHCH$_2$O- in norbornene ring), 2.92 (s, -C*H*CH$_2$CHCO- in norbornene ring), 2.36-2.25 (m, -C*H*CO- in norbornene ring), 2.07-1.87 (m, *exo*-H of -CH_2- in norbornene ring), 1.70-1.45 (m, methyl of PLLA backbone, *endo*-H of -CH_2- in norbornene ring), 1.46-1.31 (m, bridge head -CH_2- in norbornene ring).

Synthesis of *cage*$_4$-GPLLA

Method B was used for the cyclopolymerization of ***s*-(PLLA-NB)$_4$** ($M_{n,NMR}$ = 6,760 g mol^{-1}, 20.0 mg, 2.96 μmol) with G3 (49.3 μL as a 8.0 mmol L^{-1} solution in dry-CH_2Cl_2, 0.394 μmol) in dry-CH_2Cl_2 (14.8 mL) for 30 min. The byproducts and metal residue were removed by preparative SEC (solvent, $CHCl_3$) to give ***cage*$_4$-GPLLA** as a pale brown solid (15.9 mg). Yield: 79.5%

$M_{n,SEC}$ = 22,400 g mol^{-1} (THF), $Đ$ = 1.23

^{1}H NMR (400 MHz, $CDCl_3$): δ (ppm) 5.49-1.10 (br, alkenyl of poly(norbornene) backbone), 5.28-5.01 (m, methine of PLLA backbone), 4.36-3.96 (br, -CH_2O-), 1.77-1.42 (m, methyl of PLLA backbone).

Synthesis of *s*-(PTMC-OH)$_3$

Method C was used for the polymerization of trimethylene carbonate (1.50 g, 10.4 mmol) with 1,3,5-trihydroxymethylbenzene (41.2 mg, 245 μmol), and DPP (3.1 mg, 12 μmol) at 80 °C for 68 h to give ***s*-(PTMC-OH)$_3$** as a colorless viscous liquid (1.54 g). Yield: 99.9%

$M_{n,NMR}$ = 5,910 g mol^{-1}, $M_{n,SEC}$ = 9,710 g mol^{-1} (THF), $Đ$ = 1.10

^{1}H NMR (400 MHz, $CDCl_3$): δ (ppm) 7.36 (s, aromatic), 4.45 (t, J = 5.6 Hz, ArCH_2O-), 4.35-4.11 (m, -COOCH_2CH$_2$CH_2O-), 3.73 (t, J = 6.1 Hz, -CH_2OH), 2.25-1.83 (m, -

COOCH$_2$C*H*$_2$CH$_2$O-).

Synthesis of *s*-(PTMC-NB)$_4$

Method A was used for the condensation reaction of ***s*-(PTMC-OH)$_3$** ($M_{n,NMR}$ = 5,910 g mol^{-1}, 1.03 g, 174 μmol) with *exo*-NB-COOH (147 mg, 1.06 mmol), EDC (321 mg, 1.67 mmol), and DMAP (192 mg, 1.57 mmol) in CH_2Cl_2 (10.3 mL). The polymer crude was purified by reprecipitation twice from CH_2Cl_2 into cold MeOH followed by the removal of remaining impurities using preparative SEC (solvent, $CHCl_3$) to give ***s*-(PTMC-NB)$_3$** as a pale yellow viscous liquid (891 mg). Yield: 81.0%

$M_{n,NMR}$ = 6,900 g mol^{-1}, $M_{n,SEC}$ = 9,730 g mol^{-1} (THF), $Đ$ = 1.04

^{1}H NMR (400 MHz, $CDCl_3$): δ (ppm) 7.38 (s, aromatic), 6.21-6.04 (m, -C*H*=C*H*- in norbornene ring), 4.37-4.13 (m, -COOC*H*$_2$CH$_2$C*H*$_2$O-, ArC*H*$_2$O-), 3.03 (m, -C*H*CHCH$_2$O- in norbornene ring), 2.92 (s, -C*H*CH$_2$CHCO- in norbornene ring), 2.31-2.18 (-C*H*CO- in norbornene ring), 2.16-1.96 (m, -COOCH$_2$C*H*$_2$CH$_2$O-), 1.96-1.83 (m, *exo*-H of -C*H*$_2$- in norbornene ring), 1.56-1.46 (m, *endo*-H of -C*H*$_2$- in norbornene ring), 1.44-1.31 (m, bridge head -C*H*$_2$- in norbornene ring).

Synthesis of *cage*$_3$-GPTMC

Method B was used for the cyclopolymerization of ***s*-(PTMC-NB)$_3$** ($M_{n,NMR}$ = 6,900 g mol^{-1}, 49.9 mg, 7.23 μmol) with G3 (106 μL as a 8.0 mmol L^{-1} solution in dry-CH_2Cl_2, 0.848 μmol) in dry-CH_2Cl_2 (113 mL) for 40 min. The metal residue were removed by preparative SEC (solvent, $CHCl_3$) to give ***cage*$_3$-GPTMC** as a colorless viscous liquid (40.9 mg). Yield: 82.0%

$M_{n,SEC}$ = 29,400 g mol^{-1} (THF), $Đ$ = 1.19

^{1}H NMR (400 MHz, $CDCl_3$): δ (ppm) 7.38 (s, aromatic), 5.51-1.44 (br, alkenyl of

poly(norbornene) backbone), 4.50-4.00 (m, -COOC*H*$_2$CH$_2$C*H*$_2$O-, ArC*H*$_2$O-), 2.27-1.93 (m, -COOCH$_2$C*H*$_2$CH$_2$O-).

Synthesis of *s*-(PEG-NB)$_4$

Method A was used for the condensation reaction of *s*-(PEG-OH)$_4$ ($M_{n,GPC}$ = 5,200 g mol^{-1}; 2.00 g, 385 μmol) with *exo*-NB-COOH (426 mg, 3.08 mmol), EDC (877 mg, 4.57 mmol), and DMAP (553 mg, 4.53 mmol) in CH_2Cl_2 (20.0 mL). The polymer crude was purified by reprecipitation twice from CH_2Cl_2 into cold diethyl ether followed by the removal of remaining impurities using preparative SEC (solvent, $CHCl_3$) to give to give ***s*-(PEG-NB)$_4$** as a pale yellow solid (1.06 g). Yield: 45.0%

$M_{n,NMR}$ = 5,830 g mol^{-1}, $M_{n,SEC}$ = 6,260 g mol^{-1} (DMF), $Đ$ = 1.08

^{1}H NMR (400 MHz, $CDCl_3$): δ (ppm) 6.29-6.01 (m, -C*H*=C*H*- in norbornene ring), 4.38-4.17 (m, -C*H*$_2$OCO-), 3.98-3.31 (m, C(C*H*$_2$O-)$_4$, -C*H*$_2$CH$_2$O-, -CH$_2$C*H*$_2$O-), 3.05 (s, -C*H*CHCO- in norbornene ring), 2.92 (s, -C*H*CH$_2$CHCO- in norbornene ring), 2.36-2.18 (m, -CHCO- in norbornene ring), 2.04-1.85 (m, *exo*-H of -C*H*$_2$- in norbornene ring), 1.46-1.60 (m, *endo*-H of -C*H*$_2$- in norbornene ring), 1.28-1.45 (m, bridge head -C*H*$_2$- in norbornene ring).

Synthesis of *cage*$_4$-GPEG

Method B was used for the cyclopolymerization of ***s*-(PEG-NB)$_4$** ($M_{n,NMR}$ = 5,830 g mol^{-1}, 30.0 mg, 5.15 μmol) with G3 (85.8 μL as a 8.0 mM solution in dry-CH_2Cl_2, 0.686 μmol) in dry-CH_2Cl_2 (51.5 mL) for 90 min to give ***cage*$_4$-GPEG** as a pale brown solid (28.5 mg). Yield: 93.1%

$M_{n,SEC}$ = 16,600 g mol^{-1} (DMF), $Đ$ = 1.45

^{1}H NMR (400 MHz, $CDCl_3$): δ (ppm) 5.65-1.09 (br, alkenyl of poly(norbornene) backbone), 3.86-3.29 (C(C*H*$_2$O-)$_4$, -C*H*$_2$CH$_2$O-, -CH$_2$C*H*$_2$O-).

4.3 Results and Discussion

4.3.1 Cyclopolymerization of three-armed star-shaped macromonomer

To produce the GPCL with three-armed cage-shaped side-chains (*cage*$_3$-GPCL), the author initially prepared a three-armed star-shaped macromonomer (*s*-(PCL-NB)$_3$; number-average molecular weight (M_n) estimated by proton nuclear magnetic resonance spectroscopy (^{1}H NMR) ($M_{n,NMR}$) = 5,200 g mol^{-1}, M_n estimated by size exclusion chromatography (SEC) equipped with a refractive index detector using PSt standards ($M_{n,SEC}$) = 8,000 g mol^{-1}, $Đ$ = 1.10) as described in Chapter 3 (Scheme 4.1a).[31] Note that each PCL arm of the macromonomers was designed to have a number-average molecular weight of approximately 1,500 g mol^{-1} throughout this paper regardless of the number of arms. Also, the perfect functionality (>99%) of end-norbornenyl group in the star macromonomer was ensured by ^{1}H NMR analysis (Figure S4.1), by which the signal due to the methylene adjacent to the hydroxy end group (3.6 ppm) completely disappeared after the treatment with *exo*-5-norbornene carboxylic acid. Subsequently, the cyclopolymerization of *s*-(PCL-NB)$_3$ was performed in CH_2Cl_2 by adding G3 stock solution to the macromonomer solution at a [*s*-(PCL-NB)$_3$]$_0$/[G3]$_0$ = 5/1 (Table 4.1; see SI for synthetic details). Assuming the living polymerization nature of G3-mediated ROMP,[26] this should produce a GPCL containing five cage units on average if the cyclopolymerization proceeds in an accurately controlled manner. To realize an accurately controlled cyclopolymerization system, it is necessary to find an optimized reaction condition in which intramolecular cyclization takes place significantly more rapidly than intermolecular propagation. An insufficient difference in the reaction rates of the two elementary competitive reactions causes dangling chain formation, which in turn induces intermolecular crosslinking, finally leading to gelation. The author initially examined the effect of macromonomer concentration ([*s*-(PCL-NB)$_3$]$_0$). At [*s*-(PCL-NB)$_3$]$_0$ = 5.0 mM, gelation occurred upon the addition of the G3 solution, suggesting competition between the intramolecular cyclization and

intermolecular propagation, leading to significant intermolecular crosslinking. To selectively promote the intramolecular cyclization, the macromonomer was diluted further ([*s*-(PCL-NB)$_3$]$_0$ = 1.0 and 0.1 mM). Even at [*s*-(PCL-NB)$_3$]$_0$ = 1.0 mM, SEC analysis revealed a broad multimodal peak over the high-molecular region at a polymerization time of 30 min, and continuing the polymerization resulted in an insoluble product (Figure S4.2). In contrast, the reaction at [*s*-(PCL-NB)$_3$]$_0$ = 0.1 mM produced a soluble product. The SEC trace of the product clearly shifted to a higher molecular region ($M_{n,SEC}$ = 26,200 g mol^{-1}, $Đ$ = 1.20) compared to that of the macromonomer ($M_{n,SEC}$ = 8,000 g mol^{-1}, $Đ$ = 1.10), while retaining the monomodal peak shape (Figure 4.2(a)). This indicated that the intramolecular cyclization proceeded much more rapidly than intermolecular propagation under such highly diluted conditions.

Scheme 4.1. Synthesis of topological graft PCLs containing (a) three- and (b) four-armed cage-shaped side-chains via the cyclopolymerizations of the corresponding star-shaped PCLs containing a norbornenyl group at each chain-end.

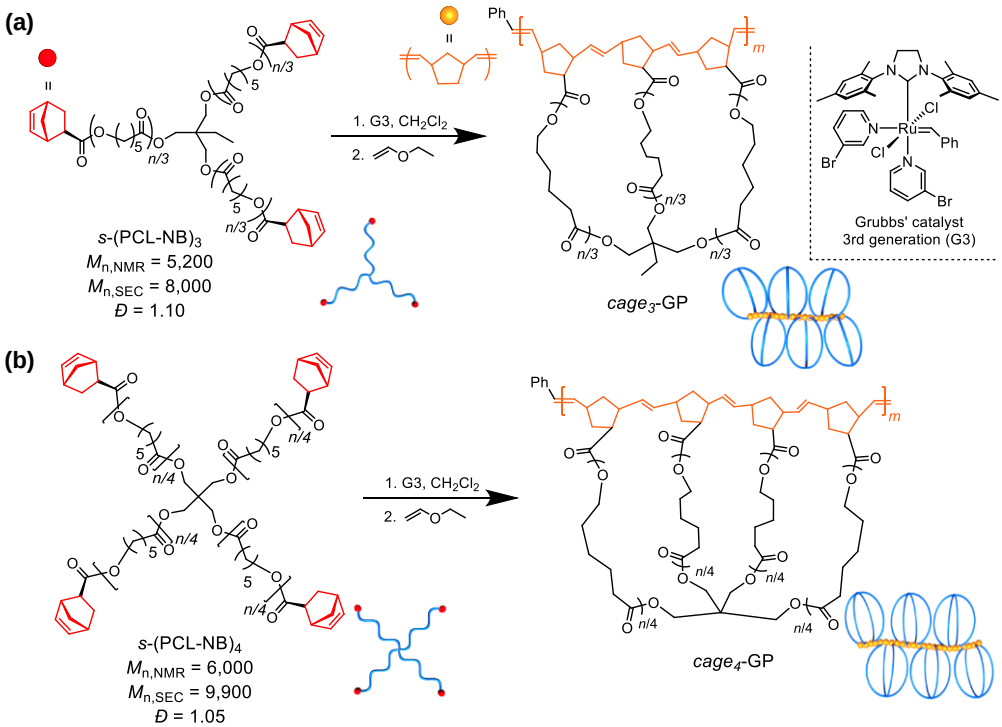

Table 4.1. Molecular characterization of graft polymers containing *cage*$_x$-shaped (x = 3 and 4) side-chains (*cage*$_x$-GPCLs (x = 3 and 4), respectively)[a].

Sample	MM	$[MM]_0/[G3]_0$	$[MM]_0$ (mol L^{-1})	time (min)	$M_{n,SEC}$ [b] (g mol^{-1})	$M_{n,MALS}$ [c] (g mol^{-1})	$Đ$ [b]	No. of graft units [d]
cage$_3$-GPCL	*s*-(PCL-NB)$_3$ ($M_{n,NMR}$ = 5,200)	5/1	0.10	30	26,200	42,900	1.20	8.3
		10/1	0.10	40	34,200	69,800	1.33	13.4
		20/1	0.20	90	58,800	118,000	1.21	22.7
		40/1	0.30	90	135,500	303,000	1.35	58.3
cage$_4$-GPCL	*s*-(PCL-NB)$_4$ ($M_{n,NMR}$ = 6,000)	3.75/1	0.20	90	24,000	40,200	1.27	6.7
		7.5/1	0.20	90	28,000	53,400	1.27	8.9
		15/1	0.30	150	44,400	95,200	1.30	15.9

[a] Polymerization conditions: temperature, r.t.; atmosphere, Ar; solvent, CH_2Cl_2. [b] Determined by SEC in tetrahydrofuran (THF) using PSt as the standard. [c] Determined by triple-detection SEC equipped with multiangle light scattering, viscosity, and refractive index detectors (SEC-MALS-Visco) in THF. [d] The number of cage repeating units in the obtained GPCLs was estimated as ($M_{n,MALS}$ of GPCL)/($M_{n,NMR}$ of MM).

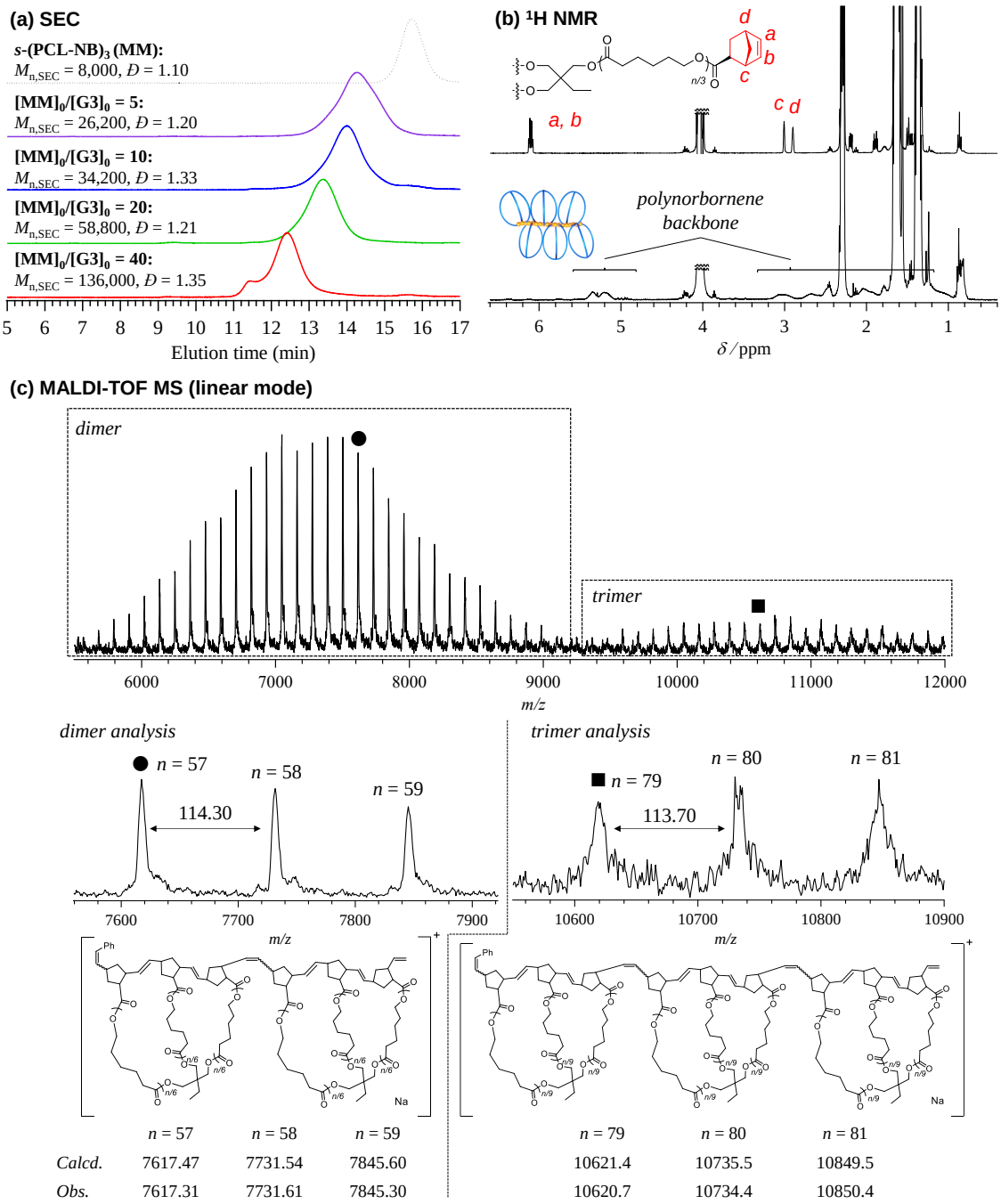

Figure 4.2. Structural analysis of graft polymers containing three-armed cage-shaped PCL side-chains (*cage*$_3$-GPCLs) prepared by cyclopolymerization using G3. (a) SEC traces of the three-armed star-shaped macromonomer (MM, namely *s*-(PCL-NB)$_3$; $M_{n,NMR}$ = 5,200 g mol^{-1}, $M_{n,SEC}$ = 8,000 g mol^{-1}, $Đ$ = 1.10; dotted line) and the *cage*$_3$-GPCLs obtained at $[MM]_0/[G3]_0$ = 5 (purple), 10 (blue), 20 (green), and 40 (red) in THF. The shoulder peak that appeared in the SEC traces of the product obtained at $[MM]_0/[G3]_0$ = 40 is due to the exclusion limit of the column (see Figure S4.3). (b) ^{1}H NMR spectra of *s*-(PCL-NB)$_3$ (upper) and *cage*$_3$-GPCL prepared at $[MM]_0/[G3]_0$ = 5 (lower) in $CDCl_3$ (400 MHz).

To prove that the polymerization of the multifunctional macromonomer proceeded via the expected cyclopolymerization mechanism, the as-obtained product was characterized by SEC equipped with multiangle light scattering and viscosity detectors (SEC-MALS-Visco), ^{1}H NMR, and matrix-assisted laser desorption/ionization-time of flight mass spectrometry (MALDI-TOF MS). The absolute number-average molecular weight determined by SEC-MALS-Visco ($M_{n,MALS}$) in THF was 42,900 g mol^{-1}, and the average number of repeating cage units was calculated to be 8.3, which is slightly higher than the theoretical value (5.0). In the ^{1}H NMR spectrum, the signals corresponding to the *exo*-norbornenyl group completely disappeared following the reaction, indicating that the ROMP proceeded quantitatively (Figure 4.2(b)). Combined with the fact that no multimerized product was found through SEC, this proves the absence of a dangling chain in the resulting GPCL. Although MALDI-TOF MS analysis can provide finer structural details, acquiring the spectrum from high-molecular-weight polymers is quite challenging. To overcome this difficulty, the author separately prepared a low-molecular-weight sample ($M_{n,SEC}$ = 12,000 g mol^{-1}, $Đ$ = 1.17) by cyclopolymerizing the macromonomer ($M_{n,NMR}$ = 4,100 g mol^{-1}, $M_{n,SEC}$ = 6,300 g mol^{-1}, $Đ$ = 1.05) at [*s*-(PCL-NB)$_3$]$_0$/[G3]$_0$ = 3. As shown in Figure 4.2(c), the MALDI-TOF MS spectrum of the product exhibited a series of periodic peaks having a regular interval of 114.30 Da, which is in good agreement with the mass of the ε-CL repeating unit. Crucially, the author found two populations of molecular weight distribution, one of which was observed between the *m*/*z* values of 5,000 and 9,000 whereas the other was observed between the *m/z* values of 9,000 and 12,000. The peaks appearing in the lower molecular weight population were assigned to the desired GPCL containing two cage units; for example, the peak denoted by ● at *m*/*z* = 7617.31 closely matches the calculated mass for the dimer containing 57 ε-CL repeating units ([M + Na]$^+$ = 7,617.47). In contrast, the peaks appearing in the higher molecular weight population were assigned to the GPCL containing three cage units; for example, the peak denoted by ■ at

m/z = 10,620.7 closely matches the calculated mass for the trimer containing 79 ε-CL repeating units ($[M + Na]^+$ = 10,621.4). No peaks attributable to possible multiple G3 adducts (such as two G3 adducts; $[M + Na]^+$ = 7,721.64, *n* = 57; Chart S4.1) were found, suggesting that the cyclopolymerization was initiated from a single G3 molecule to produce *cage*$_3$-GPCL possessing the expected chemical structure that lacks a dangling chain.

Since the cyclopolymerization of the trifunctional star-shaped macromonomer was performed in an accurately controlled manner to produce the desired *cage*-GPCL, the number of norbornenyl units in the polynorbornene backbone is expected to be an integral multiple of three. Based on this hypothesis, the author envisioned that MALDI-TOF MS analysis of the polynorbornene backbone would provide direct proof of the expected cyclopolymerization mechanism. Accordingly, the *cage*$_3$-GPCL ($M_{n,SEC}$ = 28,600 g mol^{-1}, $Đ$ = 1.16; prepared by cyclopolymerization at [*s*-(PCL-NB)$_3$]$_0$/[G3]$_0$ = 10) was subjected to methanolysis using sodium methoxide to selectively remove the PCL side-chain (see SI for the synthetic details). The MALDI-TOF MS spectrum of the methanolysis product exhibited a series of peaks that were assigned to poly(methyl norbornenecarboxylate)s consisting of 9, 12, 15, 18, and 21 repeating units (Figure 4.3). In addition, its regular peak interval (455.31 Da) was consistent with a trimer composed of methyl norbornenecarboxylate as the repeating unit (calculated mass = 456.25 Da). This result strongly supported the hypothesis that the desired *cage*-GPCL was precisely synthesized through a controlled cyclopolymerization in which intramolecular cyclization proceeded preferentially over intermolecular propagation. Overall, these structural characterizations confirm that star-shaped macromonomers are cyclopolymerized to produce GPCLs having cage-shaped topological side-chains (*i.e.*, *cage*$_3$-GPCL).

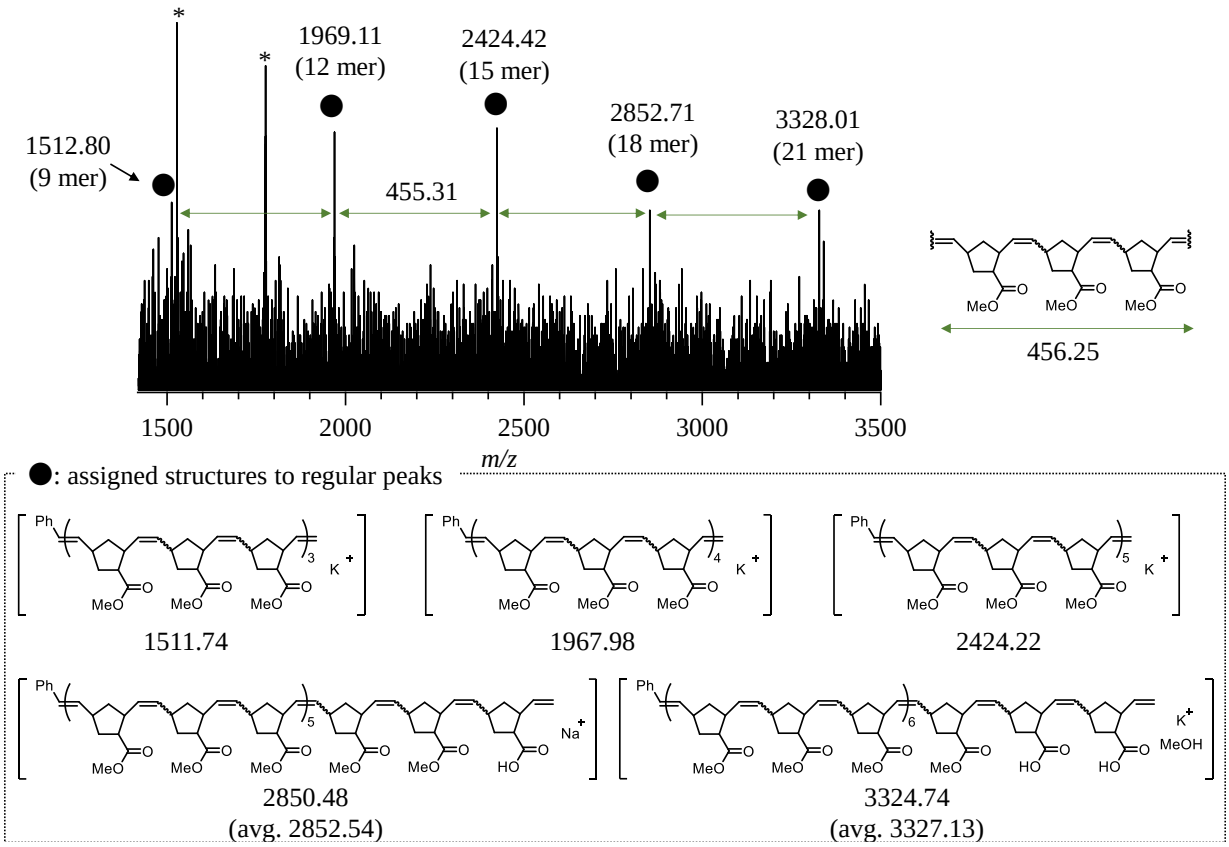

Figure 4.3. MALDI-TOF MS analysis of methanolysis product of *cage*$_3$-GPCL ($M_{n,SEC}$ = 28,600 g mol^{-1}, $Đ$ = 1.16; prepared by the cyclopolymerization with [*s*-(PCL-NB)$_3$]$_0$/[G3]$_0$ ratio of 10). The peaks marked by asterisk were not assignable to any possible methanolysis products. Note that average calculated mass (denoted as avg.) was shown below the expected chemical structures because their monoisotopic signals were hardly seen.

One might expect that the undesired reactions could occur to produce the uncyclized by-products during the cyclopolymerization of *s*-(PCL-NB)$_3$, as shown in Figure S4.4(a). However, the aforementioned detailed structural characterization of the *cage*$_3$-GPs suggested that such undesired reactions hardly occur. First of all, ^{1}H NMR of the products confirmed no unreacted norbornenyl group. Given that the by-products (i) – (iii) with dangling chains (Figure S4.4(a)) must possess unreacted norbornenyl groups, the ^{1}H NMR results can exclude the occurrence of those by-products. Moreover, MALDI-TOF MS analysis of *cage*$_3$-GP shown in Figure 4.2 revealed that all the peaks were assignable to the expected chemical structures with

the different number of PCL units. The by-products (iii) – (v) in Figure S4.4(a) are produced only when two or more G3 additions occurred. Since such multiple adducts possess one or more extra G3-derived benzylidene units, those by-products can be distinguished from *cage*$_3$-GP by MALDI-TOF MS (Figure S4(b),(c)). As mentioned before, no peak corresponding to such by-products was found in the spectra, confirming their negligibly small population. Another important evidence of successful cyclopolymerization is that no gelation occurred during the cyclopolymerizations. Given that the dangling chains exist in the products, this causes gelation through intermolecular propagation. No gelation occurred strongly supports that virtually no dangling chain formed and all the norbornenyl groups consumed for the cyclic repeating unit formations. These solid pieces of evidence proved that the cyclopolymerization of *s*-(PCL-NB)$_3$ produces the corresponding well-defined *cage*$_3$-GPs.

It has been reported that even a trace amount (˜0.1 wt%) of the linear contaminant in cyclic polymer affects the morphological and rheological properties.[32] Therefore, well-defined and highly pure samples are essential to accurately establish the structure-properties relationships. In this regard, the characterization in this study demonstrated the well-controlled synthesis of *cage*-GPs; however, detecting such a small population of structural defects and impurities is challenging. While an in-depth analysis of possible structural defects in the *cage*-GPs is outside the scope of this study, cutting-edge separation methods (such as liquid chromatography at critical conditions and temperature gradient interaction chromatography)[33,34] could facilitate not only quantifying the multicyclic polymer purity but also removing possible by-products.

4.3.2 Cyclopolymerization of four-armed star-shaped macromonomer

To further examine the controllability of the side-chain topology (*i.e.*, *cage*$_4$-GPCL), the four-armed star-shaped macromonomer (*s*-(PCL-NB)$_4$; $M_{n,NMR}$ = 6,000 g mol^{-1}, $M_{n,SEC}$ =

9,900 g mol^{-1}, $Đ$ = 1.05) was subjected to cyclopolymerization (Scheme 4.1(b)). For a reasonable comparison to the *cage*$_3$-GPCLs, the molecular weight of the PCL arm of *s*-(PCL-NB)$_4$ was fixed at ~1,500 g mol^{-1}. Note that the perfect functionality of end-norbornenyl group in the *s*-(PCL-NB)$_4$ was also confirmed by ^{1}H NMR in similar manner as *s*-(PCL-NB)$_3$ (Figure S4.5). Under the established conditions, the cyclopolymerization of *s*-(PCL-NB)$_4$ ([*s*-(PCL-NB)$_3$]$_0$/[G3]$_0$ = 3.75/1) yielded a soluble product, demonstrating that the undesired intermolecular crosslinking was sufficiently suppressed even with the tetrafunctional macromonomer (Table 4.1). Indeed, the SEC trace of the product clearly shifted to a higher molecular region ($M_{n,SEC}$ = 24000 g mol^{-1}, $Đ$ = 1.27) compared to that of *s*-(PCL-NB)$_4$ ($M_{n,SEC}$ = 9900 g mol^{-1}, $Đ$ = 1.05), while retaining the monomodal peak (Figure 4.4). Furthermore, the ^{1}H NMR analysis of the product revealed the quantitative consumption of the norbornenyl groups (Figure 4.5). The number of four-armed cage-shaped units was determined to be 6.7 from its $M_{n,MALS}$. These results support that this synthetic strategy can be applied to tetrafuctional macromonomers to produce *cage*$_4$-GPCLs containing four-armed cage-shaped side-chains.

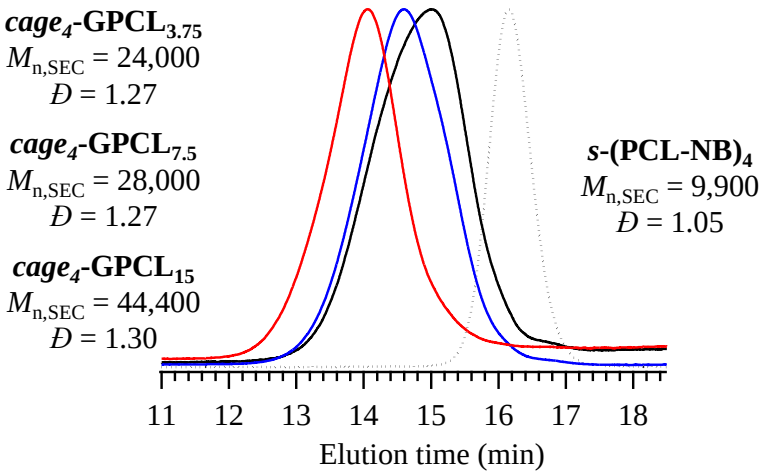

Figure 4.4. SEC traces of ***s*-(PCL-NB)$_4$** (dotted line) and ***cage*$_4$-GPCL**s with different molecular weight (black, blue, and red). The subscripted suffix of the polymer name indicates the $[MM]_0/[G3]_0$.

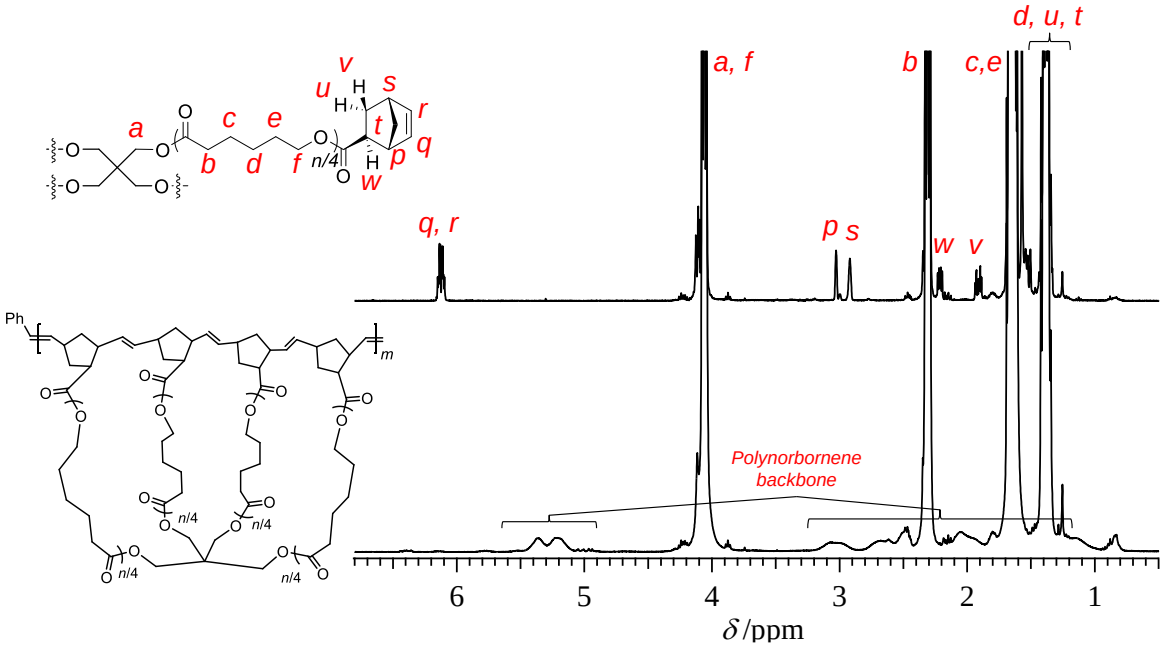

Figure 4.5. ^{1}H NMR spectra of ***s*-(PCL-NB)$_4$** (upper) and ***cage*$_4$-GPCL$_{3.75}$** (lower) in $CDCl_3$ (400 MHz).

The established cyclopolymerization system permitted reliable control over the total molecular weight of *cage*$_3$- and *cage*$_4$-GPCLs in the range of ca. 40,200–303,000 g mol^{-1} in

$M_{n,MALS}$ by varying the [macromonomer]$_0$/[G3]$_0$ ratio (Table 4.1). Although the cyclopolymerizations performed at elevated values of [macromonomer]$_0$/[G3]$_0$ (i.e., [*s*-(PCL-NB)$_3$]$_0$/[G3]$_0$ = 20) did not complete at [macromonomer]$_0$ = 0.10 mM, dosing slightly higher concentrations ([macromonomer]$_0$ = 0.20–0.30 mM) permitted quantitative polymerization. The maximum number of cage-shaped units was 58.3, which was obtained at [*s*-(PCL-NB)$_3$]$_0$/[G3]$_0$ = 40/1.

4.3.3 Kinetic study

To gain mechanistic insights into the cyclopolymerization of star-shaped macromonomers, the author performed a kinetic study by monitoring the macromonomer conversion using SEC. With this objective, the author investigated the (cyclo)polymerizations of not only *s*-(PCL-NB)$_3$ and *s*-(PCL-NB)$_4$, but also those of monofunctional (PCL-NB; $M_{n,NMR}$ = 2,040 g mol^{-1}, $M_{n,SEC}$ = 2,970 g mol^{-1}, $Đ$ = 1.12) and bifunctional (NB-PCL-NB; $M_{n,NMR}$ = 3,200 g mol^{-1}, $M_{n,SEC}$ = 5,600 g mol^{-1}, $Đ$ = 1.08) macromonomers to comprehensively understand the arm-number-dependent polymerization properties. The arm molecular weight of each macromonomer was fixed at ~1,500 g mol^{-1} to ensure a fair comparison (*i.e.*, MW of PCL-NB = 1,500 g mol^{-1}, (MW of NB-PCL-NB) = 3,000 g mol^{-1}, MW of *s*-(PCL-NB)$_3$ = 4,500 g mol^{-1}, and MW of *s*-(PCL-NB)$_4$ = 6,000 g mol^{-1}). The (cyclo)polymerization of each macromonomer was conducted at [norbornenyl group]$_0$/[G3]$_0$ = 15/1 (*i.e.*, [NB-PCL-NB]$_0$/[G3]$_0$ = 7.5/1, [*s*-(PCL-NB)$_3$]$_0$/[G3]$_0$ = 5/1, and [*s*-(PCL-NB)$_4$]$_0$/[G3]$_0$ = 3.75/1) at [macromonomer]$_0$ = 0.2 mM. As shown in Figure 4.6(a), the time-conversion plots showed that *s*-(PCL-NB)$_3$ reached complete conversion in 10 min (red plots), whereas complete conversion was observed at 30–50 min for PCL-NB and NB-PCL-NB (black and blue plots, respectively). The cyclopolymerization of *s*-(PCL-NB)$_4$ proved to be the quickest (~8 min, green plots) among the four macromonomers. These polymerizations followed first-order kinetics, exhibiting a

distinctive feature of living/controlled polymerizations (Figure 4.6(b)). More importantly, the observed trend clearly indicates that the rate of cyclopolymerization increases with decreasing number of intermolecular propagation reactions. Once the propagating chain-end (or G3 initiator) reacts to the macromonomer, the intramolecular consecutive cyclization takes place significantly more rapidly than intermolecular propagation. Therefore, intermolecular propagation is the rate-determining step of the cyclopolymerization. The cyclopolymerization mechanism is illustrated in Figure 4.6(c). The initiating step involves the addition of G3 to the norbornenyl group on the macromonomer followed by the rapid intramolecular consecutive cyclization that forms a cage-shaped unit bearing an active Ru carbene. Due to the high dilution, the addition of the active Ru carbene to the adjacent macromonomer occurs quite slowly compared to the intramolecular reaction. Therefore, possible side reactions, such as the addition of multiple G3 molecules, dangling chain formation, and crosslinking reactions, are strongly suppressed, thereby producing well-defined *cage*-GPCLs.

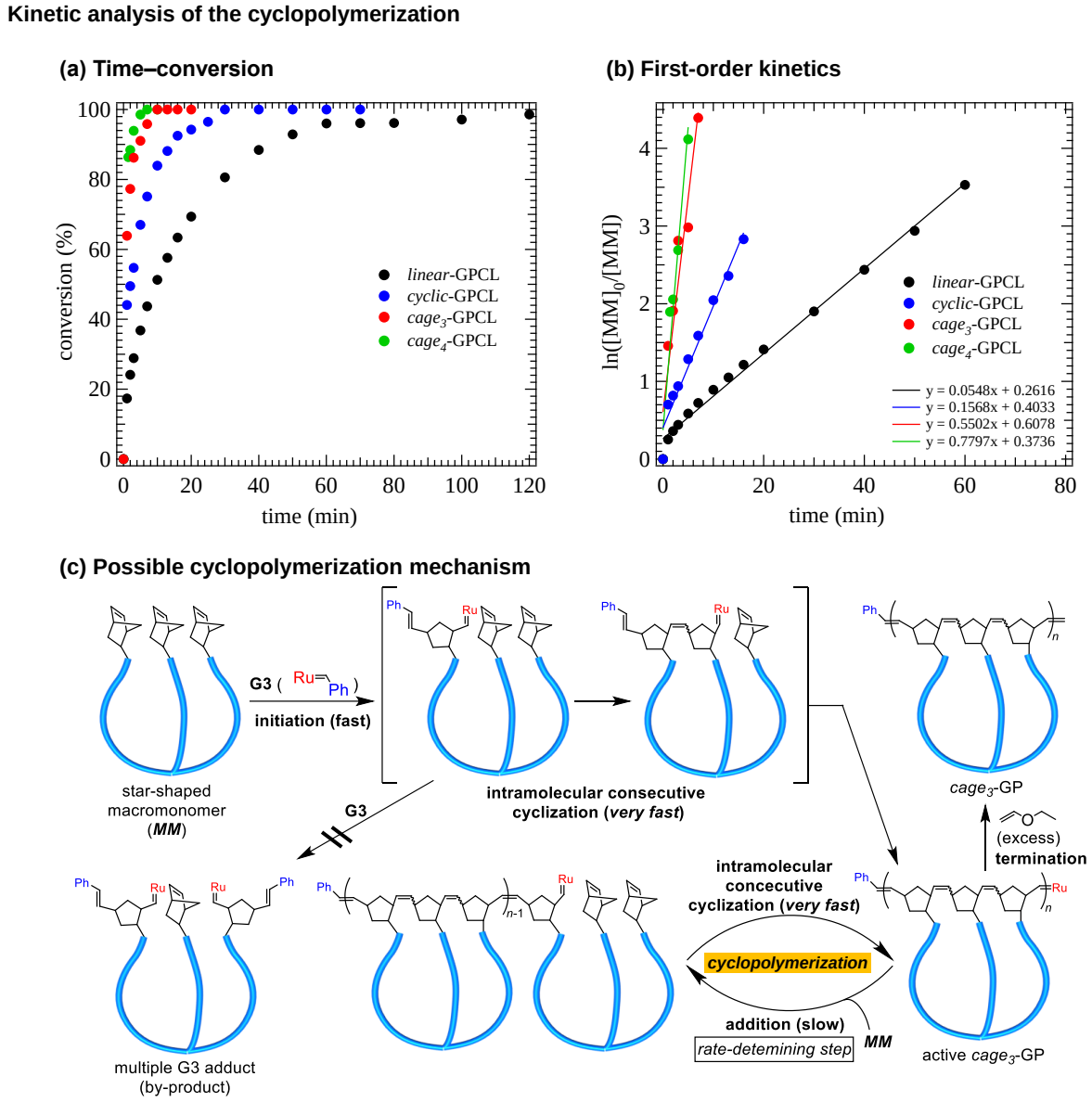

Figure 4.6. (a,b) Kinetic analyses of the (cyclo)polymerizations of PCL-NB, NB-PCL-NB, *s*-(PCL-NB)$_3$, and *s*-(PCL-NB)$_4$ ([PCL-NB]$_0$/[G3]$_0$ = 15/1; [NB-PCL-NB]$_0$/[G3]$_0$ = 7.5/1; [*s*-(PCL-NB)$_3$]$_0$/[G3]$_0$ = 5/1; [*s*-(PCL-NB)$_4$]$_0$/[G3]$_0$ = 3.75/1; [MM]$_0$ = 0.2 mM). (c) Proposed mechanism for the cyclopolymerization of three-armed star-shaped macromonomers to produce a well-defined *cage*$_3$-GPCL under a diluted condition.

4.3.4 Range of applicability to macromonomers

Thereafter, the author applied this strategy to diverse polymer species to confirm its synthetic versatility. The author performed the cyclopolymerization of a variety of norbornenyl-end-functionalized star-shaped macromonomers, such as three- and four-armed star-shaped

poly(L-lactide)s (*s*-(PLLA-NB)$_3$ and *s*-(PLLA-NB)$_4$, respectively), three-armed star-shaped poly(trimethylene carbonate) (*s*-(PTMC-NB)$_3$), and four-armed star-shaped poly(ethylene glycol) (*s*-(PEG-NB)$_4$) having a $M_{n,NMR}$ of 6,000–8,000 g mol^{-1}, to obtain the corresponding GPCLs (*cage$_x$*-GPLLA (x = 3 and 4), *cage$_3$*-GPTMC, and *cage$_4$*-GPEG, respectively; see Scheme S4.2. and Table S4.1). Specifically, the PLLA and PTMC macromonomers were prepared by the ring-opening polymerizations of L-lactide and trimethylene carbonate, respectively, using triol or tetraol initiator and tin(II) 2-ethylhexanoate and diphenyl phosphate catalysts,[30,35] followed by end-functionalization with norbornenyl carboxylic acid. Similarly, the PEG macromonomer was obtained by appending a norbornenyl group to each terminus of a commercially available four-armed star-shaped PEG. The cyclopolymerization proceeded successfully for all the macromonomers and yielded soluble products under the optimized conditions ([*s*-(PLLA-NB)$_3$]$_0$/[G3]$_0$ = 10/1 and [*s*-(PLLA-NB)$_3$]$_0$ = 0.2 mM; [*s*-(PLLA-NB)$_4$]$_0$/[G3]$_0$ = 7.5/1 and [*s*-(PLLA-NB)$_4$]$_0$ = 0.2 mM; [*s*-(PTMC-NB)$_3$]$_0$/[G3]$_0$ = 10/1 and [*s*-(PTMC-NB)$_3$]$_0$ = 0.075 mM; [*s*-(PEG-NB)$_4$]$_0$/[G3]$_0$ = 7.5/1 and [*s*-(PEG-NB)$_4$]$_0$ = 0.1 mM). While the SEC analysis revealed that the products exhibited small shoulder peaks in the higher molecular region, the major peak attested to increased molecular weights (16,600–38,500 in $M_{n,SEC}$) with respect to the corresponding macromonomer, and had narrow $Đ$ values (1.15–1.45) (Figures S4.6–S49.; also find their ^{1}H NMR spectra in Figures S4.11–S4.14). Therefore, the presented strategy is applicable to a wide range of macromonomers for producing GPs from different polymer species.

Scheme 4.2. Range of applicability to macromonomers. Cyclopolymerizations of (a,b) three- and four-armed star-shaped PLLA, (c) PTMC, and (d) PEG macromonomers to yield *cage*$_3$-GPLLA, *cage*$_4$-GPLLA, *cage*$_3$-GPTMC, and *cage*$_4$-GPEG, respectively

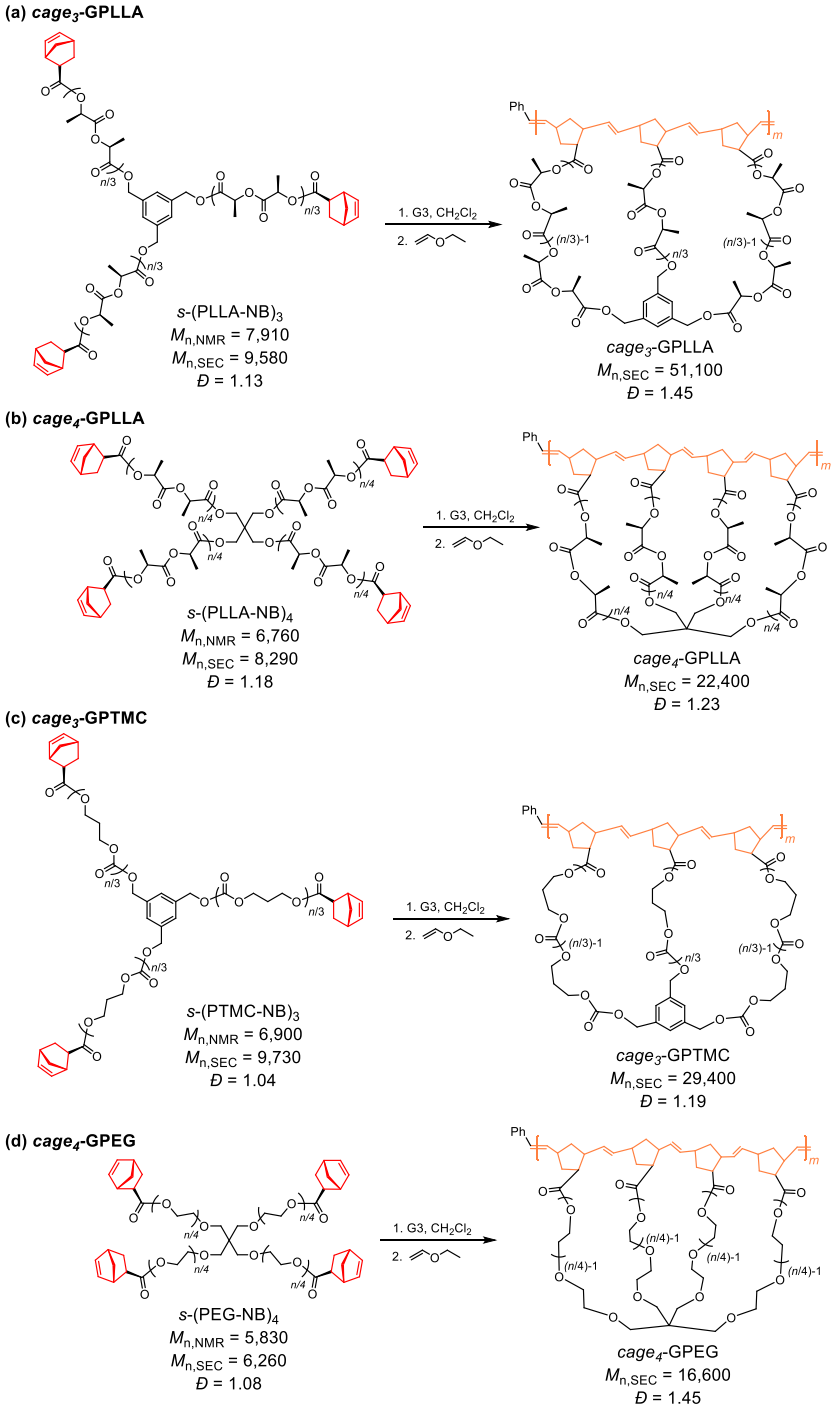

4.3.5 Structure-property relationships of *cage*-GPCLs and their linear and monocyclic counterparts

It is of fundamental interest to systematically investigate how the topology of the side-chain affects the physical properties of topological GPCLs in bulk and solution states, which could facilitate topology-directed material design. Therefore, the author initially evaluated the equilibrium melting temperature ($T_m°$) using differential scanning calorimetry (DSC). A series of linear- and cyclic-chain-grafted GPCLs (*l*-GPCLs and *c*-GPCLs, respectively) as well as monomeric cyclic and cage-shaped PCL units (PCL-NB, *c*-PCL, *cage*$_3$-PCL, and *cage*$_4$-PCL; Chart 4.1) were also prepared and subjected to DSC analyses (see Table 4.2 and Figures S4.14–4.18). Because $T_m°$ is defined as the estimated melting temperature of an infinite stack of extended chain crystals, it should provide objective and extensive insight into the crystallization properties while excluding the potential effects of the crystallization kinetics on T_m (*i.e.*, the dependence of T_m on thermal history).[36,37] The $T_m°$ value of each GPCL was determined by the linear Hoffman–Weeks extrapolation method,[36] wherein the T_m values for the isothermally crystallized samples were plotted against the crystallization temperatures (T_cs), and their linear extrapolation to the line of $T_m = T_c$ gave $T_m°$ as the intersection (see experimental section for the details of DSC measurement). Note that a series of GPCLs used in the analysis had $M_{n,MALS}$ values of 42,900–55,600 g mol^{-1}. The Hoffman–Weeks plots of the topological GPCLs shown in Figure 4.7(a) revealed a unique trend of $T_m°$ as follows: *l*-GPCL (60.6 °C) ≈ *cage*$_3$-GPCL (60.3 °C) > *c*-GPCL (56.8 °C) > *cage*$_4$-GPCL (51.8 °C). Notably, this trend is different from that of the monomeric cyclic and cage-shaped PCL units; $T_m°$ of PCL-NB, *c*-PCL, *cage*$_3$-PCL, and *cage*$_4$-PCL were similarly estimated to be 59.7, 65.0, 61.3, and 60.1 °C, respectively (see Table 4.2). Specifically, the highest $T_m°$ was calculated for *cage*$_3$-GPCL among the cyclic/cage-shaped GPCLs and for *c*-PCL among the monomeric cyclic/cage-shaped PCLs. The dense grafting of the cyclic/cage-shaped side-chain units could cause a discrepancy in the topology-

dependent trend of $T_m°$ between the monomeric cyclic/cage-shaped PCLs and GPCLs. For the cage-shaped PCLs and GPCLs, the side-chain segments around the branched points should possess lower chain mobility and be difficult to crystallize. The side-chain segments farther from the branched points should possess higher chain mobility and crystallize readily. In the case of cage-shaped GPCLs, the spatial interrelation between the neighboring cage-shaped units is determined by their junction with the polynorbornene backbone. When the side-chain segments in the cage-shaped GPCLs crystallize into the lamellar crystal, such steric constraints hinder crystallization in terms of chain mobility. However, the "fixed" spatial interrelation of the neighboring grafted cages should favor chain diffusion to the growth front of lamellar crystals. In the case of *cage*$_3$-GPCL, the side-chain segments in the same cage and perhaps neighboring segments should be located at distances and with orientations that are suitable for chain packing, resulting in an increased $T_m°$. However, further increase in the number of arms of the topological side-chain unit causes steric hindrance around the polynorbornene backbone and four-branched pentaerythritol residue,[38] which could interfere with the crystallization due to the significantly reduced chain mobility, resulting in a much lower $T_m°$ for *cage*$_4$-GPCL than for *cage*$_3$-GPCL. To gain further insight into the crystallization behavior and crystalline hierarchical structure, wide-angle X-ray diffraction (WAXD) and small-angle X-ray scattering (SAXS) experiments (Table S4.2, Figures S4.19 and S4.20) were performed on isothermally crystallized topological GPCLs ($M_{n,MALS}$ = 33,200–42,900 g mol^{-1}, crystallized at 30 °C for 48 h). As shown in Figure S4.20, each WAXD profile exhibited diffraction peaks corresponding to the (110) and (200) planes of the PCL crystal.[39,40] Similar to the cyclic/cage-shaped PCLs,[31] no significant change was observed in the positions of the diffraction peaks upon varying the side-chain topology, confirming that the side-chain topology does not affect the crystallographic unit cell (*i.e.*, chain conformation and packing). This result can be interpreted as the side-chain segments being sufficiently separated from the branched points in topological GPCLs and PCLs

crystallize in an identical conformation and packing to that of the linear PCL, whereas those around the branched points do not crystallize inherently. Correlation function analysis of the SAXS profiles (Figure S4.21) revealed the thicknesses of the crystalline lamellae (l_c) and the amorphous layer (l_a), and the long period ($L_p = l_c + l_a$). Interestingly, topological GPCLs retained a constant l_c value (4.4–4.5 nm), while the monomeric cyclic/cage-shaped PCLs exhibited an increasing trend in the l_c values from 3.2 to 4.5 nm with increase in the number of arms. The cage-shaped PCLs (*cage*$_3$-PCL and *cage*$_4$-PCL) possessed comparable values of l_c (~4.5 nm), l_a (~7.0 nm), and L_p (11.5 nm). In contrast, *cage*$_4$-GPCL possessed a longer l_a (9.4 nm) than *cage*$_3$-GPCL (7.5 nm), albeit possessing an identical l_c (4.5 nm). The crystallinity obtained from WAXD (X_{WAXD}) as well as the ratio of l_c and L_p (l_c/L_p), which is a measure of crystallinity, decreased with increasing number of arms of the cage-shaped GPCLs. In addition, the X_{WAXD} and l_c/L_p for *cage*$_3$-GPCL were comparable to those for *cage*$_3$-PCL, whereas *cage*$_4$-GPCL possessed lower X_{WAXD} and l_c/L_p compared to *cage*$_4$-PCL. These trends are consistent with the magnitude relation in $T_m°$, supporting the dense-grafting effect and the higher crystallizability of *cage*$_3$-GPCL than that of *cage*$_4$-GPCL.

Chart 4.1. List of topological counterparts used for systematic characterization. Linear and cyclic GPCLs (*l*-GPCL and *c*-GPCL) and monomeric PCLs (PCL-NB, *c*-PCL, *cage*$_3$-PCL, and *cage*$_4$-PCL)

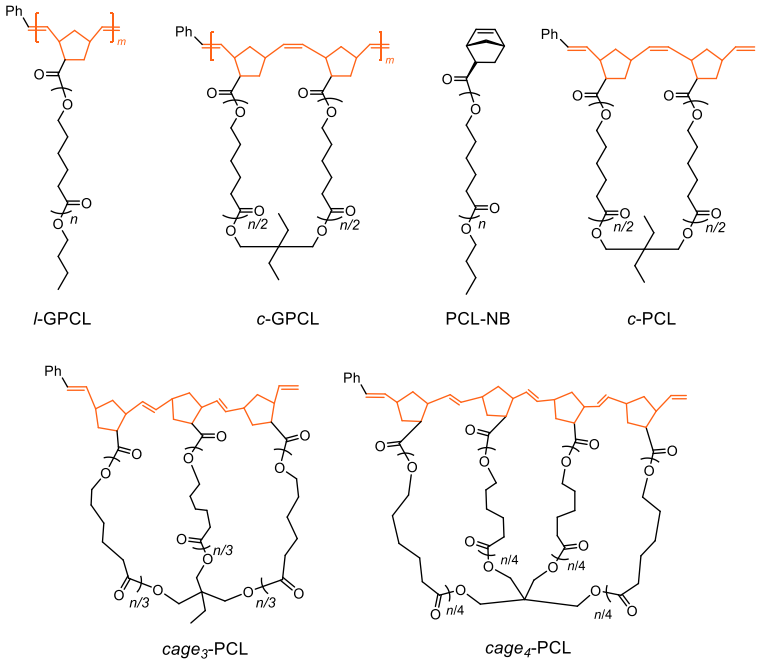

Table 4.2. Physical properties of GPCLs having various topological side-chains and their corresponding monomeric cyclic and cage-shaped PCLs

sample	Number of side-chain units [a]	$M_{n,MALS}$ [b] (g mol^{-1})	$M_{w,MALS}$ [b] (g mol^{-1})	$Đ$ [c]	T_m° (°C)	D_h [b] (nm)	[η] [b] (mL g^{-1})
l-GPCL	10.4	33,200	33,500	1.06	-[d]	9.0	16.8
	16.7	52,600	53,700	1.08	60.6	10.8	18.4
	36.8	118,000	118,000	1.11	-[d]	15.4	24.4
c-GPCL	10.7	34,300	35,100	1.14	-[d]	8.4	13.2
	17.4	55,600	56,200	1.12	56.8	10.2	14.8
	21.6	69,200	69,700	1.15	-[d]	11.2	16.0
cage$_3$-GPCL	8.3	42,900	45,700	1.19	60.3	9.2	14.0
	13.4	69,800	78,700	1.33	60.5	11.4	15.6
	22.7	118,000	122,000	1.21	60.9	14	18.1
	58.3	303,000	319,000	1.35	61.5	22.8	29.4
cage$_4$-GPCL	6.7	40,200	45,400	1.27	-[d]	8.8	12.2
	8.9	53,400	57,400	1.27	51.8	9.6	12.7
	15.9	95,200	105,000	1.30	-[d]	12.8	15.9
PCL-NB	-	1,610	1,820	1.12	59.7	2.6	8.8
c-PCL	-	3,130	3,470	1.08	65.0	3.0	6.7
cage$_3$-PCL	-	3,960	4,090	1.05	61.3	3.2	6.4
cage$_4$-PCL	-	5,550	5,600	1.05	60.1	3.6	7.0

[a] Number of linear, cyclic, or cage-shaped repeating units in the as-obtained GPCLs estimated from ($M_{n,MALS}$ of GPCL)/($M_{n,NMR}$ of MM). [b] Determined using SEC-MALS-Visco in THF. [c] Determined by SEC in THF using PSt as the standard. [d] Not determined.

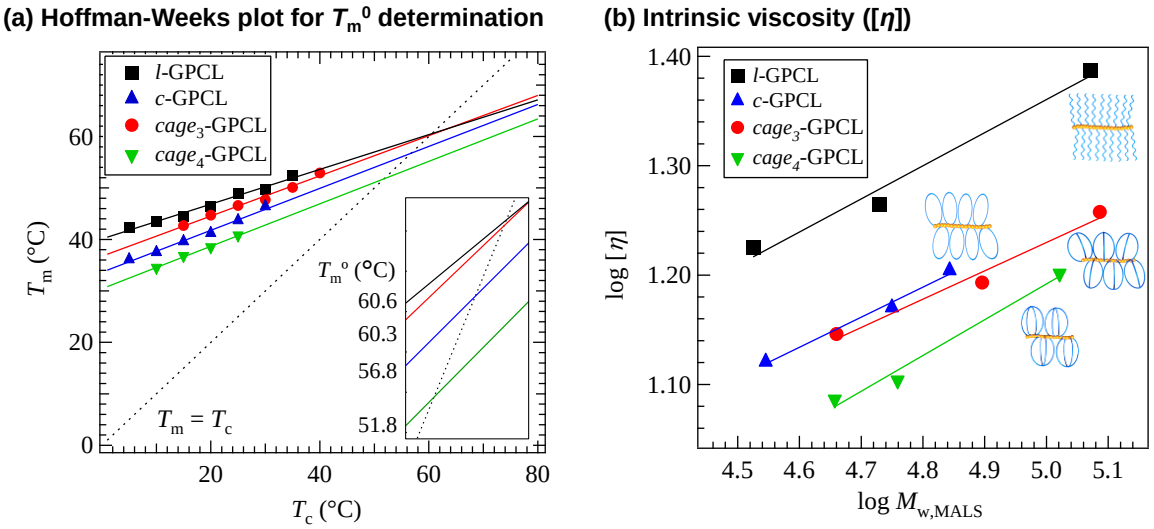

Figure 4.7. Structure-property relationships of topological GPCLs and their counterparts. (a) Hoffman-Weeks plot of GPCLs. The inset contains a magnification of the plot around the point of intersection, which represents the $T_m°$ value of each GPCL. (b) Double-logarithmic plots of $M_{w,MALS}$ versus [η] for *l*-GPCLs (black), *c*-GPCLs (blue), *cage*$_3$-GPCLs (red), and *cage*$_4$-GPCLs (green) (in THF).

Thereafter, the author evaluated the solution properties, such as intrinsic viscosity ([η]) and hydrodynamic diameter (D_h), using SEC-MALS-Visco in THF. As shown in Figure 4.7(b), [η] values of cage-type GPCLs (*cage*$_3$-GPCLs and *cage*$_4$-GPCLs; 12.2–18.1 mL g^{-1}) were found to be smaller than those of their linear and cyclic-type counterparts (13.2–24.4 mL g^{-1}). Specifically, the [η] values decreased in the following order: *l*-GPCLs > *c*-GPCLs > *cage*$_3$-GPCLs > *cage*$_4$-GPCLs. This decreasing trend in [η] with increasing number of arms is consistent with that of the monomeric cyclic/cage-shaped PCLs ([η] = 8.8, 6.7, 6.4, and 7.0 mL g^{-1} for PCL-NB, *c*-PCL, *cage*$_3$-PCL, and *cage*$_4$-PCL, respectively; See Table 4.2). While a series of monomeric PCLs appeared to have no correlation between the topology and D_h values, the D_h values of GPCLs decreased with increases in the number of arms of a repeating side-chain unit when compared between the samples possessing comparable total molecular weights (see Figure S4.22). These results confirmed that the cage-shaped topological side-chain endows

the graft polymers with reduced overall chain dimensions, significantly fewer chain entanglements, and greater side-chain density.[41–43] Such unique properties can be attractive advantages of cage-type topological GPs over cyclic GPs for applications in lubricating and antifouling coatings.

4.4 Conclusion

In this study, the author successfully demonstrated the cyclopolymerization of norbornenyl-end-functionalized star-shaped macromonomers to produce well-defined topological GPCLs possessing cage-shaped side-chains with tunable numbers of arms and cage units. The mechanistic investigation revealed that the presented cyclopolymerization proceeds in an accurately controlled manner, which is composed of the repetition of rapid intramolecular consecutive cyclization and subsequent rate-determining intermolecular addition reaction. The established cyclopolymerization system was found to be applicable to diverse macromonomers, including PLLA, PTMC, and PEG. Furthermore, the author systematically characterized a series of GPCLs with varying molecular weights and side-chain topologies, which revealed that the cage-shaped side-chain topologies significantly affected the crystallization behavior, hydrodynamic diameter, and viscosity. Overall, the simple yet robust cyclopolymerization method enabled, for the first time, the synthesis of well-defined topological graft polymers carrying controllable cage-shaped side-chains, which are difficult to obtain using conventional graft polymer synthetic approaches. Because of the structural tunability of the polymer backbone, side-chain topology, and degree of polymerization (*i.e.*, the number of side-chain units) of the topological GPs, the topology-directed molecular design of functional materials, such as surface modifiers, should be achieved. By taking advantage of the controlled/living nature of the cyclopolymerization presented herein, it could be possible to synthesize chain-end- and side-chain-functionalized topological GPs to create high-performance materials, such as ultralubricating coatings.

4.5 References

(1) Polymeropoulos, G.; Zapsas, G.; Ntetsikas, K.; Bilalis, P.; Gnanou, Y.; Hadjichristidis, N. *50th Anniversary Perspective*: Polymers with Complex Architectures. *Macromolecules* **2017**, *50*, 1253–1290.

(2) Clarson, S. J.; Semlyen, J. A. Cyclic Polysiloxanes: 1. Preparation and Characterization of Poly(Phenylmethylsiloxane). *Polymer* **1986**, *27*, 1633–1636.

(3) Zimm, B. H.; Stockmayer, W. H. The Dimensions of Chain Molecules Containing Branches and Rings. *J. Chem. Phys.* **1949**, *17*, 1301–1314.

(4) Zhu, X.; Zhou, N.; Zhang, Z.; Sun, B.; Yang, Y.; Zhu, J.; Zhu, X. Cyclic Polymers with Pendent Carbazole Units: Enhanced Fluorescence and Redox Behavior. *Angew. Chemie* **2011**, *123*, 6745–6748.

(5) Pipertzis, A.; Hossain, M. D.; Monteiro, M. J.; Floudas, G. Segmental Dynamics in Multicyclic Polystyrenes. *Macromolecules* **2018**, *51*, 1488–1497.

(6) Hossain, M. D.; Reid, J. C.; Lu, D.; Jia, Z.; Searles, D. J.; Monteiro, M. J. Influence of Constraints within a Cyclic Polymer on Solution Properties. *Biomacromolecules* **2018**, *19*, 616–625.

(7) Yamamoto, T.; Tezuka, Y. Topological Polymer Chemistry: A Cyclic Approach toward Novel Polymer Properties and Functions. *Polym. Chem.* **2011**, *2*, 1930–1941.

(8) Uehara, E.; Deguchi, T. Mean-Square Radius of Gyration and the Hydrodynamic Radius for Topological Polymers Expressed with Graphs Evaluated by the Method of Quaternions Revisited. *React. Funct. Polym.* **2018**, *133*, 93–102.

(9) Zhang, K.; Lackey, M. A.; Cui, J.; Tew, G. N. Gels Based on Cyclic Polymers. *J. Am. Chem. Soc.* **2011**, *133*, 4140–4148.

(10) Honda, S.; Yamamoto, T.; Tezuka, Y. Topology-Directed Control on Thermal Stability: Micelles Formed from Linear and Cyclized Amphiphilic Block Copolymers. *J. Am. Chem. Soc.* **2010**, *132*, 10251–10253.

(11) Liu, W.; Dong, Y.; Liu, S.; Wei, T.; Wu, Z.; Chen, H. Enhancement of Bactericidal Activity via Cyclic Poly(Cationic Liquid) Brushes. *Macromol. Rapid Commun.* **2019**, *40*, 1–6.

(12) Wei, T.; Zhou, Y.; Zhan, W.; Zhang, Z.; Zhu, X.; Yu, Q.; Chen, H. Effects of Polymer Topology on Biointeractions of Polymer Brushes: Comparison of Cyclic and Linear Polymers. *Colloids Surfaces B Biointerfaces* **2017**, *159*, 527–532.

(13) Sakurai, S.; Watanabe, H.; Takahara, A. Preparation and Characterization of Looped Polydimethylsiloxane Brushes. *Polym. J.* **2014**, *46*, 117–122.

(14) Trachsel, L.; Romio, M.; Grob, B.; Zenobi-Wong, M.; Spencer, N. D.; Ramakrishna, S. N.; Benetti, E. M. Functional Nanoassemblies of Cyclic Polymers Show Amplified Responsiveness and Enhanced Protein-Binding Ability. *ACS Nano* **2020**, *14*, 10054–

10067.

(15) Morgese, G.; Trachsel, L.; Romio, M.; Divandari, M.; Ramakrishna, S. N.; Benetti, E. M. Topological Polymer Chemistry Enters Surface Science: Linear versus Cyclic Polymer Brushes. *Angew. Chem. Int. Ed.* **2016**, *55*, 15583–15588.

(16) Wang, Y.; Quinsaat, J. E. Q.; Ono, T.; Maeki, M.; Tokeshi, M.; Isono, T.; Tajima, K.; Satoh, T.; Sato, S. ichiro; Miura, Y.; Yamamoto, T. Enhanced Dispersion Stability of Gold Nanoparticles by the Physisorption of Cyclic Poly(Ethylene Glycol). *Nat. Commun.* **2020**, *11*, 6089.

(17) Morgese, G.; Cavalli, E.; Rosenboom, J. G.; Zenobi-Wong, M.; Benetti, E. M. Cyclic Polymer Grafts That Lubricate and Protect Damaged Cartilage. *Angew. Chem. Int. Ed.* **2018**, *57*, 1621–1626.

(18) Morgese, G.; Cavalli, E.; Müller, M.; Zenobi-Wong, M.; Benetti, E. M. Nanoassemblies of Tissue-Reactive, Polyoxazoline Graft-Copolymers Restore the Lubrication Properties of Degraded Cartilage. *ACS Nano* **2017**, *11*, 2794–2804.

(19) Ramakrishna, S. N.; Morgese, G.; Zenobi-Wong, M.; Benetti, E. M. Comblike Polymers with Topologically Different Side Chains for Surface Modification: Assembly Process and Interfacial Physicochemical Properties. *Macromolecules* **2019**, *52*, 1632–1641.

(20) Lehn, J. M. Cryptates: Inclusion Complexes of Macropolycyclic Receptor Molecules. *Pure Appl. Chem.* **1978**, *50*, 871–892.

(21) Sheiko, S. S.; Sumerlin, B. S.; Matyjaszewski, K. Cylindrical Molecular Brushes: Synthesis, Characterization, and Properties. *Prog. Polym. Sci.* **2008**, *33*, 759–785.

(22) Gavrilov, M.; Amir, F.; Kulis, J.; Hossain, M. D.; Jia, Z.; Monteiro, M. J. Densely Packed Multicyclic Polymers. *ACS Macro Lett.* **2017**, *6*, 1036–1041.

(23) Liu, C.; Fei, Y. Y.; Zhang, H. L.; Pan, C. Y.; Hong, C. Y. Effective Construction of Hyperbranched Multicyclic Polymer by Combination of ATRP, UV-Induced Cyclization, and Self-Accelerating Click Reaction. *Macromolecules* **2019**, *52*, 176–184.

(24) Amir, F.; Hossain, M. D.; Jia, Z.; Monteiro, M. J. Precise Grafting of Macrocyclics and Dendrons to a Linear Polymer Chain. *Polym. Chem.* **2016**, *7*, 6598–6607.

(25) Isono, T.; Sasamori, T.; Honda, K.; Mato, Y.; Yamamoto, T.; Tajima, K.; Satoh, T. Multicyclic Polymer Synthesis through Controlled/Living Cyclopolymerization of α,ω-Dinorbornenyl-Functionalized Macromonomers. *Macromolecules* **2018**, *51*, 3855–3864.

(26) Choi, T. L.; Grubbs, R. H. Controlled Living Ring-Opening-Metathesis Polymerization by a Fast-Initiating Ruthenium Catalyst. *Angew. Chem. Int. Ed.* **2003**, *42*, 1743–1746.

(27) Hibi, Y.; Ouchi, M.; Sawamoto, M. Sequence-Regulated Radical Polymerization with a Metal-Templated Monomer: Repetitive ABA Sequence by Double Cyclopolymerization. *Angew. Chem. Int. Ed.* **2011**, *50*, 7434–7437.

(28) Kang, C.; Park, H.; Lee, J. K.; Choi, T. L. Cascade Polymerization via Controlled

Tandem Olefin Metathesis/Metallotropic 1,3-Shift Reactions for the Synthesis of Fully Conjugated Polyenynes. *J. Am. Chem. Soc.* **2017**, *139*, 11309–11312.

(29) Kakuchi, T.; Nonokawa, R.; Umeda, S.; Satoh, T.; Yokota, K. Ring-Opening and Ring-Forming Polymerization of 1,2:5,6:9,10-Triepoxydecane Leading to a Highly Regioselective Polymer Consisting of Octahydrobifuranyl Unit. *Macromolecules* **2000**, *33*, 246–247.

(30) Makiguchi, K.; Satoh, T.; Kakuchi, T. Diphenyl Phosphate as an Efficient Cationic Organocatalyst for Controlled/Living Ring-Opening Polymerization of δ-Valerolactone and ε-Caprolactone. *Macromolecules* **2011**, *44*, 1999–2005.

(31) Mato, Y.; Honda, K.; Tajima, K.; Yamamoto, T.; Isono, T.; Satoh, T. A Versatile Synthetic Strategy for Macromolecular Cages: Intramolecular Consecutive Cyclization of Star-Shaped Polymers. *Chem. Sci.* **2019**, 440–446.

(32) Kapnistos, M.; Lang, M.; Vlassopoulos, D.; Pyckhout-Hintzen, W.; Richter, D.; Cho, D.; Chang, T.; Rubinstein, M. Unexpected Power-Law Stress Relaxation of Entangled Ring Polymers. *Nat. Mater.* **2008**, *7*, 997–1002.

(33) Chang, T.; Lee, H. C.; Lee, W.; Park, S.; Ko, C. Polymer Characterization by Temperature Gradient Interaction Chromatography. *Macromol. Chem. Phys.* **1999**, *200*, 2188–2204.

(34) Ryu, J.; Chang, T. Thermodynamic Prediction of Polymer Retention in Temperature-Programmed HPLC. *Anal. Chem.* **2005**, *77*, 6347–6352.

(35) Gilding, D. K.; Reed, A. M. Biodegradable Polymers for Use in Surgery-Polyglycolic/Poly(Actic Acid) Homo- and Copolymers: 1. *Polymer* **1979**, *20*, 1459–1464.

(36) Hoffman, J. D.; Weeks, J. J. Melting Process and the Equilibrium Melting Temperature of Polychlorotrifluoroethylene. *J. Res. Natl. Bur. Stand. Sect. A Phys. Chem.* **1962**, *66A*, 13.

(37) Marand, H.; Xu, J.; Srinivas, S. Determination of the Equilibrium Melting Temperature of Polymer Crystals: Linear and Nonlinear Hoffman-Weeks Extrapolations. *Macromolecules* **1998**, *31*, 8219–8229.

(38) Ree, B. J.; Mato, Y.; Xiang, L.; Kim, J.; Isono, T.; Satoh, T. Topologically Controlled Phase Transitions and Nanoscale Film Self-Assemblies of Cage Poly(ε-Caprolactone) and Its Counterparts . *Polym. Chem.* **2021**, *12*, 744–758.

(39) Bittiger, H.; Marchessault, R. H.; Niegisch, W. D. Crystal Structure of Poly-ε-Caprolactone. *Acta Crystallogr. Sect. B Struct. Crystallogr. Cryst. Chem.* **1970**, *26*, 1923–1927.

(40) Chatani, Y.; Okita, Y.; Tadokoro, H.; Yamashita, Y. Structural Studies of Polyesters. III. Crystal Structure of Poly-ε-Caprolactone. *Polym. J.* **1970**, *1*, 555–562.

(41) Noda, T.; Doi, Y.; Ohta, Y.; Takata, S. ichi; Takano, A.; Matsushita, Y. Preparation, Characterization, and Dilute Solution Properties of Four-Branched Cage-Shaped Poly(Ethylene Oxide). *J. Polym. Sci.* **2020**, *58*, 2098–2107.

(42) Gauthier-Jaques, M.; Theato, P. Synergy of Macrocycles and Macromolecular Topologies: An Efficient [3_4]Triazolophane-Based Synthesis of Cage-Shaped Polymers. *ACS Macro Lett.* **2020**, *9*, 700–705.

(43) Oike, H.; Imaizumi, H.; Mouri, T.; Yoshioka, Y.; Uchibori, A.; Tezuka, Y. Designing Unusual Polymer Topologies by Electrostatic Self-Assembly and Covalent Fixation. *J. Am. Chem. Soc.* **2000**, *122*, 9592–9599.

4.6 Supporting Information

Table S4.1. Molecular characterization of *cage*-GPs with diverse polymer backbones[a]

sample	MM	$[MM]_0/[G3]_0$	$[MM]_0$	time (min)	$M_{n,SEC}$ [b]	$Đ$ [b]	yield (%)
cage$_3$-GPLLA	*s*-(PLLA-NB)$_3$ ($M_{n,NMR}$ =7,910, $M_{n,SEC}$ = 9,580, $Đ$ = 1.13)	10/1	0.2	40	51,100	1.45	95.9
cage$_4$-GPLLA	*s*-(PLLA-NB)$_4$ ($M_{n,NMR}$ = 6,760, $M_{n,SEC}$ = 8,290, $Đ$ = 1.18)	7.5/1	0.2	30	22,400	1.23	79.5
cage$_3$-GPTMC	*s*-(PTMC-NB)$_3$ ($M_{n,NMR}$ = 6,900, $M_{n,SEC}$ = 9,730, $Đ$ = 1.04)	10/1	0.075	40	29,400	1.19	82.0
cage$_4$-GPEG	*s*-(PEG-NB)$_4$ ($M_{n,NMR}$ = 5,830, $M_{n,SEC}$ = 6,260,[c] $Đ$ = 1.08[c])	7.5/1	0.1	90	16,600	1.45	93.1

[a] Polymerization condition: Temperature, r.t.; Atmosphere, Ar. [b] Determined by SEC in THF using PSt as standards. [c] Determined by SEC in DMF using PSt as standards.

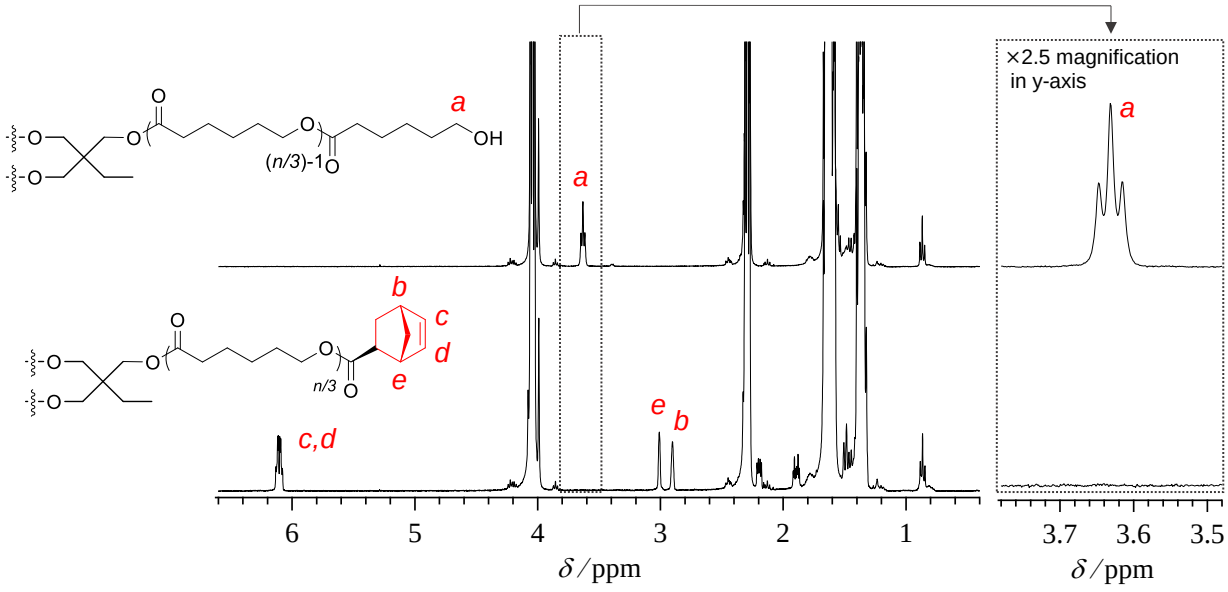

Figure S4.1. ^{1}H NMR spectra of *s*-(PCL-OH)$_3$ (upper) and *s*-(PCL-NB)$_3$ (lower) in $CDCl_3$.

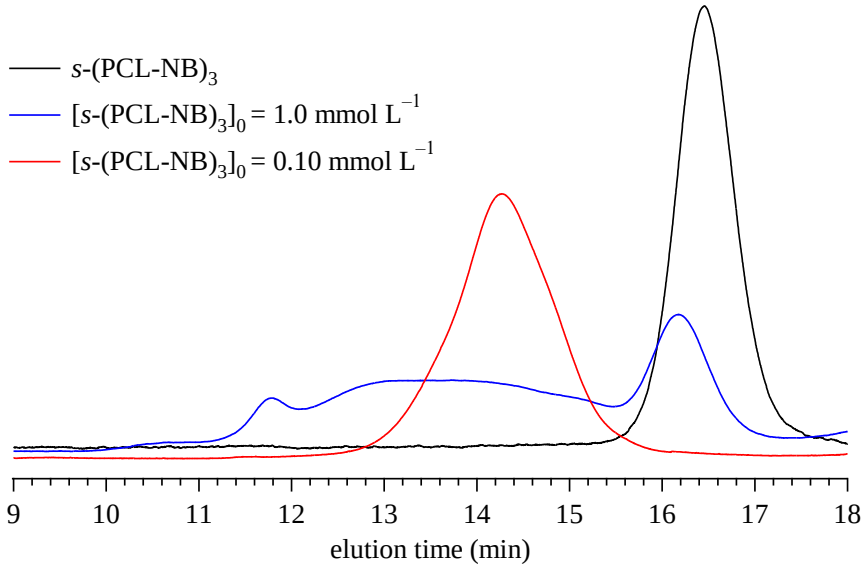

Figure S4.2. SEC traces of three-armed star-shaped macromonomer (***s*-(PCL-NB)$_3$**, red) and cyclopolymerized products under various macromonomer concentration ([***s*-(PCL-NB)$_3$**]$_0$) with 1.0 (blue) and 0.10 mmol L^{-1} (red) (RI detection; eluent, THF).

Chart S4.1. Expected chemical structures of multiple G3 adducts

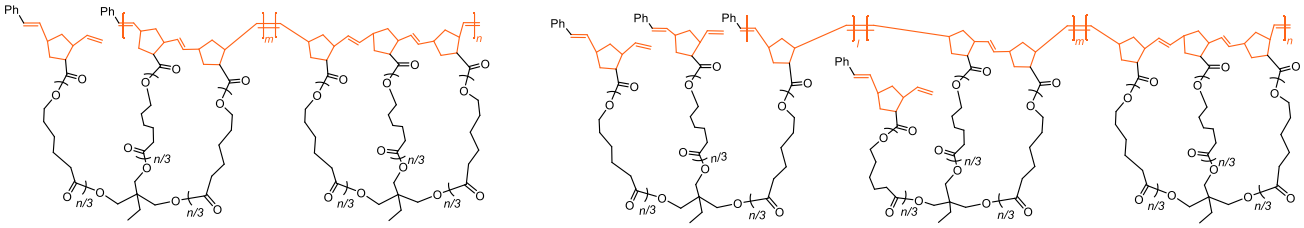

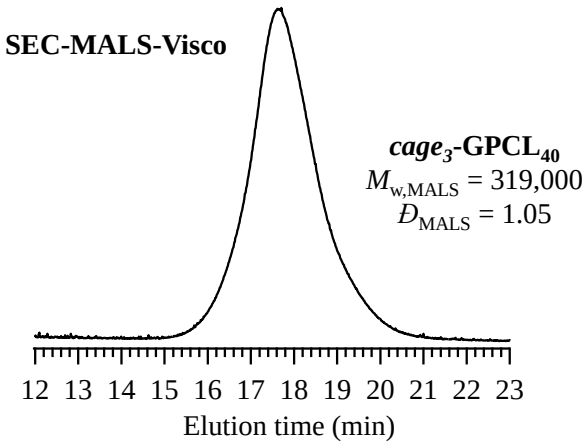

Figure S4.3. SEC trace of ***cage*$_3$-GPCL$_{40}$** obtained from SEC with higher exclusion limit (RI detection, eluent; THF).

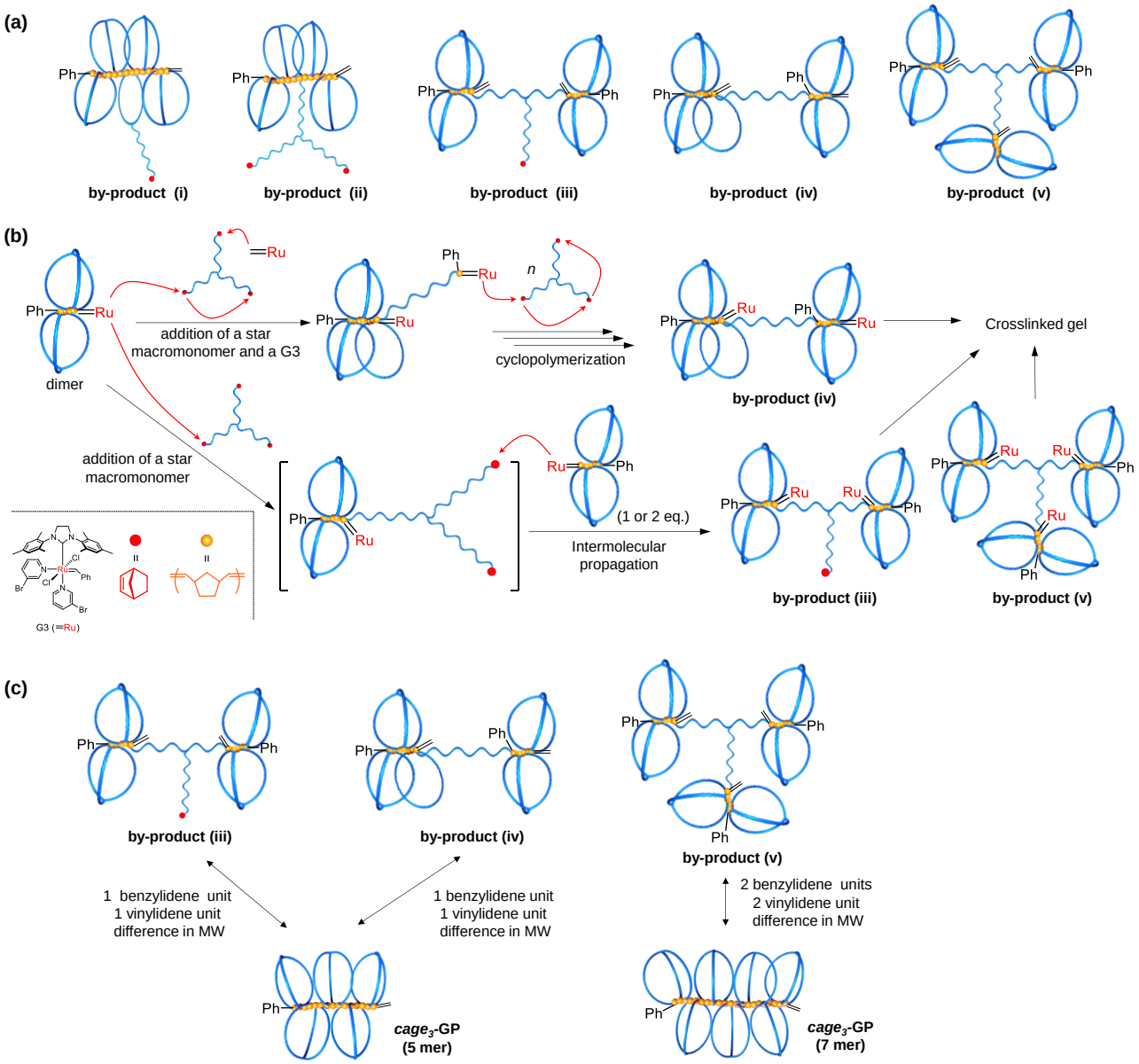

Figure S4.4. Possible by-product formations and their discrimination from the desired *cage*-GPs. (a) Various kinds of by-products possibly formed during the cyclopolymerization of *s*-(PCL-NB)$_3$. (b) Possible pathways to form the by-products (iii), (iv), and (v). (c) Structural comparisons between the by-products and desired *cage*$_3$-GPs with different number of cage units, in which the by-products show molecular-weights difference from that of *cage*-GPs due to presence of extra benzylidene groups (=CHPh) and vinylidene groups (=CH$_2$) by the multiple G3 addition. Note that the structures shown in Figure S4c are the final products obtained after quenching with ethyl vinyl ether.

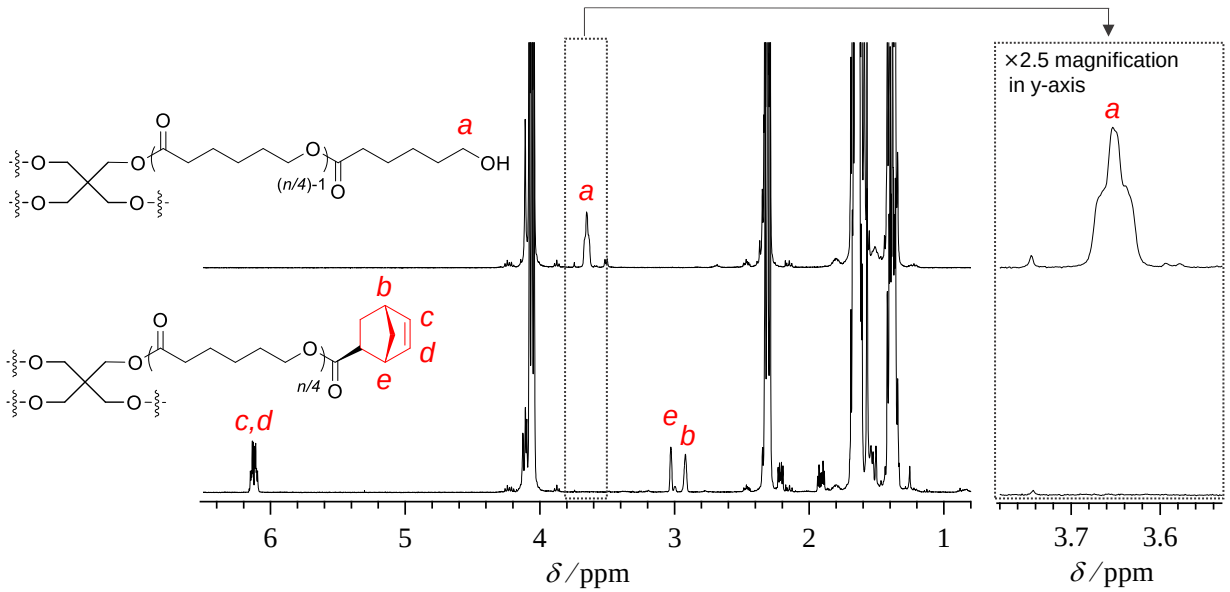

Figure S4.5. ^{1}H NMR spectra of *s*-(PCL-OH)$_4$ (upper) and *s*-(PCL-NB)$_4$ (lower) in $CDCl_3$.

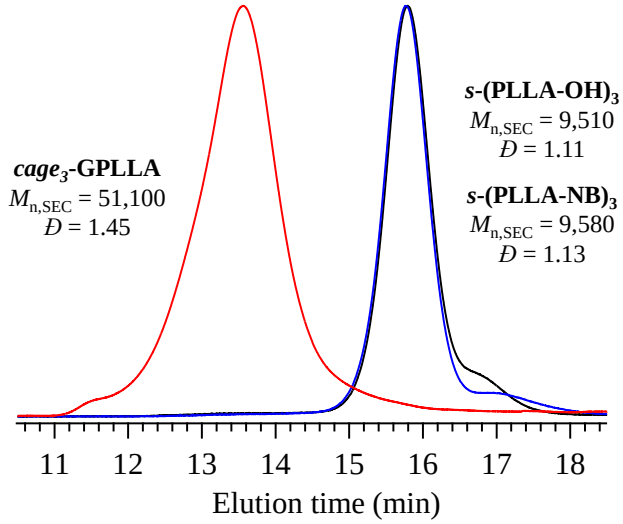

Figure S4.6. SEC traces of ***s*-(PLLA-OH)$_3$** (black), ***s*-(PLLA-NB)$_3$** (blue), and ***cage*$_3$-GPLLA** (red) in THF.

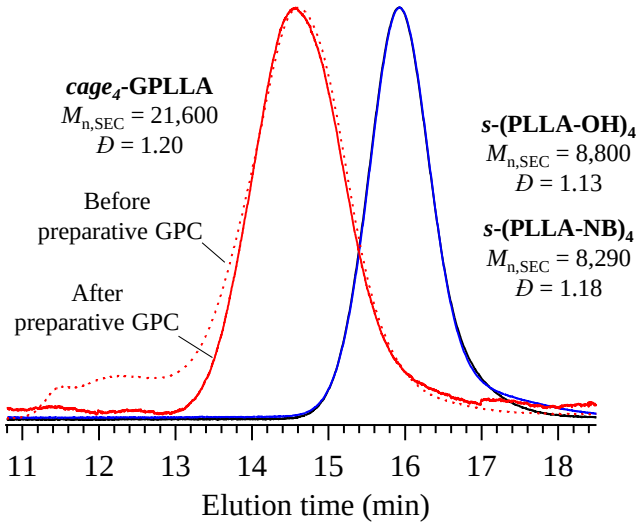

Figure S4.7. SEC traces of ***s*-(PLLA-OH)$_4$** (black), ***s*-(PLLA-NB)$_4$** (blue), and ***cage*$_4$-GPLLA** (dotted line, before purification; red solid line, after the purification using preparative SEC) in THF.

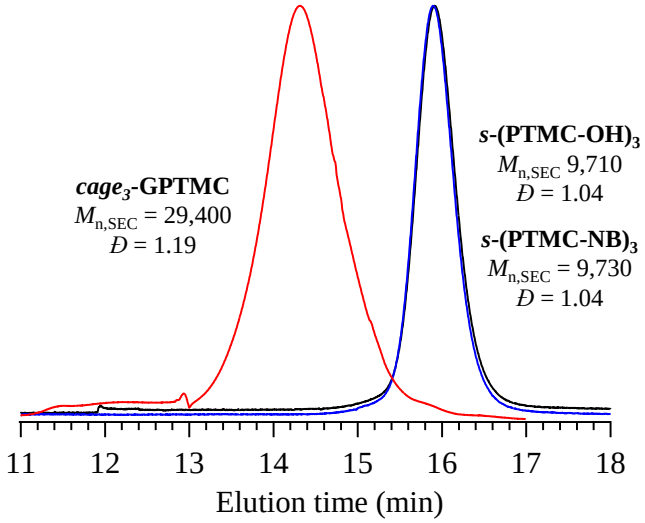

Figure S4.8. SEC traces of ***s*-(PTMC-OH)$_3$** (black), ***s*-(PTMC-NB)$_3$** (blue), and ***cage*$_3$-GPTMC** (red) in THF.

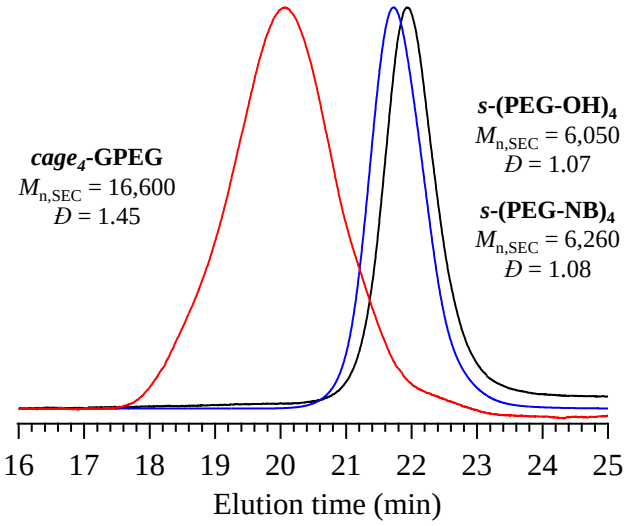

Figure S4.9. SEC traces of ***s*-(PEG-OH)$_4$** (black), ***s*-(PEG-NB)$_4$** (blue), and ***cage*$_4$-GPEG** (red) in DMF.

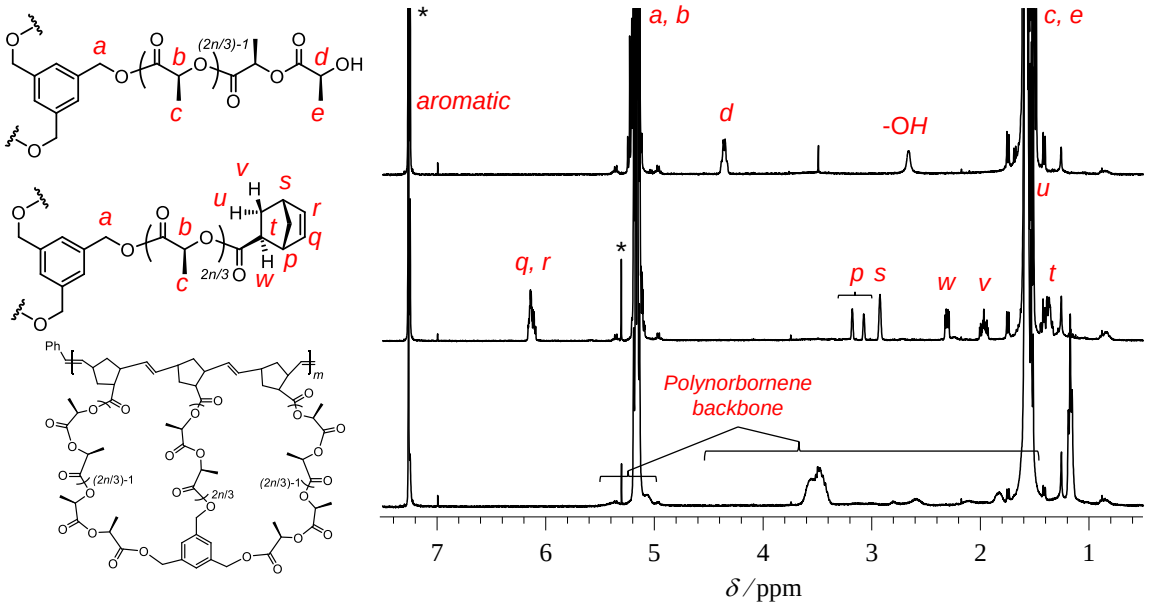

Figure S4.10. ^{1}H NMR spectra of ***s*-(PLLA-OH)$_3$** (upper), ***s*-(PLLA-NB)$_3$** (middle), and ***cage*$_3$-GPLLA** (lower) in $CDCl_3$ (400 MHz).

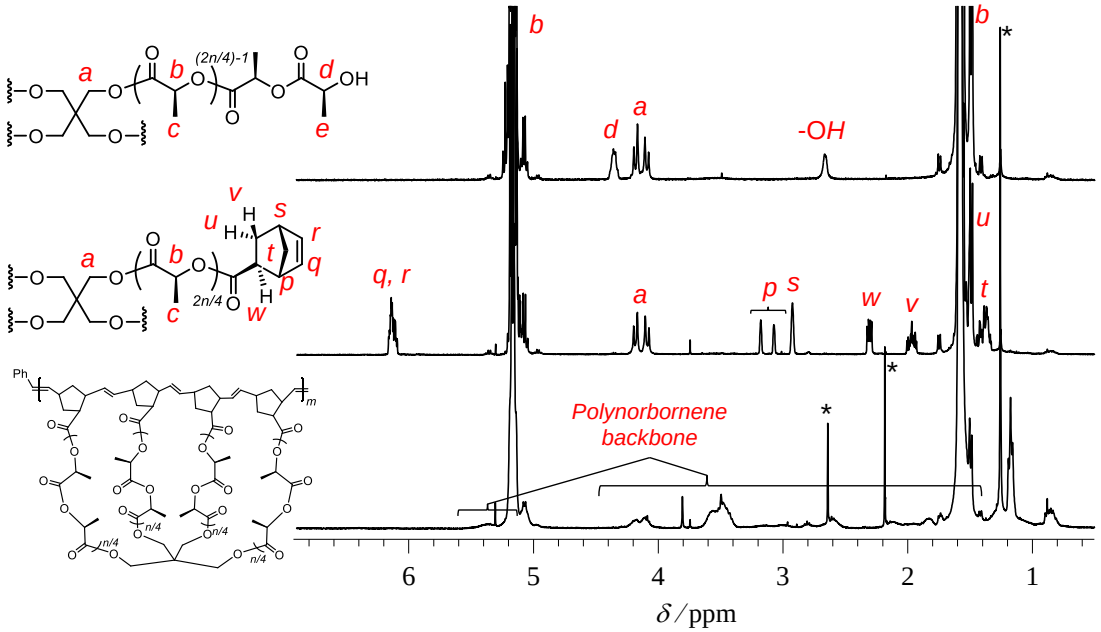

Figure S4.11. ^{1}H NMR spectra of ***s*-(PLLA-OH)$_4$** (upper), ***s*-(PLLA-NB)$_4$** (middle), and ***cage*$_4$-GPLLA** (lower) in $CDCl_3$ (400 MHz).

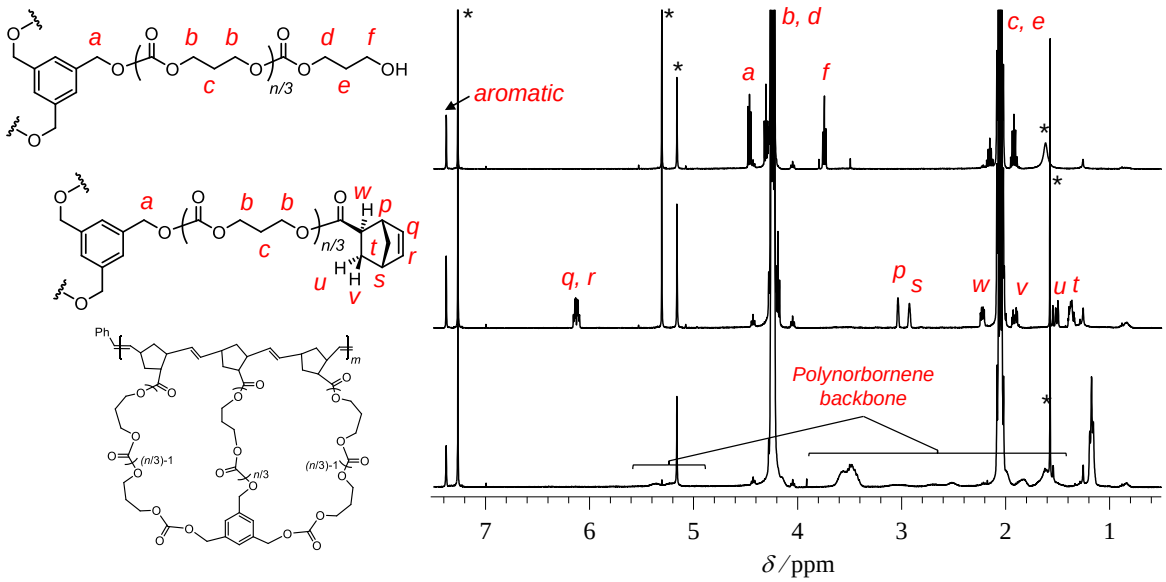

Figure S4.12. ^{1}H NMR spectra of ***s*-(PTMC-OH)$_3$** (upper), ***s*-(PTMC-NB)$_3$** (middle), and ***cage*$_3$-GPTMC** (lower) in $CDCl_3$ (400 MHz).

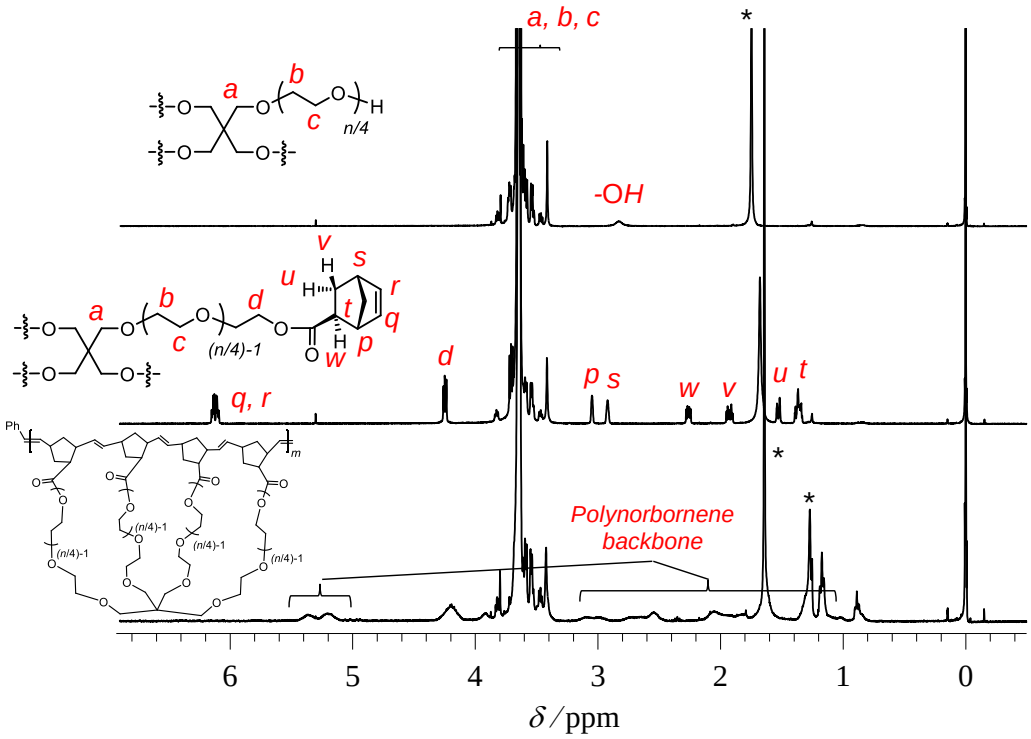

Figure S4.13. ^{1}H NMR spectra of ***s*-(PEG-OH)$_4$** (upper), ***s*-(PEG-NB)$_4$** (middle), and ***cage*$_4$-GPEG** (lower) in $CDCl_3$ (400 MHz).

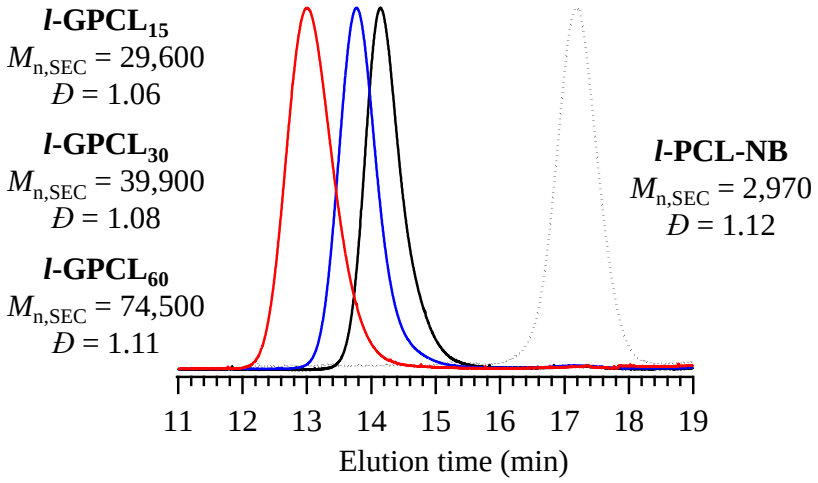

Figure S4.14. SEC traces of ***l*-PCL-NB** (dotted line) and ***l*-GPCL**s with different molecular weight (black, blue, and red).

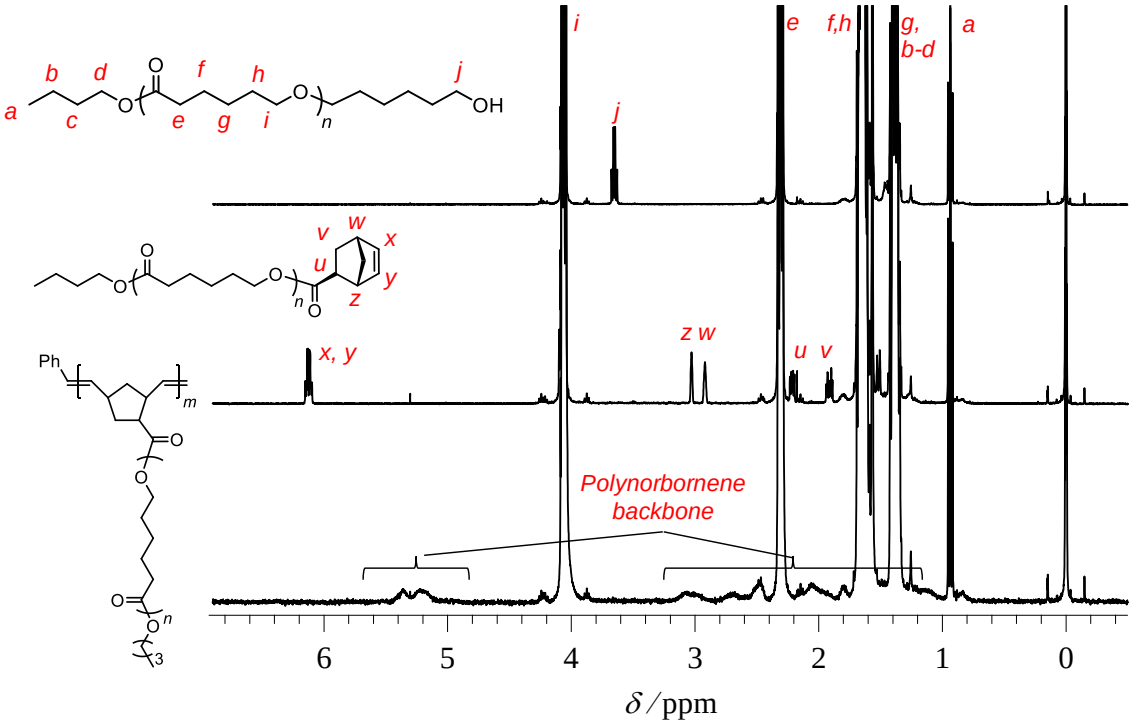

Figure S4.15. ^{1}H NMR spectra of ***l*-PCL-OH** (upper), ***l*-PCL-NB** (middle), and ***l*-GPCL** (lower) in $CDCl_3$ (400 MHz).

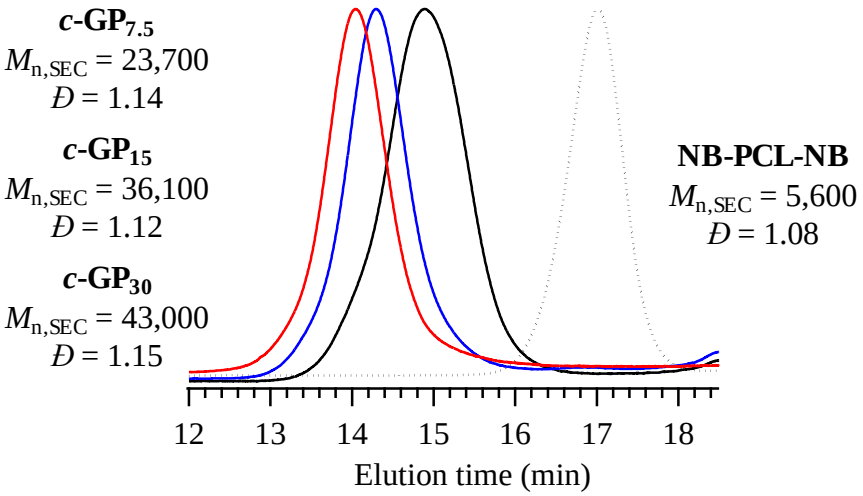

Figure S4.16. SEC traces of **NB-PCL-NB** (dotted line) and ***c*-GPCL**s with different molecular weight (black, blue, and red).

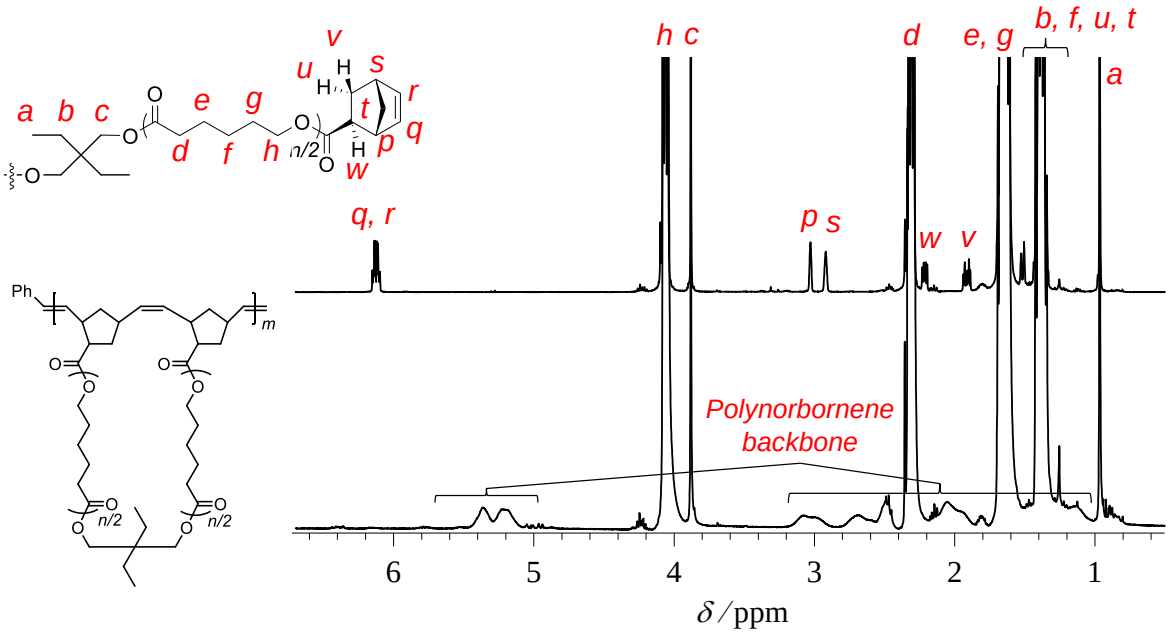

Figure S4.17. ^{1}H NMR spectra of **HO-PCL-OH** (upper), **NB-PCL-NB** (middle), and ***c*-GPCL** (lower) in $CDCl_3$ (400 MHz).

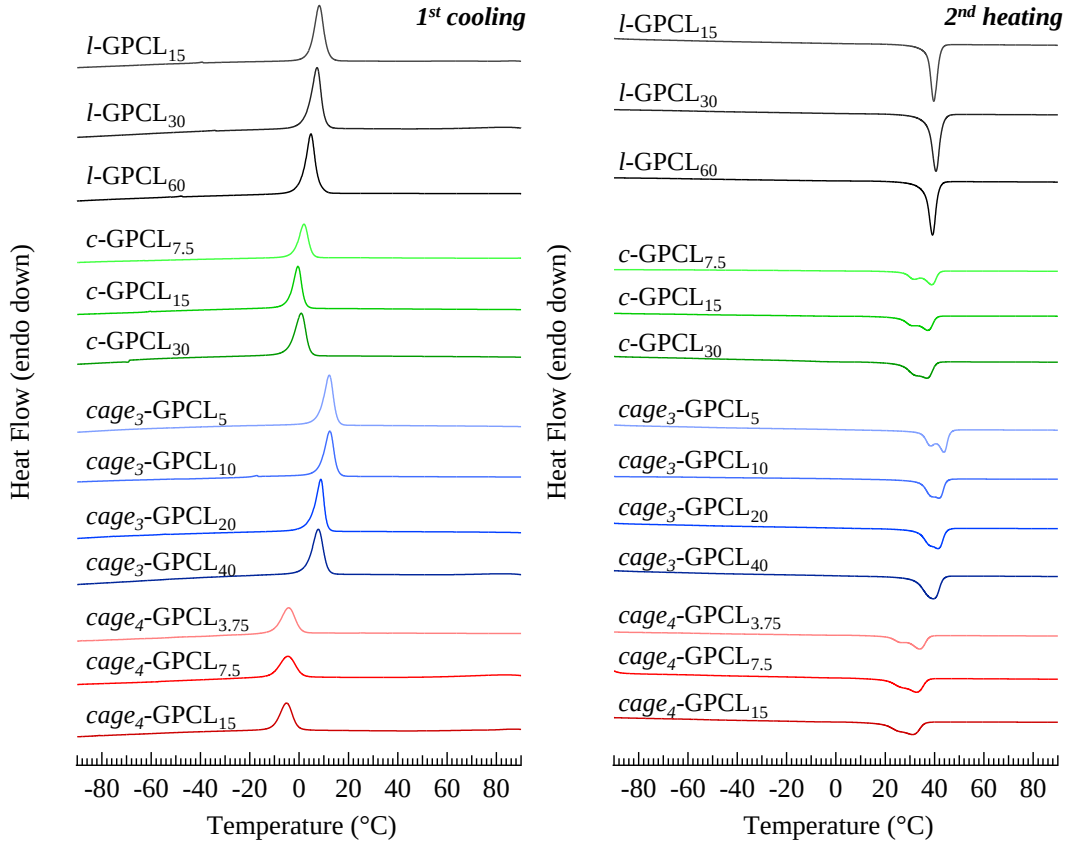

Figure S4.18. DSC thermograms during 1st cooling (left) and 2nd heating (right) of topological GPCLs (N_2 flow, heating and cooling rates: 10 and 20 °C min^{-1}, respectively).

Table S4.2. SAXS and WAXD analysis on topological GPCLs and their monomeric counterparts [a]

sample	$M_{n,MALS}$ [b] (g mol^{-1})	$Đ$ [c]	X_{WAXD} [d] (%)	l_c (nm) [e]	l_a (nm) [e]	L_p (nm) [e]	l_c/L_p (%) [e]
l-GPCL	33,200	1.06	42.1	4.5	6.7	11.2	40.0
c-GPCL	34,300	1.14	33.7	4.5	8.0	12.5	36.0
cage$_3$-GPCL	42,900	1.20	27.4	4.4	7.5	11.9	36.7
cage$_4$-GPCL	40,200	1.27	21.8	4.5	9.4	13.9	32.5
l-PCL	1,610	1.12	40.3	3.2	7.8	11.0	28.9
c-PCL	3,130	1.15	39.0	3.6	7.0	10.6	33.8
cage$_3$-PCL	3,960	1.10	27.8	4.3	7.1	11.5	37.6
cage$_4$-PCL	5,550	1.08	34.0	4.5	7.0	11.5	38.7

[a] Measurement conditions for SAXS and WAXD: temperature: r.t., sample-to-detector distance: 2.5 m, Kapton. Each sample was isothermally crystallized at 30 °C for 48 h prior to the measurements. [b] Determined by triple-detection SEC equipped with multiangle light scattering, viscosity, and refractive index detectors (SEC-MALS-Visco) in THF. [c] Determined by SEC equipped with RI detector in THF. [d] Crystallinity was determined by the peak separation of WAXD profile. [e] Determined by the correlation function analysis of SAXS profile.

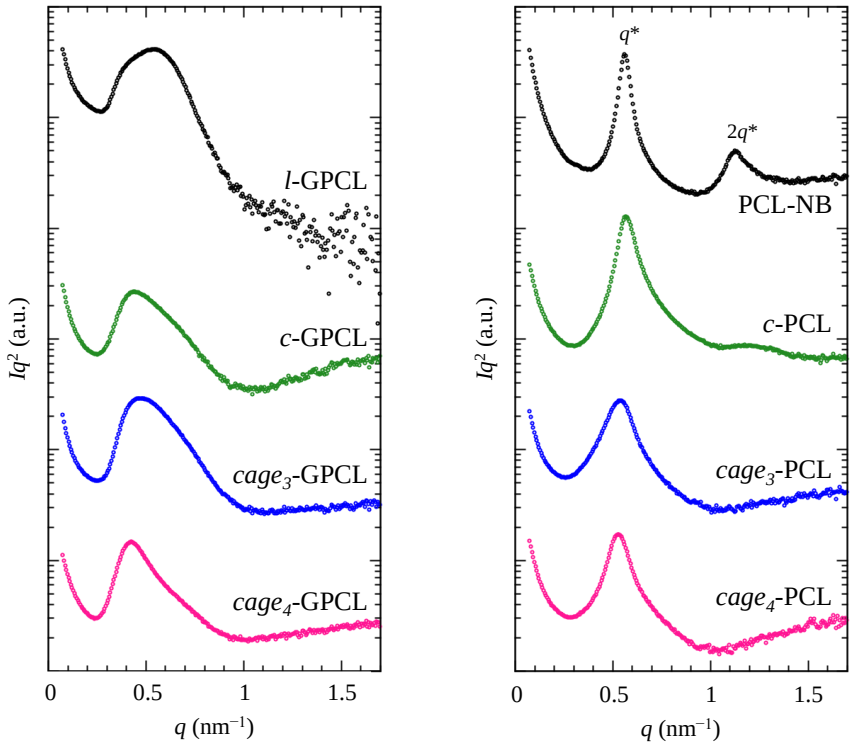

Figure S4.19. SAXS profiles of topological GPCLs (left) and corresponding monomeric counterparts (right).

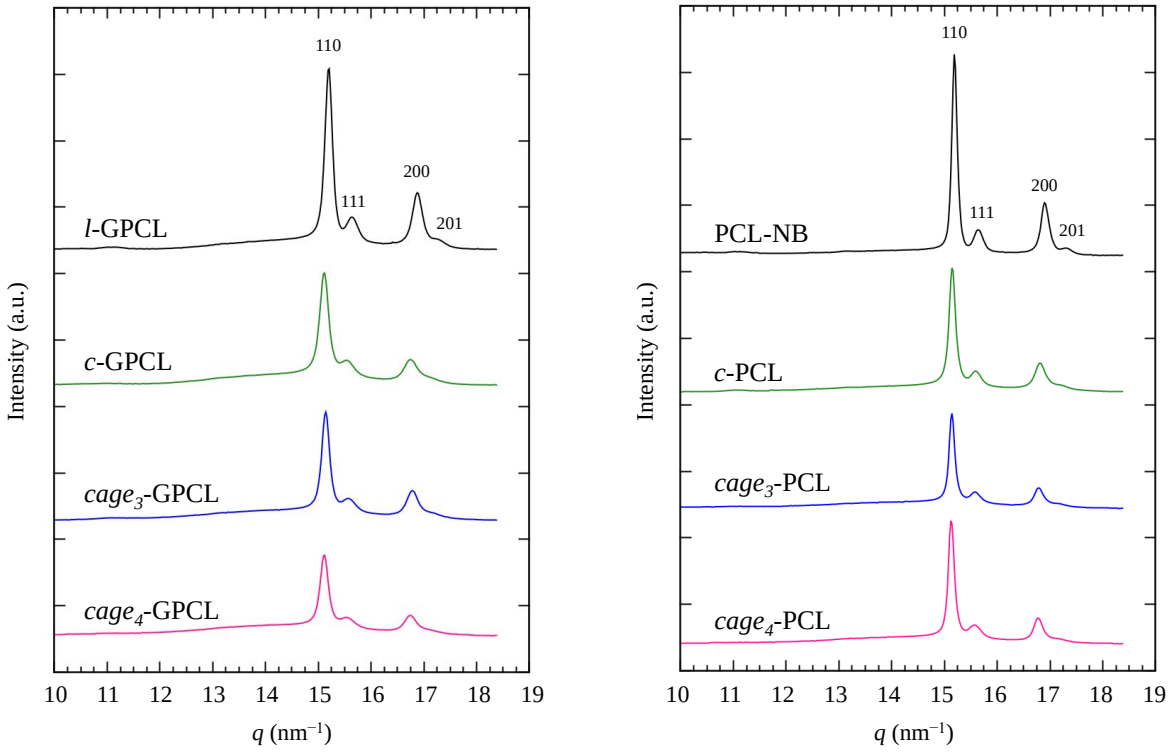

Figure S4.20. WAXD profiles of topological GPCLs (left) and corresponding monomeric counterparts (right).

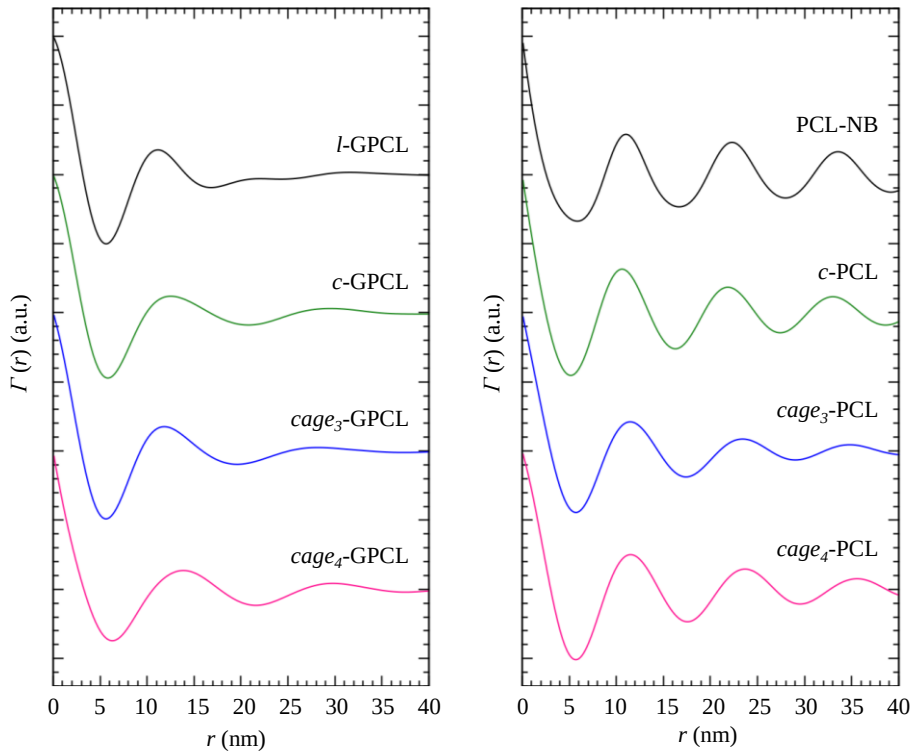

Figure S4.21. Correlation functions of SAXS profiles for topological GPCLs (left) and corresponding monomeric counterparts (right).

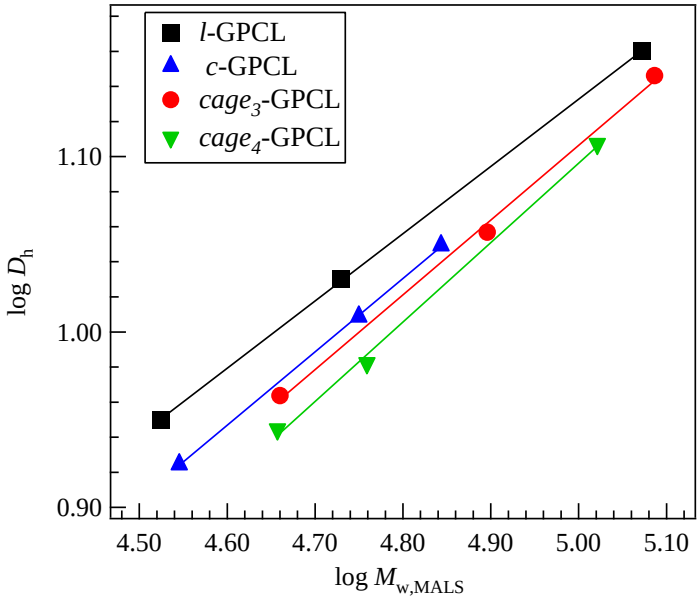

Figure S4.22. Double logarithmic plots of $M_{w,MALS}$ versus D_h for *l*-GPCLs (black), *c*-GPCLs (blue), *cage*$_3$-GPCLs (red), and *cage*$_4$-GPCLs (green).

Chapter 5

Conclusions

In this dissertation, the author proposed the “consecutive cyclization” strategy based on ring-opening metathesis polymerization (ROMP), involving intramolecular ring-opening metathesis oligomerization (ROMO) and cyclopolymerization of multifunctional precursors/macromonomers with norbornenyl groups. This novel cyclization’s concept is based on the multiple ring formation in chain-growth manner where the polymerizable groups at proper positions along the polymer chain intramolecularly reacts, while conventional cyclization technique for multicyclic polymer synthesis depends on stepwise multiple ring formation by the coupling reactions. In addition, another synthetic advantage is that this method requires no daunting preparation of specially designed catalysts, multifunctionalized linkers, and polymer precursors. Accordingly, the consecutive cyclization enabled the systematic synthesis and characterization of diverse multicyclic polymers, which is hardly achievable by conventional multicyclic polymer synthesis. In addition, the robust ROMP chemistry allowed the one-pot functionalization of multicyclic polymers as well as the use of various polymer backbones, which could facilitate the development of advanced functional materials based on multicyclic polymers. A summary of the important achievements and findings in the present study is as follows:

Chapter 2. Systematic synthesis of spiro-multicyclic polymers via intramolecular consecutive cyclization

The author successfully established the new macrocyclization method “intramolecular consecutive cyclization”, enabling the systematic synthesis of *spiro*-multicyclic (8-, trefoil-, and quatrefoil-shaped) polymers with different ring numbers and sizes in high purity. A series of linear, three-armed star-, four-armed star-shaped poly(*ε*-caprolactone)s (PCLs) with norbornenyl group at the chain center and each end were easily synthesized by the following three reaction steps: (1) ring-opening polymerization of *ε*-caprolactone using polyol initiator

having a protected hydroxyl group, (2) the deprotection reaction, and (3) end-norbornenyl-functionalization. Then, the obtained linear, three-armed star-, four-armed star-shaped polymer precursors were subjected to the intramolecular ROMO using Grubbs third-generation catalyst (G3) under a highly diluted condition to produce the 8-, trefoil-, and quatrefoil-shaped PCLs, respectively. The desired *spiro*-multicyclic topologies were successfully obtained in efficient manner with a narrow dispersity ($Đ$; < 1.1). The cyclization using different solvents under varied temperatures revealed the robustness of intramolecular ROMO. In addition, the universality of proposed cyclization strategy was confirmed by applying to diverse polymer species, such as poly(glycidyl ether) and polylactide. One-pot functionalization of the oligonorbornene chain ends was also demonstrated to make the functional multicyclic polymers for the materials applications. Comprehensive study on the structure-property relationships of the *spiro*-type multicyclic PCLs revealed enhanced crystallization ability in the 8-shaped topology.

Chapter 3. Systematic synthesis of cage-shaped polymers via intramolecular consecutive cyclization

The systematic synthesis of cage-shaped polymers (namely, macromolecular cages) with varied arm numbers and ring size via intramolecular ROMO of the end-norbornenyl-functionalized star-shaped PCL precursors was achieved. The three-, four-, six-, and eight-armed star-shaped PCL precursors were prepared in two steps: the ring-opening polymerization of ε-caprolactone using polyol initiators and subsequent end-norbornenyl-functionalization. The established intramolecular ROMO of the star-shaped precursors successfully afforded the desired cage-shaped PCL in sufficient yields with high purity. It is notable that the intramolecular consecutive cyclization enabled the facile yet precise synthesis of eight-armed cage-shaped polymers, while conventional syntheses present a practical limitation to the

systematic synthesis of macromolecular cages with arm numbers greater than six. Based on this synthetic methods, the author succeeded to prepare a series of macromolecular cages with different arm numbers and ring size for the first time. With a series of cage-PCLs, the polymer properties associated with a cage-shaped architecture have systematically evaluated for the first time, which revealed that the hydrodynamic diameter, viscosity, and crystallization behavior of macromolecular cages are strongly affected by the arm number and arm length.

Chapter 4. Systematic synthesis of graft polymers with cage-shaped side chains via cyclopolymerization of star-shaped macromonomers

The precise synthesis of novel graft polymers with macromolecular cage side chains (*cage*-GPs) through the cyclopolymerization of end-norbornenyl-functionalized star-shaped macromonomers was achieved. The three- and four-armed star-shaped macromonomers, that can be easily prepared in the same manner as described in Chapter 3, were subjected to the ROMP in the highly diluted condition to produce the $cage_x$-GPs (where x denotes the arm number of the caged-side-chain unit, x = 3 and 4). The comprehensive structural analysis revealed that the present cyclopolymerization affords the desired $cage_x$-GPs with well-defined microstructure. By taking advantage of the robustness of ROMP, the author succeeded to construct such unprecedented densely-arrayed cage topologies for the first time in a facile yet precise manner. In addition, kinetic study suggested that the cyclopolymerization of star polymer proceeds in an accurately controlled manner, which is composed of the repetition of rapid intramolecular consecutive cyclization and subsequent rate-determining intermolecular addition reaction. Systematic characterization on a series of GPCLs with varying molecular weights and side-chain topologies have elucidated the fact that the cage-shaped side-chain topologies significantly affected the crystallization behavior, hydrodynamic diameter, and viscosity.

In conclusion, the author established the simple, universal, and efficient synthetic approach “consecutive cyclization”, which is useful for creating a variety of multicyclic polymers. Over the past few decades, the synthesis of multicyclic polymers remains challenging despite their potentials for not only controlling the physical properties but also creating advanced functional materials. By taking advantage of the present approach, now one can prepare the desired multicyclic polymers to access the new fundamental science on polymer synthesis and polymer physics as well as advanced materials fabrication regarding multicyclic polymer topologies. Specifically, the established method could facilitate the multicyclic-topology-directed fabrication of advanced nanomaterials, such as polymer nanocage for large guest inclusion and polymer additive for reinforcement of network systems as described in Section 1.1. Overall, the author believes this comprehensive study could open a novel vista and platform into the next stage on elucidating and exerting the effects of multicyclic topologies.